DISSECTING THE ROLE OF PEROXISOMES IN MODULATING ENVIRONMENTAL STRESS RESPONSE AND PHOTOSYNTHESIS

By

Jiying Li

A DISSERTATION

Submitted to
Michigan State University
in partial fulfillment of the requirements
for the degree of

Genetics - Doctor of Philosophy

2015

ABSTRACT

DISSECTING THE ROLE OF PEROXISOMES IN MODULATING ENVIRONMENTAL STRESS RESPONSE AND PHOTOSYNTHESIS

By

Jiying Li

Peroxisomes are essential organelles that house a wide array of metabolic reactions important for plant growth and development. These organelles also interact with other organelles to support cellular functions. However, our knowledge regarding the role of peroxisomal proteins in various biological processes, including plant stress response and photosynthesis, is still incomplete. To address this question at the systems level, I exploited *in silico* analysis, mutant screens and in-depth physiological and biochemical characterizations. First, I used microarray data to generate a comprehensive view of transcript level changes for Arabidopsis peroxisomal genes during development and under abiotic and biotic stress conditions. Second, mutants of LON2 protease and the photorespiratory enzyme hydroxypyruvate reductase 1 (HPR1) were identified to have enhanced susceptibility to drought, suggesting the involvement of peroxisomal quality control and photorespiration in drought resistance. Third, I conducted a comprehensive peroxisomal mutant screen, in which 147 mutants of 104 Arabidopsis genes encoding peroxisomal proteins were subjected to an automated screening system, the Dynamic Environment Phenotype Imager (DEPI). This screen identified multiple peroxisomal proteins required for robust photosynthesis efficiency under dynamically changing light, including peroxisomal biogenesis and division proteins, photorespiratory proteins, and a NAD^+ transporter protein PXN, which was found to be an additional player in photorespiration. Fourth, further characterization of the photorespiratory mutants

provided insights into the molecular mechanisms regarding how the blocking of photorespiration alters photosynthetic efficiency. My data supported an integrated model for the events that occur in the photorespiration mutants, where metabolites and molecules resulting from the block of photorespiration inhibit triose phosphate isomerase (TPI) activity, compromise photosystem integrity, reduce photosystem subunit abundance, decrease proton efflux and diminish ATP synthase conductivity, induce cyclic electron flow (CEF) and activate energy dissipation. In summary, my work has provided significant insights into the connection between peroxisomal function and drought stress response and the links between photorespiration and photosynthesis. Knowledge gained from my dissertation research opens up new avenues to further investigate environmental stress response, photosynthesis, photorespiration and interorganellar communication.

ACKNOWLEDGEMENTS

First of all, I want to thank my beloved grandmother, mother and father for their endless love, encouragement and support. I would not be the person I am today and I would not have achieved so much if it was not for their constant confidence in me.

I want to express my special appreciation to Dr. Jianbing Yan, who influenced me a lot in my undergraduate study in China Agricultural University. His passion for science and his care for nurturing students enlightened my avid interest in science.

I gratefully thank my advisor Dr. Jianping Hu for giving me the opportunity to study and do research in her lab. Jianping is a great mentor, not only because of her knowledge and guidance, but also because she allowed me the freedom to explore different directions in research. What I have learned from her will be a significant impact in my future career. I also want to acknowledge present and previous Hu lab members for their great help to improve my critical thinking and experimental skills.

I appreciate the precious time and suggestions from my committee members: Drs. Kathy Osteryoung, Sheng Yang He, Christoph Benning and Thomas Sharkey, as well as the Genetic Program representative Dr. Barb Sears. I want to gratefully thank our collaborators Drs. David Kramer, Thomas Sharkey and Jin Chen, as well as members in their labs, for sharing knowledge, ideas and experimental devices. Other colleagues at MSU also offered a great deal of help to me.

I feel very fortunate to study at MSU. Besides its academic excellence, the fame of MSU's football and basketball made me very proud of being a Spartan. I have made many good friends at MSU. The time we spent in sharing stories, travelling and playing

together will be forever memorable. Our friendship will be a lifelong treasure to me. Thank you all for being a part of my life.

TABLE OF CONTENTS

LIST OF TABLES

LIST OF FIGURES

KEY TO ABBREVIATIONS

ABA	Abscisic Acid
ABRC	Arabidopsis Biological Resource Center
AGT	Alanine: Glyoxylate Aminotransferase
ATP	Adenosine-5'-Triphosphate
C	Celsius
CAT	Catalase
CBB	Calvin-Benson-Bassham
CEF	Cyclic electron flow
Cytb_6f	Cytochrome b_6f complex
DEPI	Dynamic Environment Phenotype Imager
DHAP	Dihydroxyacetone Phosphate
DRP	Dynamin Related Protein
ER	Endoplasmic Reticulum
FA	Fatty Acid
FD	Ferredoxin
FNR	FD-$NADP^+$ oxidoreductase
F_v/F_m	Maximum quantum yield
GAP	Glyceraldehyde 3-phosphate
GEO	Gene Expression Omnibus
GGT	Glutamate: Glyoxylate Aminotransferase
gH^+	ATP synthase conductivity
GL	Growth Light
GOX	Glycolate Oxidase
HL	High Light
HPR	Hydroxypyruvate Reductase

IAA	Indole-3-Acetic Acid
IBA	Indole-3-Butyric Acid
JA	Jasmonate Acid
LHC	Light Harvesting Complex
NADH	Nicotinamide Adenine Dinucleotide
NADPH	Nicotinamide Adenine Dinucleotide Phosphate
NPQ	Non-Photochemical Quenching
PC	Plastocyanin
PEX	Peroxin
P-glyc	Phosphoglycolate
PMDH	Peroxisomal Malate Dehydrogenase
pmf	Proton Motive Force
PQ	Plastoquinone
PSI	Photosystem I
PSII	Photosystem II
PXN	Peroxisomal NAD^+ carrier
qE	Energy-dependent quenching
qI	Photoinhibition quenching
ROS	Reactive Oxygen Species
SA	Salicylic Acid
SGT	Serine: Glyoxylate Aminotransferase
TPI	Triose Phosphate Isomerase
vH^+	Thylakoid membrane proton efflux
Φ2	Photosystem II operating efficiency

CHAPTER 1

Literature review: Peroxisomal functions and photosynthesis

1.1 Peroxisomal functions

1.1.1 Introduction

Peroxisomes are small and single membrane-bounded organelles found in virtually all eukaryotic cells. They were first described in 1954 (Rhodin, 1954) and later isolated from rat liver cells in 1966 (De Duve and Baudhuin, 1966). This organelle was named “peroxisome” after the discovery of several hydrogen peroxide (H_2O_2) producing oxidases and H_2O_2 degrading catalases enriched in it. In recent decades, peroxisomes have been extensively studied in different systems and increasingly recognized as an indispensable part of the subcellular compartmented system (Fagarasanu et al., 2010; Hu et al., 2012; Islinger et al., 2012; Pieuchot and Jedd, 2012; Smith and Aitchison, 2013).

Peroxisomes make critical contributions to cellular functions because of the metabolic reactions they house, including β-oxidation of fatty acids (FAs) and related metabolites and detoxification of reactive oxygen species (ROS), most of which are oxidative reactions (Fagarasanu et al., 2010; Pieuchot and Jedd, 2012). In humans, the physiological significance of the peroxisome is exemplified by a series of severe neurological, hepatic and renal diseases caused by defects in peroxisome biogenesis and metabolism, including the Zellweger syndrome, neonatal adrenoleukodystrophy and infantile refsum disease (Schrader and Fahimi, 2008; Waterham and Ebberink, 2012; Waterham and Wanders, 2012). Participation of peroxisomes in antiviral response has been revealed recently, adding another important role of peroxisomes as a signaling platform for antiviral innate immunity (Dixit et al., 2010).

In plants, peroxisomes harbor conserved metabolic processes, such as β-oxidation of FAs, production and scavenging of H_2O_2, as well as plant specific reactions, including

photorespiration, metabolism of indole-3-butyric acid (IBA) to indole-3-acetic acid (IAA) and biosynthesis of jasmonate acid (JA) and others (Hu et al., 2012; Kaur et al., 2009). Previous genetics studies have shown that mutations in peroxisomal proteins resulted in a wide range of plant growth and development defects, which indicates that peroxisomes play important roles in relevant biological processes, such as embryogenesis, seedling development, leaf senescence, stress response and others (Hu et al., 2012; Kaur et al., 2009).

1.1.2 Major peroxisomal metabolism

FA oxidation pathway: One of the well-studied peroxisomal functions in plants is FA β-oxidation, through which seed oil storage is broken down to fuel seed germination and seedling development before autotrophic ability is fully established. Seed oil storage, in the form of triacylglycerol, is firstly degraded to fatty acids before entering the peroxisomal β-oxidation cycle (Eastmond, 2006). The fatty acids and other substrates are imported into peroxisomes by the peroxisomal ABC transporter protein CTS/PXA1/PED3 (Footitt et al., 2002; Hayashi et al., 2002; Zolman et al., 2001) and subsequently activated by acyl-activating enzymes (AAEs) such as LACS6 and LACS7 (Fulda et al., 2004) before entering the β-oxidation cycle (Figure1.1). The peroxisomal FA β-oxidation cycle consists of four enzymatic steps (Goepfert and Poirier, 2007). The first step is the oxidation of acyl-CoA with production of 2-trans-enoyl-CoA, which is catalyzed by acyl-CoA oxidase (ACX) (Adham et al., 2005; Froman et al., 2000; Khan et al., 2012; Rylott et al., 2003). The second and third steps are successively catalyzed by multifunctional protein (MFP), which possesses enoyl-CoA hydratase and 3-

hydroxyacyl-CoA dehydrogenase activities thus can convert 2-trans-enoyl-CoA to 3-hydorxycayl-CoA and 3-ketoacyl-CoA, respectively (Richmond and Bleecker, 1999; Rylott et al., 2006). The last step is the cleavage of 3-ketoacyl-CoA with the generation of acyl-CoA and acetyl-CoA, catalyzed by 3-ketoacyl-CoA thiolase (KAT) (Germain et al., 2001; Wiszniewski et al., 2014). After a completed cycle, the original acyl-CoA is shortened by two carbons and one molecule of acetyl-CoA is produced as the substrate for the glyoxylate cycle and gluconeogenesis (Cornah et al., 2004). In Arabidopsis, there are 6 identified peroxisomal ACXs, which possess different but partially overlapping specificities on substrate chain length (Graham and Eastmond, 2002). Two genes encoding peroxisomal multifunctional proteins and three KATs have been identified in Arabidopsis. Many mutants of ACXs and FA β-oxidation related peroxisomal proteins exhibit germination and early seedling developmental defects (Goepfert and Poirier, 2007), solidifying the essential role of peroxisomes in seed germination and seedling establishment.

Photorespiration pathway: Photorespiration is another essential metabolic process accomplished by the peroxisome, with the cooperation of chloroplasts and mitochondria (Figure 1.2) (Bauwe et al., 2010). Photorespiration begins with the production of phosphoglycolate, a product of Rubisco oxygenase activity on ribulose-1,5-bisphosphate (RuBP), and ends with recycling phosphoglycerate back the Calvin-Benson-Bassham (CBB) cycle. Thus photorespiration is considered an alternative carbon recycling pathway operating alongside the CBB cycle (Sage et al., 2012). In chloroplasts, phosphoglycolate is dephosphorylated by phosphoglycolate phosphatase PGLP1 (Schwarte and Bauwe, 2007), and the glycolate generated is subsequently transported

outside of the chloroplasts via a plastidic glycolate glycerate transporter PLGG1 (Pick et al., 2013). After entering the peroxisome, glycolate is subjected to oxidation by glycolate oxidase (GOX) (Hofmann, 2011; Zelitch et al., 2009) to produce glyoxylate. Then an amino group is introduced to glyoxylate by glutamate: glyoxylate aminotransferase (GGT) (Igarashi et al., 2003; Liepman and Olsen, 2003) to produce glycine, which is subsequently transported to mitochondria. In mitochondria, two molecules of glycine are converted to one molecule of serine by glycine decarboxylase (GDC) (Engel et al., 2007; Timm et al., 2012) and serine hydroxymethyltransferase (SHMT) (Voll et al., 2006); meanwhile one molecule of carbon and one molecule of nitrogen are lost. Serine is transported back to peroxisomes and its amino group is removed by serine: glyoxylate aminotransferase (SGT) (Somerville and Ogren, 1980) to generate hydroxypyruvate. The last step of photorespiration in the peroxisome is catalyzed by hydroxypyruvate reductase (HPR), which reduces hydroxypyruvate to glycerate (Timm et al., 2008). NADH generated by peroxisomal malate dehydrogenase (PMDH) facilitates the reduction reaction catalyzed by HPR (Cousins et al., 2011). Glycerate is subsequently transported back to chloroplast by PLGG1, phosphorylated by glycerate kinase GLYK (Boldt et al., 2005) to generate phosphoglycerate, and finally fed into the CBB cycle. To complete photorespiration, two molecules of glycolate are converted to one molecule of glycerate at the cost of one carbon and one ammonium in mitochondria (Foyer et al., 2009). In total, five peroxisomal enzymes are found directly involved in photorespiratory metabolism, whichare encoded by two *GOX*, two *GGT*, one *HPR*, three *SGT* and two *PMDH* genes (Sage et al., 2012). Mutations in these genes cause typical photorespiratory phenotype,

that is, mutants are strongly delayed in growth or even unviable in ambient air, but can be recovered to great extent by growing in high concentrations of CO_2 (Foyer et al., 2009).

H_2O_2 detoxification: In addition to housing these two aforementioned metabolic pathways, peroxisomes are the major source of H_2O_2, a by-product generated by the oxidative reactions catalyzed ACX, GOX and other oxidases. H_2O_2 is an important signaling molecule in various stress conditions. However, if excessively accumulated and escaped to the cytosol, it could be a harmful reactive oxygen species (Mittler et al., 2011). To fine tune the equilibrium of peroxisomal H_2O_2 concentration, an efficient H_2O_2 detoxification system is implemented in the peroxisome. Catalase is the primary enzyme in degrading H_2O_2 into H_2O and O_2. There are three Arabidopsis catalases (Mhamdi et al., 2012; Takahashi et al., 1997), all of which reside in peroxisomes and have similar biochemical activities but different tissue-specific expression patterns. CAT2 is the major catalase in leaves, *CAT3* expression is mainly found in leaf vasculature, and *CAT1* shows particularly high expression in male reproductive tissues, such as anther, pollen, and stamen. Genetic evidence showed that *cat2* knockout mutant exhibited significantly increased leaf lesions in various biotic and abiotic stress conditions (Mhamdi et al., 2012), *cat1* and *cat3* mutants also exhibited obvious but less severe phenotype under the same conditions (Mhamdi et al., 2012). An auxiliary peroxisomal ROS detoxification pathway employs ascorbate peroxidase (APX), monohydroascorbate reductase MDAR, dehydroascorbate reductase (DHAR) and glutathione reductase (GR) to degrade peroxisomal H_2O_2 (Eastmond, 2007; Lisenbee et al., 2005). Peroxisomal proteins such as glutathione sulfur reductase may also be involved in H_2O_2 homeostasis (Kaur et al., 2009).

JA biosynthesis: JA is a fatty-acid-derived phytohormone that can regulate a variety of developmental and stress response processes, including fertility, sex determination, root elongation, abiotic stress and defense against pathogens and wounding (Fonseca et al., 2009). JA biosynthesis begins in chloroplasts, where polyunsaturated fatty acids are converted to the JA precursor OPDA (12-oxo-phytodienoic acid). After import into the peroxisome, OPDA is reduced by OPDA reductase OPR3 to generate OPC8:0 [3-oxo-2-(2'-[*Z*]-penenyl) cycopentane-1-octanoic acid], which is the substrate for three subsequent rounds of β-oxidation (Figure 1.1) (Wasternack and Hause, 2013). After being catalyzed by the action of ACX1 and ACX5, AIM1, and PED1/KAT2, OPC8:0 is converted to OPC6:0 after the first round, OPC4:0 after the second round and JA after the third round. Genetic studies have shown that *opcl1*, *acx1*, *aim1* and *ped1*/*kat2* mutants have decreased levels of JA, disruption of ACX1 or PED/KAT2 resulted in comprised systematic response (Cruz Castillo et al., 2004; Delker et al., 2007; Schilmiller et al., 2007), and tomato *acx1* mutant exhibited reduced defense against chewing insects (Li et al., 2005). After being exported to the cytosol, JA is modified to its bioactive form JA-isoleucine to participate in JA signaling (Fonseca et al., 2009).

Conversion of IBA to IAA: IAA (indole-3-acetic acid) is an active form of the phytohormone auxin, which regulates a plethora of processes, including cell division and elongation, leaf primordial development, phototropism, root development, fruit development and many others (Abel and Theologis, 2010; Krupinski and Jonsson, 2010). Endogenous IAA level is modulated through biosynthesis, transport, storage, and inactivation (Mano and Nemoto, 2012). An increasingly recognized aspect of IAA

regulation is the peroxisomal conversion of IBA to IAA (Strader and Bartel, 2011; Strader et al., 2010; Strader et al., 2011). IBA is structurally very similar to IAA, except that it has two more carbons in the side chain. IBA is imported into the peroxisome, activated by the addition of a CoA group, and converted to IAA through β-oxidation by the shortening of two carbons. Mutants of genes involved in FA β-oxidation, such as ABC transporter mutant *cts*/*pxa1*/*ped3* (Zolman et al., 2001), multifunctional protein mutant *mfp2* and *aim1* (Zolman et al., 2008), 3-ketoacyl-CoA thiolase mutant *ped1*/*kat2* (Zolman et al., 2008) and most of the acyl-CoA oxidase *acx* mutants (Adham et al., 2005; Eastmond et al., 2000; Rylott et al., 2003), showed reduced IBA resistance. Several other peroxisomal proteins such as IBA-RESISTANT 1 (IBR1), IBR3, IBR10 and Enoyl-CoA Hydratase 2 (ECH2), were suggested to act specifically in the conversion of IBA to IAA. IBR1, IBR3 and IBR10 were discovered in forward genetic screens searching for IBA-resistant mutants, and the mutations were later mapped to genes encoding short-chain dehydrogenase/reductase, acyl-CoA dehydrogenases/oxidases and enoyl-CoA hydratase, respectively (Hu et al., 2012). *ECH2* encodes an enoyl-CoA hydratase, and the null mutant exhibited full resistance to IBA in dark-grown Arabidopsis seedlings (Strader et al., 2011). Peroxisome biogenesis mutants, such as *pex4*, *pex5*, *pex6* and *pex7*, showed reduced IBA resistant phenotypes, further confirming the critical role of peroxisomes in IBA to IAA conversion (Strader et al., 2011).

1.1.3 The role of peroxisomes in stress response

In addition to their role in plant development and growth, recent evidence strongly suggests that peroxisomes also play a critical role in a series of biotic and abiotic stress responses (Bednarek et al., 2009; Lipka et al., 2005; McCartney et al., 2005; Rojas et al., 2012).

Striking evidence for the role of peroxisomes in plant pathogen response came from microscopic observation that peroxisomes rapidly aggregate at the fungal pathogen penetration sites, implying that peroxisomes respond to certain signals from the pathogen attack (Lipka et al., 2005). Interestingly, upon stimulation by a fine needle, peroxisomes also converged to the needle contact site in Arabidopsis epidermal cells (Hardham et al., 2008), suggesting that the physical pressure from the fungal pathogen penetration may induce peroxisome aggregation. At the molecular level, a peroxisomal protein called PEN2 has a major role in Arabidopsis broad-spectrum non-host resistance against fungal pathogens. PEN2 is a peroxisome-associated myrosinase catalyzing glucosinolate hydrolysis required for generating antimicrobial products. *pen2* mutant shows significantly reduced callose deposition, increased pathogen penetration rate and enhanced disease susceptibility (Bednarek et al., 2009; Lipka et al., 2005). Besides PEN2, a peroxisome-associated calcium-dependent protein kinase CPK1 greatly enhances plant resistance to both fungal and bacterial pathogens in a salicylic acid (SA)- dependent manner (Coca and San Segundo, 2010). Finally, both JA and SA control a wide range of signaling events in plant immunity (Afitlhile et al., 2005; Koo et al., 2006; Metraux, 2002; Schilmiller et al., 2007; Wasternack, 2007), and the peroxisomal enzymes involved in FA

β-oxidation are employed in JA and presumably SA biosynthetic pathways (Koo et al., 2006; Reumann, 2004), making peroxisomes a potential player in plant defense.

Recently, multiple isoforms of the peroxisomal glycolate oxidase (GOX) have been found as essential components of nonhost resistance against bacterial pathogen in both Arabidopsis and tobacco plants (Rojas et al., 2012). The H_2O_2 produced in the GOX-catalyzed oxidation step is believed to be utilized as a key signaling molecule during pathogen response. Several peroxisomal photorespiration enzymes, such as SGT, GGT, and HPR, are also found to confer immune response in soybean or Arabidopsis plants, possibly through photorespiratory H_2O_2 generation (Okinaka et al., 2002; Taler et al., 2004; Verslues et al., 2007). Since H_2O_2 is produced by many peroxisomal oxidative reactions, efficient ROS-scavenging systems consisting of catalases and ascorbate-glutathione cycle enzymes are implemented in the peroxisome. Suppression of *CAT1* in tobacco resulted in leaf lesion under oxidative stress-inducing conditions, such as high light and drought stress (Chamnongpol et al., 1996). Arabidopsis *cat2* null mutants exhibited enhanced leaf lesion under high light conditions (Chamnongpol et al., 1996). Exposure to H_2O_2 and UV light induces pronounced tubule-shaped extension structure called peroxule and increased peroxisome abundance, suggesting that peroxisomes are actively responding to environmental stress signals by changing morphology and abundance (Sinclair et al., 2009).

Emerging evidence indicated the roles of peroxisomal proteins in stress response, therefore a peroxisome-centered study is desired to comprehensively study how peroxisomal metabolism is connected to environmental stress response. The large amount of transcriptomic, proteomic and metabolomic data accumulated in public databases

could possibly shed light on which peroxisomal genes potentially play critical roles under specific stress conditions (Rhee et al., 2006; Schulze and Usadel, 2010; Sulpice and McKeown, 2015). The development of advanced high throughput phenotyping platform, combined with rich genetic resources, i.e. the availability of large collections of Arabidopsis mutants, may largely accelerate the discovery of those potential players (Fiorani and Schurr, 2013) .

1.2 Photosynthesis

1.2.1 Introduction

Oxygenic photosynthesis, which converts sunlight energy to ATP and NADPH for CO_2 fixation and other dark-reaction-related metabolism, is the principal reaction that drives profound changes to our planet and the life on it. The primary reaction of oxygenic photosynthesis is mediated by four protein complexes embedded in the thylakoid membrane, including photosystem II (PSII), the cytochrome b_6f complex (Cytb_6f), photosystem I (PSI) and ATP synthase (Figure 1.3). Pigments and cofactors, such as chlorophylls, carotenoids, lipids and others, are associated with these protein complexes for a diverse array of critical functions. During the past few decades, many investigations were published regarding photosynthesis in different model systems, including cyanobacteria, algae and higher plants. Our knowledge about the structure and function of the photosynthetic complexes and the dynamic regulatory mechanisms are becoming more comprehensive and in depth (Nickelsen and Rengstl, 2013). In this section, the structure, function, and regulatory mechanism of the four major photosynthetic complexes, as well as the plasticity of photosynthetic processes under dynamic environmental conditions, especially changing light conditions, will be reviewed.

Light energy is captured by the light-harvesting complex (LHC) associated with PSII and PSI. These antenna systems absorb light and channel the light excitation energy to the reaction center of PSII and PSI to generate a stable charge separation across the thylakoid membrane. In this way, PSII becomes highly oxidative and is able to split water molecules to generate electrons, protons and oxygen. The electrons will be transported through PSII, Cytb_6f and PSI, as well as small mobile electron carriers such as

plastoquinone (PQ) and plastocyanin (PC), resulting in the reduction of ferredoxin (FD) and finally the production of NAPDH (Figure1.3). In addition to the linear electron flow (LEF) from PSII to PSI, cyclic electron flow (CEF) also occurs, in which electrons are transported back to the PQ pool from the PSI. Both LEF and CEF are coupled with proton transfer from the stromal to the lumenal side of thylakoid membrane and the generation of proton gradient, which can drive the ATP synthase to produce ATP. The NAPDH and ATP produced in the oxygenic photosynthesis will fuel the reactions of carbon assimilation and other cellular metabolisms (Nelson and Junge, 2015; Rochaix, 2014).

1.2.2 PSII

PSII is a large membrane protein complex located in the thylakoid membrane of photosynthetic organisms ranging from cyanobacteria to higher plants. During the course of evolution, the core machinery for PSII has been mostly conserved. The only major difference is in the light-capturing antenna system, which is named phycobilisome in cyanobacteria and light harvesting complex (LHC) in green algae and higher plants (Shen, 2015; Suga et al., 2015). In cyanobacteria, the PSII complex consists of 20 subunits, of which 17 are transmembrane subunits and 3 are membrane-peripheral subunits, with a total molecular mass of 350 kDa. Among the transmembrane subunits, D1 and D2 constitute the core of PSII reaction center, with which all of the co-factors participate in water splitting reactions and electron transfer are associated. CP47 and CP43 are two transmembrane subunits surrounding D1 and D2, and bind to a number of chlorophyll

molecules to serve an inner light harvesting function. Besides these four large subunits, there are 13 other low-molecular-weight transmembrane subunits (<10 kDa each) that surround the PSII reaction center (Shen, 2015; Suga et al., 2015). Three membrane-peripheral proteins are associated with the lumenal side of PSII and are required to maintain the water-splitting reaction. In cyanobacteria these proteins are PsbO, PsbU and PsbV; in green algae and higher plants, PsbU and PsbV are replaced with PsbQ and PsbP, respectively (Shen, 2015; Suga et al., 2015).

P680 is the chlorophyll cluster associated with the reaction center and consists of 4 chlorophyll molecules. Upon absorption of light, one of the four chlorophyll molecules becomes excited and donates one electron to pheophytin. The electron is then transported from pheophytin to the primary and secondary plastoquinone electron acceptors, Q_A and Q_B, respectively. The oxidized P680 oxidizes the nearby D1 protein, which in turn oxidizes the Mn_4CaO_5 cluster, where the water splitting reaction happens. Once the four electrons have been extracted from the Mn_4CaO_5 cluster, two water molecules are split into four protons and one oxygen molecule, and the electron transport chain is thereby initiated in PSII (Nickelsen and Rengstl, 2013; Shen, 2015).

The first crystal structure of the PSII dimer was obtained by Zouni et al. (Zouni et al., 2000) from thermophilic cyanobacterium at the resolution of 3.8 Å. This initial structure of PSII provided information on the position of the major PSII subunits and the position of Mn_4CaO_5 cluster that catalyzes the water-splitting reaction. In subsequent studies, the resolution of the PSII structure increased gradually to 3.5 Å (Ferreira et al., 2004), 3.0 Å (Loll et al., 2005), and 2.9 Å (Guskov et al., 2009), which continuously improved our understanding of the structure of the whole complex regarding the side-

chain orientation of amino acid residues and a number of cofactors. In 2011, the resolution was significantly improved to 1.9 Å (Umena et al., 2011). At this resolution, the electron density of individual atoms in the Mn_4CaO_5 cluster was clearly separated, and the coordination environment of the metal cluster was revealed. The presence of a large number of water molecules associated with various residues in the PSII dimer was also revealed (Umena et al., 2011).

Although we have extensive knowledge about PSII structure and function, relatively little is known about the assembly process of the PSII complexes. Recent genetic and biochemical studies indicated that PSII assembly is a highly ordered process that involves many cofactors (Nixon et al., 2010; Rokka et al., 2005). Basically, PSII grows outward from the reaction center (RC), which consists of the D1, D2, cytb_{559} and PsbI subunits (Boehm et al., 2011; Keren et al., 2005). The RC complex serves as a scaffold for incorporation of CP47 and CP43, with concomitant attachment of other subunits and assembly factors (Sugimoto and Takahashi, 2003; Wei et al., 2010). After attachment of CP43, a light-driven assembly of the oxygen-evolving Mn_4CaO_5 cluster occurs (Dasgupta et al., 2008). Furthermore, PsbO, PsbP and PsbQ - the subunits that stabilize the Mn_4CaO_5 cluster, are attached to the lumenal side (Bricker et al., 2012). However, how the rest of the subunits incorporates into the complex is still unknown. Thereafter, the active PSII monomers in the thylakoid membrane will form dimers, with attachment of facilitating subunits, such as PsbI, PsbM and PsbW, and the peripheral antenna (Kouril et al., 2012; Shi et al., 2012).

Since the water-splitting reaction is extremely oxidative, PSII is highly prone to photo oxidative damage. To maintain the photosynthetic yield of PSII, efficient repair

systems have evolved (Aro et al., 2005; Kato and Sakamoto, 2009). D1 is the most vulnerable PSII subunit with a high turnover rate (Jarvi et al., 2015). Upon light-induced photodamage, D1 is degraded by the FtsH and Deg proteases on both the stromal and lumenal sides of the thylakoid membrane (Fristedt et al., 2009; Kapri-Pardes et al., 2007; Schuhmann and Adamska, 2012). The newly synthesized D1 subunit is inserted cotranslationally into the complex in the stroma lamellae on the thylakoid membrane. After the repair cycle, PSII moves back to the grana region. This repair cycle is driven by the phosphorylation and dephosphorylation of the PSII core complex (Jarvi et al., 2015).

Further elucidation of PSII water-splitting mechanism, assembly process and regulatory pathways will be important for better understanding photosynthesis and designing artificial systems capable of using sunlight energy.

1.2.3 PSI

PSI catalyzes the last step of electron transport, the oxidation of plastocyanin in the thylakoid lumen and the reduction of FD in the chloroplast stroma. After reduction of FD, electrons are distributed among five pathways, with the majority of the electrons used for NADPH production when CBB cycle is active. Other electron sinks include the reducing reaction catalyzed by nitrite reductase and sulfite reductase for nitrogen and sulfur assimilation, CEF when ATP production from LEF is insufficient, direct transfer of electrons to O_2 when PSI is overly reduced, and thioredoxin reduction useful for many chloroplast enzymes as well as the regeneration of antioxidative systems (Carmeli et al., 2007; Schottler et al., 2011).

Among the four photosynthetic complexes, PSI is the one that undergoes the most drastic evolutionary remodeling (Amunts and Nelson, 2009). In cyanobacteria, PSI functions as a trimer, with associated phycobilisome residing on top of thylakoid membrane as an additional antenna system. In eukaryotes however, PSI functions as a monomer, with associated LHC located within the thylakoid membrane. Consisting of 12 protein subunits per monomer and binding to a total of 96 chlorophylls (Jordan et al., 2001), PSI in cyanobacteria is significantly smaller than its counterpart in higher plants. The PSI monomer in higher plants contains 15 subunits that constitute the catalytically active PSI core complex, and at least four bound LHCs forming the PSI antenna system (Jordan et al., 2001).

Recently, the high-resolution structure of the PSI-LHCI supercomplex was resolved at 3.3Å and the exact positions of 173 chlorophylls and 15 carotenoids were assigned (Amunts et al., 2010). The PSI reaction center (RC) is composed of two large and essential subunits, PsaA and PsaB, which bind 80 chlorophylls and the vast majority of the redox-active cofactors. The PsaA-PsaB heterodimer catalyses the light-induced charge separation at the chlorophyll *a* special pair P700, followed by electron transfer via chlorophyll A_0, phylloquinone A_1, and the [4Fe-4S] cluster F_X to the final two [4Fe-4S] clusters, F_A and F_B. F_A and F_B are bound to the PsaC subunit, which is positioned on the stromal side of PSI. PsaC associates with PsaD and PsaE to form a so-called “stromal ridge” of PSI, which can later form a large ternary complex with FD and FNR on the top of PSI (Figure 1.3) (Schottler et al., 2011). Due to this large ternary complex protruding into the stroma, PSI is predominately residing in the stroma lamellae and rarely found in the grana stacks (Albertsson, 2001). The oxidized P700 chlorophyll *a* dimer is reduced by

plastocyanin, which interacts with PsaB, PsaF and PsaN for efficient plastocyanin oxidation (Haldrup et al., 1999).

The antenna complex of PSI in higher plants consists of four LHC proteins (LHCA1-4) that bind to the reaction center core complex in the form of two adjacent heterodimers, LHCA 1/4 and LHCA 2/3. These two heterodimers are arranged in a half-moon-shaped belt around one side of PSI, and have interactions with multiple PSI subunits, and "gap" chlorophylls on the surface of the PSI core complex (Amunts et al., 2010). On the opposite side of the LHCA belt, a nose-shaped structure is formed by PsaH, PsaI, PsaL and possibly PasO subunits (Nelson and Yocum, 2006). This part of PSI, which functions in PSI trimer formation in cyanobacteria, has been completely remodeled during the evolution in higher plants. In higher plants, the nose-shaped structure forms a docking site for at least one LHCII trimer during an adjusting process called "state transition", which is essential when plants are exposed to fluctuating light conditions (Bellafiore et al., 2005). Besides, two recently identified antenna proteins in Arabidopsis, LHCA5 and LHCA6, were suggested to involve in supercomplex formation of PSI-LHCI with the NDH complex, although their exact docking position on PSI is not determined because neither was present in the high-resolution crystal in PSI structural analysis due to their substoichiometric amounts (Ganeteg et al., 2004; Klimmek et al., 2006). The specific function of Lhca5 and Lhca6 remains to be investigated.

Although the knowledge about structure and components of PSI has become more comprehensive and detailed, the biogenesis process of PSI is not well understood (Ozawa et al., 2010). There are two obstacles for discovering the sequence of subunit integration into nascent PSI. First, the PsaA-PsaB heterodimer already constitutes nearly half of the

PSI molecular mass (165 out of 390 kDa), which makes it extremely difficult to resolve the small units attached to the heterodimer. Second, PSI assembly happens very rapidly. Although direct experimental data is lacking for the rapid assembly pathway from PsaA-PsaB heterodimer to intermediate complex, speculations were made (Ozawa et al., 2010). In the speculated process, PsaC is the first subunit to assemble onto PsaA-PsaB heterodimer after its binding to two [4Fe-4S] clusters inside the PsaA-PsaB heterodimer. Subsequently, both PsaD and PsaE bind to PsaC to complete the final formation of the stromal ridge (Ishikita et al., 2006; Nelson and Yocum, 2006). All the aforementioned PSI subunits are critical for the PSI supercomplex formation, because they provide scaffold for further binding of other subunits and LHCs and mutations in any of these subunits result in severe or even complete loss of the PSI supercomplex (Schottler et al., 2011).

Auxiliary proteins also play a critical role in PSI biogenesis. These auxiliary proteins, also called assembly factors, refer to the proteins that are not an integral part of PSI but can affect PSI biogenesis at many levels. Generally, they are divided into two functional categories: (i) proteins involved in cofactor synthesis and/or forming into nascent complex, and (ii) chaperones that function as scaffold for assembly proteins or mediate protein-protein interaction within the complex (Schottler et al., 2011). Alb3 mediates the first step of PSI assembly, i.e. membrane insertion of PsaA and PsaB, by directly interacting with them. Alb3 is a member of the conserved OxaI/YidC family of membrane protein insertases; in its absence, accumulation of PSI supercomplex is strongly reduced (Pasch et al., 2005; van der Laan et al., 2005). Ycf3 is a plastid-encoded soluble protein that interacts with PsaA and PsaD and plays a role in stromal ridge

formation; its absence leads to a complete loss of PSI. Evidence also exists that Ycf3 may mediate the rate-limiting step of PSI assembly (Albus et al., 2010; Naver et al., 2001). Other important chaperones include Y3IP1, Ycf4 and Pyg7, whose loss-of function mutants show severe or complete loss of the PSI supercomplex (Albus et al., 2010; Ozawa et al., 2009; Stockel et al., 2006). Other proteins important for PSI assembly include those involved in co-factor biogenesis and attachment, such as Apo1 and Hcf101, both of which are involved in the biogenesis of the PSI-specific cofactor phylloquinone (Gross et al., 2006; Lohmann et al., 2006). The identification of these assembly factors shed light on the intricate process of the regulatory pathway of PSI biogenesis, which seems considerably more complex than previously thought and thus needs further investigations.

1.2.4 Cytochrome b_6f

Cytochrome b_6f is a PQH_2- PC reductase found in the thylakoid membrane in chloroplasts of higher plants and green algae and in cyanobacteria. It catalyzes the oxidation of PQ and the electron transfer between PSII and PSI complexes, whereby the proton gradient across thylakoid membrane is generated by coupled proton transfer (Figure1.3) (Hasan et al., 2013).

Cytb_6f is a homo-dimer, with each monomer composed of 8 subunits that include four large and four small subunits. The large subunits contain the 25 kDa cytochrome b_6 (PetB) that has a high potential heme group, the 32 kDa cytochrome f (PetA) with a c-type cytochrome, the 19 kDa Rieske iron-sulfer protein (PetC) that contains a [2Fe-2S]

cluster, and the 17 kDa subunit IV (PetD). The small subunits range from 3 to 4 kDa in size and include PetG, PetL, PetM and PetN, which together make the total molecular weight to 217 kDa (Hasan et al., 2013; Stroebel et al., 2003). Cytb_6f contains seven prosthetic groups essential for electron transfer within the complex. The inter-mononer space between the Cytb_6f dimer is occupied by lipids, which direct the heme-to-heme electron transfer through modulation of the intra-protein environment (Baniulis et al., 2013; Cramer et al., 2005).

The electron transfer reaction occurs through the Q cycle, where the electron from the PQH_2 is transferred through high- and low- potential pathways to PC, PSI and finally to generate NADPH. In addition, attachment of FNR to Cytb_6f was recently found to be important for CEF. When $NADP^+$ is not sufficient to accept electrons from reduced FD, they are returned to PQ and then Cytb_6f to reduce PC. Meanwhile the electron transfer creates proton transfer from stroma to lumen (Baniulis et al., 2009; Laisk et al., 2005; Munekage et al., 2004). ATP is produced without generation of NADPH in CEF, therefore it is speculated that CEF helps maintain the proper ratio of ATP to NADPH needed for carbon fixation, especially when the ATP/NADPH is low under environmental stresses (Munekage et al., 2004).

1.2.5 ATP synthase

ATP synthase is ubiquitous on energy producing membranes such as chloroplast thylakoid membrane, mitochondrial inner membrane, and bacterial plasma membrane, and participate in photosynthesis and respiration. The electron transport in photosynthesis

and respiration is coupled with generation of proton gradient across the membrane, which activates ATP synthase to produce ATP from ADP and phosphate. The ATP synthase holoenzyme is composed of the soluble membrane-peripheral sector F_1 and the hydrophobic membrane-spanning sector F_O (Groth and Pohl, 2001; Stock et al., 1999; von Ballmoos et al., 2009).

F_1 consists of five subunits in a stoichiometry of $\alpha_3\beta_3\gamma_1\delta_1\varepsilon_1$. The α- and β-subunits are arranged in alternation into a hexagon $(\alpha\beta)_3$, within which the γ subunit is located in the center axis as a rotary shaft. Three key catalytic sites for ATP synthesis are located on the β subunits at the interface with the α- subunit, and the center shaft γ unit is functionally important to confer catalytic cooperation within the three catalytic sites (Abrahams et al., 1994; Bowler et al., 2007). Relative rotation between the $(\alpha\beta)_3$ hexagon and the γ subunit was first postulated by P.D. Boyer based on the analysis of the catalytic sites (Gresser et al., 1982). In 1997, H. Noji et al. verified this speculation using video-recording of unidirectional spin of an actin filament attached to the γ subunit of the $\alpha_3\beta_3\gamma_1$ core subcomplex (Noji et al., 1997). In this experiment, the F_1 subunit from the thermophilic *Bacillus* PS3 was used, and later the rotation of the γ subunit in *E. coli* F_1 (Omote et al., 1999) and chloroplast F_1 (CF_1) (Hisaboria et al., 1999) was demonstrated using the same method, thereby the rotation model was confirmed in all major F_1-ATPases.

The membrane-spanning F_O is composed of $a_1b_2c_{8\text{-}14}$. Different numbers of the c subunit were reported for complexes from different organelles, such as chloroplasts and mitochondria. A high resolution structure of the entire F_O is still lacking (Junge and Nelson, 2015). A common feature of the F_O portion of ATP synthase from different

organisms is the homo-oligomeric ring of the c-subunit, which is the only portion of F_O with a high resolution structure (Meier et al., 2005; Stock et al., 1999; Vollmar et al., 2009). The c-ring faces the a-subunit, which is a four-helix bundle plus one transmembrane helix. The a-subunit associates with two transmembrane helixes of the b-subunits that connect F_O to the top of the $(\alpha\beta)_3$ hexagon of F_1. All three subunits are required for promoting proton conduction by F_O. The c-subunit carries an ionizable residue in the middle of the membrane, around which the pocket for binding of proton is located. The copy number of c-subunits is believed to determine the proton-to-ATP ratio. Since one proton binds to one c-subunit, the more c-subunits there are, the more protons are needed to produce one ATP. There are 8 c-subunits in bovine mitochondria, 10 in yeast mitochondria, and 14 in chloroplasts, which is consistent with the level of ATP demand in each organism. Organisms with higher proton motive force (PMF) benefit from running at high-speed gear (low c-subunit number), while those exposed to variable PMF (chloroplast) benefit from high torque and low-speed gear (high c-subunit number) (Meier et al., 2005; Stock et al., 1999; Vollmar et al., 2009).

In higher plants, photosynthesis takes place in the thylakoid membrane, whereas respiration occurs in the crista membrane of mitochondria. To prevent futile consumption of chloroplast ATP by mitochondria, the chloroplast enzyme is downregulated in the dark (Petersen et al., 2012; Saroussi et al., 2012). Therefore, the low PMF under dark and high PMF under light constitutes a key regulation of ATP synthase activity. Chloroplast F_OF_1 is regulated by the thioredoxin-dependent thiol-activation. Two cysteine residues in the bottom of the chloroplast γ subunit are the targets of modulation (Kim et al., 2011). In

addition, tightly bound ADP and the ε subunit are involved in ATP synthase activity regulation (Saroussi et al., 2012).

Lastly, the photosynthetic thylakoid membrane contains PSII, PSI, Cytb_6f, and ATP synthase with a relative ratio 2:2:1:1, thus it is highly crowded (Menke, 1962; Stolz and Walz, 1988). Each thylakoid is a highly-folded spherical bleb, in which hundreds of electron transport chain complexes and ATP synthase molecules are electrically coupled with each other. Biochemical analyses and electron microscopy established the heterogeneous lateral distribution of the membrane proteins (Figure1.3) (Mustardy et al., 2008). PSI and ATP synthase are located mainly in the stroma lamellae, and also in the top and bottom surface of grana. PSII is almost exclusively found within the grana area, and Cytb_6f is found at the connection between grana and lamellae (Albertsson, 2001; Daum et al., 2010). The separation of PSII and PSI are thought to be beneficial for efficient light distribution and to facilitate the PSII repair cycle (Nelson and Junge, 2015).

1.2.6 Adaptive mechanisms to changing light conditions

Due to diurnal and seasonal changes, photosynthetic organisms are subjected to a constantly changing environment. As one of the most important input for photosynthesis, light is shifting considerably in intensity and spectral quality. To adjust to changing light conditions, plants have evolved numerous biochemical and developmental processes, such as photoreceptor-dependent shade avoidance, movement of leaves and chloroplasts, and changing antenna size through genes expression regulation and proteolysis (Rochaix, 2014). Other environmental parameters, such as CO_2 concentration, water availability,

nutrient limitation and temperature variation can also significantly affect the need for ATP and NADPH (Kaiser et al., 2015). Regulating the operation of the photosynthetic machinery accordingly is necessary to maintain optimal photosynthetic efficiency and protect organisms from photodamage (Rochaix, 2014).

One of the key components in the adaptive processes is the light harvesting complex, which is involved in both efficient light capture for driving the primary photochemical reactions, and sensing and dissipating excessive light. To achieve this goal, photosynthetic organisms have developed two main strategies (Horton and Ruban, 2005). The first strategy is to regulate the amount of absorbed light energy that is used for the photochemical reaction by dissipating excessive absorbed energy as heat when light exceeds the capacity of the photochemical machinery. This process is also called energy-dependent nonphotochemical quenching (qE-NPQ) (Niyogi and Truong, 2013). The second strategy balances the excitation energy absorbed by LHCII and LHCI antenna systems and adjusts the electron transfer chain upon fluctuating light to optimize photosynthetic electron flow, by re-distributing of the mobile LHCII antenna between PSII and PSI. This process is called state transition (Horton, 2012; Wollman, 2001). Both strategies will be discussed in detail.

1.2.7 NPQ

Upon light absorption by the antenna system, a chlorophyll (Chl) *a* molecule is excited to singlet-state (^{1}Chl*). The energy released during the return of the singlet-state Chl *a* to ground state could be used for photochemistry, emitted as chlorophyll

fluorescence, dissipated as heat, or used for generating triplet state (^{3}Chl*), which is very dangerous to the organism because it could be used to generate highly damaging singlet oxygen ($^1O_2$*) (Muller et al., 2001).

The heat dissipation process is associated with a decrease of chlorophyll fluorescence, it is therefore referred to as nonphotochemical quenching (NPQ). Based on the relaxation kinetics in the dark, there are at least three components of NPQ: (i) energy-dependent quenching (qE), which depends on the proton gradient across the thylakoid membrane and relaxes within seconds; (ii) qT, which is caused by state transitions and relaxes within minutes; and (iii) qI, which is induced by photoinhibition of PSII and relaxes relatively slow (Goss and Lepetit, 2015).

As mentioned above, qE is triggered by light-induced proton gradient across the thylakoid membrane. Proton deposition and decrease of pH in the thylakoid lumen lead to the activation of the violaxanthin de-epoxidase named NPQ1, which coverts violaxanthin to zeaxanthin (Havaux et al., 2000). This reaction is a part of the xanthophyll cycle, and it is reversible by zeaxanthin epoxidase named NPQ2 (Niyogi et al., 1998). Zeaxanthin subsequently binds to LHCII and induces LHCII's conformational changes, thereby switching LHCII from the light-harvesting state to photoprotective state, in which light excitation energy is harmlessly dissipated as heat (Johnson et al., 2008). Besides the enzymes that are involved in zeaxanthin conversion in the xanthophyll cycle, several LHCII components have been found necessary for generation of NPQ in *Arabidopsis* (Ruban et al., 2007). The absence of CP29 or CP24 decreases qE by 30% and 50%, respectively (Andersson et al., 2001; Kovacs et al., 2006). Loss of the major LHCB1 and LHCB2 proteins decreases qE by 35% (Andersson et al., 2003). These results confirmed

that LHCII is the major site for qE, and also indicated that additional components and sites exist for qE generation. Besides the *npq1* and *npq2* mutants, which were identified in a genetic screen of mutants with altered chlorophyll fluorescence properties, another component named PsbS (identified in mutant *npq4*) was found essential for qE generation (Li et al., 2000). PsbS belongs to a superfamily of LHC proteins and contains four transmembrane domains. It acts as a sensor of the lumenal pH and stimulates qE rapidly. The protonation of PsbS is presumably required for the activation PsbS-dependent activation of qE, and it is thought to promote rearrangement of the PSII supercomplex for efficient heat dissipation (Holt et al., 2004; Li et al., 2000; Niyogi et al., 2005). Although PsbS is necessary for qE *in vivo*, isolated thylakoids lacking PsbS still exhibit qE in the presence of an unusually high ΔpH, suggesting that direction protonation of the LHC antenna proteins by extremely high ΔpH can bypass the need for PsbS (Sylak-Glassman et al., 2014).

1.2.8 State transition

The light harvesting systems of PSII and PSI have different chlorophyll compositions. LHCII is enriched in chlorophyll *b*, whereas LHCI is rich in chlorophyll *a* that can absorb far-red light (Croce et al., 2002; Lama et al., 1984). Changes in light quality and quantity can thus alter the distribution of absorbed light excitation energy between PSII and PSI (Yokono et al., 2011). Under fluctuating light conditions, the "state transition" is activated, during which the LHC system is able to sense the redox poise of the PQ pool through a signal network consisting of Cytb_6f, protein kinase and

phosphatase. Specifically, upon over-excitation of PSII relative to PSI, the PQ pool is highly reduced (Minagawa, 2011). The redox state of PQ is sensed by a protein kinase STN7, which is activated by binding of PQH_2 to Cytb_6f and subsequently phosphorylates a portion of LHCII. The phosphorylated LHCII disassociates from PSII and binds to PSI, thereby readjusting the excitation energy between PSII and PSI and restoring the redox poise of the PQ pool (Mullineaux and Emlyn-Jones, 2005). This process is reversible, where oxidation of the PQ pool by PSI absorbed light results in deactivation of STN7 (Bellafiore et al., 2005) and the phosphatase PPH1 subsequently dephosphorylates LHCII to return LHCII to PSII (Shapiguzov et al., 2010). STN8 is a homologue of STN7 that carries partially overlapping function (Vainonen et al., 2005) and its counterpart phosphatase called PBCP can dephosphorylate LHCII (Samol et al., 2012). Thus, the two kinases STN7 and STN8 and two phosphatases PPH1 and PBCP constitute the central system for state transition in higher plant.

Recent studies indicate that the mobile LHCII without binding to PSII or PSI acts as a highly efficient antenna for PSI under various light conditions and remains associated with PSI after long-term acclimation. The mobile LHCII returns to PSII only under specific conditions, such as after a sudden increase in light intensity or when PSI is overexcited by far-red light (Wientjes et al., 2013; Wientjesa et al., 2012).

1.2.9 Cyclic electron flow

The ATP and NADPH generated in light reactions are mainly consumed in CO_2 assimilation, which theoretically requires an ATP-to-NADPH ratio of 1.5.

Photorespiration, which inevitably occurs in ambient air, raises this ratio to 1.66 (Osmond, 1981). However, the ATP-to-NADPH ratio provided by LEF is about 1.33, which is too low to sustain the CBB cycle and other metabolism (Kramer and Evans, 2011). CEF is considered a major compensation pathway to make up the deficiency of ATP supply in normal and many stress conditions. In this pathway (Figure1.3), electrons are recycled from NAD(P)H or FD to PQ, and the coupled proton transport to the lumen can generate ΔpH and promote ATP synthesis. A main difference between CEF and LEF, is that CEF is exclusively involved in ATP synthesis whereas LEF generates both ATP and NADPH. In addition to ATP production, ΔpH, which is partially contributed by CEF, acts as a key factor in inducing rapid response to fluctuating light intensity and high light (Hasan et al., 2013; Heber and Walker, 1992; Iwai et al., 2010; Zhang et al., 2001).

The mechanism of CEF remains a controversial subject. Two major pathways have been proposed and studied (Figure1.3). In the first pathway, electrons are transferred to PQ by the plastid encoded PQ reductases NDHs, which are homologues to subunits of the mitochondrial NADH dehydrogenase complex (complex I) (Matsubayashi et al., 1987). The cyanobacterial *ndhB* mutant, which is defective in a subunit of the NDH complex, has impaired CEF activity (Ogawa, 1991). Knockout lines of the tobacco *NDH* genes displayed clear alternation of electron transport (Shikanai et al., 1998). Although no obvious growth phenotype was observed in *NDH* knockout tobacco lines under normal conditions,, these mutants exhibited compromised tolerance to various environmental stresses, such as high light (Miyake et al., 2004), drought (Hundhausen et al., 2005) and high and low temperatures (Wang et al., 2006). These results suggested

that the NDH complex is involved in alleviating oxidative stress, which is probably generated from PSI associated excessive energy.

The second key pathway is sensitive to antimycin and involves two thylakoid proteins, PGR5 (proton gradient regulation 5) and PGRL1 (PGR-like 1). PGR5 is a small soluble protein without any known motif like the typical electron-binding prosthetic motif, and thus is believed to be indirectly involved in CEF as a regulator (Munekage et al., 2004; Munekage et al., 2002). PGRL1 is a thylakoid transmembrane protein that physically interacts with PGR5 and transiently interacts with PSI, thus serving as an anchor protein to bring PGR5 to PSI (DalCorso et al., 2008). Recently, PGRL1 has been biochemically characterized as the long-sought FD-PQ reductase (FQR) that accepts electron from FD in a PGR5-dependent manner, and reduces PQ in an antimycin-sensitive fashion (Hertle et al., 2013). Genetic studies showed that *pgr5* and *pgrl1* mutants exhibited highly similar CEF perturbation, NPQ reduction, and lower $P700^{+}$-to-P700 ratio under high light, which further confirmed their participation in CEF (Munekage et al., 2004; Munekage et al., 2002). Meanwhile, NDH activity is not inhibited in *pgr5* mutant background, suggesting that the PGR5-PGRL1 pathway is independent of the NDH-dependent pathway (DalCorso et al., 2008; Kukuczka et al., 2014).

The *crr2 pgr5* double mutant, which is defective in both NDH- and PGR5-dependent CEF, lost almost all of the PSI CEF activity, indicating that these two key pathways contribute to major production of CEF. Meanwhile, the double mutant exhibited strongly delayed growth, suggesting that CEF around PSI is essential for

efficient photosynthesis even under normal growth conditions (Hashimoto et al., 2003; Munekage et al., 2004).

1.3. Aims of dissertation research

My dissertation is aimed at defining the role of peroxisomes in modulating environmental stress response and photosynthesis at a systems level. Progress in proteomics studies of peroxisomes and *in silico* analysis, followed by *in vivo* targeting verification largely increased the number of known peroxisomal proteins in Arabidopsis. Increasing evidence indicated the roles of peroxisomal proteins in environmental stress response, and the metabolic connections between peroxisomes and chloroplasts, prompting us to check into these aspects systematically and in more depth. My first aim was to use transcriptomic analysis combined with mutant screens to identify peroxisomal proteins involved in stress response. In Chapter 2, I examined the transcriptional regulation of all the genes encoding peroxisomal proteins in Arabidopsis across different developmental stages and under various environmental stress conditions. Developmental stage- and stress- specific gene expression patterns were identified. Two peroxisomal proteins, LON2 protease and the photorespiratory enzyme hydroxypyruvate reductase 1 (HPR1), were found necessary in conferring robust drought resistance. My second aim was to investigate the role of peroxisomal metabolism in modulating photosynthesis. In Chapter 3, I used the Dynamic Environment Phenotype Imager (DEPI) to screen 147 mutants of 104 Arabidopsis genes encoding peroxisomal proteins, hoping to identify mutants with photosynthetic defects under dynamic light conditions. Our systematic

screen identified a number of peroxisomal proteins required for robust photosynthesis efficiency under dynamically changing light. These include peroxisomal biogenesis and division proteins, photorespiratory proteins and an NAD^+ transporter protein PXN, which was later found to be an additional player in photorespiration. Further characterization of photorespiratory mutants suggested an integrated model that depicts the molecular events that occur as a result of the block of photorespiration: 1) increased level of phosphoglycolate leads to the inhibition of the activity of an enzyme involved in CBB cycle; 2) decreased amount of glycerate slows down the CBB cycle, and leads to accumulation of unused stromal ATP. Accumulation of stromal ATP inhibits ATP synthase conductivity and subsequent higher proton motive force (*pmf*) and qE; and 3) enhanced oxidative stress causes compromised photosystem integrity, reduced photosystem subunit abundance and enhanced photoinhibition.

APPENDIX

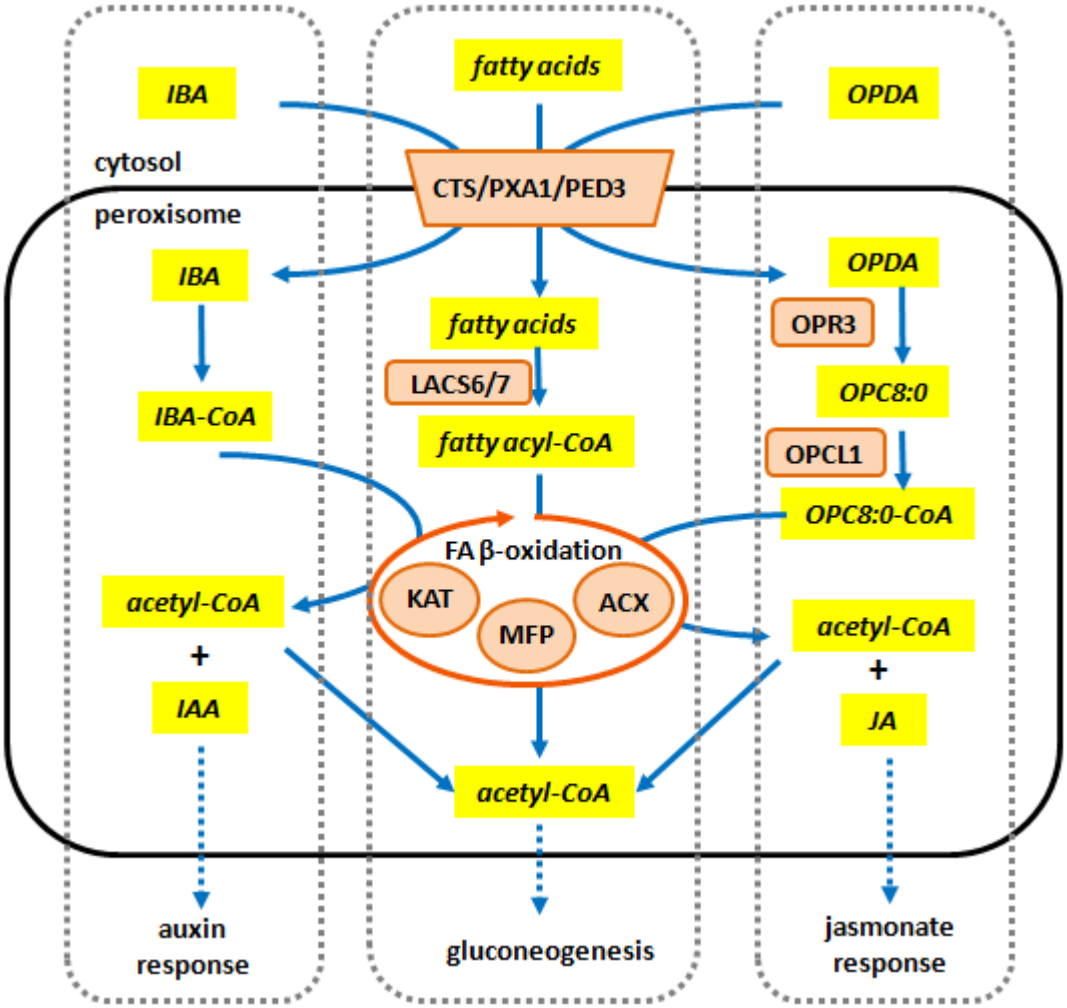

Figure 1.1. Some peroxisomal metabolic pathways share a core set of β-oxidation enzymes. (Modified from Hu et al., 2012)

FA β-oxidation (center box) involves peroxisomal import of FAs by the ABC transporter CTS/PXA1/PED3, activation of FAs by acyl-activating enzymes LACS6 and LACS7, β-oxidation catalyzed by a core set of enzymes including acyl-CoA oxidase (ACX), multiple function protein (MFP) and 3-ketoacyl-CoA thiolase (KAT). After each cycle of β-oxidation, the substrate is shortened by two carbons, which are used to generate acetyl-CoA for further energy-providing metabolism in gluconeogenesis. Metabolism of IBA to

Figure 1.1. (cont'd)

IAA (left box) and biosynthesis of JA (right box) utilize the core enzymes in FA β-oxidation. After import and activation, IBA-CoA undergoes one round of FA β-oxidation to produce IAA, and the JA intermediate, OPC8:0-CoA, undergoes three rounds of β-oxidation to generate JA. IAA and JA are then exported to the cytosol. Metabolites involved are shown in yellow boxes, and the key enzymes are shown in orange boxes. Blue arrows indicate the metabolic flow, and dashed arrows indicate further biological function of the metabolites.

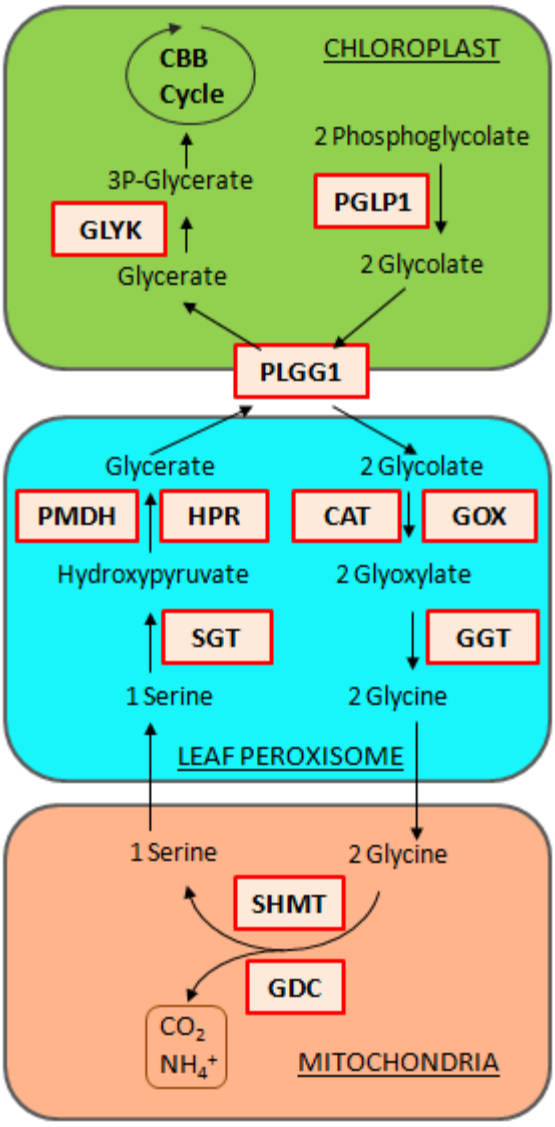

Figure 1.2. Peroxisomes play a central role in photorespiration.

Photorespiration is accomplished by the cooperation of peroxisomes, chloroplasts and mitochondria. It starts with phosphoglycolate, which is the product of Rubisco oxygenase activity on ribulose-1,5-bisphosphate (RuBP), and ends with the production of phosphoglycerate as the substrate for the Calvin-Benson-Bassham (CBB) cycle. The enzymes directly involved in metabolic conversion and metabolite transport (in

Figure 1.2. (cont'd)

red boxes) include phosphoglycolate phosphatase PGLP1, glycolate glycerate transporter PLGG1, glycolate oxidase (GOX), glutamate: glyoxylate aminotransferase (GGT), serine hydroxymethyltransferase (SHMT), glycine decarboxylase (GDC), serine:

glyoxylate aminotransferase (SGT), hydroxypyruvate reductase (HPR), peroxisomal malate dehydrogenase (PMDH) and glycerate kinase GLYK.

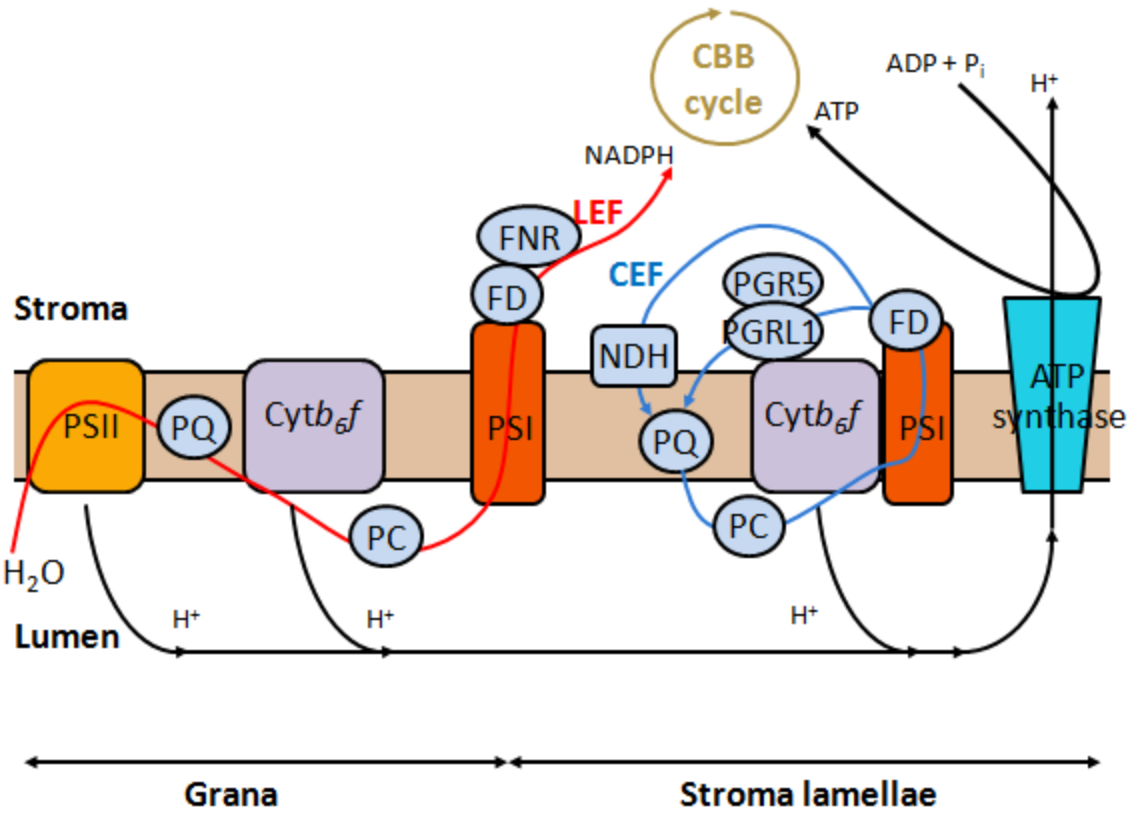

Figure 1.3. Overview of photosynthetic complexes and processes on the thylakoid membrane. (Modified from Rochaix, 2014)

Linear electron flow (LEF) and cyclic electron flow (CEF) are shown in red and blue curved lines, respectively, with arrows indicating the direction of the flow. The LEF involves major photosynthetic complexes photosystem II (PSII), cytochrome b_6f complex (Cytb_6f), photosystem I (PSI) and the ATP synthase, as well as small mobile electron carriers such as plastoquinone (PQ), plastocyanin (PC), ferredoxin (FD) and FD-NADP$^+$ oxidoreductase (FNR). The electron is used to generate NADPH. CEF, on the other hand, is only driven by PSI. Besides complexes shared with LEF, CEF also involves specific components, including NADPH dehydrogenase complex (NDH), an unknown soluble protein PGR5 and a FD-PQ oxidoreductase PGRL1. Both LEF and CEF contribute to

Figure 1.3. (cont'd)

proton transfer to the lumen, which creates proton gradient across the thylakoid membrane. ATP synthase is activated by the proton gradient and generate ATP from ADP and phosphate. NAPDH and ATP are used by the CBB cycle. Lateral heterogeneity of the thylakoid membrane is shaped by preferential distribution of each complex. PSI and ATP synthase are located mainly in the stromal lamellae, with a large protrusion into the stroma. PSII is almost exclusively located within the grana area, and Cytb_6f is found at the junction between grana and lamellae.

REFERENCES

REFERENCES

Abel, S., and Theologis, A. (2010). Odyssey of auxin. Cold Spring Harb Perspect Biol 2, a004572.

Abrahams, J.P., Leslie, A.G., Lutter, R., and Walker, J.E. (1994). Structure at 2.8 A resolution of F1-ATPase from bovine heart mitochondria. Nature 370, 621-628.

Adham, A.R., Zolman, B.K., Millius, A., and Bartel, B. (2005). Mutations in Arabidopsis acyl-CoA oxidase genes reveal distinct and overlapping roles in beta-oxidation. Plant J 41, 859-874.

Afitlhile, M.M., Fukushige, H., Nishimura, M., and Hildebrand, D.F. (2005). A defect in glyoxysomal fatty acid beta-oxidation reduces jasmonic acid accumulation in Arabidopsis. Plant Physiol Biochem 43, 603-609.

Albertsson, P. (2001). A quantitative model of the domain structure of the photosynthetic membrane. Trends Plant Sci 6, 349-358.

Albus, C.A., Ruf, S., Schottler, M.A., Lein, W., Kehr, J., and Bock, R. (2010). Y3IP1, a nucleus-encoded thylakoid protein, cooperates with the plastid-encoded Ycf3 protein in photosystem I assembly of tobacco and Arabidopsis. Plant Cell 22, 2838-2855.

Amunts, A., and Nelson, N. (2009). Plant photosystem I design in the light of evolution. Structure 17, 637-650.

Amunts, A., Toporik, H., Borovikova, A., and Nelson, N. (2010). Structure determination and improved model of plant photosystem I. J Biol Chem 285, 3478-3486.

Andersson, J., Walters, R.G., Horton, P., and Jansson, S. (2001). Antisense inhibition of the photosynthetic antenna proteins CP29 and CP26: implications for the mechanism of protective energy dissipation. Plant Cell 13, 1193-1204.

Andersson, J., Wentworth, M., Walters, R.G., Howard, C.A., Ruban, A.V., Horton, P., and Jansson, S. (2003). Absence of the Lhcb1 and Lhcb2 proteins of the light-harvesting complex of photosystem II - effects on photosynthesis, grana stacking and fitness. Plant J 35, 350-361.

Aro, E.M., Suorsa, M., Rokka, A., Allahverdiyeva, Y., Paakkarinen, V., Saleem, A., Battchikova, N., and Rintamaki, E. (2005). Dynamics of photosystem II: a proteomic approach to thylakoid protein complexes. J Exp Bot 56, 347-356.

Baniulis, D., Hasan, S.S., Stofleth, J.T., and Cramer, W.A. (2013). Mechanism of enhanced superoxide production in the cytochrome b(6)f complex of oxygenic photosynthesis. Biochemistry 52, 8975-8983.

Baniulis, D., Yamashita, E., Whitelegge, J.P., Zatsman, A.I., Hendrich, M.P., Hasan, S.S., Ryan, C.M., and Cramer, W.A. (2009). Structure-Function, Stability, and Chemical Modification of the Cyanobacterial Cytochrome b6f Complex from Nostoc sp. PCC 7120. J Biol Chem 284, 9861-9869.

Bauwe, H., Hagemann, M., and Fernie, A.R. (2010). Photorespiration: players, partners and origin. Trends Plant Sci 15, 330-336.

Bednarek, P., Pislewska-Bednarek, M., Svatos, A., Schneider, B., Doubsky, J., Mansurova, M., Humphry, M., Consonni, C., Panstruga, R., Sanchez-Vallet, A., et al. (2009). A glucosinolate metabolism pathway in living plant cells mediates broad-spectrum antifungal defense. Science 323, 101-106.

Bellafiore, S., Barneche, F., Peltier, G., and Rochaix, J.D. (2005). State transitions and light adaptation require chloroplast thylakoid protein kinase STN7. Nature 433, 892-895.

Boehm, M., Romero, E., Reisinger, V., Yu, J., Komenda, J., Eichacker, L.A., Dekker, J.P., and Nixon, P.J. (2011). Investigating the early stages of photosystem II assembly in Synechocystis sp. PCC 6803: isolation of CP47 and CP43 complexes. J Biol Chem 286, 14812-14819.

Boldt, R., Edner, C., Kolukisaoglu, U., Hagemann, M., Weckwerth, W., Wienkoop, S., Morgenthal, K., and Bauwe, H. (2005). D-GLYCERATE 3-KINASE, the last unknown enzyme in the photorespiratory cycle in Arabidopsis, belongs to a novel kinase family. Plant Cell 17, 2413-2420.

Bowler, M.W., Montgomery, M.G., Leslie, A.G., and Walker, J.E. (2007). Ground state structure of F1-ATPase from bovine heart mitochondria at 1.9 A resolution. J Biol Chem 282, 14238-14242.

Bricker, T.M., Roose, J.L., Fagerlund, R.D., Frankel, L.K., and Eaton-Rye, J.J. (2012). The extrinsic proteins of Photosystem II. Biochim Biophys Acta 1817, 121-142.

Carmeli, I., Frolov, L., Carmeli, C., and Richter, S. (2007). Photovoltaic activity of photosystem I-based self-assembled monolayer. J Am Chem Soc 129, 12352-12353.

Chamnongpol, S., Willekens, H., Langebartels, C., Montagu, M.V., Inzé, D., and Camp, W.V. (1996). Transgenic tobacco with a reduced catalase activity develops necrotic lesions and induces pathogenesis-related expression under high light. the Plant Journal.

Coca, M., and San Segundo, B. (2010). AtCPK1 calcium-dependent protein kinase mediates pathogen resistance in Arabidopsis. Plant J.

Cornah, J.E., Germain, V., Ward, J.L., Beale, M.H., and Smith, S.M. (2004). Lipid utilization, gluconeogenesis, and seedling growth in Arabidopsis mutants lacking the glyoxylate cycle enzyme malate synthase. J Biol Chem 279, 42916-42923.

Cousins, A.B., Walker, B.J., Pracharoenwattana, I., Smith, S.M., and Badger, M.R. (2011). Peroxisomal hydroxypyruvate reductase is not essential for photorespiration in Arabidopsis but its absence causes an increase in the stoichiometry of photorespiratory CO2 release. Photosynth Res 108, 91-100.

Cramer, W.A., Yan, J., Zhang, H., Kurisu, G., and Smith, J.L. (2005). Structure of the cytochrome b6f complex: new prosthetic groups, Q-space, and the 'hors d'oeuvres hypothesis' for assembly of the complex. Photosynth Res 85, 133-143.

Croce, R., Canino, G., Ros, F., and Bassi, R. (2002). Chromophore organization in the higher-plant photosystem II antenna protein CP26. Biochemistry 41, 7334-7343.

Cruz Castillo, M., Martinez, C., Buchala, A., Metraux, J.P., and Leon, J. (2004). Gene-specific involvement of beta-oxidation in wound-activated responses in Arabidopsis. Plant Physiol 135, 85-94.

DalCorso, G., Pesaresi, P., Masiero, S., Aseeva, E., Schunemann, D., Finazzi, G., Joliot, P., Barbato, R., and Leister, D. (2008). A complex containing PGRL1 and PGR5 is involved in the switch between linear and cyclic electron flow in Arabidopsis. Cell 132, 273-285.

Dasgupta, J., Ananyev, G.M., and Dismukes, G.C. (2008). Photoassembly of the Water-Oxidizing Complex in Photosystem II. Coord Chem Rev 252, 347-360.

Daum, B., Nicastro, D., Austin, J., 2nd, McIntosh, J.R., and Kuhlbrandt, W. (2010). Arrangement of photosystem II and ATP synthase in chloroplast membranes of spinach and pea. Plant Cell 22, 1299-1312.

De Duve, C., and Baudhuin, P. (1966). Peroxisomes (microbodies and related particles). Physiol Rev 46, 323-357.

Delker, C., Zolman, B.K., Miersch, O., and Wasternack, C. (2007). Jasmonate biosynthesis in Arabidopsis thaliana requires peroxisomal beta-oxidation enzymes--additional proof by properties of pex6 and aim1. Phytochemistry 68, 1642-1650.

Dixit, E., Boulant, S., Zhang, Y., Lee, A.S., Odendall, C., Shum, B., Hacohen, N., Chen, Z.J., Whelan, S.P., Fransen, M., et al. (2010). Peroxisomes are signaling platforms for antiviral innate immunity. Cell 141, 668-681.

Eastmond, P.J. (2006). SUGAR-DEPENDENT1 encodes a patatin domain triacylglycerol lipase that initiates storage oil breakdown in germinating Arabidopsis seeds. Plant Cell 18, 665-675.

Eastmond, P.J. (2007). MONODEHYROASCORBATE REDUCTASE4 is required for seed storage oil hydrolysis and postgerminative growth in Arabidopsis. Plant Cell 19, 1376-1387.

Eastmond, P.J., Hooks, M.A., Williams, D., Lange, P., Bechtold, N., Sarrobert, C., Nussaume, L., and Graham, I.A. (2000). Promoter trapping of a novel medium-chain acyl-CoA oxidase, which is induced transcriptionally during Arabidopsis seed germination. J Biol Chem 275, 34375-34381.

Engel, N., van den Daele, K., Kolukisaoglu, U., Morgenthal, K., Weckwerth, W., Parnik, T., Keerberg, O., and Bauwe, H. (2007). Deletion of glycine decarboxylase in Arabidopsis is lethal under nonphotorespiratory conditions. Plant Physiol 144, 1328-1335.

Fagarasanu, A., Mast, F.D., Knoblach, B., and Rachubinski, R.A. (2010). Molecular mechanisms of organelle inheritance: lessons from peroxisomes in yeast. Nat Rev Mol Cell Biol 11, 644-654.

Ferreira, K.N., Iverson, T.M., Maghlaoui, K., Barber, J., and Iwata, S. (2004). Architecture of the photosynthetic oxygen-evolving center. Science 303, 1831-1838.

Fiorani, F., and Schurr, U. (2013). Future scenarios for plant phenotyping. Annu Rev Plant Biol 64, 267-291.

Fonseca, S., Chico, J.M., and Solano, R. (2009). The jasmonate pathway: the ligand, the receptor and the core signalling module. Curr Opin Plant Biol 12, 539-547.

Footitt, S., Slocombe, S.P., Larner, V., Kurup, S., Wu, Y., Larson, T., Graham, I., Baker, A., and Holdsworth, M. (2002). Control of germination and lipid mobilization by COMATOSE, the Arabidopsis homologue of human ALDP. EMBO J 21, 2912-2922.

Foyer, C.H., Bloom, A.J., Queval, G., and Noctor, G. (2009). Photorespiratory metabolism: genes, mutants, energetics, and redox signaling. Annu Rev Plant Biol 60, 455-484.

Fristedt, R., Willig, A., Granath, P., Crevecoeur, M., Rochaix, J.D., and Vener, A.V. (2009). Phosphorylation of photosystem II controls functional macroscopic folding of photosynthetic membranes in Arabidopsis. Plant Cell 21, 3950-3964.

Froman, B.E., Edwards, P.C., Bursch, A.G., and Dehesh, K. (2000). ACX3, a novel medium-chain acyl-coenzyme A oxidase from Arabidopsis. Plant Physiol 123, 733-742.

Fulda, M., Schnurr, J., Abbadi, A., Heinz, E., and Browse, J. (2004). Peroxisomal Acyl-CoA synthetase activity is essential for seedling development in Arabidopsis thaliana. Plant Cell 16, 394-405.

Ganeteg, U., Klimmek, F., and Jansson, S. (2004). Lhca5--an LHC-type protein associated with photosystem I. Plant Mol Biol 54, 641-651.

Germain, V., Rylott, E.L., Larson, T.R., Sherson, S.M., Bechtold, N., Carde, J.P., Bryce, J.H., Graham, I.A., and Smith, S.M. (2001). Requirement for 3-ketoacyl-CoA thiolase-2 in peroxisome development, fatty acid beta-oxidation and breakdown of triacylglycerol in lipid bodies of Arabidopsis seedlings. Plant J 28, 1-12.

Goepfert, S., and Poirier, Y. (2007). Beta-oxidation in fatty acid degradation and beyond. Curr Opin Plant Biol 10, 245-251.

Goss, R., and Lepetit, B. (2015). Biodiversity of NPQ. J Plant Physiol 172, 13-32.

Graham, I.A., and Eastmond, P.J. (2002). Pathways of straight and branched chain fatty acid catabolism in higher plants. Prog Lipid Res 41, 156-181.

Gresser, M.J., Myers, J.A., and Boyer, P.D. (1982). Catalytic site cooperativity of beef heart mitochondrial F1 adenosine triphosphatase. Correlations of initial velocity, bound intermediate, and oxygen exchange measurements with an alternating three-site model. J Biol Chem 257, 12030-12038.

Gross, J., Cho, W.K., Lezhneva, L., Falk, J., Krupinska, K., Shinozaki, K., Seki, M., Herrmann, R.G., and Meurer, J. (2006). A plant locus essential for phylloquinone (vitamin K1) biosynthesis originated from a fusion of four eubacterial genes. J Biol Chem 281, 17189-17196.

Groth, G., and Pohl, E. (2001). The structure of the chloroplast F1-ATPase at 3.2 A resolution. J Biol Chem 276, 1345-1352.

Guskov, A., Kern, J., Gabdulkhakov, A., Broser, M., Zouni, A., and Saenger, W. (2009). Cyanobacterial photosystem II at 2.9-A resolution and the role of quinones, lipids, channels and chloride. Nat Struct Mol Biol 16, 334-342.

Haldrup, A., Naver, H., and Scheller, H.V. (1999). The interaction between plastocyanin and photosystem I is inefficient in transgenic Arabidopsis plants lacking the PSI-N subunit of photosystem I. Plant J 17, 689-698.

Hardham, A.R., Takemoto, D., and White, R.G. (2008). Rapid and dynamic subcellular reorganization following mechanical stimulation of Arabidopsis epidermal cells mimics responses to fungal and oomycete attack. BMC Plant Biol 8, 63.

Hasan, S.S., Yamashita, E., Baniulis, D., and Cramer, W.A. (2013). Quinone-dependent proton transfer pathways in the photosynthetic cytochrome b6f complex. Proc Natl Acad Sci U S A 110, 4297-4302.

Hashimoto, M., Endo, T., Peltier, G., Tasaka, M., and Shikanai, T. (2003). A nucleus-encoded factor, CRR2, is essential for the expression of chloroplast ndhB in Arabidopsis. Plant J 36, 541-549.

Havaux, M., Bonfils, J.P., Lutz, C., and Niyogi, K.K. (2000). Photodamage of the photosynthetic apparatus and its dependence on the leaf developmental stage in the npq1 Arabidopsis mutant deficient in the xanthophyll cycle enzyme violaxanthin de-epoxidase. Plant Physiol 124, 273-284.

Hayashi, M., Nito, K., Takei-Hoshi, R., Yagi, M., Kondo, M., Suenaga, A., Yamaya, T., and Nishimura, M. (2002). Ped3p is a peroxisomal ATP-binding cassette transporter that might supply substrates for fatty acid beta-oxidation. Plant Cell Physiol 43, 1-11.

Heber, U., and Walker, D. (1992). Concerning a dual function of coupled cyclic electron transport in leaves. Plant physiology 100, 1621-1626.

Hertle, A.P., Blunder, T., Wunder, T., Pesaresi, P., Pribil, M., Armbruster, U., and Leister, D. (2013). PGRL1 is the elusive ferredoxin-plastoquinone reductase in photosynthetic cyclic electron flow. Mol Cell 49, 511-523.

Hisaboria, T., Kondoha, A., and Yoshidaa, M. (1999). The γ subunit in chloroplast F1-ATPase can rotate in a unidirectional and counter-clockwise manner. FEBS Lett 463, 35-38.

Hofmann, N.R. (2011). The evolution of photorespiratory glycolate oxidase activity. Plant Cell 23, 2805.

Holt, N.E., Fleming, G.R., and Niyogi, K.K. (2004). Toward an understanding of the mechanism of nonphotochemical quenching in green plants. Biochemistry 43, 8281-8289.

Horton, P. (2012). Optimization of light harvesting and photoprotection: molecular mechanisms and physiological consequences. Philos Trans R Soc Lond B Biol Sci 367, 3455-3465.

Horton, P., and Ruban, A. (2005). Molecular design of the photosystem II light-harvesting antenna: photosynthesis and photoprotection. J Exp Bot 56, 365-373.

Hu, J., Baker, A., Bartel, B., Linka, N., Mullen, R.T., Reumann, S., and Zolman, B.K. (2012). Plant peroxisomes: biogenesis and function. Plant Cell 24, 2279-2303.

Hundhausen, C., Bosch-Saadatmandi, C., Augustin, K., Blank, R., Wolffram, S., and Rimbach, G. (2005). Effect of vitamin E and polyphenols on ochratoxin A-induced cytotoxicity in liver (HepG2) cells. J Plant Physiol 162, 818-822.

Igarashi, D., Miwa, T., Seki, M., Kobayashi, M., Kato, T., Tabata, S., Shinozaki, K., and Ohsumi, C. (2003). Identification of photorespiratory glutamate:glyoxylate aminotransferase (GGAT) gene in Arabidopsis. Plant J 33, 975-987.

Ishikita, H., Stehlik, D., Golbeck, J.H., and Knapp, E.W. (2006). Electrostatic influence of PsaC protein binding to the PsaA/PsaB heterodimer in photosystem I. Biophys J 90, 1081-1089.

Islinger, M., Grille, S., Fahimi, H.D., and Schrader, M. (2012). The peroxisome: an update on mysteries. Histochem Cell Biol 137, 547-574.

Iwai, M., Takizawa, K., Tokutsu, R., Okamuro, A., Takahashi, Y., and Minagawa, J. (2010). Isolation of the elusive supercomplex that drives cyclic electron flow in photosynthesis. Nature 464, 1210-1213.

Jarvi, S., Suorsa, M., and Aro, E.M. (2015). Photosystem II repair in plant chloroplasts - Regulation, assisting proteins and shared components with photosystem II biogenesis. Biochim Biophys Acta 1847, 900-909.

Johnson, M.P., Davison, P.A., Ruban, A.V., and Horton, P. (2008). The xanthophyll cycle pool size controls the kinetics of non-photochemical quenching in Arabidopsis thaliana. FEBS Lett 582, 262-266.

Jordan, P., Fromme, P., Witt, H.T., Klukas, O., Saenger, W., and Krauss, N. (2001). Three-dimensional structure of cyanobacterial photosystem I at 2.5 A resolution. Nature 411, 909-917.

Junge, W., and Nelson, N. (2015). ATP synthase. Annu Rev Biochem 84, 631-657.

Kaiser, E., Morales, A., Harbinson, J., Kromdijk, J., Heuvelink, E., and Marcelis, L.F. (2015). Dynamic photosynthesis in different environmental conditions. J Exp Bot 66, 2415-2426.

Kapri-Pardes, E., Naveh, L., and Adam, Z. (2007). The thylakoid lumen protease Deg1 is involved in the repair of photosystem II from photoinhibition in Arabidopsis. Plant Cell 19, 1039-1047.

Kato, Y., and Sakamoto, W. (2009). Protein quality control in chloroplasts: a current model of D1 protein degradation in the photosystem II repair cycle. J Biochem 146, 463-469.

Kaur, N., Reumann, S., and Hu, J. (2009). Peroxisome biogenesis and function. Arabidopsis Book 7, e0123.

Keren, N., Liberton, M., and Pakrasi, H.B. (2005). Photochemical competence of assembled photosystem II core complex in cyanobacterial plasma membrane. J Biol Chem 280, 6548-6553.

Khan, B.R., Adham, A.R., and Zolman, B.K. (2012). Peroxisomal Acyl-CoA oxidase 4 activity differs between Arabidopsis accessions. Plant Mol Biol 78, 45-58.

Kim, Y., Konno, H., Sugano, Y., and Hisabori, T. (2011). Redox regulation of rotation of the cyanobacterial F1-ATPase containing thiol regulation switch. J Biol Chem 286, 9071-9078.

Klimmek, F., Sjodin, A., Noutsos, C., Leister, D., and Jansson, S. (2006). Abundantly and rarely expressed Lhc protein genes exhibit distinct regulation patterns in plants. Plant Physiol 140, 793-804.

Koo, A.J., Chung, H.S., Kobayashi, Y., and Howe, G.A. (2006). Identification of a peroxisomal acyl-activating enzyme involved in the biosynthesis of jasmonic acid in Arabidopsis. J Biol Chem 281, 33511-33520.

Kouril, R., Dekker, J.P., and Boekema, E.J. (2012). Supramolecular organization of photosystem II in green plants. Biochim Biophys Acta 1817, 2-12.

Kovacs, L., Damkjaer, J., Kereiche, S., Ilioaia, C., Ruban, A.V., Boekema, E.J., Jansson, S., and Horton, P. (2006). Lack of the light-harvesting complex CP24 affects the structure and function of the grana membranes of higher plant chloroplasts. Plant Cell 18, 3106-3120.

Kramer, D.M., and Evans, J.R. (2011). The importance of energy balance in improving photosynthetic productivity. Plant Physiol 155, 70-78.

Krupinski, P., and Jonsson, H. (2010). Modeling auxin-regulated development. Cold Spring Harb Perspect Biol 2, a001560.

Kukuczka, B., Magneschi, L., Petroutsos, D., Steinbeck, J., Bald, T., Powikrowska, M., Fufezan, C., Finazzi, G., and Hippler, M. (2014). Proton Gradient Regulation5-Like1-Mediated Cyclic Electron Flow Is Crucial for Acclimation to Anoxia and Complementary to Nonphotochemical Quenching in Stress Adaptation. Plant Physiol 165, 1604-1617.

Laisk, A., Eichelmann, H., Oja, V., and Peterson, R.B. (2005). Control of cytochrome b6f at low and high light intensity and cyclic electron transport in leaves. Biochim Biophys Acta 1708, 79-90.

Lama, E., Ortizb, W., and Malkin, R. (1984). Chlorophyll a/b proteins of Photosystem I. FEBS Lett.

Li, C., Schilmiller, A.L., Liu, G., Lee, G.I., Jayanty, S., Sageman, C., Vrebalov, J., Giovannoni, J.J., Yagi, K., Kobayashi, Y., et al. (2005). Role of beta-oxidation in jasmonate biosynthesis and systemic wound signaling in tomato. Plant Cell 17, 971-986.

Li, X.P., Bjorkman, O., Shih, C., Grossman, A.R., Rosenquist, M., Jansson, S., and Niyogi, K.K. (2000). A pigment-binding protein essential for regulation of photosynthetic light harvesting. Nature 403, 391-395.

Liepman, A.H., and Olsen, L.J. (2003). Alanine aminotransferase homologs catalyze the glutamate:glyoxylate aminotransferase reaction in peroxisomes of Arabidopsis. Plant Physiol 131, 215-227.

Lipka, V., Dittgen, J., Bednarek, P., Bhat, R., Wiermer, M., Stein, M., Landtag, J., Brandt, W., Rosahl, S., Scheel, D., et al. (2005). Pre- and postinvasion defenses both contribute to nonhost resistance in Arabidopsis. Science 310, 1180-1183.

Lisenbee, C.S., Lingard, M.J., and Trelease, R.N. (2005). Arabidopsis peroxisomes possess functionally redundant membrane and matrix isoforms of monodehydroascorbate reductase. Plant J 43, 900-914.

Lohmann, A., Schottler, M.A., Brehelin, C., Kessler, F., Bock, R., Cahoon, E.B., and Dormann, P. (2006). Deficiency in phylloquinone (vitamin K1) methylation affects prenyl quinone distribution, photosystem I abundance, and anthocyanin accumulation in the Arabidopsis AtmenG mutant. J Biol Chem 281, 40461-40472.

Loll, B., Kern, J., Saenger, W., Zouni, A., and Biesiadka, J. (2005). Towards complete cofactor arrangement in the 3.0 A resolution structure of photosystem II. Nature 438, 1040-1044.

Mano, Y., and Nemoto, K. (2012). The pathway of auxin biosynthesis in plants. J Exp Bot 63, 2853-2872.

Matsubayashi, T., Wakasugi, T., Shinozaki, K., Yamaguchi-Shinozaki, K., Zaita, N., Hidaka, T., Meng, B.Y., Ohto, C., Tanaka, M., Kato, A., et al. (1987). Six chloroplast genes (ndhA-F) homologous to human mitochondrial genes encoding components of the respiratory chain NADH dehydrogenase are actively expressed: determination of the splice sites in ndhA and ndhB pre-mRNAs. Mol Gen Genet 210, 385-393.

McCartney, A.W., Greenwood, J.S., Fabian, M.R., White, K.A., and Mullen, R.T. (2005). Localization of the tomato bushy stunt virus replication protein p33 reveals a peroxisome-to-endoplasmic reticulum sorting pathway. Plant Cell 17, 3513-3531.

Meier, T., Polzer, P., Diederichs, K., Welte, W., and Dimroth, P. (2005). Structure of the rotor ring of F-Type Na+-ATPase from Ilyobacter tartaricus. Science 308, 659-662.

Menke, W. (1962). Structure and Chemistry of Plastids. Annual Review of Plant Physiology.

Metraux, J.P. (2002). Recent breakthroughs in the study of salicylic acid biosynthesis. Trends Plant Sci 7, 332-334.

Mhamdi, A., Noctor, G., and Baker, A. (2012). Plant catalases: peroxisomal redox guardians. Arch Biochem Biophys 525, 181-194.

Minagawa, J. (2011). State transitions--the molecular remodeling of photosynthetic supercomplexes that controls energy flow in the chloroplast. Biochim Biophys Acta 1807, 897-905.

Mittler, R., Vanderauwera, S., Suzuki, N., Miller, G., Tognetti, V.B., Vandepoele, K., Gollery, M., Shulaev, V., and Van Breusegem, F. (2011). ROS signaling: the new wave? Trends Plant Sci 16, 300-309.

Miyake, C., Shinzaki, Y., Miyata, M., and Tomizawa, K. (2004). Enhancement of cyclic electron flow around PSI at high light and its contribution to the induction of non-photochemical quenching of chl fluorescence in intact leaves of tobacco plants. Plant Cell Physiol 45, 1426-1433.

Muller, P., Li, X.P., and Niyogi, K.K. (2001). Non-photochemical quenching. A response to excess light energy. Plant Physiol 125, 1558-1566.

Mullineaux, C.W., and Emlyn-Jones, D. (2005). State transitions: an example of acclimation to low-light stress. J Exp Bot 56, 389-393.

Munekage, Y., Hashimoto, M., Miyake, C., Tomizawa, K., Endo, T., Tasaka, M., and Shikanai, T. (2004). Cyclic electron flow around photosystem I is essential for photosynthesis. Nature 429, 579-582.

Munekage, Y., Hojo, M., Meurer, J., Endo, T., Tasaka, M., and Shikanai, T. (2002). PGR5 is involved in cyclic electron flow around photosystem I and is essential for photoprotection in Arabidopsis. Cell 110, 361-371.

Mustardy, L., Buttle, K., Steinbach, G., and Garab, G. (2008). The three-dimensional network of the thylakoid membranes in plants: quasihelical model of the granum-stroma assembly. Plant Cell 20, 2552-2557.

Naver, H., Boudreau, E., and Rochaix, J.D. (2001). Functional studies of Ycf3: its role in assembly of photosystem I and interactions with some of its subunits. Plant Cell 13, 2731-2745.

Nelson, N., and Junge, W. (2015). Structure and energy transfer in photosystems of oxygenic photosynthesis. Annu Rev Biochem 84, 659-683.

Nelson, N., and Yocum, C.F. (2006). Structure and function of photosystems I and II. Annu Rev Plant Biol 57, 521-565.

Nickelsen, J., and Rengstl, B. (2013). Photosystem II assembly: from cyanobacteria to plants. Annu Rev Plant Biol 64, 609-635.

Nixon, P.J., Michoux, F., Yu, J., Boehm, M., and Komenda, J. (2010). Recent advances in understanding the assembly and repair of photosystem II. Ann Bot 106, 1-16.

Niyogi, K.K., Grossman, A.R., and Bjorkman, O. (1998). Arabidopsis mutants define a central role for the xanthophyll cycle in the regulation of photosynthetic energy conversion. Plant Cell 10, 1121-1134.

Niyogi, K.K., Li, X.P., Rosenberg, V., and Jung, H.S. (2005). Is PsbS the site of non-photochemical quenching in photosynthesis? J Exp Bot 56, 375-382.

Niyogi, K.K., and Truong, T.B. (2013). Evolution of flexible non-photochemical quenching mechanisms that regulate light harvesting in oxygenic photosynthesis. Curr Opin Plant Biol 16, 307-314.

Noji, H., Yasuda, R., Yoshida, M., and Kinosita, K., Jr. (1997). Direct observation of the rotation of F1-ATPase. Nature 386, 299-302.

Ogawa, T. (1991). A gene homologous to the subunit-2 gene of NADH dehydrogenase is essential to inorganic carbon transport of Synechocystis PCC6803. Proc Natl Acad Sci U S A 88, 4275-4279.

Okinaka, Y., Yang, C.H., Herman, E., Kinney, A., and Keen, N.T. (2002). The P34 syringolide elicitor receptor interacts with a soybean photorespiration enzyme, NADH-dependent hydroxypyruvate reductase. Mol Plant Microbe Interact 15, 1213-1218.

Omote, H., Sambonmatsu, N., Saito, K., Sambongi, Y., Iwamoto-Kihara, A., Yanagida, T., Wada, Y., and Futai, M. (1999). The gamma-subunit rotation and torque generation in F1-ATPase from wild-type or uncoupled mutant Escherichia coli. Proc Natl Acad Sci U S A 96, 7780-7784.

Osmond, C.B. (1981). Photorespiration and photoinhibition: Some implications for the energetics of photosynthesis.

Biochimica et Biophysica Acta- Bioenergetics.

Ozawa, S., Nield, J., Terao, A., Stauber, E.J., Hippler, M., Koike, H., Rochaix, J.D., and Takahashi, Y. (2009). Biochemical and structural studies of the large Ycf4-photosystem I assembly complex of the green alga Chlamydomonas reinhardtii. Plant Cell 21, 2424-2442.

Ozawa, S., Onishi, T., and Takahashi, Y. (2010). Identification and characterization of an assembly intermediate subcomplex of photosystem I in the green alga Chlamydomonas reinhardtii. J Biol Chem 285, 20072-20079.

Pasch, J.C., Nickelsen, J., and Schunemann, D. (2005). The yeast split-ubiquitin system to study chloroplast membrane protein interactions. Appl Microbiol Biotechnol 69, 440-447.

Petersen, J., Forster, K., Turina, P., and Graber, P. (2012). Comparison of the H+/ATP ratios of the H+-ATP synthases from yeast and from chloroplast. Proc Natl Acad Sci U S A 109, 11150-11155.

Pick, T.R., Brautigam, A., Schulz, M.A., Obata, T., Fernie, A.R., and Weber, A.P. (2013). PLGG1, a plastidic glycolate glycerate transporter, is required for photorespiration and defines a unique class of metabolite transporters. Proc Natl Acad Sci U S A 110, 3185-3190.

Pieuchot, L., and Jedd, G. (2012). Peroxisome assembly and functional diversity in eukaryotic microorganisms. Annu Rev Microbiol 66, 237-263.

Reumann, S. (2004). Specification of the peroxisome targeting signals type 1 and type 2 of plant peroxisomes by bioinformatics analyses. Plant Physiol 135, 783-800.

Rhee, S.Y., Dickerson, J., and Xu, D. (2006). Bioinformatics and its applications in plant biology. Annu Rev Plant Biol 57, 335-360.

Rhodin, J. (1954). Correlation of ultrastructural organization and function in normal and experimentally changed proximal tubule cells of the mouse kidney. Doctorate Thesis, Karolinska Institutet, Stockholm.

Richmond, T.A., and Bleecker, A.B. (1999). A defect in beta-oxidation causes abnormal inflorescence development in Arabidopsis. Plant Cell 11, 1911-1924.

Rochaix, J.D. (2014). Regulation and dynamics of the light-harvesting system. Annu Rev Plant Biol 65, 287-309.

Rojas, C.M., Senthil-Kumar, M., Wang, K., Ryu, C.M., Kaundal, A., and Mysore, K.S. (2012). Glycolate oxidase modulates reactive oxygen species-mediated signal

transduction during nonhost resistance in Nicotiana benthamiana and Arabidopsis. Plant Cell 24, 336-352.

Rokka, A., Suorsa, M., Saleem, A., Battchikova, N., and Aro, E.M. (2005). Synthesis and assembly of thylakoid protein complexes: multiple assembly steps of photosystem II. Biochem J 388, 159-168.

Ruban, A.V., Berera, R., Ilioaia, C., van Stokkum, I.H., Kennis, J.T., Pascal, A.A., van Amerongen, H., Robert, B., Horton, P., and van Grondelle, R. (2007). Identification of a mechanism of photoprotective energy dissipation in higher plants. Nature 450, 575-578.

Rylott, E.L., Eastmond, P.J., Gilday, A.D., Slocombe, S.P., Larson, T.R., Baker, A., and Graham, I.A. (2006). The Arabidopsis thaliana multifunctional protein gene (MFP2) of peroxisomal beta-oxidation is essential for seedling establishment. Plant J 45, 930-941.

Rylott, E.L., Rogers, C.A., Gilday, A.D., Edgell, T., Larson, T.R., and Graham, I.A. (2003). Arabidopsis mutants in short- and medium-chain acyl-CoA oxidase activities accumulate acyl-CoAs and reveal that fatty acid beta-oxidation is essential for embryo development. J Biol Chem 278, 21370-21377.

Sage, R.F., Sage, T.L., and Kocacinar, F. (2012). Photorespiration and the evolution of C4 photosynthesis. Annu Rev Plant Biol 63, 19-47.

Samol, I., Shapiguzov, A., Ingelsson, B., Fucile, G., Crevecoeur, M., Vener, A.V., Rochaix, J.D., and Goldschmidt-Clermont, M. (2012). Identification of a photosystem II phosphatase involved in light acclimation in Arabidopsis. Plant Cell 24, 2596-2609.

Saroussi, S., Schushan, M., Ben-Tal, N., Junge, W., and Nelson, N. (2012). Structure and flexibility of the C-ring in the electromotor of rotary F(0)F(1)-ATPase of pea chloroplasts. PLoS One 7, e43045.

Schilmiller, A.L., Koo, A.J., and Howe, G.A. (2007). Functional diversification of acyl-coenzyme A oxidases in jasmonic acid biosynthesis and action. Plant Physiol 143, 812-824.

Schottler, M.A., Albus, C.A., and Bock, R. (2011). Photosystem I: its biogenesis and function in higher plants. J Plant Physiol 168, 1452-1461.

Schrader, M., and Fahimi, H.D. (2008). The peroxisome: still a mysterious organelle. Histochem Cell Biol 129, 421-440.

Schuhmann, H., and Adamska, I. (2012). Deg proteases and their role in protein quality control and processing in different subcellular compartments of the plant cell. Physiol Plant 145, 224-234.

Schulze, W.X., and Usadel, B. (2010). Quantitation in mass-spectrometry-based proteomics. Annu Rev Plant Biol 61, 491-516.

Schwarte, S., and Bauwe, H. (2007). Identification of the photorespiratory 2-phosphoglycolate phosphatase, PGLP1, in Arabidopsis. Plant Physiol 144, 1580-1586.

Shapiguzov, A., Ingelsson, B., Samol, I., Andres, C., Kessler, F., Rochaix, J.D., Vener, A.V., and Goldschmidt-Clermont, M. (2010). The PPH1 phosphatase is specifically involved in LHCII dephosphorylation and state transitions in Arabidopsis. Proc Natl Acad Sci U S A 107, 4782-4787.

Shen, J.R. (2015). The Structure of Photosystem II and the Mechanism of Water Oxidation in Photosynthesis. Annu Rev Plant Biol 66, 23-48.

Shi, L.X., Hall, M., Funk, C., and Schroder, W.P. (2012). Photosystem II, a growing complex: updates on newly discovered components and low molecular mass proteins. Biochim Biophys Acta 1817, 13-25.

Shikanai, T., Endo, T., Hashimoto, T., Yamada, Y., Asada, K., and Yokota, A. (1998). Directed disruption of the tobacco ndhB gene impairs cyclic electron flow around photosystem I. Proc Natl Acad Sci U S A 95, 9705-9709.

Sinclair, A.M., Trobacher, C.P., Mathur, N., Greenwood, J.S., and Mathur, J. (2009). Peroxule extension over ER-defined paths constitutes a rapid subcellular response to hydroxyl stress. Plant J 59, 231-242.

Smith, J.J., and Aitchison, J.D. (2013). Peroxisomes take shape. Nat Rev Mol Cell Biol 14, 803-817.

Somerville, C.R., and Ogren, W.L. (1980). Photorespiration mutants of Arabidopsis thaliana deficient in serine-glyoxylate aminotransferase activity. Proc Natl Acad Sci U S A 77, 2684-2687.

Stock, D., Leslie, A.G., and Walker, J.E. (1999). Molecular architecture of the rotary motor in ATP synthase. Science 286, 1700-1705.

Stockel, J., Bennewitz, S., Hein, P., and Oelmuller, R. (2006). The evolutionarily conserved tetratrico peptide repeat protein pale yellow green7 is required for photosystem I accumulation in Arabidopsis and copurifies with the complex. Plant Physiol 141, 870-878.

Stolz, B., and Walz, D. (1988). The absorption spectrum of single blebs and the specific surface of thylakoids. Mol Cell Biol.

Strader, L.C., and Bartel, B. (2011). Transport and metabolism of the endogenous auxin precursor indole-3-butyric acid. Mol Plant 4, 477-486.

Strader, L.C., Culler, A.H., Cohen, J.D., and Bartel, B. (2010). Conversion of endogenous indole-3-butyric acid to indole-3-acetic acid drives cell expansion in Arabidopsis seedlings. Plant Physiol 153, 1577-1586.

Strader, L.C., Wheeler, D.L., Christensen, S.E., Berens, J.C., Cohen, J.D., Rampey, R.A., and Bartel, B. (2011). Multiple facets of Arabidopsis seedling development require indole-3-butyric acid-derived auxin. Plant Cell 23, 984-999.

Stroebel, D., Choquet, Y., Popot, J.L., and Picot, D. (2003). An atypical haem in the cytochrome b(6)f complex. Nature 426, 413-418.

Suga, M., Akita, F., Hirata, K., Ueno, G., Murakami, H., Nakajima, Y., Shimizu, T., Yamashita, K., Yamamoto, M., Ago, H., et al. (2015). Native structure of photosystem II at 1.95 A resolution viewed by femtosecond X-ray pulses. Nature 517, 99-103.

Sugimoto, I., and Takahashi, Y. (2003). Evidence that the PsbK polypeptide is associated with the photosystem II core antenna complex CP43. J Biol Chem 278, 45004-45010.

Sulpice, R., and McKeown, P.C. (2015). Moving toward a comprehensive map of central plant metabolism. Annu Rev Plant Biol 66, 187-210.

Sylak-Glassman, E.J., Malnoe, A., De Re, E., Brooks, M.D., Fischer, A.L., Niyogi, K.K., and Fleming, G.R. (2014). Distinct roles of the photosystem II protein PsbS and zeaxanthin in the regulation of light harvesting in plants revealed by fluorescence lifetime snapshots. Proc Natl Acad Sci U S A 111, 17498-17503.

Takahashi, H., Chen, Z., Du, H., Liu, Y., and Klessig, D.F. (1997). Development of necrosis and activation of disease resistance in transgenic tobacco plants with severely reduced catalase levels. Plant J 11, 993-1005.

Taler, D., Galperin, M., Benjamin, I., Cohen, Y., and Kenigsbuch, D. (2004). Plant eR genes that encode photorespiratory enzymes confer resistance against disease. Plant Cell 16, 172-184.

Timm, S., Florian, A., Arrivault, S., Stitt, M., Fernie, A.R., and Bauwe, H. (2012). Glycine decarboxylase controls photosynthesis and plant growth. FEBS Lett 586, 3692-3697.

Timm, S., Nunes-Nesi, A., Parnik, T., Morgenthal, K., Wienkoop, S., Keerberg, O., Weckwerth, W., Kleczkowski, L.A., Fernie, A.R., and Bauwe, H. (2008). A cytosolic pathway for the conversion of hydroxypyruvate to glycerate during photorespiration in Arabidopsis. Plant Cell 20, 2848-2859.

Umena, Y., Kawakami, K., Shen, J.R., and Kamiya, N. (2011). Crystal structure of oxygen-evolving photosystem II at a resolution of 1.9 A. Nature 473, 55-60.

Vainonen, J.P., Hansson, M., and Vener, A.V. (2005). STN8 protein kinase in Arabidopsis thaliana is specific in phosphorylation of photosystem II core proteins. J Biol Chem 280, 33679-33686.

van der Laan, M., Nouwen, N.P., and Driessen, A.J. (2005). YidC--an evolutionary conserved device for the assembly of energy-transducing membrane protein complexes. Curr Opin Microbiol 8, 182-187.

Verslues, P.E., Kim, Y.S., and Zhu, J.K. (2007). Altered ABA, proline and hydrogen peroxide in an Arabidopsis glutamate:glyoxylate aminotransferase mutant. Plant Mol Biol 64, 205-217.

Voll, L.M., Jamai, A., Renne, P., Voll, H., McClung, C.R., and Weber, A.P. (2006). The photorespiratory Arabidopsis shm1 mutant is deficient in SHM1. Plant Physiol 140, 59-66.

Vollmar, M., Schlieper, D., Winn, M., Buchner, C., and Groth, G. (2009). Structure of the c14 rotor ring of the proton translocating chloroplast ATP synthase. J Biol Chem 284, 18228-18235.

von Ballmoos, C., Wiedenmann, A., and Dimroth, P. (2009). Essentials for ATP synthesis by F1F0 ATP synthases. Annu Rev Biochem 78, 649-672.

Wang, P., Duan, W., Takabayashi, A., Endo, T., Shikanai, T., Ye, J.Y., and Mi, H. (2006). Chloroplastic NAD(P)H dehydrogenase in tobacco leaves functions in alleviation of oxidative damage caused by temperature stress. Plant Physiol 141, 465-474.

Wasternack, C. (2007). Jasmonates: an update on biosynthesis, signal transduction and action in plant stress response, growth and development. Ann Bot 100, 681-697.

Wasternack, C., and Hause, B. (2013). Jasmonates: biosynthesis, perception, signal transduction and action in plant stress response, growth and development. An update to the 2007 review in Annals of Botany. Ann Bot 111, 1021-1058.

Waterham, H.R., and Ebberink, M.S. (2012). Genetics and molecular basis of human peroxisome biogenesis disorders. Biochim Biophys Acta 1822, 1430-1441.

Waterham, H.R., and Wanders, R.J. (2012). Metabolic functions and biogenesis of peroxisomes in health and disease. Biochim Biophys Acta 1822, 1325.

Wei, L., Guo, J., Ouyang, M., Sun, X., Ma, J., Chi, W., Lu, C., and Zhang, L. (2010). LPA19, a Psb27 homolog in Arabidopsis thaliana, facilitates D1 protein precursor processing during PSII biogenesis. J Biol Chem 285, 21391-21398.

Wientjes, E., Drop, B., Kouril, R., Boekema, E.J., and Croce, R. (2013). During state 1 to state 2 transition in Arabidopsis thaliana, the photosystem II supercomplex gets phosphorylated but does not disassemble. J Biol Chem 288, 32821-32826.

Wientjesa, E., Amerongenb, H.v., and Croce, R. (2012). LHCII is an antenna of both photosystems after long-term acclimation. Biochimica et Biophysica Acta - Bioenergetics.

Wiszniewski, A.A., Bussell, J.D., Long, R.L., and Smith, S.M. (2014). Knockout of the two evolutionarily conserved peroxisomal 3-ketoacyl-CoA thiolases in Arabidopsis recapitulates the abnormal inflorescence meristem 1 phenotype. J Exp Bot 65, 6723-6733.

Wollman, F.A. (2001). State transitions reveal the dynamics and flexibility of the photosynthetic apparatus. EMBO J 20, 3623-3630.

Yokono, M., Murakami, A., and Akimoto, S. (2011). Excitation energy transfer between photosystem II and photosystem I in red algae: larger amounts of phycobilisome enhance spillover. Biochim Biophys Acta 1807, 847-853.

Zelitch, I., Schultes, N.P., Peterson, R.B., Brown, P., and Brutnell, T.P. (2009). High glycolate oxidase activity is required for survival of maize in normal air. Plant Physiol 149, 195-204.

Zhang, H., Whitelegge, J.P., and Cramer, W.A. (2001). Ferredoxin:NADP+ oxidoreductase is a subunit of the chloroplast cytochrome b6f complex. J Biol Chem 276, 38159-38165.

Zolman, B.K., Martinez, N., Millius, A., Adham, A.R., and Bartel, B. (2008). Identification and characterization of Arabidopsis indole-3-butyric acid response mutants defective in novel peroxisomal enzymes. Genetics 180, 237-251.

Zolman, B.K., Silva, I.D., and Bartel, B. (2001). The Arabidopsis pxa1 mutant is defective in an ATP-binding cassette transporter-like protein required for peroxisomal fatty acid beta-oxidation. Plant Physiol 127, 1266-1278.

Zouni, A., Jordan, R., Schlodder, E., Fromme, P., and Witt, H.T. (2000). First photosystem II crystals capable of water oxidation. Biochim Biophys Acta 1457, 103-105.

CHAPTER 2

Using co-expression analysis and stress-based screens to uncover Arabidopsis peroxisomal proteins involved in drought response

---

Data in this chapter has been published in: Li, J. and Hu, J. (2015) Using co-expression analysis and stress-based screens to uncover Arabidopsis peroxisomal proteins involved in drought response. PLoS ONE 10(9): e0137762doi:10.1371/journal.pone.0137762

2.1. Abstract

Peroxisomes are essential organelles that house a wide array of metabolic reactions important for plant growth and development. However, our knowledge regarding the role of peroxisomal proteins in various biological processes, including plant stress response, is still incomplete. Recent proteomic studies of plant peroxisomes significantly increased the number of known peroxisomal proteins and greatly facilitated the study of peroxisomes at the systems level. The objectives of this study were to determine whether genes that encode peroxisomal proteins with related functions are co-expressed in Arabidopsis and identify peroxisomal proteins involved in stress response using *in silico* analysis and mutant screens. Using microarray data from online databases, we performed hierarchical clustering analysis to generate a comprehensive view of transcript level changes for Arabidopsis peroxisomal genes during development and under abiotic and biotic stress conditions. Many genes involved in the same metabolic pathways exhibited co-expression, some genes known to be involved in stress response are regulated by the corresponding stress conditions, and function of some peroxisomal proteins could be predicted based on their co-expression pattern. Since drought caused expression changes to the highest number of genes that encode peroxisomal proteins, we subjected a subset of Arabidopsis peroxisomal mutants to a drought stress assay. Mutants of the LON2 protease and the photorespiratory enzyme hydroxypyruvate reductase 1 (HPR1) showed enhanced susceptibility to drought, suggesting the involvement of peroxisomal quality control and photorespiration in drought resistance. Our study provided a global view of how genes that encode peroxisomal proteins respond to developmental and environmental cues and began to reveal additional peroxisomal

proteins involved in stress response, thus opening up new avenues to investigate the role of peroxisomes in plant adaptation to environmental stresses.

2.2. Introduction

Peroxisomes are small and single membrane-delimited organelles that house numerous oxidative reactions connected to metabolism and development. These organelles are dynamic in nature, as their abundance, morphology and protein composition can be remodeled in response to developmental and environmental cues to adapt to the need of the organism (Hu et al., 2012; Pieuchot and Jedd, 2012; Smith and Aitchison, 2013). Plant peroxisomes perform conserved functions such as β-oxidation of fatty acids and related metabolites and detoxification of reactive oxygen species (ROS), as well as plant-specific functions including photorespiration and metabolism of hormones such as jasmonate (JA) and auxin. Peroxisomes are crucial to virtually every developmental stage in plants, from embryogenesis, seedling development, vegetative and reproductive development, to senescence, and were recently shown to be involved in plant response to biotic and abiotic stresses (Hu et al., 2012; Kaur et al., 2009b). The number of known peroxisomal proteins has risen to ~170 in Arabidopsis, largely due to recent peroxisomal proteome analyses followed by *in vivo* protein targeting verifications (Kaur and Hu, 2011).

Peroxisomes possess many oxidative reactions that produce H_2O_2, as well as ROS-scavenging enzymes such as catalase and ascorbate-glutathione cycle enzymes (Del Rio, 2011; Kaur et al., 2009b). ROS is a key component in stress responses (Kotchoni and Gachomo, 2006). Suppression of catalase 1 in tobacco resulted in necrotic lesions in high light and increased susceptibility to paraquat, salt and ozone (Willekens et al., 1997). Mutants of Arabidopsis catalase 2 develop photoperiod-dependent leaf lesions (Queval et al., 2007). Evidence from melon, Arabidopsis and tobacco suggested the involvement of

several peroxisomal photorespiratory enzymes, e.g., hydroxypyruvate reductase (HPR), serine:glyoxylate aminotransferase (SGT), alanine:glyoxylate aminotransferase (AGT), and glycolate oxidase (GOX) in immune response, possibly through ROS production (Okinaka et al., 2002; Rojas et al., 2012a; Taler et al., 2004).

Peroxisomes are also involved in stress response through mechanisms other than ROS homeostasis. Arabidopsis Ca^{2+}-dependent protein kinase CPK1 is physically associated with peroxisomes and functions in a SA-dependent signaling pathway that leads to plant resistance to both fungal and bacterial pathogens (Coca and San Segundo, 2010; Dammann et al., 2003). Arabidopsis PEN2 is a peroxisome-associated myrosinase involved in callose deposition and glucosinolate hydrolysis necessary to generate antimicrobial products, thus is required for plant resistance against a broad spectrum of nonhost fungal pathogens, (Bednarek et al., 2009; Clay et al., 2009; Lipka et al., 2005; Maeda et al., 2009; Westphal et al., 2008). Furthermore, JA biosynthetic enzymes, some of which reside in peroxisomes, have been shown to affect systemic acquired resistance (SAR) to varying degrees (Spoel and Dong, 2012). It was suggested that the final step of SA biosynthesis, i.e., cinnamate to SA via the reduction of two carbons, may occur through β–oxidation in the peroxisome (Reumann, 2004), thus making the peroxisome a potential player in SAR signaling. Interestingly, some virus species can hijack peroxisomes for viral RNA replication, causing the proliferation of peroxisome-like vesicle structures and leading to plant necrosis (McCartney et al., 2005; Rochon et al., 2014), which adds another layer of peroxisomal involvement in plant-pathogen interaction.

Despite these findings, there are still substantial knowledge gaps in the role of peroxisomes in stress response and how the functions of these peroxisomal proteins may be connected. To further identify peroxisomal proteins involved in plant response to various stress conditions, a peroxisome-centered systematic approach is needed. Recent advances in genome-wide transcriptomic and gene ontology enrichment analyses have provided valuable information on gene functions and mechanisms of biological processes. An important finding from these analyses is that genes functioning in the same pathway are often co-regulated by shared transcriptional regulatory systems and thus co-express across development and/or under many stress conditions (Schmid et al., 2005). To this end, we performed a genome-wide transcriptomic analysis of genes that encode peroxisomal proteins in Arabidopsis, trying to determine whether peroxisomal genes involved in the same biochemical pathways are co-expressed and whether we could identify new peroxisomal proteins involved in stress response using this type of *in silico* analysis. We followed up the *in silico* analysis with a pilot drought-based mutant screen, which identified the role of the peroxisomal LON2 protease and the photorespiratory enzyme hydroxypyruvate reductase 1 (HPR1) in drought resistance. Our study marks the beginning of systematic identifications of peroxisomal proteins involved in plant adaptation to stresses.

2.3. Result

2.3.1. Co-expression analysis of genes that encode peroxisomal proteins during development and in response to stresses

Microarray datasets containing expression data of Arabidopsis peroxisomal genes from various tissues at different developmental stages and under biotic and abiotic stresses were downloaded from the AtGenExpress database and NCBI Gene Expression Omnibus (GEO) database, respectively (Table 2.1). Developmental data were obtained from different tissues from seedlings, adult and senescing leaves, flowers, and siliques and seeds at various maturation stages. Abiotic stress conditions included high light, cold, hypoxia, drought, salt, and the major stress hormone abscisic acid (ABA). Biotic stresses included the bacterial pathogen *Pseudomonas syringae* pv. *tomato* (*pst*) DC3000, fungal pathogen *Botrytis cinerea*, and Pathogen-Associated Molecular Patterns (PAMPs) such as the 22-amino-acid fragment of bacterial flagellin, flg22, the 18-amino-acids fragment bacterial elongation factor, elf18, and the fungal elicitor chitin (Table 2.1). Expression profiles of 160 peroxisomal genes (Table 2.2) were extracted from the whole-genome expression profile, clustered by hierarchical clustering analysis based on the extent of co-expression, and visualized by heatmaps.

Not surprisingly, many peroxisomal genes that function in the same metabolic pathways are co-regulated during development (Figure 2.1). For example, genes that encode glyoxylate cycle enzymes isocitrate lyase (ICL), malate synthase (MLS), and citrate synthase 1 (CSY1) are clustered together and co-up-regulated during seed maturation but co-repressed in other developmental stages (Figure 2.1). This is consistent

with the fact that the glyoxylate cycle, a pathway that converts the β–oxidation product acetyl-CoA to succinate and malate to be used for gluconeogenesis, is primarily if not exclusively active in seeds and early seedling development (Hu et al., 2012; Pracharoenwattana and Smith, 2008). In agreement with their roles in photorespiration, which recycles 2-phosphoglycolate produced by the oxygenase activity of Rubisco back to the CBB cycle (Bauwe et al., 2010), the expression of genes for the peroxisomal photorespiratory enzymes hydroxypyruvate reductase 1 (HPR1), glycolate oxidase 1 and 2 (GOX1 and GOX2, which are indistinguishable in microarrays due to high sequence identity), and peroxisomal malate dehydrogenase MDH2 is high in vegetative tissues but diminished during seed development. In contrast to these three clustered genes, genes that encode two other photorespiratory enzymes, glutamate: glyoxylate aminotransferase 1 (GGT1) and alanine: glyoxylate aminotransferase 1 (AGT1), are expressed during seed development as well, indicating that photorespiration may not be the only process that these two enzymes participate. Interestingly, genes that encode the JA biosynthetic enzymes 12-oxophytodienoate reductase 3 (OPR3) and OPC-8:0 CoA ligase 1 (OPCL1), disease related protein PEN2, and the small heat shock protein ACD31.2 are clustered together and also co-expressed with the photorespiration genes *HPR1*, *GOX1/2* and *MDH2* throughout development. This pattern indicates that these stress-related and development-related (in the case of JA biosynthesis) genes might be under similar regulatory circuitry as those photorespiration genes. As the major H_2O_2 detoxification enzymes, the three catalases are mostly constitutively expressed throughout development (Figure 2.1).

Transcriptional reprogramming during stresses is an important mechanism to confer stress tolerance (Gehan et al., 2015; Yamaguchi-Shinozaki and Shinozaki, 2006). Many genes that encode peroxisomal proteins are significantly regulated by abiotic stresses (Figure 2.2A). Among them, the small heat shock protein-encoding gene *AtHsp15.7* showed >150-fold increase in expression under high light (Figure 2.2B) and had to be removed from the heatmap in Figure 2.2A to prevent it from masking the changes in other genes in the heatmap. Genes encoding the peroxisomal proliferation factors PEX11b, PEX11c and PEX11d are all up-regulated by hypoxia (Figure 2.2A), which is consistent with a previous finding that hypoxia stress can rapidly stimulate peroxisomal extension over endoplasmic reticulum (Sinclair et al., 2009). *CAT2* and *CAT3* expressions are also significantly up-regulated during drought stress (Figure 2.2A), consistent with their role as major ROS detoxification enzymes in stress response (Kaur et al., 2009a). The glyoxylate cycle genes *ICL*, *MLS* and *CSY1* are again clustered (Figure 2.2A), suggesting the tight regulation of this pathway by abiotic stress factors. Genes encoding the photorespiration enzymes GOX1/2, HPR1, MDH2, AGT1 and the chloroplast/peroxisome dual localized organelle division protein dynamic related protein 5B (DRP5B) are clustered (Figure 2.2A), raising the interesting possibility that photorespiration and the proliferation of peroxisomes are co-regulated during plant adaptation to abiotic stresses.

In response to biotic stresses, genes for some peroxisomal proteins previously shown to be involved in defense exhibited strong transcriptional reprogramming. For example, *PEN2* (*Penetration 2*) is induced by two PAMPs, flg22 and chitin (Figure 2.3), supporting its major role as a myrosinase in PAMP-triggered immunity (Clay et al., 2009;

Lipka et al., 2005). The two JA biosynthetic genes *OPR3* and *OPCL1* are co-up-regulated by flg22, chitin, *P. syringae* and *B. cinerea* (Figure 2.3), consistent with JA's role as an important defense hormone (Browse, 2009). Interestingly, photorespiratory genes such as *HPR1*, *CAT2*, *GOX1/2*, *MDH2*, *AGT1* and *GGT2* are co-down-regulated by elf18, *P. syringae* and *B. cinerea* (Figure 2.3), which is in agreement with the idea that photorespiration may play a defense role against pathogens through H_2O_2-dependent and -independent metabolism (Sorhagen et al., 2013). The peroxisomal elongation factor gene *PEX11b* is again co-expressed with several photorespiratory genes during biotic stresses (Figure 2.3), which is in accordance with its co-expression with photorespiratory genes in response to light (Kaur et al., 2013) and the role of PEX11b in inducing peroxisomal proliferation during dark-to-light transition (Desai and Hu, 2008). This data also indicated a potential need to increase peroxisomal abundance during pathogen defense.

2.3.2. A drought tolerance mutant screen revealed the role of the LON2 protease and the photorespiratory enzyme hydroxypyruvate reductase 1 (HPR1) in drought response

Based on the rule of "guilt-by-association" (Schmid et al., 2005), those peroxisomal genes that showed significant up-regulation of transcript levels by some stresses may have a potential to play a role in these specific conditions. To test this hypothesis, we decided to choose a stress condition, under which significant regulation of expression is seen for the highest number of peroxisomal genes, to screen for mutants with altered response.

Among the abiotic and biotic stress conditions examined, drought and the bacterial PAMP elf18 trigger expression changes to the highest number of peroxisomal genes (Figure 2.4). Drought is one of the most common environmental stresses that limit plant growth and development. Plants have evolved sophisticated adaptive drought tolerance mechanisms, including increased level of water transporting capacity, decrease of water evaporation, up-regulation of osmolytes and chaperone proteins, activation of Ca^{2+}-dependent, ABA-dependent and other signaling pathways, and regulation of the transcript levels of the genes involved (Zhu, 2002). Mutant plants defective in these processes may exhibit increased drought sensitivity, such as increased water loss and ion leakage, decrease of photosynthesis rate, degradation of chlorophyll, and eventually cell death and plant withering (Zhu, 2002). As such, we used a drought tolerance assay as an initial screen to test the prediction from *in silico* analysis.

We have a collection of Arabidopsis mutants, which has facilitated discovering functions of newly identified peroxisomal proteins in previous studies (Cassin-Ross and Hu, 2014a, b; Quan et al., 2013). To identify peroxisomal proteins involved in drought stress response, we first selected 26 mutants for 18 genes, most of which showed transcript level changes under drought or the drought stress hormone ABA. These included the up-regulated genes *CAT2, GOX3, Hsp15.7, CSY3, Macrophage Migration Inhibitory Factor 1* (*MIF1*) and *LON2* protease, and the down-regulated genes polyamine oxidase *PAO2*, thiolase *KAT5* and acyl-CoA activating enzyme *AAE14*. We also included mutants of proteins involved in major peroxisomal pathways (photorespiration and fatty acids β-oxidation) but do not show obvious changes in transcript levels under drought, i.e. *hpr1*, *gox1*, *acx3, acx6,* and *acx1 acx5*. Mutants of mildly regulated genes, such as

peroxisomal NAD^+ transporter *PXN* and beta-hydroxyisobutyryl-CoA hydrolase *CHY1* were assayed as well (Table 2.3).

For an efficient and quantitative drought tolerance assessment, we used the photosynthetic efficiency F_v/F_m as a drought susceptibility indicator in our screen. Each mutant was grown in the same pot with the wild type plant for 3.5 weeks with periodic irrigation, followed by an 18-day drought period, at the end of which F_v/F_m was measured. The positive control, ABA biosynthetic mutant *aba1* (Xiong et al., 2002), and mutants for the LON2 protease and photorespiratory enzyme HPR1, showed statistically significant decrease in F_v/F_m after drought treatment (Figure 2.5).

The *lon2* and *hpr1* mutants were further analyzed to assess defects in drought resistance. Prior to drought treatment, *lon2* and *hpr1* mutants exhibited similar F_v/F_m values to that of the wild type (Figures 2.6A and 2.6B), suggesting that the drought sensitive phenotypes we observed were specific to drought stress and not a result from general growth defect. Compared with watered plants and drought-treated wild type plants, drought-treated *lon2-2*, *hpr1-1* and *hpr1-2* displayed an age-dependent gradient of photosynthetic defect, which was stronger in older leaves and milder in young leaves (Figures 2.6C and 2.6D). These mutants also showed defects in other drought stress indicators, including reduced anthocyanin induction (Figure 2.6F), accelerated chlorophyll degradation (Figure 2.6G), and lower relative water content (Figure 2.6H).

2.4. Discussion

We have constructed peroxisome-centered transcriptomic heatmaps using Arabidopsis microarray data from various developmental stages and under biotic and

abiotic stresses. Results obtained from the *in silico* analysis not only showed correlation between protein function and expression regulation for many proteins with known function, but also provided information from which previously unknown roles may be inferred for some peroxisomal proteins. For example, out of the two peroxisomal *MDH* isoforms, *MDH2* is tightly co-expressed with *HPR1* and *GOX1/2*, suggesting that MDH2 is the major MDH isoform that functions in photorespiration. Among all the genes analyzed, *AtHsp15.7*, shows the strongest up-regulation by high light, suggesting that the small heat shock protein Hsp15.7, which was shown to be a stress-inducible constituent of the peroxisome (Ma et al., 2006), may facilitate the re-folding of proteins that have been partially unfolded or damaged under high light stress. Up-regulation of peroxisome elongation factors such as *PEX11b*, *PEX11c* and *PEX11d* under hypoxial and biotic stresses suggests that increased volume of peroxisome might be a mechanism for the plant to deal with enhanced oxidative stress. Finally, the fact that unknown protein UP6, which was previously shown to play a minor role in β–oxidation (Cassin-Ross and Hu, 2014b; Quan et al., 2010; Reumann et al., 2009), is strongly up-regulated during late seed developmental stages, indicates a possible role for this protein in seed maturation.

Following the transcriptome analysis, we used a drought stress assay to test promising gene candidates, and identified LON2 and HPR1 as contributors to drought tolerance. HPR1 converts hydroxypyruvate to glycerate during photorespiration (Hu et al., 2012) . It is possible that drought induces stomatal closure, which limits the atmospheric uptake of CO_2, thus increasing the oxygenase activity of Rubisco and thus, photorespiration. In *hpr1*, the accumulated photorespiratory metabolites may inhibit Rubisco activity and slow down the Calvin-Benson cycle due to decreased supply of

glycerate, thus leading to accumulated NADPH and ROS that cause a series of oxidative damages. Mutants for the other two genes directly (*GOX1*) or indirectly (*CAT2*) involved in photorespiration did not show a drought phenotype, possibly due to their functional redundancy with *GOX2* and *CAT1/CAT3*, respectively.

LON2 is a protease with unknown substrates and a role in peroxisomal matrix protein import and degradation (Farmer et al., 2013; Lingard and Bartel, 2009). Our transcriptomic analysis found *LON2* to be up-regulated by ABA by 4-fold, which is consistent with its 8-fold induction by ABA in guard cells (Leonhardt et al., 2004), suggesting that LON2 may play a role in drought response through ABA signaling and peroxisomal protein quality control pathways. Since peroxisomal degradation via autophagy was shown to be enhanced in the *lon2* mutant, especially in older leaves (Farmer et al., 2013; Goto-Yamada et al., 2014), it is possible that there are insufficient peroxisomes in the *lon2* mutant to carry out photorespiration, which is critical for plant survival under drought conditions. This may also explain why *lon2* and *hpr1* display stronger phenotypes than the ABA biosynthetic mutant *aba1* in the initial F_v/F_m screen, because our screen measured photosynthetic efficiency, which is directly impacted by photorespiration deficiencies in these two peroxisomal mutants.

Although *in silico* analysis is powerful for function prediction, mutants for many genes whose transcript levels are regulated by drought did not exhibit obvious drought tolerance defects. Given the manageable size of the peroxisomal proteome and available mutants, stress-based mutant screens should be a more direct way to identify peroxisomal proteins involved in stress response. In this initial screen, we identified strong drought sensitive phenotypes in the knockout mutants of the LON2 protease and the

photorespiratory enzyme HPR1, suggesting that future larger-scale screens would be promising to investigate the role of peroxisomes in plant adaptation to environmental stresses comprehensively. The next step would be to link these peroxisomal proteins with the global stress response networks.

2.5. Materials and methods

2.5.1. Plant materials and growth conditions

Arabidopsis thaliana ecotype Col-0 was used as wild type (WT). T-DNA insertion mutant lines were obtained from the Arabidopsis Biological Resource Center (ABRC; http://www.arabidopsis.org/) and confirmed by PCR genotyping. Seeds were sown in the soil, stratified in the dark at 4 °C for 3 days, and plants were grown in a controlled growth chamber at 22 °C under long-day conditions (16 hrs white light at 100 µmol photons m^{-2} s^{-1} and 8 hrs dark) for 3.5 weeks before drought treatment.

2.5.2. Microarray data analysis and heatmap visualization

Microarray datasets containing expression data of Arabidopsis peroxisomal genes from various tissues at different developmental stages were obtained from the AtGenExpress database, and expression data under biotic and abiotic stresses were downloaded from NCBI Gene Expression Omnibus (GEO) database (Table 2.1). Peroxisomal gene expression data obtained from various developmental stages were directly extracted from the whole-genome data and used for generating the heatmap. For data on biotic and abiotic stresses, log2-normalized data were extracted for peroxisomal genes from the whole-genome expression profile, using methods previously described (Quan et al., 2013). Analysis was performed using the Bioconductor software (Gentleman et al., 2004) with the statistical computing language R (version 2.15.2). Normalization of gene expression values was carried out with the robust multi-array average (RMA) algorithm (Irizarry et al., 2003) implemented in the Affy package of Bioconductor. Statistical significance of the differential expression values were assessed with Linear

models for microarray (limma) package (Smyth, 2004). Hierarchical clustering of the differentially expressed genes was visualized by creating heatmaps using the color palette package RColorBrewer and the gplots package (Warnes et al., 2015).

2.5.3. Chlorophyll fluorescence measurements

Chlorophyll fluorescence images of intact plants were obtained from a custom-designed plant imager chamber, using a previously described method (Attaran et al., 2014). Plants in the pots were placed in the imaging chamber in the dark for 20 min for dark adaptation before minimal chlorophyll fluorescence F_o was measured. Later, maximal fluorescence F_m was measured when a saturating pulse of light was applied. $F_v/F_m = (F_m-F_o)/F_m$. Fluorescence images were analyzed by ImageJ (Schneider et al., 2012).

2.5.4. Drought stress assays

For the drought tolerance screen, each selected mutant (two plants) and two WT plants were grown in the same pot under long day conditions (specified above) for 3.5 weeks, after which point plants stopped receiving water for 18 days before F_v/F_m measurement was conducted. For the follow-up analysis of the *lon2* and *hpr1* mutants, F_v/F_m measurement was repeated in the same way as in the primary screen, and watered plants were added as the control. Leaf samples from the drought-treated and control

plants were harvested for chlorophyll content measurement, relative water content (RWC) and anthocyanin quantification as described previously (Pandey et al., 2013).

For chlorophyll measurement, rosette leaves were weighed and placed into 2 ml 80% acetone in the dark for 3 days. Absorbance at 645 nm and 663 nm was measured using a spectrophotometer. Total chlorophyll content = (22.22 x A_{645} + 9.05 x A_{663}) µg/ml x 2 ml /leaf fresh weight in mg.

To measure relative water content, rosette leaves were cut and immediately weighed as fresh weight (FW), and then placed in distilled deionized water at 4 °C in the dark for 24 hrs, and the weight was recorded as turgid weight (TW). Then the rosette leaf sample was placed at 60 °C for 2 days and the weight was recorded as dry weight (DW). Relative water content = (FW-DW) / (TW-DW) X 100%.

For anthocyanin measurement, rosette leaves were weighed, frozen by liquid nitrogen, and ground to powder. After adding 2 ml extraction buffer (1% HCl in methanol), the samples were placed at 4 °C overnight. Later, an equal amount of chloroform was added, and the mixture was centrifuged for 5 min. After the top supernatant was transferred to a new tube, equal volume of 60 % extraction buffer was added. Absorbance of each tube at 530 nm and 657 nm were measured with a spectrophotometer. Anthocyanin content = (A_{530}-A_{657}) /weight.

2.6. Acknowledgement

We would like to thank David Hall for assistance with F_v/F_m measurement, Dr. Jin Chen and Sahra Uygun for help with microarray data analysis, the Arabidopsis Biological Resource Center for providing the T-DNA insertion mutant lines, Dr. David Kramer for sharing the *gox1* mutant and Dr. Gregg Howe for sharing the *acx1 acx5* double mutant. No conflict of interest declared.

APPENDIX

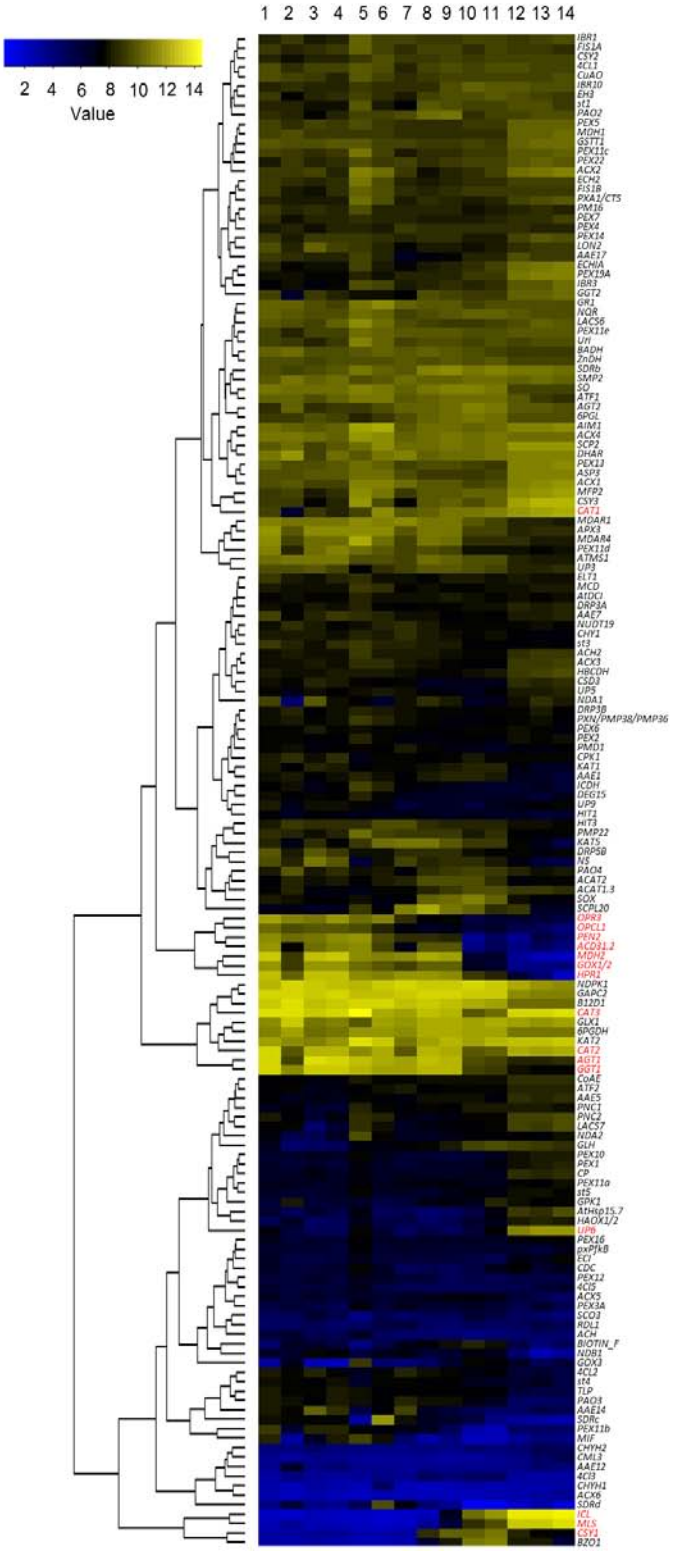

Figure 2.1. Heatmap of transcript levels of peroxisomal genes in various developmental stages.

Figure 2.1. (cont'd)

Absolute gene expression values downloaded from the AtGenExpress database were used for heatmap generation. Genes discussed in the text are in red. Developmental stages include: 1. seedling_cotyledons; 2. seedling_hypocotyl; 3. seedling_leaves1+2; 4. adult_leaves; 5. senescing leaves; 6. flower; 7. silique_stage3; 8. silique_stage4; 9. silique_stage5; 10. seed_stage6; 11. seed_stage7; 12. seed_stage8; 13. seed_stage9; 14. seed_stage10.

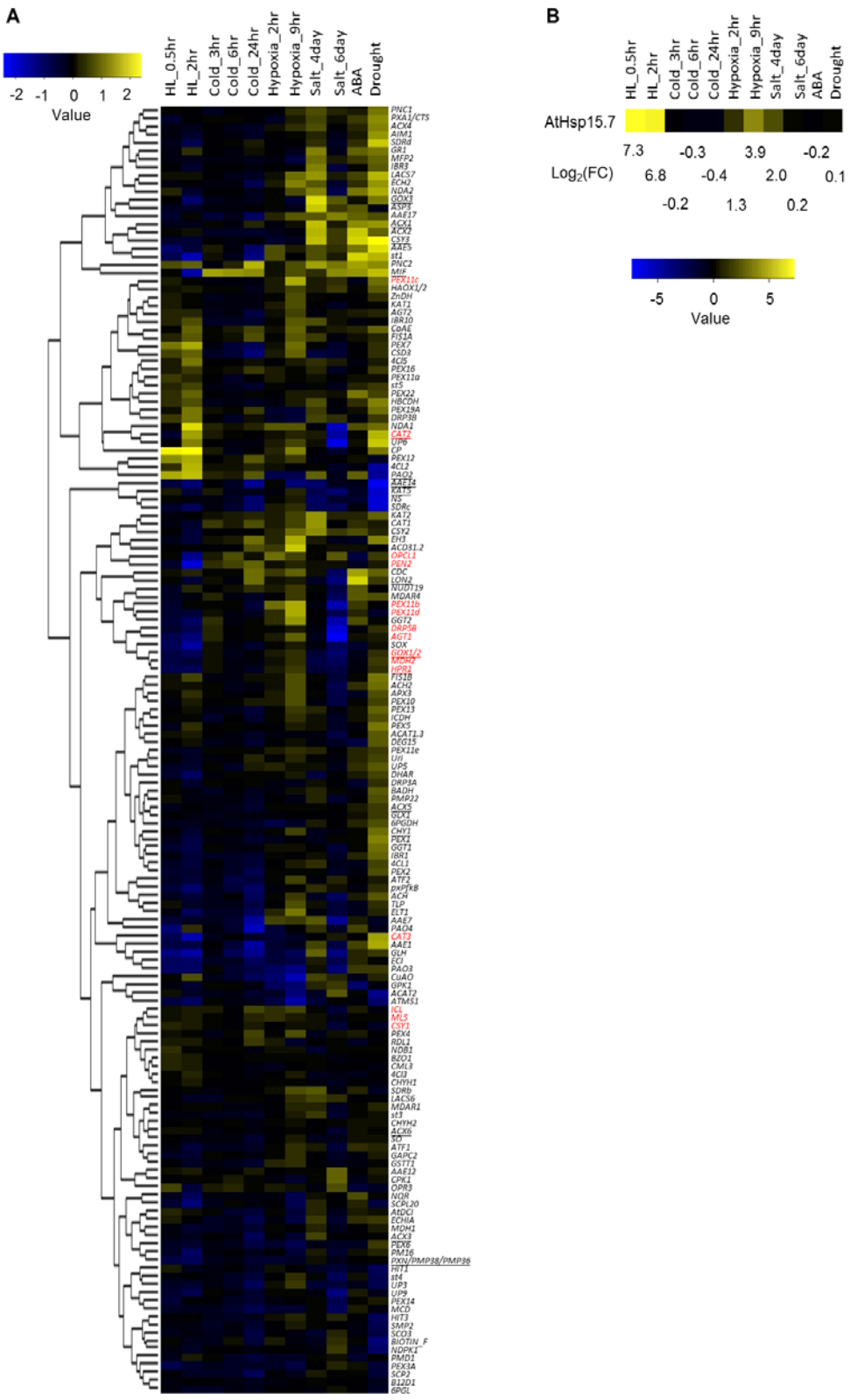

Figure 2.2. Heatmap of transcript levels of peroxisomal genes under abiotic stresses.

Figure 2.2. (cont'd)

Expression values are log2 normalized fold changes against untreated plants. (A) All genes are included, except *AtHsp15.7* (Figure 2.2B) due to its significantly higher upregulation. Genes discussed in the text are in red. Genes subjected to mutant analysis are underscored. (B) Expression of the small heat shock protein gene *AtHsp15.7* in response to abiotic stresses. FC, fold change.

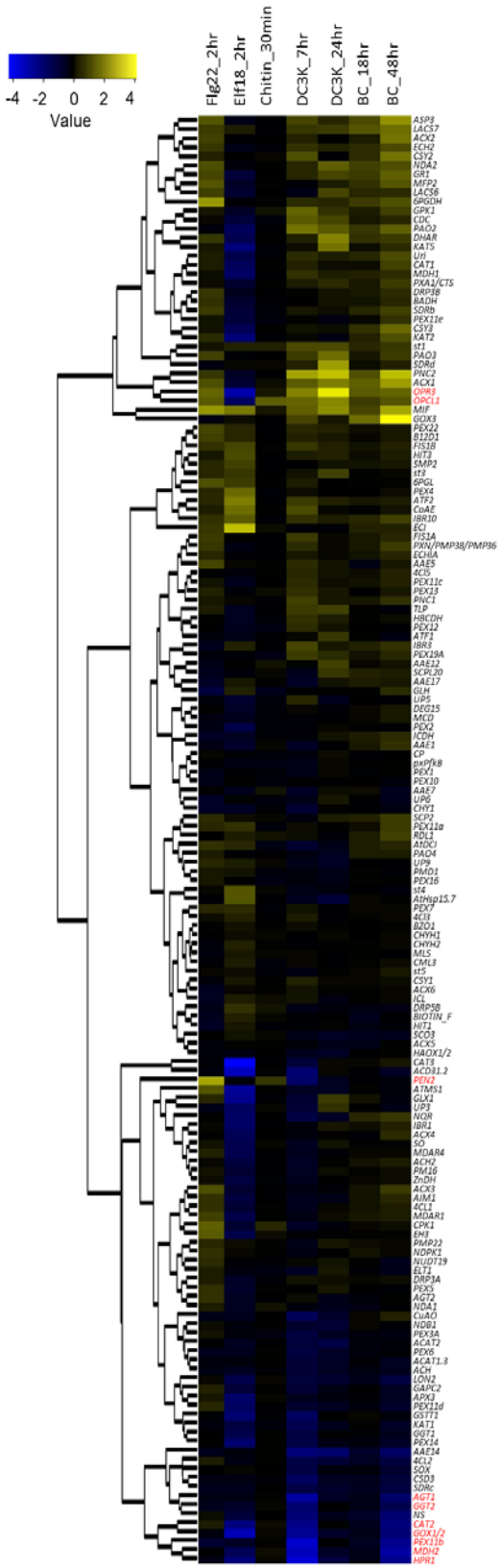

Figure 2.3. Heatmap of transcript levels of peroxisomal genes under biotic stresses.

Figure 2.3. (cont'd)

Expression values are log2 normalized fold changes against untreated plants. Genes discussed in the text are in red.

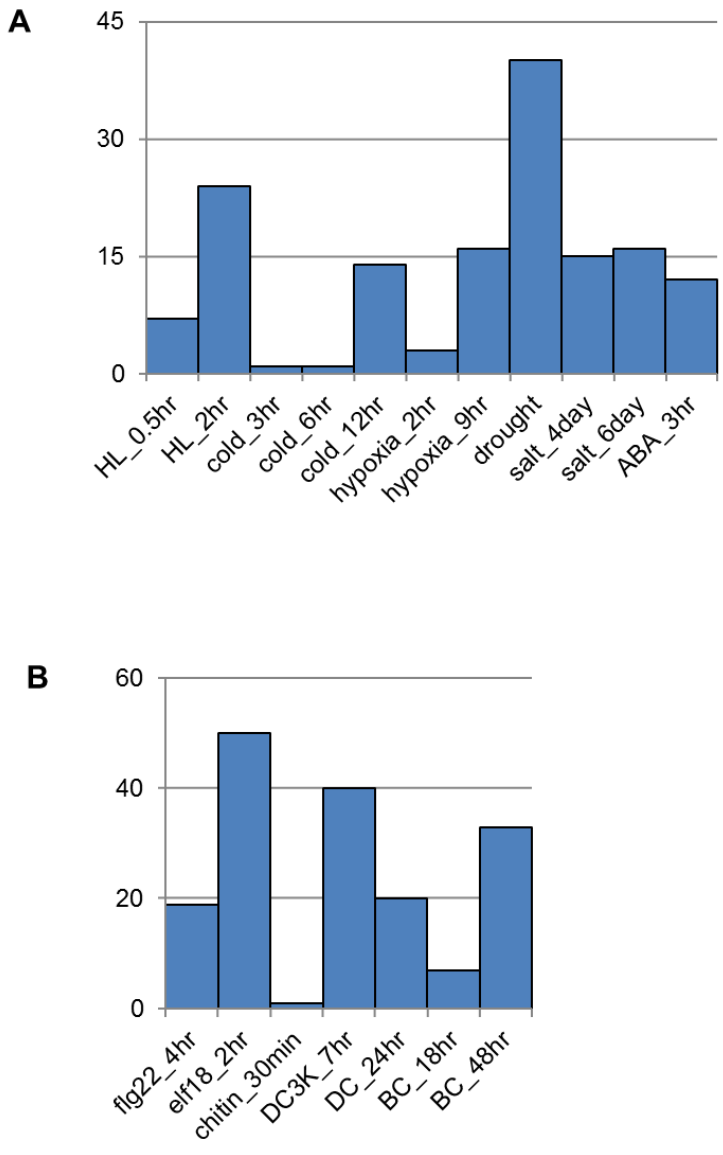

Figure 2.4. Total number of peroxisomal genes with significantly changed expression levels in response to stresses. (A) Abiotic stresses. (B) Biotic stresses. Genes that have log2 normalized fold change >1 or <-1 are considered as significantly regulated.

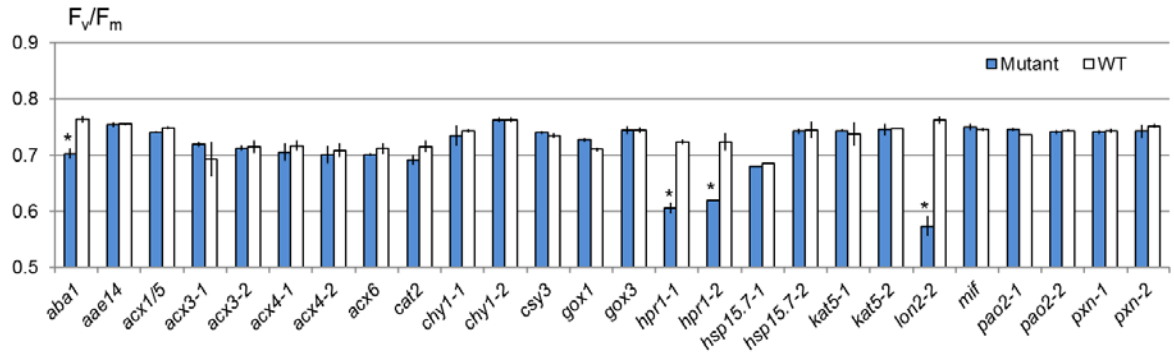

Figure 2.5. F_v/F_m of the selected peroxisomal mutants after drought treatment.

Mutants and wild type plants were grown in the same pot. The *aba1* mutant (salk_059469) was used as a positive control. Two biological replicates were used for each genotype. Asterisk indicates p-value < 0.01 in Student's *t* test.

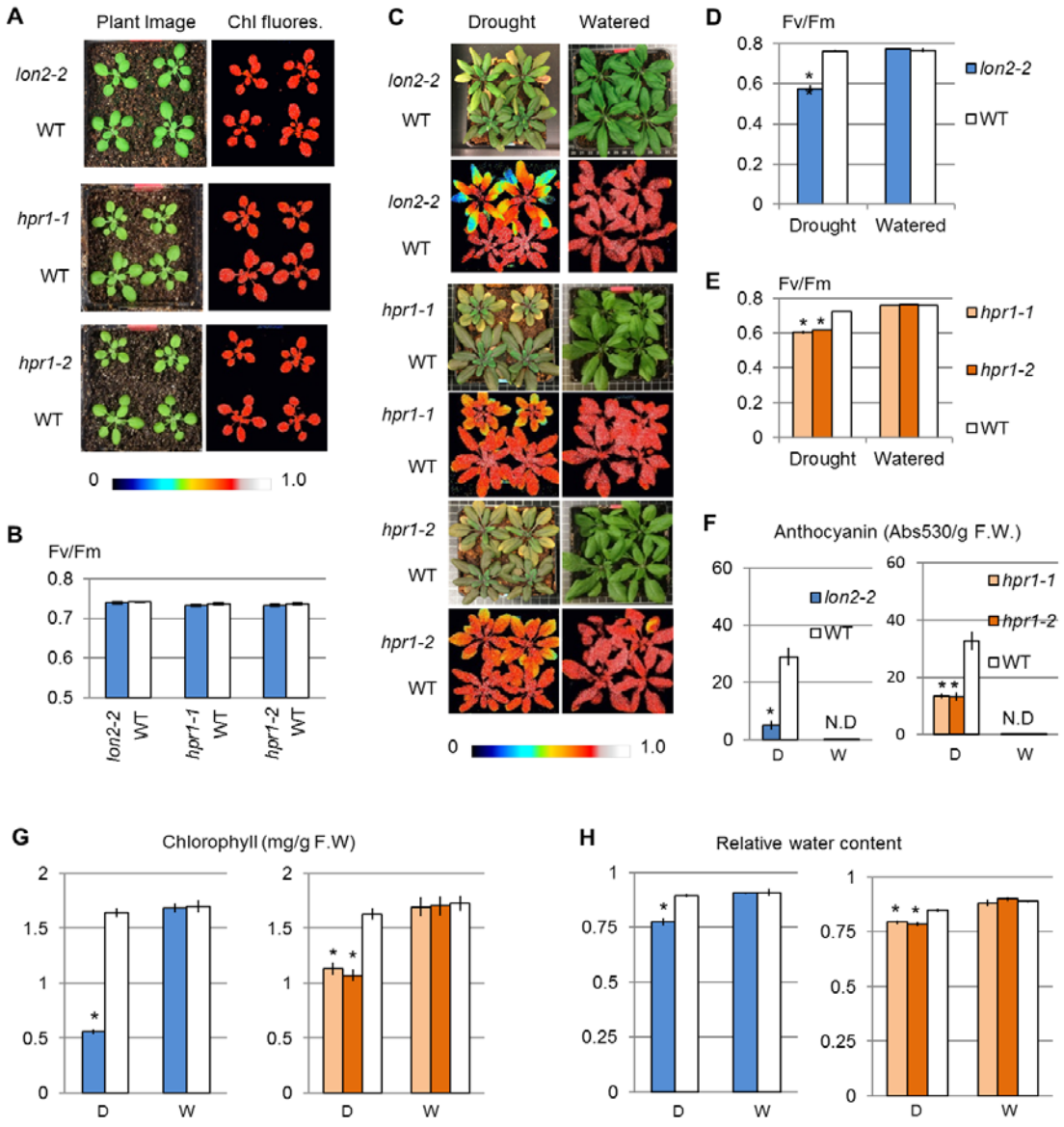

Figure 2.6. Drought resistance phenotypes of *lon2* and *hpr1* mutants.

(A) Images of plants (left) and color-coded chlorophyll fluorescence that indicates F_v/F_m values (right). (B) F_v/F_m comparison between mutants and wild type. Four biological replicates of each genotype were used. No significant difference in F_v/F_m was observed. (C) Plant images and color-coded chlorophyll fluorescence images that indicate F_v/F_m values. (D-E) F_v/F_m comparison between mutants and wild type. Two biological

Figure 2.6. (cont'd)

replicates were used for each genotype under each condition. Asterisk, $p < 0.01$ in Students' *t* test. (F-H) Quantification of anthocyanin (F), chlorophyll (G), and relative water content (H) in mutants and wild type plants. Three biological replicates were used for each genotype under each condition. Asterisk indicates $p < 0.01$ in Students' *t* test; N.D, not detectable; D, drought; W, watered.

Table 2.1. Microarray datasets used in this study

Abbreviation in heatmap/figure legend	Dataset series number	Experiment design and description of used dataset	Reference or link
Developmental			
Abbreviation in Heatmap	Stage#	Stage description	All data for Developmental stages were downloaded from AtGenExpress: http://arabidopsis.org/servlets/TairObject?type=expression_set&id=1006710873
seedling_cotyledon	1	ATGE_1 development baseline Wt cotyledons 7 days continuous light soil	
seedling_hypocotyl	2	ATGE_2 development baseline Wt hypocotyl 7 days continuous light soil	
seeding_leaves1+2	5	ATGE_5 development baseline Wt leaves 1 + 2 7 days continuous light soil	
adult_leaves	15	ATGE_15 development baseline Wt rosette leaf # 8 17 days continuous light soil	
senescing leaves	25	ATGE_25 development baseline Wt senescing leaves 35 days continuous light soil	
Flower	39	ATGE_39 development baseline Wt flowers stage 15 21+ days continuous light soil	
silique_stage3	76	ATGE_76 seed & silique development Wt siliques, w/ seeds stage 3; mid globular to early heart embryos 8 wk long day (16/8) soil	
silique_stage4	77	ATGE_77 seed & silique development Wt siliques, w/ seeds stage 4; early to late heart embryos 8 wk long day (16/8) soil	
silique_stage5	78	ATGE_78 seed & silique development Wt siliques, w/ seeds stage 5; late heart to mid torpedo embryos 8 wk long day (16/8) soil	
seed_stage6	79	ATGE_79 seed & silique development Wt seeds, stage 6, w/o siliques; mid to late torpedo embryos 8 wk long day (16/8) soil	

Table 2.1. (cont'd)

seed_stage7	81	ATGE_81 seed & silique development Wt seeds, stage 7, w/o siliques; late torpedo to early walking-stick embryos 8 wk long day (16/8) soil	
seed_stage8	82	ATGE_82 seed & silique development Wt seeds, stage 8, w/o siliques; walking-stick to early curled cotyledons embryos 8 wk long day (16/8) soil	
seed_stage9	83	ATGE_83 seed & silique development Wt seeds, stage 9, w/o siliques; curled cotyledons to early green cotyledonsembryos 8 wk long day (16/8) soil	
seed_stage10	84	ATGE_84 seed & silique development Wt seeds, stage 10, w/o siliques; green cotyledons embryos 8 wk long day (16/8) soil	
abiotic stress			
HL_0.5hr, HL_2hr	E-MTAB-403	Col-0 plants were grown in growth chambers for 3.5 weeks. Plant leaf tissue was incubated for at least 6 h in a LL growth chamber (light intensity was 65 µmol photons /m^2·s, 22 °C) and then collected as control sample. The leaf tissue was exposed for 0.5 hr and 2 hr to light with an intensity of 1,300 µmol photons /m^2·s, (22 °C).	Jung, H.S., Crisp, P.A., Estavillo, G.M., Cole, B., Hong, F., Mockler, T.C., Pogson, B.J., and Chory, J. (2013). Subset of heat-shock transcription factors required for the early response of Arabidopsis to excess light. Proc Natl Acad Sci USA 110, 14474-14479.
cold_3hr, cold_6hr, cold_24hr	GSE3326	The wild-type seeds were plated on MS agar plates supplemented with 3% sucrose. Seedlings were grown at 22℃ with 16-h-light and 8-h-dark cycles for 2 weeks before being harvested. To avoid variations due to circadian rhythm, all cold treatments were started at 12 PM at 0℃ under light and continued for 0 (untreated control), 3, 6, and 24 h.	Lee, B.H., Henderson, D.A., and Zhu, J.K. (2005). The Arabidopsis cold-responsive transcriptome and its regulation by ICE1. Plant Cell 17, 3155-3175.

Table 2.1. (cont'd)

hypoxia_2hr, hypoxia_9hr	GSE9719	Seedlings grown in vertical orientation for 7–14 d on solid Murashige–Skoog medium containing 1% sucrose were treated with mixed gases in humidified chambers. Seedlings were deprived of O_2 as well as CO_2 in chambers which were purged with 99.99% Ar(gas), as control. Alternatively, treatment was with 2% O2, 370 ppm CO2, in a balance of N2 for 2hr and 9hr.	Sorenson, R., and Bailey-Serres, J. (2014). Selective mRNA sequestration by OLIGOURIDYLATE-BINDING PROTEIN 1 contributes to translational control during hypoxia in Arabidopsis. Proc Natl Acad Sci USA 111, 2373-2378.
Drought	GSE10643	Wild-type plants were grown under normal watering conditions for 24 days and then stressed by completely depriving of irrigation for 10 days.	Zhang, Y., Xu, W., Li, Z., Deng, X.W., Wu, W., and Xue, Y. (2008). F-box protein DOR functions as a novel inhibitory factor for abscisic acid-induced stomatal closure under drought stress in Arabidopsis. Plant Physiol 148, 2121-2133.
salt_4day	GSE53308	Wild type Arabidopsis Col-0 plants were grown hydroponically and treated with or without 150mM NaCl and harvested after 4 days of treatment.	Allu, A.D., Soja, A.M., Wu, A., Szymanski, J., and Balazadeh, S. (2014). Salt stress and senescence: identification of cross-talk regulatory components. J Exp Bot 65, 3993-4008.
salt_6day	GSE16765	Arabidopsis Col-0 were grown in the growth chamber in the absence and presence of salt stress. Plants of 2 weeks were subject to salt treatment for 6 days and were used for RNA extraction.	Chan, Z., Grumet, R., and Loescher, W. (2011). Global gene expression analysis of transgenic, mannitol-producing, and salt-tolerant Arabidopsis thaliana indicates widespread changes in abiotic and biotic stress-related genes. J Exp Bot 62, 4787-4803.
ABA	RIKEN-GODA17& 21	Wild-type seedlings were treated with ABA and mock for 3 hr.	Nemhauser, J.L., Hong, F., and Chory, J. (2006). Different plant hormones regulate similar processes through largely nonoverlapping transcriptional responses. Cell *126*, 467-475. http://arabidopsis.org/servlets/TairObject?type=hyb_descr_collection&id=1007964750

Table 2.1. (cont'd)

biotic stress			
flg22_4hr	GSE11807	Six-week old Col-0 plants were infiltrated with 1 µM flg22 or ddH2O and harvested 4 hours later. Total RNA was extracted, biotinlabeled and hybridized to the Affymetrix ATH1 chip. Gene expression values from treated sample were compared to that of mock-treated sample	Bethke G, Unthan T, Uhrig JF, Poschl Y, Gust AA, et al. (2009) Flg22 regulates the release of an ethylene response factor substrate from MAP kinase 6 in Arabidopsis thaliana via ethylene signaling. Proc Natl Acad Sci USA 106: 8067-8072.
elf18_2hr	GSE34047	3-week old Col-0 plants were infiltrated with 10 µM elf18 or mock and harvested after 2 hrs. Three biological replicates were included	Pajerowska-Mukhtar KM, Wang W, Tada Y, Oka N, Tucker CL, et al. (2012) The HSF-like transcription factor TBF1 is a major molecular switch for plant growth-to-defense transition. Curr Biol 22: 103-112.
chitin_30min	GSE28227	2-week old MS medium-grown seedlings were treated with chitooctaose at a final concentration of 1 µM for 30 minutes. The controls were similarly treated with an equivalent amount of ddH2O. Seedlings were harvested for RNA isolation. Three biological replicates were conducted for the experiment	http://www.ncbi.nlm.nih.gov/geo/query/acc.cgi?acc=GSE28227
DC3K_7hr; DC3K_24hr	GSE5520	4-week old Arabidopsis leaves were treated with bacterial pathogen Pseudomonas syringae pv. Tomato DC3000. The first leaf sample was treated with bacteria at the concentration of 10*8 bacteria/ml and sampled 7 hours later, and the second leaf sample was treated with bacteria at the concentration of 10*6 bacteria/ml and sampled 24 hours later	Thilmony R, Underwood W, He SY (2006) Genome-wide transcriptional analysis of the Arabidopsis thaliana interaction with the plant pathogen Pseudomonas syringae pv. tomato DC3000 and the human pathogen Escherichia coli O157:H7. Plant J 46: 34-53.
BC_18hr; BC_48hr	GSE5684	Adult Col-0 leaves were inoculated by placing 4 5-µl drops of 5x10*5 Botrytis cinerea spore solution. Control leaves were spotted with droplets of 24g/L potato dextrose broth medium. Samples were collected at 18 hrs and 48 hrs after inoculation.	http://www.ncbi.nlm.nih.gov/geo/query/acc.cgi?acc=GSE5684

Table 2.2. Arabidopsis peroxisomal gene list

160 peroxisomal genes have expression data and were used for co-expression analysis. The last eight genes do not have microarray probes.

Order	Gene name	A.t Locus	Microarray probe ID	Annotation
1	*ACH2*	AT1G01710	261560_at	acyl-CoA thioesterase family protein
2	*PEX11c*	AT1G01820	261534_at	PEX11c, peroxisome elongation
3	*PEX6*	AT1G03000	263170_at	peroxin6
4	*st4*	AT1G04290	263661_at	thioesterase family protein
5	*KAT1*	AT1G04710	264608_at	3-keto-acyl-CoA thiolase 1
6	*ACX3*	AT1G06290	260789_s_at	acyl-CoA oxidase 3
7	*ACX6*	AT1G06310	259419_at	acyl-CoA oxidase 6
8	*ACD31.2*	AT1G06460	262629_at	alpha-crystallin domain 31.2
9	*NDA1*	AT1G07180	256057_at	alternative NAD(P)H dehydrogenase 1
10	*GLX1*	AT1G11840	264372_at	glyoxalase i homolog 1
11	*GAPC2*	AT1G13440	259361_at	glyceraldehyde-3-phosphate dehydrogenase
12	*UP6*	AT1G16730	255763_at	unknown protein 6
13	*DHAR*	AT1G19570	261149_s_at	dehydroascorbate reductase 1
14	*4Cl3*	AT1G20480	259569_at	4-coumaroyl-CoA synthase family protein
15	*OPCL1*	AT1G20510	259518_at	opc-8:0 -CoA ligase1
16	*AAE1*	AT1G20560	259545_at	acyl-activating enzyme 1
17	*CAT3*	AT1G20620	259544_at	catalase 3
18	*CAT1*	AT1G20630	259517_at	catalase 1
19	*ATF1*	AT1G21770	262499_at	acyl-CoA n-acyltransferases
20	*GGT1*	AT1G23310	262988_at	alanine-2-oxoglutarate aminotransferase 1
21	*DEG15*	AT1G28320	245687_at	Endopeptidase
22	*UP9*	AT1G29120	260889_at	unknown protein 9
23	*PEX7*	AT1G29260	260844_at	peroxin 7

Table 2.2. (cont'd)

24	*AAE14*	AT1G30520	261801_at	acyl-activating enzyme 14
25	*PEX11a*	AT1G47750	261739_at	PEX11a, peroxisome elongation
26	*st1*	AT1G48320	262237_at	thioesterase family protein
27	*pxPfkB*	AT1G49350	262398_at	pfkb-type carbohydrate kinase family protein
28	*NQR*	AT1G49670	261601_at	involved in oxidative stress tolerance.
29	*ICDH*	AT1G54340	262962_at	isocitrate dehydrogenase
30	*NS*	AT1G60550	264920_at	naphthoate synthase
31	*ECI*	AT1G65520	264627_at	enoyl-CoA hydratase/isomerase family protein
32	*PAO4*	AT1G65840	262933_at	polyamine oxidase 4
33	*BZO1*	AT1G65880	261915_at	benzoate-CoA ligase
34	*AAE12*	AT1G65890	261922_at	acyl-activating enzyme 12
35	*HPR1*	AT1G68010	260014_at	hydroxypyruvate reductase 1
36	*GGT2*	AT1G70580	260309_at	glutamate:glyoxylate aminotransferase 2
37	*ECH2*	AT1G76150	261771_at	monofunctional enoyl-CoA hydratase 2
38	*ATF2*	AT1G77540	259706_at	histone acetyltransferase
39	*PEX2*	AT1G79810	261348_at	peroxin2
40	*SMP2*	AT2G02510	267239_at	NADH dehydrogenase
41	*OPR3*	AT2G06050	265530_at	OPDA-reductase 3
42	*AGT1*	AT2G13360	263350_at	alanine:glyoxylate aminotransferase
43	*DRP3B*	AT2G14120	263278_at	dynamin-related protein 3B
44	*MDH1*	AT2G22780	266457_at	peroxisomal NAD-malate dehydrogenase 1
45	*SOX*	AT2G24580	263788_at	sarcosine oxidase family protein
46	*Uri*	AT2G26230	267374_at	uricase/urate oxidase putative
47	*PEX10*	AT2G26350	267433_at	peroxin 10
48	*CoAE*	AT2G27490	265637_at	dephospho-CoA kinase
49	*st5*	AT2G29590	266298_at	thioesterase family protein

Table 2.2. (cont'd)

50	*NDA2*	AT2G29990	266835_at	alternative NAD(P)H dehydrogenase 2
51	*CHYH1*	AT2G30650	267571_at	3-hydroxyisobutyryl-coenzyme a hydrolase
52	*CHYH2*	AT2G30660	267572_at	3-hydroxyisobutyryl-coenzyme a hydrolase
53	*UP3*	AT2G31670	263449_at	unknown protein 3
54	*KAT2*	AT2G33150	245168_at	3-keto-acyl-CoA thiolase 2
55	*ACX5*	AT2G35690	265843_at	acyl-CoA oxidase 5
56	*GLH*	AT2G38180	267096_at	gdsl-motif lipase/hydrolase family protein
57	*PXN/PMP38/PMP36*	AT2G39970	267363_at	peroxisomal membrane protein 36
58	*PM16*	AT2G41790	260554_at	peptidase m16 family protein
59	*CuAO*	AT2G42490	265882_at	copper amine oxidase
60	*CSY3*	AT2G42790	263986_at	citrate synthase 3
61	*PAO2*	AT2G43020	265244_at	polyamine oxidase 2
62	*PEN2*	AT2G44490	267392_at	o-glycosyl compounds hydrolase
63	*PEX16*	AT2G45690	267512_at	peroxin 6
64	*PEX11d*	AT2G45740	266925_at	PEX11d, peroxisome elongation
65	*SO*	AT3G01910	258948_at	sulfite oxidase
66	*SDRc*	AT3G01980	258976_at	short-chain dehydrogenase/reductase (sdr) family protein
67	*6PGDH*	AT3G02360	256328_at	6-phosphogluconate dehydrogenase family protein
68	*PEX19A*	AT3G03490	259052_at	peroxin 19-1
69	*PEX12*	AT3G04460	258627_at	peroxin 22
70	*PNC1*	AT3G05290	259306_at	peroxisomal adenine nucleotide carrier 1
71	*LACS6*	AT3G05970	258563_at	long-chain acyl-CoA synthetase 6
72	*IBR3*	AT3G06810	258525_at	acyl-CoA dehydrogenase
73	*MFP2*	AT3G06860	258555_at	multifunctional protein 2
74	*CML3*	AT3G07490	259064_at	calcium ion binding

Table 2.2. (cont'd)

75	*PEX13*	AT3G07560	259068_at	peroxin 13
76	*SDRb*	AT3G12800	257687_at	short-chain dehydrogenase
77	*HAOX1/2*	AT3G14130, AT3G14150	257004_s_at	putative glycolate oxidase
78	*GOX1/2*	AT3G14415, AT3G14420	258359_s_at	glycolate oxidase
79	*HBCDH*	AT3G15290	257052_at	3-hydroxybutyryl-CoA dehydrogenase, putative
80	*AAE7*	AT3G16910	257880_at	acyl-activating enzyme 7
81	*GPK1*	AT3G17420	257295_at	glyoxysomal protein kinase 1
82	*PEX3A*	AT3G18160	258150_at	peroxin 3a
83	*SCO3*	AT3G19570	257047_at	snowy cotyledon3
84	*DRP5B*	AT3G19720	257045_at	dynamin-related protein 5B
85	*ICL*	AT3G21720	257947_at	isocitrate lyase
86	*PEX22*	AT3G21865	257953_at	peroxin 22
87	*GR1*	AT3G24170	257252_at	glutathione-disulfide reductase 1
88	*MDAR4*	AT3G27820	257227_at	monodehydroascorbate reductase 4
89	*PEX11b*	AT3G47430	252411_at	PEX11b, peroxisome elongation
90	*B12D1*	AT3G48140	252348_at	senescence-associated protein
91	*BADH*	AT3G48170	252354_at	betaine aldehyde dehydrogenase
92	*MIF*	AT3G51660	252076_at	macrophage migration inhibitory factor family protein
93	*ACX4*	AT3G51840	246304_at	acyl-CoA oxidase 4
94	*MDAR1*	AT3G52880	252024_at	monodehydroascorbate reductase
95	*SDRd*	AT3G55290	251780_s_at	short-chain dehydrogenase/reductase (sdr) family protein]
96	*CDC*	AT3G55640	251757_at	mitochondrial substrate carrier family protein
97	*ZnDH*	AT3G56460	251687_at	zinc-binding dehydrogenase
98	*HIT3*	AT3G56490	251707_at	histidine triad family protein

Table 2.2. (cont'd)

99	*FIS1A*	AT3G57090	251659_at	fission protein 1A
100	*CP*	AT3G57810	251558_at	OTU-like cysteine protease
101	*CSY1*	AT3G58740	251540_at	citrate synthase 1
102	*CSY2*	AT3G58750	251541_at	citrate synthase 2
103	*PMD1*	AT3G58840	251556_at	peroxisome and mitochodria division protein
104	*PAO3*	AT3G59050	251505_at	polyamine oxidase 3
105	*PEX11e*	AT3G61070	251352_at	PEX11e, peroxisome elongation
106	*st3*	AT3G61200	251307_at	thioesterase family protein
107	*ACH*	AT4G00520	255679_at	acyl-CoA thioesterase family protein
108	*EH3*	AT4G02340	255525_at	putative epoxide hydrolase
109	*MCD*	AT4G04320	255327_at	malonyl-CoA decarboxylase family protein
110	*PMP22*	AT4G04470	255338_at	peroxisomal membrane protein 22
111	*4CL1*	AT4G05160	255263_at	putative 4-coumaroyl-CoA synthase
112	*IBR1*	AT4G05530	255240_at	short-chain dehydrogenase
113	*NDPK1*	AT4G09320	255089_at	nucleoside diphosphate kinase 1
114	*SCPL20*	AT4G12910	254791_at	serine carboxypeptidase-like 20
115	*IBR10*	AT4G14430	245359_at	enoyl-CoA hydratase/isomerase family protein
116	*ECHIA*	AT4G16210	245484_at	enoyl-CoA hydratase/isomerase family protein
117	*HIT1*	AT4G16566	245337_at	histidine triad family protein
118	*ACX1*	AT4G16760	245249_at	acyl-CoA oxidase 1
119	*GOX3*	AT4G18360	254630_at	putative glycolate oxidase
120	*4Cl5*	AT4G19010	254600_at	4-coumaroyl-coa synthase family protein
121	*NDB1*	AT4G28220	253810_at	NAD(P)H dehydrogenase b
122	*AIM1*	AT4G29010	253759_at	abnormal inflorescence meristem1 , enoyl-CoA hydratase
123	*DRP3A*	AT4G33650	253306_at	dynamin-related protein 3A
124	*APX3*	AT4G35000	253223_at	ascorbate peroxidase 3

Table 2.2. (cont'd)

125	*CAT2*	AT4G35090	253174_at	catalase 2
126	*RDL1*	AT4G36880	246250_at	cysteine-type peptidase
127	*AGT2*	AT4G39660	252855_at	alanine:glyoxylate aminotransferase 2
128	*PXA1/CTS*	AT4G39850	252830_at	peroxisomal ABC transporter 1
129	*MLS*	AT5G03860	250868_at	malate synthase
130	*BIOTIN_F*	AT5G04620	250837_at	7-keto-8-aminopelargonic acid synthase
131	*CPK1*	AT5G04870	246955_at	calcium-dependent protein kinase isoform
132	*PEX1*	AT5G08470	250520_at	peroxin 1, ATPase
133	*MDH2*	AT5G09660	250498_at	peroxisomal NAD-malate dehydrogenase 2
134	*ASP3*	AT5G11520	250385_at	aspartate aminotransferase 3
135	*ELT1*	AT5G11910	250299_at	esterase/lipase/thioesterase family protein
136	*FIS1B*	AT5G12390	245178_at	mitochodria and peroxisome fission protein
137	*AAE5*	AT5G16370	250114_s_at	acyl-activating enzyme 5
138	*ATMS1*	AT5G17920	259343_s_at	methionine synthesis 1
139	*CSD3*	AT5G18100	250016_at	copper superoxide dismutase 3
140	*NUDT19*	AT5G20070	246126_at	nudix hydrolase homolog 19
141	*AAE17*	AT5G23050	249869_at	acyl-activating enzyme 17
142	*6PGL*	AT5G24400	249733_at	6-phosphoglucunolactonase
143	*PEX4*	AT5G25760	246862_at	peroxin4, ubiquitin-protein ligase
144	*PNC2*	AT5G27520	246779_at	peroxisomal adenine nucleotide carrier 2
145	*LACS7*	AT5G27600	246789_at	long-chain acyl-CoA synthetase 7
146	*AtHsp15.7*	AT5G37670	249575_at	15.7 kda class i-related small heat shock protein-like
147	*GSTT1*	AT5G41210	249291_at	glutathione s-transferase (class theta) 1
148	*SCP2*	AT5G42890	249178_at	sterol carrier protein 2
149	*AtDCI*	AT5G43280	249145_at	delta(3,5),delta(2,4)-dienoyl-CoA isomerase 1
150	*UP5*	AT5G44250	249064_at	unknown protein 5

Table 2.2. (cont'd)

151	*LON2*	AT5G47040	248818_at	lon protease homolog 2
152	*ACAT1.3*	AT5G47720	248779_at	putative acetyl-CoA c-acyltransferase
153	*ACAT2*	AT5G48230	248690_at	acetoacetyl-CoA thiolase 2
154	*KAT5*	AT5G48880	248625_at	3-keto-acyl-CoA thiolase 5
155	*PEX5*	AT5G56290	248010_at	peroxin 5, peroxisome matrix targeting signal-1 binding protein
156	*TLP*	AT5G58220	247858_at	transthyretin-like protein
157	*PEX14*	AT5G62810	247422_at	peroxin 14
158	*4CL2*	AT5G63380	247380_at	4-coumarate-CoA ligase family protein
159	*ACX2*	AT5G65110	247176_at	acyl-CoA oxidase 2
160	*CHY1*	AT5G65940	247117_at	beta-hydroxyisobutyryl-CoA hydrolase 1
161	*AAE18*	AT1G48635	no probe	acyl-activating enzyme 18
162	*PEX3B*	AT1G50510	no probe	peroxin 3B
163	*IndA*	AT1G55320	no probe	indigoidine synthase a family protein
164	*NADK3*	AT1G78590	no probe	NADH kinase
165	*APEM9*	AT3G10572	no probe	required for both pts1- and pts2-dependent protein transport
166	*PEX19B*	AT5G17550	no probe	peroxin 19B
167	*MIA40*	AT5G23395	no probe	mitochondrial intermembrane space assembly machinery 40
168	*HIT2*	AT5G48545	no probe	histidine triad nucleotide-binding 3

Table 2.3. Mutants used in the primary screen for drought tolerance

KO, knock-out; KD, knock-down。

Mutant	SALK_ID	Gene expression	Transcriptional regulation by drought, log_2(FC)	Reference
aba1	SALK_059469	KO	Control	(Riboni et al., 2013)
hpr1-1	SALK_067724	KO	limited up-regulation, 0.44	(Timm et al., 2008)
hpr1-2	SALK_143584	KO		
cat2	SALK_076998	KO	up-regulated by drought, 1.70	(Shibata et al., 2013)
gox1	SAIL_177_G11	KO	limited up-regulation by drought, 0.42	(Rojas et al., 2012)
gox3	SALK_020909	KO	up-regulated by drought, 1.10	(Quan et al., 2013)
hsp15.7-1	SALK_038951	KD	up-regulated by drought, 2.05	(Ma, 2005)
hsp15.7-2	SALK_107711	KO		
pao2-1	SALK_046281	KO	down-regulated by drought, -1.37	(Kim et al., 2014)
pao2-2	SALK_062035			
pxn-1	SALK_038951	KO	limited up-regulation by drought, 0.03	(Bernhardt et al., 2012)
pxn-2	SALK_107711	KD		
csy3	SALK_076319	KO	up-regulated by drought, 2.23	
Mif	SALK_037373		up-regulated by drought, 1.79	
lon2-2	SALK_043857	KO	up-regulated by ABA/drought, 1.98/0.51	(Lingard and Bartel, 2009)
kat5-1	SALK_132871		down-regulated by drought, -1.93	
kat5-2	SALK_144464	KD		(Wiszniewski, 2011)
acx3-1	SALK_128947		limited up-regulation by drought, 0.05	
acx3-2	SALK_044956	KO		(Adham et al., 2005)
acx4-1	SALK_000879	KO	up-regulated by drought, 1.21	(Adham et al., 2005)
acx4-2	SALK_065013	KO		

Table 2.3. (cont'd)

acx6	SALK_023093	KO	limited up-regulation by drought, 0.01	(Adham et al., 2005)
acx1/5	SALK_041464/SALK_009998	KO	up-regulated by drought, 1.38/0.51	(Schilmiller et al., 2007)
aae14	SALK_038308		down-regulated by drought, -2.27	
chy1-1	SALK_025417	KO	limited up-regulation by drought, 0.82	(Ibdah and Pichersky, 2009)
chy1-2	SALK_102725			

REFERENCES

REFERENCES

Adham, A.R., Zolman, B.K., Millius, A., and Bartel, B. (2005). Mutations in Arabidopsis acyl-CoA oxidase genes reveal distinct and overlapping roles in beta-oxidation. Plant J *41*, 859-874.

Attaran, E., Major, I.T., Cruz, J.A., Rosa, B.A., Koo, A.J., Chen, J., Kramer, D.M., He, S.Y., and Howe, G.A. (2014). Temporal Dynamics of Growth and Photosynthesis Suppression in Response to Jasmonate Signaling. Plant Physiol *165*, 1302-1314.

Bauwe, H., Hagemann, M., and Fernie, A.R. (2010). Photorespiration: players, partners and origin. Trends Plant Sci *15*, 330-336.

Bednarek, P., Pislewska-Bednarek, M., Svatos, A., Schneider, B., Doubsky, J., Mansurova, M., Humphry, M., Consonni, C., Panstruga, R., Sanchez-Vallet, A., *et al.* (2009). A glucosinolate metabolism pathway in living plant cells mediates broad-spectrum antifungal defense. Science *323*, 101-106.

Bernhardt, K., Wilkinson, S., Weber, A.P., and Linka, N. (2012). A peroxisomal carrier delivers NAD(+) and contributes to optimal fatty acid degradation during storage oil mobilization. Plant J *69*, 1-13.

Browse, J. (2009). Jasmonate passes muster: a receptor and targets for the defense hormone. Annu Rev Plant Biol *60*, 183-205.

Cassin-Ross, G., and Hu, J. (2014a). A simple assay to identify peroxisomal proteins involved in 12-oxo-phytodienoic acid metabolism. Plant Signal Behav *9*, e29464.

Cassin-Ross, G., and Hu, J. (2014b). Systematic phenotypic screen of Arabidopsis peroxisomal mutants identifies proteins involved in beta-oxidation. Plant Physiol *166*, 1546-1559.

Clay, N.K., Adio, A.M., Denoux, C., Jander, G., and Ausubel, F.M. (2009). Glucosinolate metabolites required for an Arabidopsis innate immune response. Science *323*, 95-101.

Coca, M., and San Segundo, B. (2010). AtCPK1 calcium-dependent protein kinase mediates pathogen resistance in *Arabidopsis*. Plant J *63*, 526-540.

Dammann, C., Ichida, A., Hong, B., Romanowsky, S.M., Hrabak, E.M., Harmon, A.C., Pickard, B.G., and Harper, J.F. (2003). Subcellular targeting of nine calcium-dependent protein kinase isoforms from Arabidopsis. Plant Physiol *132*, 1840-1848.

Del Rio, L.A. (2011). Peroxisomes as a cellular source of reactive nitrogen species signal molecules. Arch Biochem Biophys *506*, 1-11.

Desai, M., and Hu, J. (2008). Light induces peroxisome proliferation in Arabidopsis seedlings through the photoreceptor phytochrome A, the transcription factor HY5 HOMOLOG, and the peroxisomal protein PEROXIN11b. Plant Physiol *146*, 1117-1127.

Farmer, L.M., Rinaldi, M.A., Young, P.G., Danan, C.H., Burkhart, S.E., and Bartel, B. (2013). Disrupting autophagy restores peroxisome function to an Arabidopsis lon2 mutant and reveals a role for the LON2 protease in peroxisomal matrix protein degradation. Plant Cell *25*, 4085-4100.

Gehan, M.A., Greenham, K., Mockler, T.C., and McClung, C.R. (2015). Transcriptional networks - crops, clocks, and abiotic stress. Current opinion in plant biology *24*, 39-46.

Gentleman, R.C., Carey, V.J., Bates, D.M., Bolstad, B., Dettling, M., Dudoit, S., Ellis, B., Gautier, L., Ge, Y., Gentry, J., *et al.* (2004). Bioconductor: open software development for computational biology and bioinformatics. Genome Biol *5*, R80.

Goto-Yamada, S., Mano, S., Nakamori, C., Kondo, M., Yamawaki, R., Kato, A., and Nishimura, M. (2014). Chaperone and protease functions of LON protease 2 modulate the peroxisomal transition and degradation with autophagy. Plant Cell Physiol *55*, 482-496.

Hu, J., Baker, A., Bartel, B., Linka, N., Mullen, R.T., Reumann, S., and Zolman, B.K. (2012). Plant peroxisomes: biogenesis and function. Plant Cell *24*, 2279-2303.

Ibdah, M., and Pichersky, E. (2009). Arabidopsis Chy1 null mutants are deficient in benzoic acid-containing glucosinolates in the seeds. Plant Biol (Stuttg) *11*, 574-581.

Irizarry, R.A., Hobbs, B., Collin, F., Beazer-Barclay, Y.D., Antonellis, K.J., Scherf, U., and Speed, T.P. (2003). Exploration, normalization, and summaries of high density oligonucleotide array probe level data. Biostatistics *4*, 249-264.

Kaur, N., and Hu, J. (2011). Defining the plant peroxisomal proteome: from Arabidopsis to rice. Front Plant Sci *2*, 103.

Kaur, N., Li, J., and Hu, J. (2013). Peroxisomes and photomorphogenesis. Subcell Biochem *69*, 195-211.

Kaur, N., Reumann, S., and Hu, J. (2009a). Peroxisome biogenesis and function. Arabidopsis Book *7*, e0123.

Kaur, N., Reumann, S., and Hu, J. (2009b). Peroxisome biogenesis and function. The Arabidopsis Book *7*, e0123. doi: 0110.1199/tab.0123.

Kim, D.W., Watanabe, K., Murayama, C., Izawa, S., Niitsu, M., Michael, A.J., Berberich, T., and Kusano, T. (2014). Polyamine Oxidase5 Regulates Arabidopsis Growth through Thermospermine Oxidase Activity. Plant Physiol *165*, 1575-1590.

Kotchoni, S.O., and Gachomo, E.W. (2006). The reactive oxygen species network pathways:an essential prerequisite for perception of pathogen attack and the acquired disease resistance in plants. J Biosci *31*, 389-404.

Leonhardt, N., Kwak, J.M., Robert, N., Waner, D., Leonhardt, G., and Schroeder, J.I. (2004). Microarray expression analyses of Arabidopsis guard cells and isolation of a recessive abscisic acid hypersensitive protein phosphatase 2C mutant. Plant Cell *16*, 596-615.

Lingard, M.J., and Bartel, B. (2009). Arabidopsis LON2 is necessary for peroxisomal function and sustained matrix protein import. Plant Physiol *151*, 1354-1365.

Lipka, V., Dittgen, J., Bednarek, P., Bhat, R., Wiermer, M., Stein, M., Landtag, J., Brandt, W., Rosahl, S., Scheel, D., *et al.* (2005). Pre- and postinvasion defenses both contribute to nonhost resistance in Arabidopsis. Science *310*, 1180-1183.

Ma, C. (2005). Subcellular and functional analyses of two small heat shock proteins and protein kinases from peroxisomes of Arabidopsis thaliana L. PhD Dissertatoin.

Ma, C., Haslbeck, M., Babujee, L., Jahn, O., and Reumann, S. (2006). Identification and characterization of a stress-inducible and a constitutive small heat-shock protein targeted to the matrix of plant peroxisomes. Plant Physiol *141*, 47-60.

Maeda, K., Houjyou, Y., Komatsu, T., Hori, H., Kodaira, T., and Ishikawa, A. (2009). AGB1 and PMR5 contribute to PEN2-mediated preinvasion resistance to *Magnaporthe oryzae* in *Arabidopsis thaliana*. Mol Plant Microbe Interact *22*, 1331-1340.

McCartney, A.W., Greenwood, J.S., Fabian, M.R., White, K.A., and Mullen, R.T. (2005). Localization of the tomato bushy stunt virus replication protein p33 reveals a peroxisome-to-endoplasmic reticulum sorting pathway. Plant Cell *17*, 3513-3531.

Okinaka, Y., Yang, C.H., Herman, E., Kinney, A., and Keen, N.T. (2002). The P34 syringolide elicitor receptor interacts with a soybean photorespiration enzyme, NADH-dependent hydroxypyruvate reductase. Mol Plant Microbe Interact *15*, 1213-1218.

Pandey, N., Ranjan, A., Pant, P., Tripathi, R.K., Ateek, F., Pandey, H.P., Patre, U.V., and Sawant, S.V. (2013). CAMTA 1 regulates drought responses in Arabidopsis thaliana. BMC Genomics *14*, 216.

Pieuchot, L., and Jedd, G. (2012). Peroxisome assembly and functional diversity in eukaryotic microorganisms. Annu Rev Microbiol *66*, 237-263.

Pracharoenwattana, I., and Smith, S.M. (2008). When is a peroxisome not a peroxisome? Trends Plant Sci *13*, 522-525.

Quan, S., Switzenberg, R., Reumann, S., and Hu, J. (2010). In vivo subcellular targeting analysis validates a novel peroxisome targeting signal type 2 and the peroxisomal localization of two proteins with putative functions in defense in Arabidopsis. Plant Signal Behav *5*, 151-153.

Quan, S., Yang, P., Cassin-Ross, G., Kaur, N., Switzenberg, R., Aung, K., Li, J., and Hu, J. (2013). Proteome analysis of peroxisomes from etiolated Arabidopsis seedlings identifies a peroxisomal protease involved in beta-oxidation and development. Plant Physiol *163*, 1518-1538.

Queval, G., Issakidis-Bourguet, E., Hoeberichts, F.A., Vandorpe, M., Gakiere, B., Vanacker, H., Miginiac-Maslow, M., Van Breusegem, F., and Noctor, G. (2007). Conditional oxidative stress responses in the Arabidopsis photorespiratory mutant *cat2* demonstrate that redox state is a key modulator of daylength-dependent gene expression, and define photoperiod as a crucial factor in the regulation of H_2O_2-induced cell death. Plant J *52*, 640-657.

Reumann, S. (2004). Specification of the peroxisome targeting signals type 1 and type 2 of plant peroxisomes by bioinformatics analyses. Plant Physiol *135*, 783-800.

Reumann, S., Quan, S., Aung, K., Yang, P., Manandhar-Shrestha, K., Holbrook, D., Linka, N., Switzenberg, R., Wilkerson, C.G., Weber, A.P., *et al.* (2009). In-depth proteome analysis of Arabidopsis leaf peroxisomes combined with in vivo subcellular targeting verification indicates novel metabolic and regulatory functions of peroxisomes. Plant Physiol *150*, 125-143.

Riboni, M., Galbiati, M., Tonelli, C., and Conti, L. (2013). GIGANTEA enables drought escape response via abscisic acid-dependent activation of the florigens and SUPPRESSOR OF OVEREXPRESSION OF CONSTANS. Plant Physiol *162*, 1706-1719.

Rochon, D., Singh, B., Reade, R., Theilmann, J., Ghoshal, K., Alam, S.B., and Maghodia, A. (2014). The p33 auxiliary replicase protein of Cucumber necrosis virus targets peroxisomes and infection induces de novo peroxisome formation from the endoplasmic reticulum. Virology *452*, 133-142.

Rojas, C.M., Senthil-Kumar, M., Wang, K., Ryu, C.M., Kaundal, A., and Mysore, K.S. (2012a). Glycolate oxidase modulates reactive oxygen species-mediated signal transduction during nonhost resistance in *Nicotiana benthamiana* and Arabidopsis. Plant Cell *24*, 336-352.

Rojas, C.M., Senthil-Kumar, M., Wang, K., Ryu, C.M., Kaundal, A., and Mysore, K.S. (2012b). Glycolate oxidase modulates reactive oxygen species-mediated signal transduction during nonhost resistance in Nicotiana benthamiana and Arabidopsis. Plant Cell *24*, 336-352.

Schilmiller, A.L., Koo, A.J., and Howe, G.A. (2007). Functional diversification of acyl-coenzyme A oxidases in jasmonic acid biosynthesis and action. Plant Physiol *143*, 812-824.

Schmid, M., Davison, T.S., Henz, S.R., Pape, U.J., Demar, M., Vingron, M., Scholkopf, B., Weigel, D., and Lohmann, J.U. (2005). A gene expression map of Arabidopsis thaliana development. Nat Genet *37*, 501-506.

Schneider, C.A., Rasband, W.S., and Eliceiri, K.W. (2012). NIH Image to ImageJ: 25 years of image analysis. Nat Methods *9*, 671-675.

Shibata, M., Oikawa, K., Yoshimoto, K., Kondo, M., Mano, S., Yamada, K., Hayashi, M., Sakamoto, W., Ohsumi, Y., and Nishimura, M. (2013). Highly oxidized peroxisomes are selectively degraded via autophagy in Arabidopsis. Plant Cell *25*, 4967-4983.

Sinclair, A.M., Trobacher, C.P., Mathur, N., Greenwood, J.S., and Mathur, J. (2009). Peroxule extension over ER-defined paths constitutes a rapid subcellular response to hydroxyl stress. Plant J *59*, 231-242.

Smith, J.J., and Aitchison, J.D. (2013). Peroxisomes take shape. Nat Rev Mol Cell Biol *14*, 803-817.

Smyth, G.K. (2004). Linear models and empirical bayes methods for assessing differential expression in microarray experiments. Stat Appl Genet Mol Biol *3*, Article3.

Sorhagen, K., Laxa, M., Peterhansel, C., and Reumann, S. (2013). The emerging role of photorespiration and non-photorespiratory peroxisomal metabolism in pathogen defence. Plant Biology *15*, 723-736.

Spoel, S.H., and Dong, X. (2012). How do plants achieve immunity? Defense without specialized immune cells. Nat Rev Immunol *12*, 89-100.

Taler, D., Galperin, M., Benjamin, I., Cohen, Y., and Kenigsbuch, D. (2004). Plant eR genes that encode photorespiratory enzymes confer resistance against disease. Plant Cell *16*, 172-184.

Timm, S., Nunes-Nesi, A., Parnik, T., Morgenthal, K., Wienkoop, S., Keerberg, O., Weckwerth, W., Kleczkowski, L.A., Fernie, A.R., and Bauwe, H. (2008). A cytosolic pathway for the conversion of hydroxypyruvate to glycerate during photorespiration in Arabidopsis. Plant Cell *20*, 2848-2859.

Warnes, G.R., Bolker, B., Bonebakker, L., Gentleman, R., Liaw, W.H.A., Lumley, T., Maechler, M., Magnusson, A., Moeller, S., Schwartz, M., *et al.* (2015). gplots: Various R Programming Tools for Plotting Data. http://cran.r-project.org/web/packages/gplots/index.html.

Westphal, L., Scheel, D., and Rosahl, S. (2008). The *coi1-16* mutant harbors a second site mutation rendering PEN2 nonfunctional. Plant Cell *20*, 824-826.

Willekens, H., Chamnongpol, S., Davey, M., Schraudner, M., Langebartels, C., Van Montagu, M., Inze, D., and Van Camp, W. (1997). Catalase is a sink for H_2O_2 and is indispensable for stress defence in C3 plants. Embo J *16*, 4806-4816.

Wiszniewski, A. (2011). Dissecting functions of members of β-oxidation multi-gene families in Arabidopsis. PhD Dissertatoin.

Xiong, L., Lee, H., Ishitani, M., and Zhu, J.K. (2002). Regulation of osmotic stress-responsive gene expression by the LOS6/ABA1 locus in Arabidopsis. J Biol Chem *277*, 8588-8596.

Yamaguchi-Shinozaki, K., and Shinozaki, K. (2006). Transcriptional regulatory networks in cellular responses and tolerance to dehydration and cold stresses. Annu Rev Plant Biol *57*, 781-803.

Zhu, J.K. (2002). Salt and drought stress signal transduction in plants. Annu Revi Plant Biol *53*, 247-273.

CHAPTER 3

Dissecting the role of peroxisomes in modulating photosynthesis under dynamic light conditions

3.1. Abstract

In plant cells, peroxisomes cooperate with other subcellular compartments such as chloroplasts, mitochondria, lipid bodies and cytoplasm to support cellular functions. Emerging evidence also suggested physical connections between peroxisomes and chloroplasts, leading to the question of how general peroxisomal metabolism affects photosynthesis. To comprehensively investigate the impact of peroxisomes on photosynthesis, a systematic mutant screen was conducted. One hundred and forty-seven mutants of 104 Arabidopsis genes encoding peroxisomal proteins were subjected to an automated screen system, Dynamic Environment Phenotype Imager (DEPI), which measures a suite of photosynthetic parameters continuously and non-invasively. Photosynthetic defects were revealed under dynamically changing light conditions for a subset of peroxisomal mutants. A peroxisomal NAD^+ transporter PXN was identified to play a role in modulating photosynthesis via photorespiration, which suggests that peroxisomal NAD^+ homeostasis is critical for photorespiration under dynamic light condition. In addition, although photorespiration is known to be linked to photosynthesis, detailed molecular mechanisms regarding how the blocking of photorespiration alters photosynthetic efficiency were poorly understood. We have found that the block of photorespiration alters various photosynthetic processes including inhibition of the activity of triose phosphate isomerase (TPI) by the accumulated phosphoglycolate, diminished ATP synthase conductivity, increased proton motive force (*pmf*) and energy-dependent quenching (qE), compromised photosystem integrity, reduced photosystem subunit abundance, induced CEF and less induction of anthocyanin. In summary, our systematic mutant screen identified multiple peroxisomal proteins required for robust

photosynthetic efficiency under dynamically changing light and discovered an additional player, the NAD^+ transporter PXN, in photorespiration. Further characterization of photorespiratory mutants provided a deeper understanding of the connection between photorespiration and photosynthesis. Knowledge gained from this study will enhance our understanding of peroxisome function, photosynthesis and interorganellar communication.

3.2. Introduction

Peroxisomes are small and single-membrane delimited organelles that exist in almost all eukaryotic cells (Fagarasanu et al., 2010; Hu et al., 2012; Pieuchot and Jedd, 2012; Smith and Aitchison, 2013). The peroxisome houses conserved metabolic functions across different kingdoms, such as fatty acid β-oxidation and hydrogen peroxide (H_2O_2) detoxification (Islinger et al., 2012; Schrader and Fahimi, 2008; Waterham and Wanders, 2012). Plant specific metabolism, such as photorespiration, conversion of indole-3-butyric acid (IBA) to indole-3-acetic acid (IAA) and jasmonic acid (JA) biosynthesis, take place in peroxisomes as well (Hu et al., 2012).

Besides the metabolism that exclusively occurs in peroxisomes, peroxisomes also coordinate with other subcellular compartments to support important cellular functions. Numerous studies have shown that subcellular organelles often coordinate in response to and integrating various signals and exchanging metabolites, thereby sustaining optimal plant growth and development (Fu and Dong, 2013; Sulpice and McKeown, 2015; Wang and Wu, 2013). For example, chloroplasts and mitochondria interact with the nucleus through retrograde signaling, in which signals from organelles to nucleus play critical roles in coordinating nuclear gene expression (Chi et al., 2013; Hartl and Finkemeier, 2012). Chloroplast retrograde signals, which are derived from chloroplastic metabolites, redox status and ROS, are critical for chloroplast development and the maintenance of optimal chloroplast function under a series of stress conditions (Chi et al., 2013; Fernandez and Strand, 2008). Mitochondria, another important energy organelle, also use retrograde signaling to coordinate with the nucleus under a variety of environmental perturbations, such as cold, drought and high light (Ng et al., 2013a; Ng et al., 2013b).

Organelles also act in concert in metabolism. In plant cells, photorespiration is a well-known carbon recycling metabolic pathway that requires the collaboration of the chloroplast, peroxisome, mitochondrion and cytosol (Bauwe et al., 2010). A lipase Sugar-Dependent 1 (SDP1), which is critical for efficient lipid mobilization in seed germination, can migrate from peroxisomes to oil bodies through peroxisomal extension, indicating that protein transport complexes may exist between peroxisomes and lipid bodies (Thazar-Poulot et al., 2015). It was also shown that mitochondria-derived vesicles (MDVs) can fuse with peroxisomes for transporting metabolites, proteins and membranes in mammalian cells (McBride and Sedwick, 2014; Neuspiel et al., 2008; Schumann and Subramani, 2008).

Peroxisomes can dynamically interact with other organelles. Microscopic studies revealed that tightly associated membranes exist between peroxisomes and chloroplasts (Oikawa et al., 2015), lipid bodies (Thazar-Poulot et al., 2015) and the endoplasmic reticulum (Mullen and Trelease, 2006), which suggested that interorganellar channels may facilitate protein and metabolite exchange. A recent study reported the light-induced physical interaction between peroxisomes and chloroplasts, which plays a critical role in ensuring efficient interorganellar metabolite flow (Oikawa et al., 2015). Finally, snowy cotyledon 3 (SCO3) is a microtubule-associated peroxisomal protein, which is important for chloroplast biogenesis in the cotyledon and robust photosynthetic efficiency under changed CO_2 conditions in mature plants with an unknown mechanism (Albrecht et al., 2010).

Since emerging evidence suggested the physical and functional connections between peroxisomes and chloroplasts, one of our interests was to study how

peroxisomal metabolism modulates photosynthesis in the chloroplast. Photosynthesis is a principal and complex pathway, which converts sunlight energy to ATP and NADPH for CO_2 fixation and other dark reaction related metabolisms. To explore the interaction between peroxisomal metabolism and photosynthesis at a systems level, a large collection of mutants of genes encoding peroxisomal proteins, as well as a high-throughput photosynthesis phenotyping platform were needed to enable efficient phenotype discovery. Thanks to the recent peroxisomal proteomic analyses followed by *in vivo* subcellular protein targeting verifications, the total number of known peroxisome proteins has been increased to ~170 (Kaur and Hu, 2011; Quan et al., 2010; Quan et al., 2013). The collection of mutants of genes encoding these peroxisomal proteins laid a foundation for various phenotypic assays. For example, our lab has successfully uncovered the involvement of novel peroxisomal proteins in fatty acid β-oxidation, conversion of IBA to IAA and stress response by screening peroxisomal mutants using a series of physiological assays (Cassin-Ross and Hu, 2014; Quan et al., 2013).

Given the complexity and dynamics of photosynthetic processes, a robust assay is needed for the screen. Approaches used to study photosynthesis include chlorophyll fluorescence, absorption spectroscopy, gas exchange and biochemical analyses of photosynthetic complexes (Hunt, 2003; Kügler et al., 1997; Long and Bernacchi, 2003; Tanaka and Makino, 2009). Chlorophyll fluorescence measurement has become a commonly used method because it is non-destructive, quantitative and applicable to high throughput phenotyping (Baker, 2008). Photosynthetic parameters that reflect basic properties of photosynthesis , such as maximum quantum yield (F_v/F_m) of photosynthesis, photosystem II (PSII) operating efficiency (Φ2), non-photochemical quenching (NPQ),

energy-dependent quenching (qE) and photoinhibition quenching (qI), can be measured through this method.

One system that suits our purpose is the recently developed Dynamic Environment Phenotype Imager (DEPI), which allows continuous, highly sensitive, non-invasive and simultaneous measurement of photosynthetic parameters (Attaran et al., 2014; Dutta et al., 2015; Kramer et al., 2013). DEPI can reveal phenotypes that emerge under dynamic light conditions and otherwise may not show under constant light conditions, thus these new phenotypes are called emerging phenotypes (Attaran et al., 2014; Dutta et al., 2015). To acclimate to constantly changing light in the natural environment, plants have evolved sophisticated biophysical, biochemical and physiological strategies to fine tune the balance between photosynthesis and photodamage. For example, plants tend to redistribute chloroplasts to the periphery of cells to minimize light absorption under high light exposure (Kasahara et al., 2002). Activation of NPQ, phosphorylation of light-harvesting complex II (LHCII), and accelerated repair cycle of core subunits in photosystem (PS) I and PSII can together efficiently dissipate and partition excessively absorbed energy under dynamic light conditions (Bellafiore et al., 2005; Eberhard et al., 2008; Fristedt et al., 2009; Niyogi and Truong, 2013). Interruption of the Calvin-Benson-Bassham (CBB) cycle and other dark metabolism can largely affect photosynthetic efficiency (Eberhard et al., 2008). Mutants that are defective in the primary light reaction, the CBB cycle and their regulation can potentially be discovered through the DEPI screen.

3.3. Result

3.3.1. Collecting mutants for genes encoding peroxisomal proteins

Recent advances in Arabidopsis peroxisome studies using proteomics, *in silico* prediction and *in vivo* targeting confirmation identified more than three dozen novel peroxisomal proteins (Quan et al., 2013; Reumann et al., 2009). The number of known peroxisomal proteins in Arabidopsis has been expanded to ~170, which enabled us to start a comprehensive peroxisome-centered analysis and genetic screens for target phenotypes (Cassin-Ross and Hu, 2014). By collecting T-DNA insertion mutants from Arabidopsis Biological Research Center (ABRC, https://abrc.osu.edu/) and other research groups, followed by PCR-based genotyping, our lab has collected 147 homozygous mutants for 104 peroxisomal genes (Table 3.1).

3.3.2. Mutant screen and photosynthetic data analysis

In DEPI system, dynamically changing light conditions are imposed over a 5-day experiment (Figure 3.1A). Simultaneously, Φ2, NPQ, qE and qI are measured at multiple time points across five days. On Day 1, plants were exposed to constant illumination typical of that used in a growth chamber (100 μmol m^{-2} s^{-1}). On Day 2, the light was programmed “sinusoidal” to mimic solar radiation with maximal intensity of 500 μmol m^{-2} s^{-1}. On Day 3, plants were exposed to a regime of fluctuating light to simulate changing light conditions that occur in natural environment, under which strong phenotypes were revealed in mutants defective in photoprotective process (Kulheim et al., 2002; Tikkanen et al., 2012). Light intensity was changed every 30 minutes following the

sinusoidal curve as on Day 2, but with superimposed fluctuations. Each light interval consisted of an 18-min period at an "ambient" light peaking at 500 μmol m^{-2} s^{-1}, followed by an 8-min period of twice the ambient intensity ("fluctuating" intensity). Day 4 was a repeat of Day 1 and Day 5 was a repeat of Day 3.

Photosynthetic parameters from 16, 32, 64, 16 and 64 time points were collected from Day 1 to Day 5, summing up to a total of 192 time points. Using software OLIVER (Tessmer *et al.*, submitted), I generated heatmaps that were linked to each other by mutant name-based linking curves. Each heatmap represents the values of Φ2, NPQ, qE or qI for 147 peroxisomal mutants, as log-fold changes in each mutant relative to the wild-type Col-0 control (Figure 3.1B). The x axis represents the time points across five days, and the y axis represents the screened mutants. In each heatmap, mutants were positioned from top to bottom based on the sum of all values across 5 days (low to high). A subset of mutants that exhibited significantly lower Φ2 was indicated within the black box in heatmap of Φ2 (Figure 3.1B). The corresponding locations of this subset of mutants in each heatmap were indicated by the linking curves. Consistent with the lower Φ2, these mutants showed higher NPQ, as indicated by their position at the bottom of the NPQ heatmap (data for generating heatmaps is in Supplemental Table 1).

The subset of mutants that exhibited significantly reduced Φ2 include: i) peroxisome biogenesis and division mutants *pex14*, *drp5B, drp3A drp3B* double, and *drp3A drp3B drp5B* triple; ii) photorespiratory mutants *hpr1-1*, *hpr1-2*, *gox1-3* and *cat2-1*, and iii) mutants of the NAD^+ transporter PXN, *pxn-1* and *pxn-2* (Figure 3.1C). Only the peroxisomal protein import mutant *pex14*, which is often used as a control for peroxisome function assays, exhibited strong reduce of Φ2 on Day 1. The other mutants

exhibited distinguished phenotypes mainly under dynamic illumination on Day 2, Day 3 and Day 5.

3.3.3. Peroxisomal biogenesis and division mutants exhibited reduced photosynthetic efficiency under various light conditions

To examine the overall impact of peroxisomes on photosynthesis, we first assessed the peroxisome protein import mutant *pex14* and peroxisome division mutants *drp5B*, *drp3A drp3B* and *drp3A drp3B drp5B*, as these mutants should display general defects in peroxisomal functions. PEX14 is a peroxisomal membrane protein required for efficient peroxisome protein targeting and import (Hayashi et al., 2000), and DRP3 and DRP5B are shared factors in the division of mitochondria and peroxisomes (DRP3) (Aung and Hu, 2012; Zhang and Hu, 2009) and peroxisomes and chloroplasts (DRP5B) (Aung and Hu, 2012; Zhang and Hu, 2010).

Not surprisingly, *pex14* showed an up to 30% decrease in Φ2 under constant light on Day 1 (Figure 3.2). Under sinusoidal light on Day 2 and fluctuating light on Day 3, the decrease in Φ2 became more severe, and more energy was dissipated as heat, as indicated by higher NPQ (Figure 3.2). Interestingly, qI, rather than qE, was the major quenching in *pex14*. After a recovery period on Day 4, *pex14* exhibited similar phenotypes as exhibited on Day 3 under the second round of fluctuating light conditions on Day 5 (Figure 3.2).

In the peroxisomal division mutants, photosynthetic performance was similar to that of WT under constant light on Day 1 (Figure 3.3). However, mutants began to show lower Φ2 as light intensity increased to 350 μmol m^{-2} s^{-1} and became more severely

affected under higher intensities. On Day 2 under sinusoidal light, *drp5B* had higher qE, while *drp3A drp3B* and *drp3A drp3B drp5B* had higher qI, which were consistent with an enhanced reduction of Φ2 in the double and triple mutants. Under fluctuating light conditions, which consisted of lower bound "ambient light" and upper bound "fluctuating light", these mutants behaved similarly. All three mutants had lower Φ2, with the triple mutant showing the greatest reduction. NPQ under lower bound ambient light was higher in all mutants than in WT, but NPQ under upper bound fluctuating light was lower in double and triple mutants. A similar pattern was found in qE. Meanwhile, qI was strongly activated under both ambient and fluctuating light in the double and triple mutants. After two days of dynamic light treatment, all three mutants (especially the triple mutant) exhibited lower Φ2. Under the second round of fluctuating light treatment on Day 5, all mutants showed similar defects as those shown under the first round of fluctuating light conditions (Day 3), but the difference from the WT became less obvious (Figure 3.3).

Overall, both peroxisome biogenesis mutant *pex14* and the organelle division mutants showed impaired photosynthetic performance, indicating that peroxisomes play a crucial role in robust photosynthesis under dynamic light.

3.3.4. Photorespiratory mutants displayed various levels of deficiencies in photosynthetic performance under high light and fluctuating light conditions

Glycolate oxidases (GOX1 and GOX2) and hydroxypyruvate reductase 1 (HPR1) respectively catalyze the first and last step of the peroxisomal portion of the photorespiration pathway. Catalase 2 (CAT2) is the major catalase enzyme in the

peroxisome that breaks down H_2O_2 produced by photorespiration. Two peroxisomal malate dehydrogenases (PMDH1 and PMDH2) produce NADH to facilitate the reduction reaction by HPR1 (Cousins et al., 2008b). As previously reported (Timm et al., 2008; Vanderauwera et al., 2005), null mutants *hpr1-1*, *hpr1-2* and *cat2-1* showed typical photorespiratory phenotypes, i.e. retarded growth and smaller rosette leaves when grown in ambient air. Semi-quantitative RT-PCR analysis was performed on the mutant alleles of *GOX1*. The *gox1-1* and *gox1-2* mutants sustained similar amount of transcript as WT (Figure 3.4A), and *gox1-3* appeared to be a knockout mutant (Rojas et al., 2012). Two mutant alleles of *GOX2*, which is highly similar to *GOX1*, were examined as well, and the result suggested that they are knockout mutants (Figure 3.4A). A knockout mutant of *PMDH1*, which grew normally under ambient air (Figure 3.4B), was also included in the screen. Null mutants *gox1-3*, *gox2-1* and *gox2-2* grew as well as the WT in ambient air, which is possibly due to the functional redundancy between GOX1 and GOX2 under ambient conditions (Figure 3.4B). Likewise, null mutant *pmdh1* did not show typical photorespiratory phenotype, which is possibly due to the functional redundancy between *PMDH1* and *PMDH2* despite the fact that the expression of *PMDH2* is much higher than that of *PMDH1* in leaves (Li and Hu, 2015). However, *hpr1-1*, *hpr1-2*, *cat2-1*, and interestingly, *gox1-3* as well, exhibited strong phenotypes under dynamic light conditions, which will be described below.

Day 1 and Day 2: Under constant light on Day 1, there were limited differences between photorespiratory mutants and WT in photosynthetic performance (Figure 3.5). However, under sinusoidal light on Day 2, Φ2 was reduced in all four mutants, with *hpr1-1* and *hpr1-2* showing the fastest and strongest decrease and *gox1-3* and *cat2-1*

displaying weaker but significant decreases. The fast decay of Φ2 began at 170 μmol m^{-2} s^{-1} in *hpr1-1* and *hpr1-2*, and at ~300 μmol m^{-2} s^{-1} in *gox1-3* and ~330 μmol m^{-2} s^{-1} in *cat2-1* (Figure 3.5A). Φ2 in *hpr1-1* and *hpr1-2* kept decreasing to around 0.2 at the highest light intensity. The lowest Φ2 in *gox1-3* and *cat2-1* were both around 0.4, with a faster decrease in *gox1-3*. Φ2 gradually recovered as light intensity decreased and by the end of the day, WT recovered to around 95% of its starting level, while in *hpr1-1*, *hpr1-2*, *gox1-3* and *cat2-1*, it was 57%, 60%, 83% and 77%, respectively (Figure 3.5A). Pseudo fluorescence images of Φ2 in *hpr1-1* and *gox1-3* also reflected the change of Φ2 during the course of sinusoidal light on Day 2 (Figure 3.6).

For NPQ, *hpr1-1*, *hpr1-2*, *gox1-3* and *cat2-1* started to show an exponential increase at around 170, 170, 300 and 330 μmol photons m^{-2} s^{-1}, respectively, corresponding to the light intensities that triggered the drastic decay of Φ2 in each mutant (Figure 3.5B). *hpr1-1* and *hpr1-2* exhibited the highest NPQ, followed by *gox1-3* and *cat2-1*. qE is the fast relaxing component of NPQ, and qI is the slowly relaxing component of NPQ (Rochaix, 2014).

All four mutants had much higher qE than WT. *hpr1-1* and *hpr1-2* had a large peak of qE between 120 and 300 μmol photons m^{-2} s^{-1}, and the response gradually relaxed even when the light was increasing (Figure 3.5C). On the other hand, *gox1-3* and *cat2-1* had a fast increase of qE at around 250 and 290 μmol photons m^{-2} s^{-1} respectively, and kept increasing as light intensity increased (Figure 3.5C). At the end of the day, there was residual qE in *hpr1-1*, *hpr1-2* and *cat2-1*, but not *gox1-3*. *hpr1-1* and *hpr1-2* exhibited the highest qI, followed by *gox1-3* and *cat2-1*. *hpr1-1*, *hpr1-2* and *cat2-1* showed gradually increased qI, which reached the highest value after the highest light

intensity, while the kinetics of qI in *gox1-3* and WT correlated with light intensity changes (Figure 3.5D). There were residual qI in *hpr1-1*, *hpr1-2* and *cat2-1*, which is in line with their enhanced reduction of Φ2.

Day 3: Under fluctuating light conditions on Day 3, Φ2, NPQ, qE and qI were clearly distinct between mutants and WT. *hpr1-1*, *hpr1-2* and *cat2-1* started with lower Φ2 that resulted from light stress on Day 2, and continued to decrease faster than the WT under both lower bound ambient light and upper bound fluctuating light (Figure 3.5A). Starting with a lower Φ2, *gox1-3* had faster reduction than WT in Φ2 under both ambient light and fluctuating light, but to a lesser extent than that of *hpr1-1*, *hpr1-2* and *cat2-1* (Figure 3.5A). All the mutants have overall higher NPQ than WT, especially under ambient light. *hpr1-1*, *hpr1-2* and *cat2-1* had much smaller ranges of qE, indicating impaired qE adaptation to fluctuating light (Figure 3.5C). However, qE in *gox1-3* was overall higher than WT under both ambient and fluctuating light, indicating that *gox1-3* sustained robust adaptive qE response under fluctuating light conditions (Figure 3.5C). Compared with the wild type, *hpr1-1*, *hpr1-2* and *cat2-1* had significantly higher qI under both ambient light and fluctuating light, while *gox1-3* had significantly higher qI under fluctuating light (Figure 3.5D).

Day 4: After light stress on Day 2 and Day 3, Φ2 of all four mutants significantly dropped from the starting value on Day 2, to 47% in *hpr1-1*, 48% in *hpr1-2*, 57% in *cat2-1*, 77% in *gox1-3* in and 62% in WT, suggesting strongly enhanced photoinhibition in most mutants (Figure 3.5A). Since NPQ, qE and qI are activated under high light conditions, NPQ, qE and qI showed no change under constant low light on Day 4 (Figure 3. 5B-D)

Day 5: Under the repeated fluctuating light conditions on Day 5, Φ2 in *hpr1-1* and *hpr1-2* not only decreased faster than WT, similar to the trend in Day 3, but also exhibited a quick decay similar to that of Day 2. So were *cat2-1* and *gox1-3*, but to a lesser extent (Figure 3.5A). Compared with Day 3, qE in *hpr1-1*, *hpr1-2* and *cat2-1* were responding more robustly to light fluctuation, and *gox1-3* was responding as strongly as on Day 3 (Figure 3.5C). qI in both *hpr1-1* and *hpr1-2* had two peaks, one was before and one was after the highest light intensity. qI in *cat2-1* and *gox1-3* was as responsive to the fluctuating light conditions as on Day 3 (Figure 3.5D). The difference in Φ2, qE and qI between Day 3 and Day 5 might be due to the light conditions prior to that day, which was sinusoidal for Day 3 and constant moderate light for Day 5.

3.3.5. The peroxisomal NAD^+ carrier PXN modulates photosynthesis under fluctuating light conditions

PXN is a peroxisomal NAD^+ carrier delivering cytosolic NAD^+ into peroxisomes for the production of NADH, a reducing equivalent that presumably facilitates photorespiration (Cousins et al., 2008a), fatty acid β-oxidation, conversion of IBA to IAA and others (Bernhardt et al., 2012). Two T-DNA insertion mutants, the knockout *pxn-1* and the strong knock-down *pxn-2* (Bernhardt et al., 2012) were analyzed in this study.

Limited phenotypic difference was observed on Day 1 and Day 2. However, under fluctuating light conditions on Day 3, both *pxn* alleles exhibited emerging phenotypes. *pxn-1* and *pxn-2* showed lower Φ2 than WT as light intensity increased to

high levels under both lower bound ambient light and upper bound fluctuating light (Figure 3.7A). Pseudo fluorescence images of Φ2 in *pxn-1* and *pxn-2* also reflected the change of Φ2 under the fluctuating light during the 1st half period of Day 3 (Figure 3.8).

Meanwhile, *pxn-1* and *pxn-2* exhibited higher NPQ than WT, especially under ambient light (Figure 3.7B). Correspondingly, the kinetics of qE largely resembled that of NPQ (Figure 3.7C), and qI in both *pxn* alleles were higher than WT under fluctuating light (Figure 3.7D). After recovering on Day 4, *pxn-1* and *pxn*-2 did not show altered response to repeated fluctuating light condition on Day 5, as measured by Φ2, qE, qI and NPQ (Figure 3.7), suggesting that *pxn-1* and *pxn-2* may have "memorized" the fluctuating light conditions via certain adaptive mechanisms, or that the emerging phenotype on Day 3 was dependent on the light stress on Day 2, i.e. was an accumulative effect from light stress on both Day 2 and Day 3.

3.3.6. Supply of CO_2 rescued the phenotypes of the photorespiratory mutants and the *pxn* mutants

Typical phenotypes exhibited on photorespiratory mutants, including reduced photosynthetic rate, altered primary metabolism and compromised stress tolerance, can be complemented by supply of high concentration CO_2, which suppresses the oxygenase activity of Rubisco (Foyer et al., 2009). To test whether the emerging phenotypes in the mutants were dependent on photorespiration, we tested the mutants in the same five-day experiment in DEPI under saturated concentration of CO_2 (3000 ppm). The measurement of Φ2, NPQ, qE and qI were acquired as in the previous five-day DEPI screen. The

photorespiratory mutants and *pxn* mutants were all completely rescued by elevated CO_2 and no phenotypic differences were observed between mutants and WT (Figure 3.9). This result suggested that PXN modulates photosynthesis under fluctuating light through photorespiration, and confirmed that it was the impairment of photorespiration in the photorespiratory mutants that caused the emerging phenotypes.

3.3.7. Fast increase in proton motive force contributes to fast qE response in photorespiratory mutants

Through the five-day chlorophyll fluorescence-based screen by DEPI, we identified photorespiratory mutants that had strongly reduced photosynthetic capacities under high light (HL) and fluctuating light conditions. Enhanced photoinhibition by HL was indicated by decreased Φ2 and increased qI in the mutants. The highly elevated NPQ and qE in the mutants prompted us to investigate whether the proton motive force (*pmf*) is increased as well, because *pmf* is the indicator of the buildup of ΔpH across thylakoid membranes, which in turn leads to the generation of qE (Takizawa et al., 2007). To this end, we measured *pmf* using a spectrophotometer and simultaneously measured other relevant parameters such as the thylakoid membrane proton efflux (vH^+), conductivity of ATP synthase (gH^+), linear electron flow (LEF), Φ2, NPQ, qE and qI. Another photorespiratory mutant *plgg1*, which lacks a plastidic glycolate/glycerate transporter (Pick et al., 2013), was added into the photorespiratory mutant group. Since *hpr1-1* and *hpr1-2* are both knockout mutants and exhibited the same phenotype, we only used *hpr1-*

1 hereafter. For the rest of this chapter, *hpr1*, *cat2* and *gox1* represented *hpr1-1*, *cat2-1* and *gox1-3* respectively.

Indeed, *pmf* was higher in photorespiratory mutants at high light intensities. *hpr1* and *plgg1* exhibited rapid increases of *pmf* at moderate light intensities (100 and 250 μmol m^{-2} s^{-1}), but the increases were quickly relaxed in spite of increasing light intensities (500 and 750 μmol m^{-2} s^{-1}), which suggested a rapid increase and a fast buildup of ΔpH (Figure 3.10A). The buildup of ΔpH could result from increased proton influx and/or decrease of proton efflux. Since LEF, which is coupled with proton influx (Takizawa et al., 2007), was largely decreased in *hpr1* and *plgg1*, a decrease of proton efflux seemed more likely to be the case. Indeed, we found that *hpr1* and *plgg1* exhibited strong decrease in proton efflux, indicated by lower vH^+ at high light intensities (250, 500 and 750 μmol m^{-2} s^{-1}) (Figure 3.10A). Consistently, *hpr1* and *plgg1* also showed reduced ATP synthase conductivity, as indicated by lower gH^+ at high light intensities (250, 500 and 750 μmol m^{-2} s^{-1}). vH^+ and gH^+ in *cat2* and *gox1* was similar to those of WT under all light intensities, suggesting that proton efflux rate and ATP synthase conductivity were not affected in *cat2* and *gox1*. Furthermore, all mutants had lower LEF as light intensity increased to 250 μmol m^{-2} s^{-1} and higher (Figure 3.10A), which was in line with a strongly reduced PSII quantum yield Φ2. Consistent with results from the chlorophyll fluorescence-based assays, all mutants displayed lower Φ2 and higher NPQ, qE and qI under higher light intensities (250, 500 and 750 μmol m^{-2} s^{-1}) (Figure 3.10B).

3.3.8. Activation of CEF in *hpr1* under high light conditions

CEF around PSI is considered an important mechanism to balance the ATP/NADPH energy budget in photosynthesis (Shikanai, 2007). Under stress conditions, CEF is activated to meet higher demand of ATP/NADPH, which cannot be sufficiently provided by LEF (Joliot and Johnson, 2011). The photorespiratory mutants showed reduced LEF and lower proton efflux through ATP synthase (vH^+) (Figure 3.11A), which indicated an altered ATP/NADPH ratio and activated CEF.

To test CEF in the mutants, we first plotted vH^+ as a function of LEF to qualitatively analyze CEF related contribution of vH^+. Under low light intensities (50 and 100 μmol photons m^{-2} s^{-1}), all photorespiratory mutants showed similar vH^+-to-LEF ratio as the WT (Figure 3.11A). However, as light intensity increased to over 250 μmol photons m^{-2} s^{-1}, all four mutants shifted to a higher vH^+/LEF ratio, and *hpr1* exhibited the largest shift (30% increase to WT, p-value < 0.01). This result indicated that CEF was enhanced to compensate for reduced LEF to sustain adequate vH^+ and ATP/NADPH in the photorespiratory mutants, especially *hpr1*.

Since *hpr1* showed the strongest phenotypes in the first assay, we used post-illumination chlorophyll fluorescence rise signal as an independent assessment of CEF in *hpr1* (Gotoh et al., 2010). In principle, the fluorescence rise signal following imposition of darkness is mainly attributed to CEF-related reduction of the PQ pool through the NAD(P)H dehydrogenase (NDH) complex, thus the kinetics of fluorescence rise can be used to reflect CEF induction (Gotoh et al., 2010; Shikanai et al., 1998). As shown in Figure 3.11B, *hpr1* and WT exhibited similar kinetics of fluorescence rise under growth

light (GL) – i.e. 100 μmol photons m^{-2} s^{-1}. However, after 6 hours of HL (1000 μmol photons m^{-2} s^{-1}) treatment, *hpr1* showed a much more rapid and stronger fluorescence rise than WT. The signal in *hpr1* kept increasing and even surpassed the signal under actinic light. These two independent approaches together demonstrated the higher activation of CEF in photorespiratory mutants, especially *hpr1*, under HL.

3.3.9. Interaction between photorespiration and excessive energy dissipation

It is known that robust induction of qE requires the thylakoid membrane protein PsbS as a pH sensor and zeaxanthin (Niyogi and Truong, 2013). Rapid increase of qE and elevated proton gradient across the thylakoid membrane (as indicated by high level of *pmf*) exhibited on the photorespiratory mutants suggested that these mutants provide ideal systems to study the relationship between ΔpH and qE. To this end, double mutants were constructed between photorespiratory mutants (*hpr1*, *gox1* and *plgg1*) and mutants defective in the biosynthesis of the photoprotective zeaxanthin (*npq1,* which has a lower level of zeaxanthin), the conversion of zeaxanthin to violaxanthin (*npq2,* which has a higher level of zeaxanthin), and the pH sensor PsbS (*npq4*, a knockout of PsbS that has no qE under high light). All the mutants were subjected to the five-day experiment in DEPI.

Under sinusoidal light on Day 2, *hpr1* exhibited highly elevated qE compared to WT (Figure 3.12A). Similar to previous report (Havaux et al., 2000), *npq1* had very limited qE due to reduced level of zeaxanthin. However, *hpr1 npq1* had significantly decreased qE than *hpr1*, but higher qE than that of WT and *npq1* (Figure 3.12A). The initial phase of qE increase in *hpr1* and *hpr1 npq1* were well synchronized, suggesting

that the gain of qE in *hpr1 npq1* was due to activation of qE by the mutation in *hpr1*. This data suggested that higher qE in *hpr1* is partially dependent on zeaxanthin level. The increased ΔpH might bypass zeaxanthin and directly activate qE via protonation of the pH sensor PsbS protein. Consistent with previous studies, *npq2* showed faster buildup and a higher level of qE compared to WT as a result of sustaining higher levels of zeaxanthin (Niyogi et al., 1998). *hpr1 npq2* showed lower qE than *hpr1*, and higher qE than *npq2* (Figure 3.12B), suggesting that a higher level of zeaxanthin might not always enhance qE, or that the equilibrium between zeaxanthin and violaxanthin might be more important for robust qE production. As previously reported, *npr4* showed no qE due the absence of the pH sensor PsbS (Li et al., 2000). Adding *npq4* to the *hpr1* background completely abolished high qE in *hpr1*, which suggested that qE in *hpr1* is completely dependent on PsbS (Figure 3.12C). Similar patterns have been found in double mutants *gox1 npq1*, *gox1 npq2*, *gox1 npq4*, *plgg1 npq1*, *plgg1 npq2*, and *plgg1 npq4* (Figure 3.13). Since *gox1* and *plgg1* had lower qE than *hpr1*, they exhibited less effect in qE production in *npq1* and *npq2* background. Consistently, *gox1 npq4* and *plgg1 npq4* showed no qE (Figure 3.13).

Measurement of Φ2, NPQ, and qI was also made under sinusoidal light on Day 2. Φ2s in *hpr1*, *hpr1 npq1*, *hpr1 npq2* and *hpr1 npq4* were similarly decreased, but qIs in *hpr1* and *hpr1 npq2* were much higher than those of *hpr1 npq1* and *hpr1 npq4* (Figure 3.14-3.16), indicating that PsbS and zeaxanthin were also required for qI generation in *hpr1*. Photosynthetic measurements of double mutants, including *gox1 npq1*, *gox1 npq2* and *gox1 npq4*, were also measured under dynamically changing light conditions (Figure 3.17-3.19). Φ2s in *gox1*, *gox1 npq1* and *gox1 npq4* were similarly decreased, but Φ2 in

gox1 npq2 was partially rescued, suggesting that zeaxanthin can protect photosystem from photoinhibition in *gox1*. qIs in *gox1 npq1, gox1 npq2* and *gox1 npq4* were all decreased than that in *gox1*, suggesting that PsbS and zeaxanthin were also required for qI generation in *gox1*, consistent with the result of *hpr1 npq* double mutants. Photosynthetic parameters of double mutants, including *plgg1 npq1*, *plgg1 npq2*, and *plgg1 npq4*, were measured under dynamically changing light conditions (Figure 3.20-3.22). Φ2s in *plgg1*, *plgg1 npq1*, *plgg1 npq2* and *plgg1 npq4* were similarly decreased, but qIs in *plgg1 npq1* and *plgg1 npq4*, suggesting that that PsbS and zeaxanthin were also required for qI generation in *plgg1*.

Overall, we conclude that the activation of qE in the photorespiratory mutants is completely dependent on PsbS, and partially dependent on zeaxanthin, and that qI is also partially dependent on PsbS and zeaxanthin.

3.3.10. Elevated ROS burst, faster chlorophyll degradation and anthocyanin deficiency in the photorespiratory mutants under high light

We have shown that the photorespiratory mutants displayed enhanced photoinhibition under sinusoidal and fluctuating light conditions. Since these are short-term HL treatments, we were interested in investigating how these mutants adapt to long term HL stress. Three-week-old plants were treated with 3 days of HL stress (6 hours of 1000 μmol m^{-2} s^{-1} daily) or kept under 100 μmol m^{-2} s^{-1}. Measurements of F_v/F_m, chlorophyll and anthocyanin were conducted for each genotype. *hpr1*, *plgg1* and *cat2* showed pale green leaves after long term HL stress, with faster chlorophyll degradation as well as pronounced reduction of F_v/F_m (Figure 3.23A and 3.23B). Stronger

photoinhibition and accelerated chlorophyll degradation were previously shown to be resulted from elevated levels of ROS in photorespiratory mutants (Nishiyama et al., 2006). To follow up on this possibility, we took leaf samples of plants after one day of HL treatment or grown under GL, and stained for a major stable ROS, H_2O_2, using 3, 3-diaminobenzidine (DAB). Under GL all the plants exhibited similarly low levels of ROS. Under HL however, *hpr1*, *plgg1* and *cat2* displayed significantly increased levels of H_2O_2, which were observed as dark brown stains on discolored leaves (Figure 3.23C). Higher levels of ROS burst was further confirmed by quantitative RT-PCR analysis of two oxidative-stress responsive gene markers, a heat shock protein gene *17.6B-CI* (*HSP 17.6B-CI*) and a transcription factor gene (*WRKY30*), which were shown to be strongly induced in expression by HL in *hpr1*, *plgg1* and *cat2* (Figure 3.23C).

Another aspect of acclimation to long term HL is the induction of anthocyanin, a pigment that protects plants by absorbing excessive UV light (Page et al., 2012; Zeng et al., 2010). While leaves of WT and *gox1* turned dark purple due to anthocyanin accumulation, this adaptive response was largely missing in *hpr1*, *plgg1* and *cat2* (Figure 3.23A and 3.23B). To gain insight into the anthocyanin deficiency, we used quantitative RT-PCR to quantify the transcripts of six representative genes involved in anthocyanin biosynthesis or regulation. Two known regulatory MYB transcription factor genes that control the accumulation of anthocyanin, *Production of Anthocyanin Pigment 1* (*PAP1*) and *PAP2* (Borevitz et al., 2000; Winkel-Shirley, 2002), and four genes that are involved in anthocyanin biosynthesis, including *phenylalanine ammonia-lyase 2* (*PAL2*), *chalcone synthase (CHS*), *dihydroflavonol 4-reductase* (*DFR*) and *flavonol-7-o-rhamnosyltransferase* (*UGT89C1*) (Gou et al., 2011; Winkel-Shirley, 2002), were tested

(Figure 3.23D). *PAP1*, *PAL2*, and *CHS* were less up-regulated by HL in *hpr1*, *plgg1* and *cat2*, indicating that they were still HL-responsive but not as strong as in WT (Figure 3.23D). *PAP2*, *DFR* and *UGT89C1* were even suppressed by HL in *hpr1*, *plgg1* and *cat2* (Figure 3.23D). Overall, expression patterns of the six anthocyanin-related genes correlated with the amount of anthocyanin in the mutants, and the transcriptional regulation in *hpr1*, *cat2* and *plgg1* seemed insufficient to stimulate accumulation of anthocyanin. Earlier studies reported the inhibitory effect of H_2O_2 on anthocyanin biosynthesis (Fahnenstich et al., 2008; Hou et al., 2015; Vanderauwera et al., 2005). Here our data support the view that under HL in the photorespiratory mutants, elevated ROS inhibits anthocyanin biosynthesis through transcriptional regulation.

3.3.11. Compromised integrity of photosynthetic complexes and decreased abundance of photosynthetic subunits in photorespiratory mutants under high light

Optimal performance of photosynthesis requires structural and functional integrity of photosynthetic complexes embedded in thylakoid membranes (Liu and Last, 2015; Rochaix, 2014). The enhanced photoinhibition, induced CEF, and deficiencies in photosynthetic capacities in the photorespiratory mutants led to the hypothesis that the integrity of the photosysthetic complexes may be compromised in the mutants.

To test this hypothesis, we first used blue native polyacrylamide gel electrophoresis (BN-PAGE) to examine the integrity of the native forms of photosysthetic complexes. Thylakoid membranes were isolated from wild type and mutants treated with 3 days of HL or grown under GL, and subsequently used for BN-

PAGE analysis. The overall distribution and abundance of most complexes were similar between mutants and WT under either GL or HL. However, under HL the abundance of the protein corresponding to the PSI/PSII dimer was reduced in *hpr1*, *plgg1* and *cat2* compared to WT (Figure 3.24A). This data was in line with the severe photoinhibition observed in *hpr1*, *plgg1* and *cat2*, since photoinhibition can directly result in decrease of PSII complex abundance.

We also performed immunoblot analysis to analyze the abundance of representative subunits of each complex. Equal amounts of isolated thylakoid membranes were loaded for standard SDS-PAGE, followed by western blotting with specific antibodies (Figure 3.24B). After HL treatment, the levels of the PSII core reaction center subunits D1 and D2 were dramatically decreased in *hpr1* (10% for D1 and 30% for D2), *plgg1* (20% for D1 and 45% for D2) and *cat2* (35% for D1 and 50% for D2) relative to that of WT. Levels of the PSI reaction center protein PsaA and antenna protein LHCA2 were also reduced in *hpr1* (40% and 50%, respectively) and *plgg1* (40% and 80%, respectively) after HL treatment. Interestingly, the Cyt.b_6f subunit Cyt.*f* was much less abundant in *hpr1* compared to WT (15% of WT) after HL treatment. However, the ATP synthase subunit CF1-β remained largely unchanged in all the mutants relative to WT (Figure 3.24B). The decreased levels of PSII reaction center D1 and D2 proteins, as well as the reduction of the PSI/PSII dimer collectively indicate accelerated damage of photosystems and/or inhibited repair processes in *hpr1*, *plgg1* and *cat2*. Both data were also consistent with reduced F_v/F_m and LEF in these mutants. The decrease of PSI reaction center protein PsaA and antenna protein Lhca2 in *hpr1* after HL suggested that PSI complex is also vulnerable to strong photooxidative stress upon disruption of

photorespiration. In addition to defects in PSII and PSI, the decrease of the Cyt.b_6f subunit Cyt.*f* in *hpr1* could also account for the severely reduced LEF in *hpr1* under HL, since Cyt.b_6f significantly limits photosynthetic electron transport (Rochaix, 2011; Yamori et al., 2011). Although the conductivity of ATP synthase is significantly decreased in *hpr1* under HL, the abundance of ATP synthase was not reduced, which suggests that other mechanisms could account for the reduced ATP synthase conductivity in *hpr1*.

Taken together, the compromised integrity of photosynthetic complexes and decreased levels of photosynthetic proteins are consistent with the impairment of photosynthesis in the photorespiratory mutants.

3.3.12. Evidence for the inhibition of triose phosphate isomerase activity and activation of the oxidative pentose phosphate pathway in *hpr1* under high light

Previous studies have shown that multiple photorespiration intermediates are accumulated in photorespiratory mutants under ambient conditions (Foyer et al., 2009; Pick et al., 2013; Timm et al., 2013; Timm et al., 2012b). Among these intermediates, phosphoglycolate (P-glyc) was speculated to be toxic in directly affecting the activity of enzymes participating in the CBB cycle in the chloroplast (Eisenhut et al., 2008; Schwarte and Bauwe, 2007). A previous study showed that Rubisco activity was inhibited in a glycolate oxidase-deficient rice mutant *glo*, possibly by high levels of P-glyc (Xu et al., 2009). An early report showed that triose phosphate isomerase (TPI) is strongly inhibited by P-glyc *in vitro* (Anderson, 1971). Triose phosphate isomerase

converts glyceraldehyde 3-phosphate (GAP) to dihydroxyacetone phosphate (DHAP). Both of these triose phosphates are required to regenerate ribulose 1,5-bisphosphate (RuBP) to make starch; they can also be exported to the cytosol for sucrose synthesis.

A block in stromal TPI could be overcome by export of GAP to the cytosol, where it is converted to DHAP, followed by the import of DHAP back to the chloroplast (Athanasiou et al., 2010; Dyson et al., 2015). An alternative to the import of DHAP is to process the carbon to glucose 6-phosphate (G6P), which can be imported to the chloroplast by the glucose-6-phosphate transporter GPT2 (Athanasiou et al., 2010; Dyson et al., 2015). Induced expression of *GPT2* would increase the protein amount of GPT2, which provides a higher capacity for reimport of carbon into the stroma.

To test whether *GPT2* is up-regulated, we first extracted RNA from leaf samples of each genotype after one day of HL treatment or grown under GL, and examined the expression level of *GPT2* by quantitative RT-PCR. Under GL, as the WT, all tested photorespiratory mutants showed similarly low expression levels of *GPT2* (Figure 3.25A). HL treatment induced the expression of *GPT2* in all mutants and WT, but to a much larger extent in *hpr1* and *plgg1*, which was consistent with the other profound phenotypes displayed in these two mutants. The stronger up-regulation of *GPT2* by high light suggested that there could be a significant flux of G6P from the cytosol to the chloroplast in these two mutants.

We also measured the levels of GAP and DHAP in HL-treated *hpr1*. The average level of DHAP was higher in *hpr1* than WT, but the difference was not statistically significant (Figure 3.25B). However, the level of GAP in *hpr1* was over two-fold higher

than WT (p-value < 0.01). The ratio of DHAP to GAP was lower in *hpr1* than WT (Figure 3.25B) and well below isomerase equilibrium (Sharkey and Weise, 2012). Since TPI converts GAP to DHAP, the lower DHAP/GAP indicates that TPI activity was inhibited. It was previously shown that *hpr1* accumulates higher levels of P-glyc in ambient air, and HL can stimulate photorespiration and probably enhance P-glyc accumulation (Timm et al., 2008). Our results support the model that high levels of P-glyc in *hpr1* under high light inhibits TPI activity and consequently disrupts the equilibrium of DHAP/GAP. As a bypass to inhibited TPI activity and disrupted equilibrium of DHAP/GAP, the export of GAP to the cytosol allows the conversion of GAP to G6P, which can then be re-imported back to the chloroplast to allow photosynthesis to proceed. Re-import of G6P also stimulates the oxidative branch of the pentose phosphate pathway, in which $NADP^+$ is reduced to NADPH using energy from the conversion of glucose-6-phosphate to ribulose 5-phosphate (Schnarrenberger et al., 1995) . Activation of the oxidative branch of the pentose phosphate pathway results in a futile cycle (Sharkey and Weise, 2012) that in turn leads to a higher demand of ATP. The increased CEF in *hpr1* under HL condition may be a mechanism to supply the extra ATP.

3.4. Discussion

In recent years considerable progress has been made in identifying novel peroxisomal proteins, charactering their biochemical functions, and discovering their involvements in metabolic pathways and stress response. Towards understanding the function of peroxisomes at a systems level, the methodology that utilizes rich genetic

materials combined with powerful high-throughput phenotyping platforms has proven to be an efficient way for discovering a wide range of phenotypes. Increasing evidence suggested the physical and functional connections between peroxisomes and chloroplasts. Here we report the first comprehensive peroxisome-centered reverse genetics screen, which was aimed at discovering peroxisomal proteins that contribute to robust photosynthetic capacity under dynamic light conditions, followed by detailed characterization of a group of photorespiratory mutants identified from the screen.

3.4.1. Photorespiration is the major peroxisomal function that connects to photosynthesis

The mutant screen reported here is the first comprehensive peroxisomal mutant screen in terms of the large coverage of peroxisomal proteins and the number of tested mutants. Mutants of genes involved in major peroxisomal functions, i.e. fatty acid β-oxidation, glyoxylate cycle, biosynthesis of JA, conversion of IBA to IAA, photorespiration, H_2O_2 detoxification and others were included, yet only mutants deficient in photorespiration-related proteins were identified, suggesting that photorespiration is the primary and dominant peroxisomal pathway that significantly impacts photosynthesis.

Novel emerging phenotypes displayed by the NAD^+ transporter mutant *pxn* under fluctuating light suggested that peroxisomal NADH homeostasis is important for robust photosynthesis. CO_2 can rescue the phenotype of *pxn*, suggesting that peroxisomal NADH homeostasis modulates photosynthesis through photorespiration. Previous studies

showed that NADH produced by PMDHs facilitates the reducing reaction catalyzed by HPR1 (Cousins et al., 2008a), and that the double mutant *pmdh1 pmdh2* exhibited relatively subtle but statistically significant changes in photosynthesis (Cousins et al., 2008a). NAD^+ delivered by PXN could be used by PMDH to generate NADH, thus contributing to photorespiration. Both PMDH and PXN may also be involved in fatty acid degradation during seed germination, as the knockout mutants exhibited germination defect (Bernhardt et al., 2012; Pracharoenwattana et al., 2007). Thus, PMDH and PXN seem to play dual roles in fatty acid β-oxidation during seed germination and photorespiration in adult plants.

We have shown in this study that previously reported peroxisomal photorespiratory mutants, such as *hpr1* and *cat2*, exhibited profound phenotypes under dynamic light, which makes sense because *hpr1* and *cat2* already grew slowly in ambient air. For *gox1*, which grew as well as WT in ambient air, the emerging phenotype could not be revealed without subjecting the mutant to stress conditions and monitoring real-time photosynthetic capacity, which proved the high sensitivity of phenotype discovery by DEPI.

The general growth abnormality exhibited in the peroxisome biogenesis mutant *pex14*, such as extremely small rosette and pale green leaves, correlated with its strongly affected photosynthetic capacity. In this study, peroxisomal division mutants also displayed significant phenotypes. DRP3 proteins are involved in both mitochondrial and peroxisomal division, and double mutant *drp3A drp3B* showed growth retardation (Zhang and Hu, 2009). DRP5B participates in both chloroplast and peroxisome division, with a stronger role in the chloroplast (Zhang and Hu, 2010). The affected growth in *drp5B*

mutant could be recovered by CO_2, suggesting that the emerging phenotype exhibited in *drp5B* is mostly due to insufficient photorespiration. The strongest emerging phenotype exhibited in the triple mutant *drp3A drp3B drp5B* should be an additive effect of the photorespiratory defects caused by impaired division of all three organelles (chloroplasts, peroxisomes and mitochondria) involved in photorespiration.

3.4.2. Various enzymes in photorespiration play quantitatively and kinetically different roles in photorespiration under dynamic light conditions

Extensive real-time monitoring of *in vivo* physiological parameters, in our case photosynthetic capacities, provides valuable information on the specific importance of each enzyme in the same pathway. GOX1 and HPR1 are metabolic enzymes directly involved in the photorespiratory metabolic flux. CAT2, on the other hand, is responsible for degrading H_2O_2 produced in photorespiration and other oxidative reactions, thus it is indirectly involved in photorespiratory metabolism (Mhamdi et al., 2012). Our results showed that HPR1 has the most significant impact on photosynthesis, as the *hpr1* mutant showed the strongest phenotype under dynamic light conditions. Although a cytosolic HPR2 was identified as a bypass to the peroxisomal HPR1, the metabolic conversion from hydroxypyruvate to glycerate is still predominately catalyzed by HPR1 (Timm et al., 2008). Due to functional redundancy between the highly identical genes *GOX1* and *GOX2*, *gox1* knockout only exhibited emerging phenotype, which can also explain why the fast decay of Φ2 in *gox1* under sinusoidal light happened later than in *hpr1*. Mutant *cat2* showed the later decay of Φ2 than *hpr1*, which is possibly due to the redundant role

between CAT2, CAT1 and CAT3, although CAT2 is the mostly highly expressed in leaves. Both *hpr1* and *cat2* exhibited remaining qI and decreased Φ2 under dynamic light conditions, indicating that photorespiration is critical in protecting photosystem from photoinhibition.

Under fluctuating light conditions, the degree of responsive adaptation in *gox1* is more robust than in *hpr1* and *cat2*, as indicated by the range of qE fluctuation. This suggested that *GOX2* still largely, although not fully, functionally substituted *GOX1*, and that the photodamage in *hpr1* and *cat2* may also inhibit components responsible for qE build up.

3.4.3. Highly elevated qE in photorespiratory mutants is due to rapid buildup of proton gradient across thylakoid membrane and largely dependent on PsbS and zeaxanthin

Stimulated energy-dependent quenching under high light results from the buildup of proton gradient across the thylakoid membrane (Niyogi and Truong, 2013). Photorespiration mutants analyzed in this study, especially *hpr1* and *plgg1*, exhibited a nice correlation between qE and *pmf*. *pmf* is an indicator of the proton gradient across the thylakoid membrane (Takizawa et al., 2007), thus higher *pmf* in *hpr1* and *plgg1* indicated elevated proton gradient. Inhibited activity of ATP synthase, which pumps out proton from lumen to stroma, was probably the major reason for the buildup of the proton gradient in these mutants. The exact inhibitory effect on ATP synthase activity in the photorespiratory mutants remains to be investigated. One speculation is that the depletion

of glycerate to CBB cycle, as a result from blocking of photorespiration, slows down the CBB cycle, which in turn leads to accumulation of ATP in the stroma. It is possible that accumulated stromal ATP has a negative feedback regulation on ATP synthase conductivity.

The highly activated qE and *pmf* in *hpr1* provide a useful *in vivo* system to study the relationship between strong ΔpH and NPQ components in generating NPQ. Adding *hpr1* into the *npq4* background, which lacks the key pH sensor PsbS, did not change the qE phenotype in *npq4* (Figure 3.12C), suggesting that PsbS is downstream from HPR1 in generating qE, i.e. HPR1 acts through PsbS in qE generation. However, the addition of *hpr1* to *npq1*, which has diminished level of zeaxanthin and qE, led to a significant stimulation of qE (Figure 3.12A), suggesting that the qE in *hpr1* is only partially dependent on zeaxanthin. Besides, qE in double mutant *hpr1 npq2* was between that of *hpr1* and *npq2*, suggesting that higher zeaxanthin cannot always enhance qE or the equilibrium between zeaxanthin and violaxanthin is more important for enhancement of qE (Figure 3.12B). Evidence from the double mutant analysis indicated that activated qE by increased ΔpH in *hpr1* was completely dependent on the PsbS protein, and partially dependent on zeaxanthin. Other double mutants, including *gox1 npq1*, *gox1 npq2*, *gox1 npq4*, *plgg1 npq1*, *plgg1 npq2*, and *plgg1 npq4*, showed similar patterns of the relationship between photorespiration and NPQ components regarding qE generation, based on which we can make the same conclusions as from results of the *hpr1 npq* double mutant analysis. Previous reports showed that unusually high ΔpH was able to bypass PsbS and stimulate qE through direct protonation of LHC in vitro (Sylak-Glassman et al., 2014), whereas our evidence indicated that the high ΔpH *in vivo* is unable to stimulate qE.

3.4.4. Activation of CEF and inhibition of TPI occurs in photorespiratory mutants under high light

We have shown that photorespiratory mutants had lower LEF under high light, and *hpr1* and *plgg1*, in particular, had the lowest LEF. Meanwhile, *hpr1* and *plgg1* showed strongly reduced proton efflux vH^+. The disrupted ratio between LEF and vH^+ may result from the activation of CEF. Indeed, *hpr1* showed higher CEF under HL, as shown in two independent assays (Figure 3.11). Our evidence suggested the reasons for activated CEF in *hpr1*. ROS and H_2O_2 have been shown as direct and indirect players in activating CEF (Casano et al., 2001; Strand et al., 2015), and we showed that the amount of H_2O_2 and transcripts of oxidative stress responsive genes were increased after short term HL treatment (Figure 3.23C). In addition, we have shown that under HL, the enzymatic activity of TPI was inhibited, possibly by the toxic levels of P-glyco in *hpr1*, as shown by the disequilibrium of GAP and DHAP (Figure 3.25B). As a bypass of this inhibition, re-import of G6P from cytosol to the chloroplast stroma may allow photosynthesis to proceed, but with a trade-off that the oxidative branch of pentose phosphate may be simulated and higher ATP demand is created. Previous studies suggested that the disruption of photorespiration interrupts the CBB cycle, which results in accumulated ATP and NADPH to generate ROS (Takahashi et al., 2007). Here we provided the evidence supporting that the oxidative branch of the pentose phosphate pathway is another pathway for a source of ROS production in *hpr1*.

3.4.5. Photorespiratory mutants exhibited compromised PS complex integrity, diminished PS subunit abundance and reduced stress resistance after HL treatment

Multiple lines of evidence suggested the molecular basis of the strong photoinhibition in photorespiratory mutants. The level of the PSII-PSI dimer was reduced in *hpr1* after HL treatment. Subunits in PS systems, such as D1 and D2 in PSII reaction center, PsaA in the PSI core, LHCAII in PSI antenna and Cyt.*f* in Cyt.b_6f, were significantly reduced in level. Decrease of D1 in other photorespiratory mutants, such as *glyk*, was demonstrated in previous studies (Takahashi et al., 2007). D2, as shown here, was decreased as well, which correlated with lower Φ2 and enhanced photoinhibition in the mutants. Although PSI is more stable than PSII under photodamage, we showed decreased levels of the PSI core protein and PSI antenna protein in *hpr1* after HL treatment. Decreased level of Cyt.b_6f, together with reduced abundance of the PSII core protein, correlated with decreased LEF in the mutants, since Cyt.b_6f is the rate-limiting step in photosynthetic electron transport (Rochaix, 2011; Yamori et al., 2011).

In addition to short term HL stress, photorespiratory mutants also demonstrated strong phenotypes after 3 days of HL treatment. Fast degradation of chlorophyll, which was possibly caused by over accumulation of ROS over time, resulted in pale green leaves. Deficiency in the induction of photoprotective pigment anthocyanin due to transcriptional repression of enzymes in the anthocyanin biosynthetic pathway was also shown in the photorespiratory mutants after long term HL. H_2O_2 was shown as a signal in repressing anthocyanin biosynthesis in *cat2* (Vanderauwera et al., 2005). Our data confirmed this result in *cat2*, and in addition found similar phenotype and mechanism in *hpr1* and *plgg1*. In addition to the inhibitory effect of ROS on anthocyanin biosynthesis

through transcriptional regulation, disrupted amino acid metabolism resulted from the blocking of photorespiration may also negatively affect anthocyanin biosynthesis by depriving the anthocyanin biosynthetic precursors. It was previously reported that supplementing phenyalanine can increase anthocyanin content in plants (Voll et al., 2004), and expressing Phenylalanine Ammonia-Lyase (PAL), which converts phenylalanine to ammonia in anthocyanin biosynthesis pathway, in *Daucus carota* induced accumulation of anthocyanin (Heinzmann and Seitz, 1977). Drastic changes in amino acid metabolism were identified in photorespiratory mutants (Pick et al., 2013; Timm et al., 2012b; Timm et al., 2008), and the herbicide glyphosate inhibits amino acid biosynthesis pathway, including phenylalanine, as well as enzymatic activity of proteins involved in photorespiration (Vivancos et al., 2011). It is also possible that the disrupted level of phenyalanine is the cause of anthocyanin deficiency in the photorespiration mutants.

3.4.6. Conclusion.

To conclude, our study has helped us to come up with an integrated model for the events that occur in the photorespiration mutants (Figure 3.26). First, increased photorespiration under high light increases the accumulation of phosphoglycolate in photorespiratory mutants. Phosphoglycolate inhibits TPI activity, which leads to the activation of the oxidative branch of pentose pathway that requires more ATP and increases oxidative stress. Second, depletion of the CBB cycle intermediates slows down the CBB cycle, which causes accumulation of unused ATP and NADPH. The unused

ATP in stroma inhibits the ATP synthase conductivity and leads to increased *pmf* and subsequent higher NPQ to dissipate excessive energy. Less consumed NADPH can be used to generate more ROS and creates enhance oxidative stress as well. Third, the increased oxidative stress, resulted from the two effects mentioned above, activates CEF to supply higher ATP/NADPH. Besides, elevated ROS impacts various photosynthetic processes, such as photoinhibition, compromised photosystem integrity, damaged photosystem subunit.

In summary, our comprehensive peroxisomal mutant screen has identified peroxisomal proteins involved in modulating photosynthesis and photorespiration under dynamic light conditions. Further characterization of the mutants also helped to dissect the qualitative and quantitative contribution of different proteins in the photorespiratory pathway to photosynthesis, providing new insight into the connection between photorespiration and photosynthesis. Knowledge gained from this study opens an avenue for future research on photosynthesis, photorespiration and interorganelle communication.

3.5. Materials and methods

3.5.1. Plant materials and growth conditions

Arabidopsis thaliana ecotype Col-0 and Ws-4 were used as wild type (WT). T-DNA insertion mutant lines were obtained from the Arabidopsis Biological Resource Center (ABRC; http://www.arabidopsis.org/) and confirmed by PCR-based genotyping. Information on gene locus and annotation of all the tested mutants is in Table 3.1. For constructing the double mutants, *npq1* and *npq2* are the same as *npq1-2* and *npq2-1* in a previous study (Niyogi et al., 1998), and *npq4* is *npq4-1* in Li et al (2000) (Li et al., 2000). Seeds were sown in the soil, stratified in the dark at 4 °C for 3 days, and plants were grown under 16/8-h light/dark cycle of 100 μmol photons m^{-2} s^{-1} of white light at 22 °C and 60% humidity. Plants that were screened in the Dynamic Environment Photosynthesis Imager (DEPI) were grown with black foam masks covering the soil for better background separation from the rosette leaves for fluorescence imaging. To allow for acclimation, plants were transferred to the imaging chamber 1-2 days before the 5-day experiment. Growth conditions in the imaging chambers were similar to those described above.

3.5.2. Fluorescence measurements, image processing and data analysis

Fluorescence measurements were performed in the Dynamic Environment Photosynthesis Imager (DEPI), as described in Kramer *et al.*, 2013, US patent WO 2013181433 A2. The initial fluorescence, F_0, was determined by turning on the weak measuring light. F_m was obtained by exposing the plants to a 0.3 s saturation flash of

approximately 10,000 μmol photons m^{-2} s^{-1}. Detailed methods were described in a previous study (Dutta et al., 2015).

Chlorophyll fluorescence images were processed using Visual Phenomics software (Tessmer et al., 2013). The maximum quantum efficiency of PSII photochemistry (F_v/F_m) was calculated as $(F_m - F_0)/F_m$ (Krause and Jahns, 2003; Krause and Weis, 1991), where F_0 is the fluorescence of the dark-adapted plant and F_m is the maximum fluorescence. The quantum yield of PSII (Φ2) was calculated as $(F_m' - F_s)/F_m'$, where F_s is the steady-state fluorescence and F_m' is the fluorescence maximum at steady state (Baker, 2008). NPQ was calculated as $(F_m - F_m')/ F_m'$ (Baker, 2008), qE as $F_m/F_m' - F_m/F_m''$, and qI as $(F_m - F_m'')/F_m''$, where F_m'' is the post-illumination fluorescence maximum (Baker, 2008; Krause and Jahns, 2003).

At least three replicates for each genotype were tested. All imaging data were put in Origin (OriginLab, Northampton, MA) for data analysis. Heatmaps were generated with OLIVER software (Tessmer *et al.*, submitted).

3.5.3. In vivo spectroscopic assays

All spectroscopic measurements were made using intact and fully expanded leaves in 25-30-day-old plants just before bolting. Plants were dark adapted for 10 min before analysis. Actinic light intensities ranged between 50 and 750 μmol photons m^{-2} s^{-1}. Chlorophyll a fluorescence yield changes and light-induced absorbency changes were measured using a laboratory-built spectrophotometer/fluorimeter (Hall et al., 2013) using the techniques described in Livingston et al., (2010). Saturation pulse chlorophyll a

fluorescence yield parameters (F_0, F_m, F_s, F_m', F_m'') were recorded as described (Avenson et al., 2004; Baker, 2008; Baker et al., 2007; Kanazawa and Kramer, 2002), using 1-s saturation pulses of 10,000 μmol photons m^{-2} s^{-1}. These measurements were used to estimate Φ2, LEF, NPQ, qE and qI (Edwards and Baker, 1993; Genty et al., 1989). LEF was calculated as (Φ2 * light intensity * 0.5). Φ2, NPQ, qE and qI were calculated using the same equations mentioned above. Leaf absorptivity of all the mutants did not differ from WT (p-value > 0.15, n=4). The ECS measurements, which were used to calculate *pmf*, vH^+ and gH^+, were normalized for variations in leaf thickness and pigmentation by the extent of the rapid-rise single-turnover flash-induced ECS (Avenson et al., 2004; Livingston et al., 2010). The ECSt and τ_{ECS} parameters were taken from a first order exponential decay fit to ECS dark interval relaxation kinetics as described in (Baker et al., 2007). *pmf* was calculated as amplitude of the ECS first order exponential decay, vH^+ was calculated as the slope during the initial linear phase of ECS first order exponential decay, and gH^+ was calculated as $1/\tau_{ECS}$.

3.5.4. Measurements of CEF

LEF, with no contributions from CEF, should produce a constant ratio of proton flux to electron transfer through PSII (Sacksteder et al., 2000), which in our measurements should result in a constant, linear slope of vH^+ plotted against LEF. The relative rates of CEF can then be estimated by the increase in the slope of vH^+ versus LEF above the baseline slope for LEF alone (Livingston et al., 2010).

Post-illumination transient chlorophyll fluorescence was measured as described (Gotoh et al., 2010). Leaves were illuminated for 40 s with 150 μmol photons m^{-2} s^{-1}, followed by a 10-s dark interval. The plastoquinone pool was then oxidized by two 200-ms flashes of 730-nm light at 10 s apart.

3.5.5. Statistical analysis

Descriptive statistics and figures were generated using Origin 9.0 software (Microcal Software), and statistical analyses were performed using MATLAB R2012a (The MathWorks, Inc.) or Microsoft Excel. Except for calculating the difference of slope of vH^+ against LEF, which I used ANCOVA (analysis of covariance), Student's t- test were used for evaluating the differences of other parameters.

3.5.6. Thylakoid membrane preparation

Thylakoid membranes were prepared as previously described (Zhang et al., 1999). The leaves were homogenized in an ice-cold isolation buffer containing 400 mM sucrose, 50 mM HEPES-KOH, pH 7.8, 10 mM NaCl, and 2 mM $MgCl_2$ with a chilled mortar and pestle and filtrated through two layers of cheesecloth. The filtrate was centrifuged at 5000g for 10 min. The thylakoid pellets were washed with isolation buffer, re-centrifuged, and suspended in isolation buffer. The resulting thylakoid membrane pellets were either used freshly or frozen in liquid N_2 and stored at –70 °C before use. The chlorophyll

content was determined by spectrophotometer measurement according to (Wellburn, 1994).

3.5.7. BN-PAGE and immunoblot analyses

BN-PAGE was performed by modification of a previously described protocol (Liu et al., 2012), and thylakoid membranes were solubilized using 2% dodecyl-β-D-maltopyranoside. Electrophoresis was performed using a Native PAGE™ Novex@ 4–16% Bis/Tris mini gel and an XCellSureLock mini-cell (Life Technologies, https://www.lifetechnologies.com) at 4°C according to the manufacturer's instructions.

Immunoblotting was performed according to standard techniques by probing with specific antibodies after electroblotting of thylakoid membranes on SDS–PAGE gels onto nitrocellulose membranes (GE Healthcare, http://www3.gehealthcare.com) (Liu et al., 2012). Rabbit primary antibodies were purchased from Agrisera (http://www.agrisera.com). Primary antibodies were diluted 20,000-fold for antibodies against D1 and D2, 5000-fold for LHCAII, cytochrome *f* and CF1β, and 2500-fold for α-PsaA (all antibodies were generously shared from Dr. Rob Last Lab). Signals from horseradish peroxidase-conjugated goat anti-rabbit IgG (H+L) were visualized using Clarity Western ECL substrate (Bio-rad, http://www.bio-rad.com/en-us/product/clarity-ecl-western-blotting-substrate) and analyzed using software Image LabTM (version 5.0) (Bio–Rad, http://www.bio-rad.com). Protein accumulation was normalized to the amount of Coomassie Brilliant Blue-stained LHCII of PSII as an internal standard and was quantified from ChemiDoc™ XRS+ scans of the membrane using Image Lab™ software

(http://www.bio-rad.com/en-mx/sku/170-8265-chemidoc-xrssystem-with-image-lab-software).

3.5.8. Quantitative RT-PCR

Arabidopsis total RNA was isolated using a Plant RNeasy kit according to the manufacturer's instructions (Qiagen, https://www.qiagen.com), and treated with DNase I. 500 ng of each RNA sample was used for cDNA synthesis with random primers and iScript^{TM} cDNA Synthesis Kit (Bio-rad, http://www.bio-rad.com/). Quantitative real-time PCR was performed using a 7500 Fast Real-Time PCR System with Fast SYBR Green Master Mix (Applied Biosystems, http://www.appliedbiosystems.com). Relative gene expression was normalized to *ACTIN2* (At3g18780). Expression was determined in triplicate biological measurements.

3.5.9. Measurement of chlorophyll and anthocyanin

For chlorophyll measurement, rosette leaves were weighed and placed into 2 ml 80% acetone in the dark for 3 days. Absorbance at 645 nm and 663 nm was measured using a spectrophotometer. Total chlorophyll content = $(22.22 \times A_{645} + 9.05 \times A_{663})$ µg/ml x 2 ml /leaf fresh weight in mg (Wellburn, 1994). For anthocyanin measurement, rosette leaves were weighed, frozen by liquid nitrogen, and ground to powder. After adding 2 ml extraction buffer (1% HCl in methanol), the samples were placed at 4 °C overnight. Later, an equal amount of chloroform was added, and the mixture was

centrifuged for 5 min. After the top supernatant was transferred to a new tube, equal volume of 60 % extraction buffer was added. Absorbance of each tube at 530 nm and 657 nm were measured with a spectrophotometer. Anthocyanin content = (A_{530}-A_{657}) /weight (Zeng et al., 2010).

3.5.10. In situ detection of H_2O_2

In situ detection of H_2O_2 was performed by treating plants with DAB-HCl as previously described (Thordal-Christensen et al., 2002). Detached rosette leaves were vacuum-infiltrated with 5mM DAB-HCl, pH 3.8, for 5 min, and incubated in the same solution under growth light or HL for 6 h. Stained leaves were boiled in an acetic acid: glycerol: ethanol (1:1:3 [v/v/v]) solution for 5 min and photographed.

3.5.11. Measurement of GAP and DHAP

~500 mg F.W. of leaves were immediately frozen in liquid N_2, weighed and fully pulverized using Retsch Mill M300 (Retsch, http://www.retsch.com/). Cold 3.5% perchloric acid (2 µl per mg tissue), was added with tissues in eppendorf tubes, and tubes were placed on ice for 5 min incubation. Extracts were centrifuged at maximum speed at 4 °C for 10 min. Approx. 500 µl supernatant was recovered. Neutralizing buffer (2M KOH, 150 mM HEPES and 10mM KCl), in the ratio of 0.25µl per µl of recovered supernatant, was added to the supernatant to bring the pH to ~7. pH sticks were used to check pH, volume of neutralizing buffer was adjusted accordingly, and volume of

neutralizing buffer was recorded. Samples were frozen and thawed to precipitate salts, and centrifuged at maximum speed for 2 min. Supernatant was pipette off for immediate GAP and DHAP assays, or frozen at -80 °C for future assays. (Adapted protocol from Dr. Thomas Sharkey Lab at MSU)

The amount of GAP and DHAP was measured using dual λ spectrophotometer. 50 µl supernatant was added to 800 µl reaction buffer (100 mM HEPES buffer pH 7.6, 1 M DTT, 1M KH_2AsO_4, 50 mM NAD and 50 Mm ADP) in a cuvette, which was inserted to the cuvette holder in the spectrophotometer. 5 µl of glyceraldehydes-phosphate dehydrogenase GAPDH (Sigma G-5537) was added into cuvette and immediately mixed using a clean plastic stick. Absorbency of NADH at 340nm was recorded throughout the reaction, which reflected the reaction kinetics. The difference of abs (340) between the baseline and the maximum level was measured to estimate the level of GAP. Next, 5 µl of triose phosphate isomerase TPI (Sigma T-6285) was added into cuvette and immediately mixed by a clean plastic stick. Absorbance of NADH at 340nm was recorded throughout the reaction, and the difference of abs at 340 nm between the baseline and the maximum level was measured to estimate the level of DHAP. This protocol was adapted from Dr. Thomas Sharkey Lab and modified from (OH and JV, 1972; Shirokane et al., 2000).

3.6. Acknowledgement

I thank Dr. David Kramer for constant support, share of devices and insightful discussions. I also want to give appreciations to the great helps from Kramer Lab

members: Dr. Jeffery Cruz for teaching me chlorophyll fluorescence measurement techniques and data analysis, Linda Savage for scheduling my experiments, Dr. Deserah Strand for technical support on in vivo spectroscopic assays and CEF measurements, Geoffry Davis for sharing *npq1*, *npq2* and *npq4* mutants and help with data analysis, David Hall for image processing, Dr. Mio Sato-Cruz and Ruby Carrillo for sharing devices. I want to especially thank Dr. Jun Liu for teaching me BN-PAGE techniques, doing western blot of all the photosynthetic subunits and constant encouragements. I want to express my gratitude to other collaborators: Dr. Jin Chen for teaching me using R programming and data analysis, Dr. Thomas Sharkey and Dr. Sean Weise for providing ideas and helping with GAP and DHAP measurements. Finally, I would like to thank Center for Advanced Algal and Plant Phenotyping (CAAPP) at MSU-PRL for strong technical support.

APPENDIX

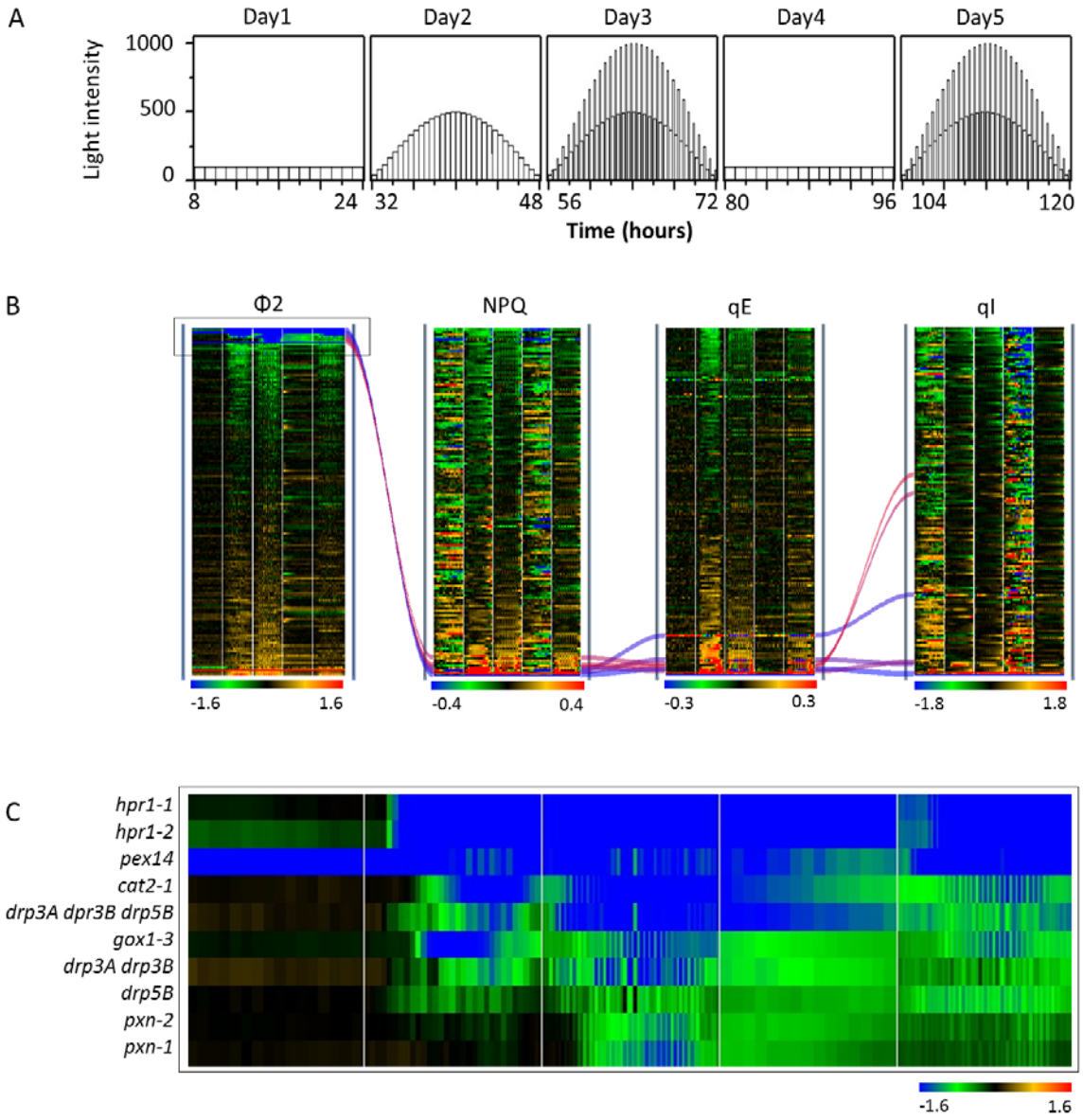

Figure 3.1. Revealing photosynthetic phenotypes of peroxisomal mutants under dynamic light conditions using DEPI.

(A) 5-day dynamically changing light conditions. The x axis represents time. The y axis represents light intensity. (B) Heatmaps of Φ2, NPQ, qE and qI, based on log fold-change in mutant relative to the WT. In each heatmap, the x axis represents time points, and the y

Figure 3.1. (cont'd)

axis represents the 147 screened peroxisomal mutants. Mutants are positioned from top to bottom based on the sum of all values (low to high) across 5 days. Corresponding color codes are under each heatmap. (C) Φ2 heatmap of the group of mutants that showed significant difference from WT. It is a zoom-in picture of the area in the black rectangle in Figure 3.1B. The x axis represents time points, and the y axis represents mutants. Color code is under the heatmap.

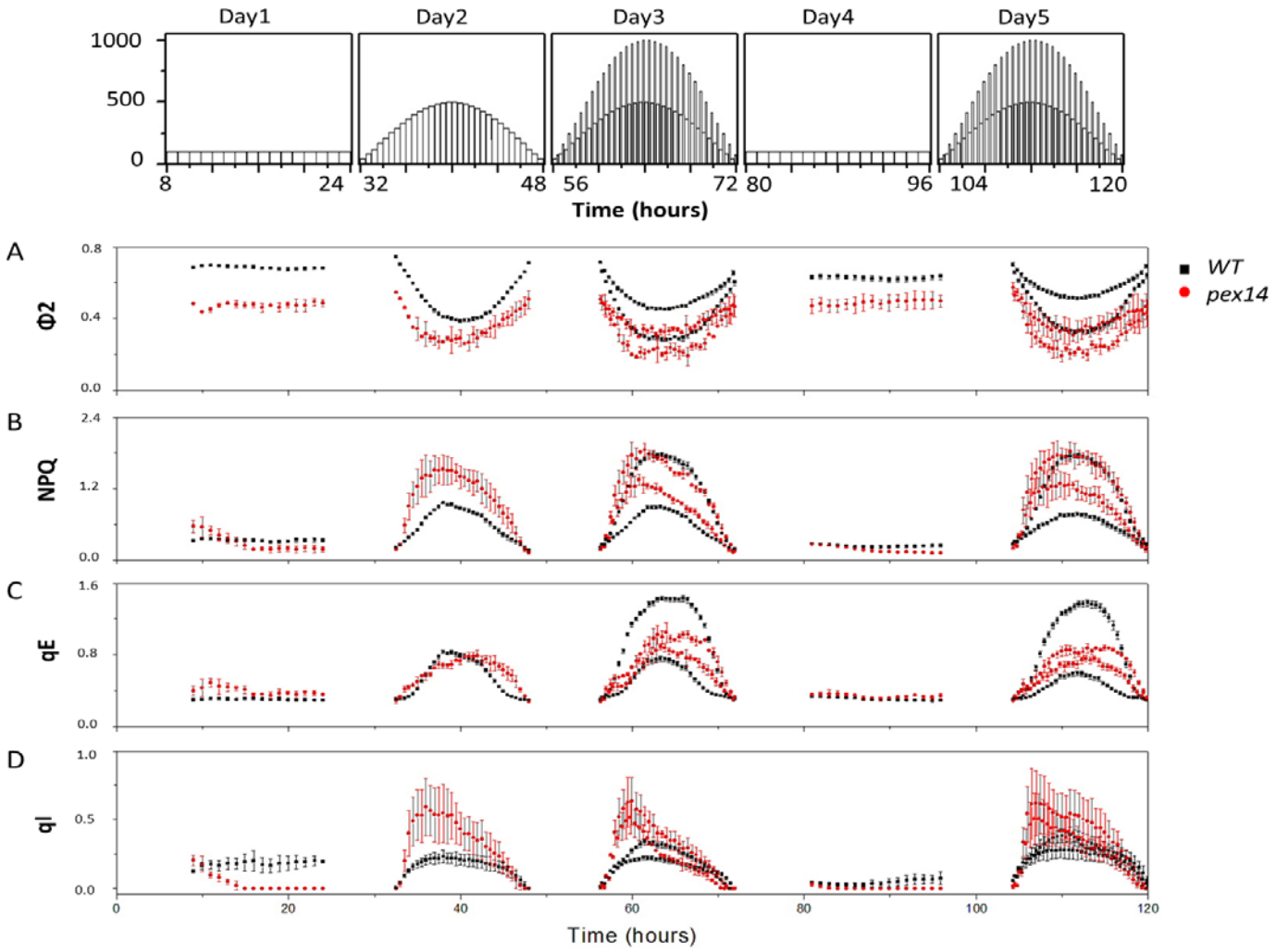

Figure 3.2. Photosynthetic performance of the *pex14* mutant under dynamically changing light conditions.

Figure 3.2. (cont'd)

The positive control *pex14* was tested in DEPI under dynamically changing light conditions. Each horizontal panel shows the measurement of a photosynthetic parameter across 5 days. The x axis represents time points, and y axis represents the value of the corresponding parameter. Three biological replicates were used for each genotype.

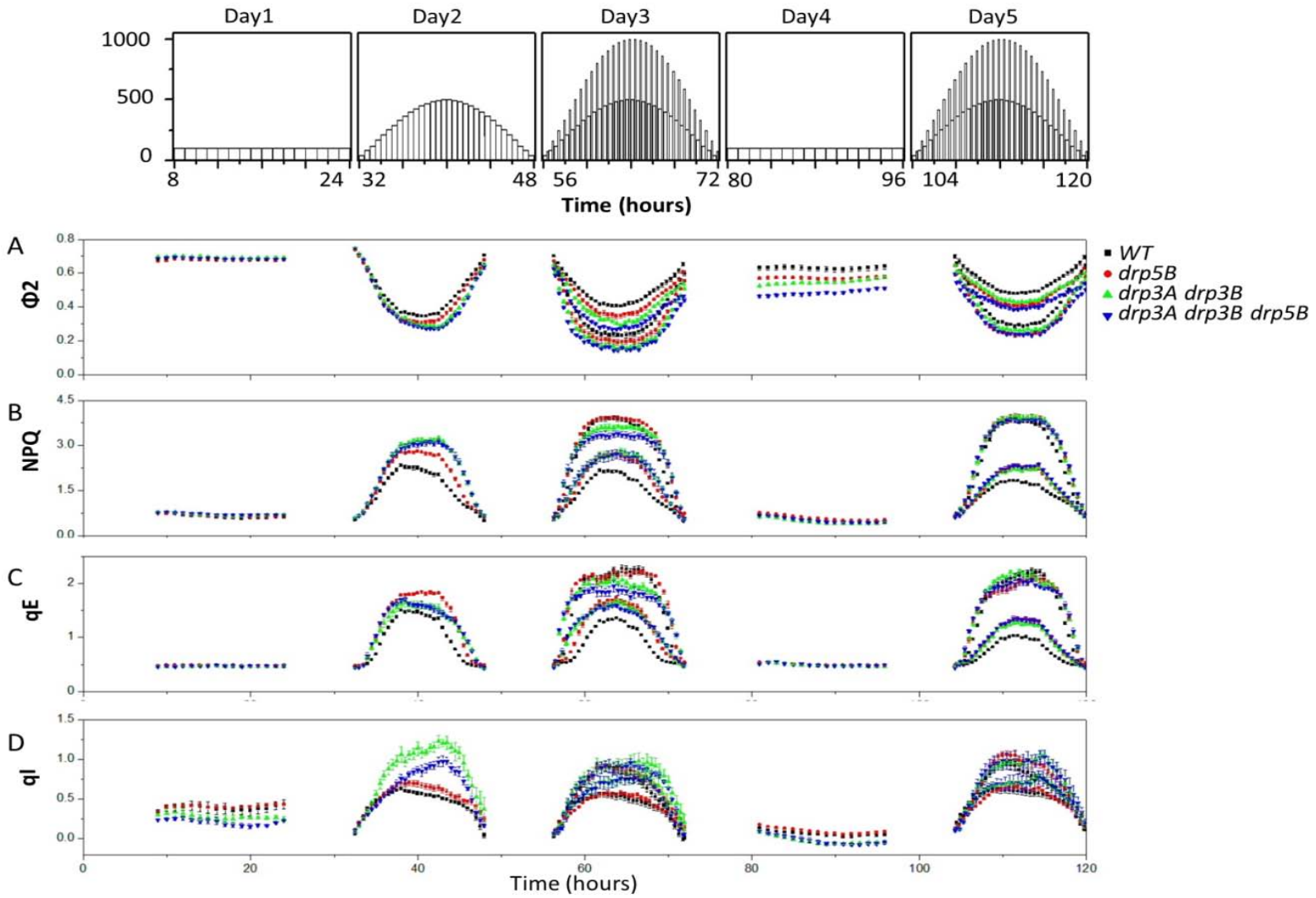

Figure 3.3. Photosynthetic capabilities of peroxisomal division mutants under dynamically changing light conditions.

Figure 3.3. (cont'd)

Peroxisomal division mutants *drp5B, drp3A drp3B,* and *drp3A drp3B drp5B,* were tested in DEPI under high light and fluctuating light conditions. Each horizontal panel shows the measurement of a photosynthetic parameter across 5 days. The x axis represents time points, and y axis represents the value of corresponding parameter. Three biological replicates were used for each genotype.

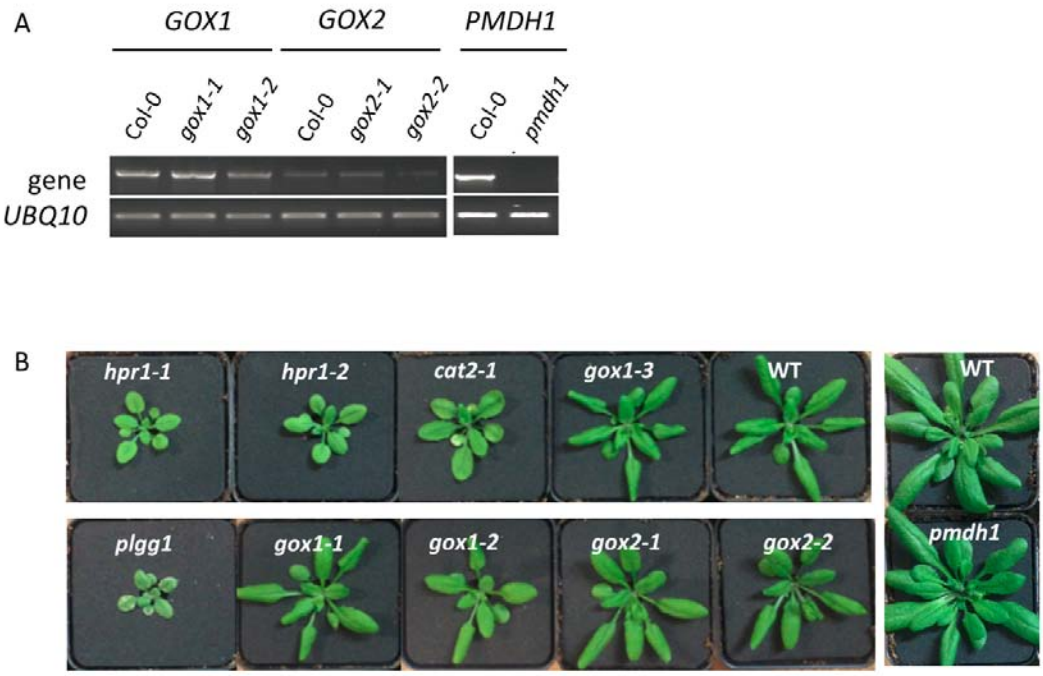

Figure 3.4. Gene expression analysis and growth appearance of photorespiratory mutants.

(A) Semi quantitative RT-PCR analysis of gene expression of the photorespiratory mutants that had not been reported before, including *gox1-1*, *gox1-2*, *gox2-1*, *gox2-2* and *pmdh1*. (B) Growth phenotype of photorespiratory mutants that had been growing under ambient air for 3-3.5 weeks.

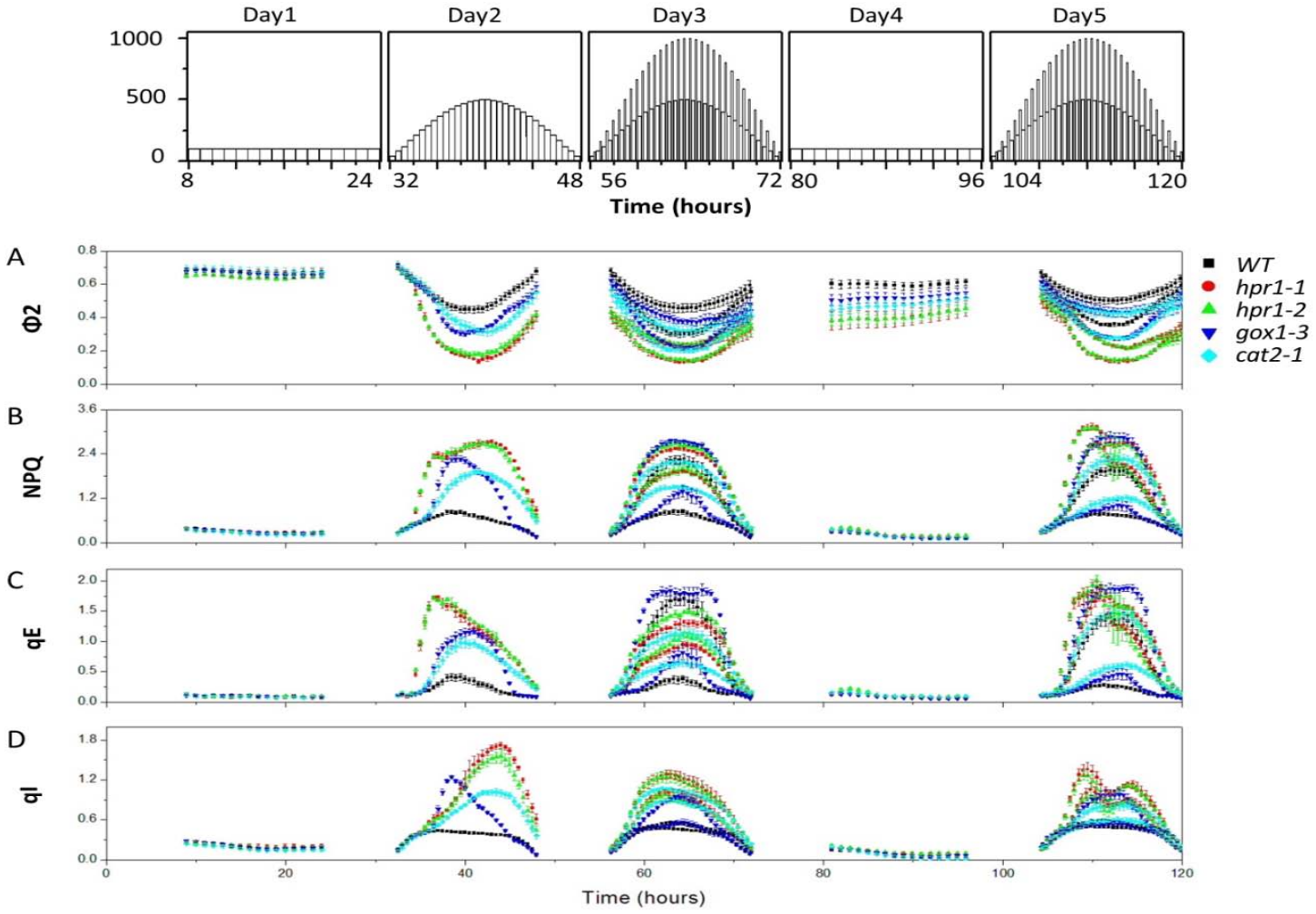

Figure 3.5. Photosynthetic performance of photorespiratory mutants under high light and fluctuating light conditions.

Figure 3.5. (cont'd)

Photorespiratory mutants, including *hpr1-1*, *hpr1-2*, *gox1-3* and *cat2-1*, and WT were tested in DEPI under high light and fluctuating light conditions. Each horizontal panel shows the measurement of a photosynthetic parameter across 5 days. The x axis represents the time points, and y axis represents the value of the corresponding parameter. Three biological replicates were used for each genotype.

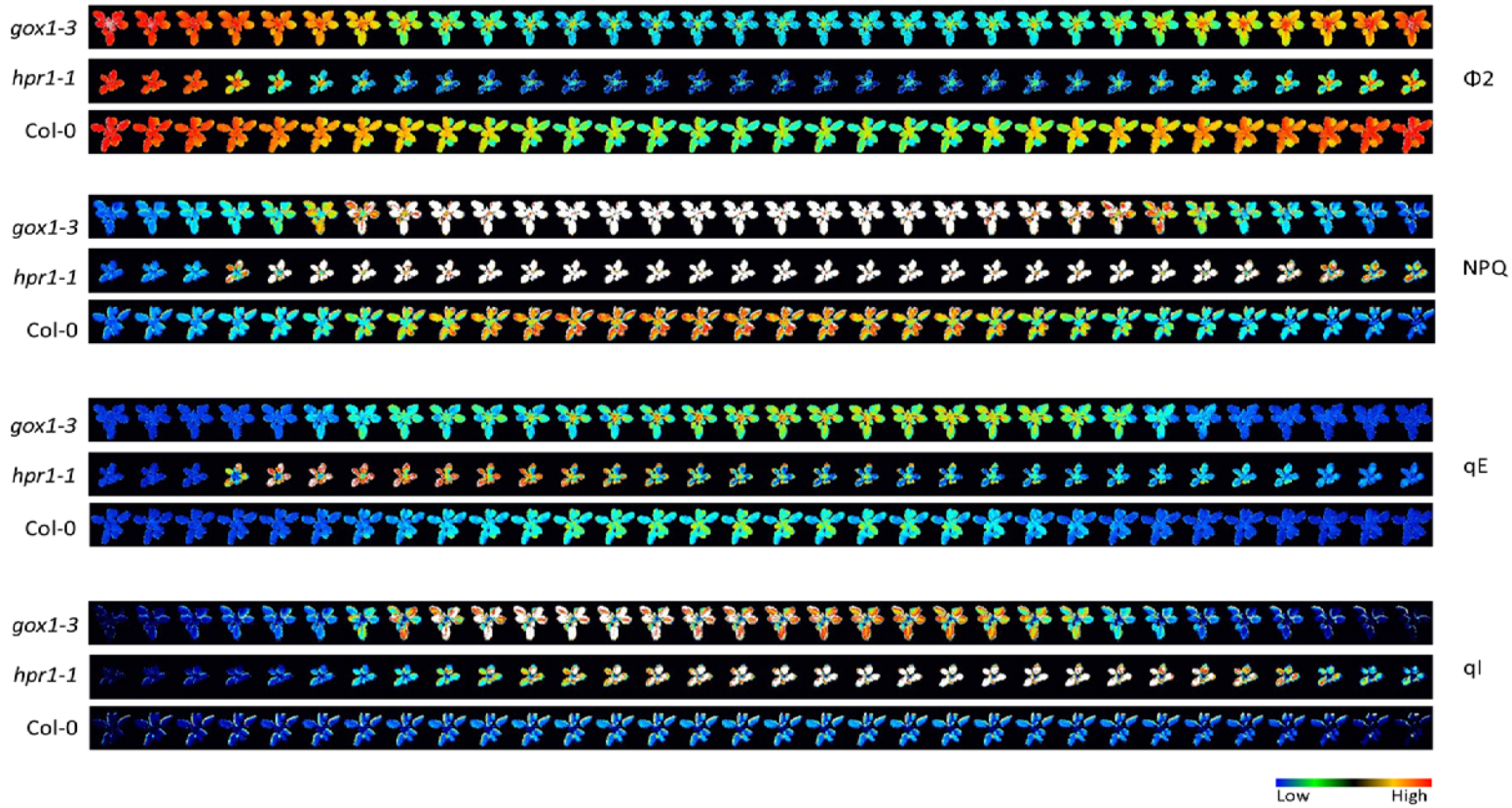

Figure 3.6. Chlorophyll fluorescence images of representative photorespiratory mutants under sinusoidal light on Day 2

Figure 3.6. (cont'd)

Pseudo fluorescence images of *hpr1-1*, *gox1-3* and WT are shown. Each horizontal panel shows the measurement of a photosynthetic parameter. Images for individual plants are arranged from left to right according to the chronological order of each measurement under sinusoidal light on Day 2, which include measurements at 32 time points.

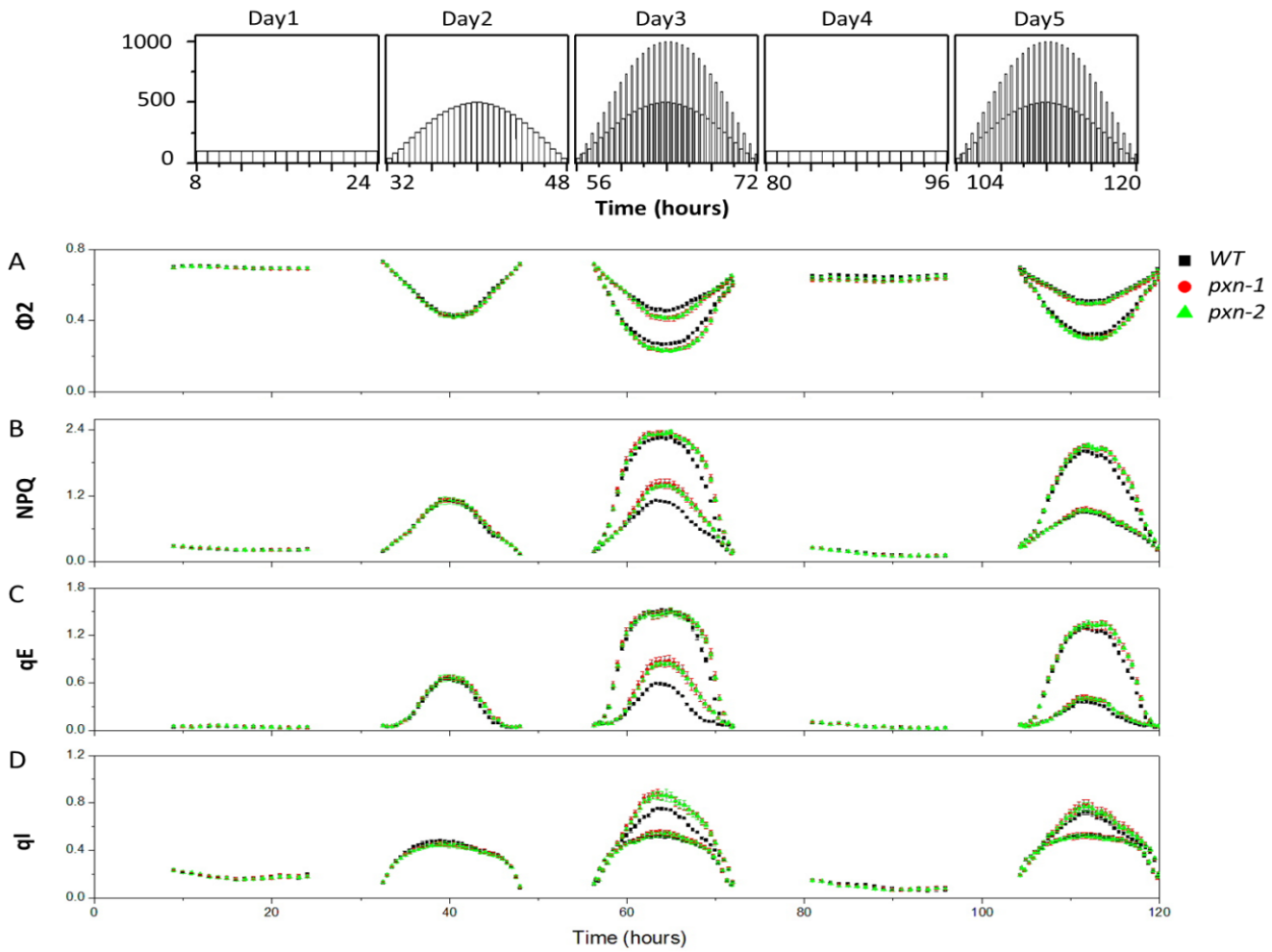

Figure 3.7. Mutants of the peroxisomal NAD$^+$ transporter PXN, *pxn-1* and *pxn-2*, exhibit emerging phenotype under fluctuating light conditions.

Figure 3.7. (cont'd)

Each horizontal panel shows the measurement of a photosynthetic parameter across 5 days. The x axis represents the time points, and y axis represents the value of the corresponding parameter. Three biological replicates were used for each genotype.

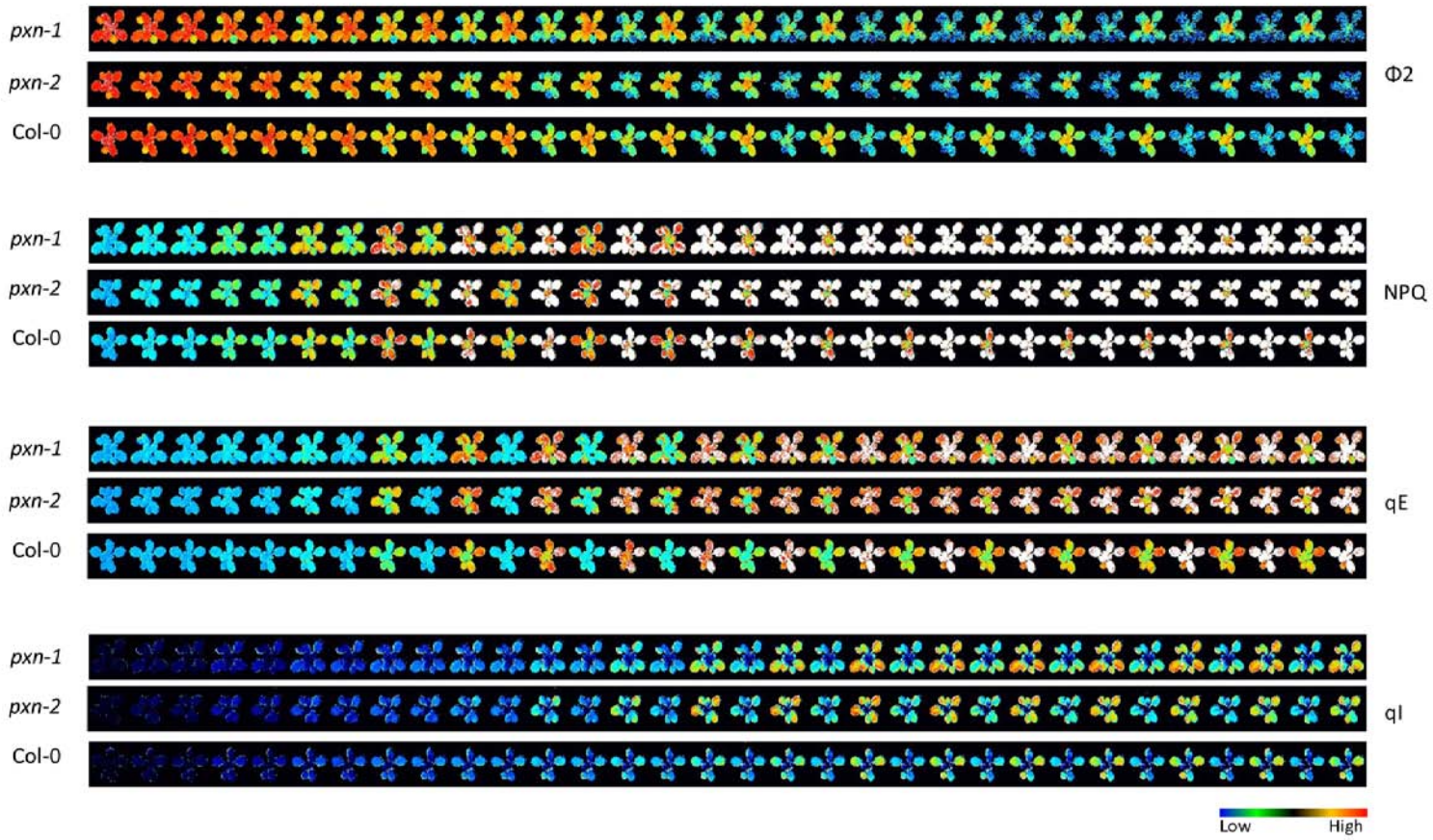

Figure 3.8. Chlorophyll fluorescence image of *pxn* under the first half period of fluctuating light on Day 3.

Figure 3.8. (cont'd)

Pseudo fluorescence images of *pxn-1*, *pxn-2* and WT are shown. Each horizontal panel shows the measurement of a photosynthetic parameter. Images for individual plant are arranged from left to right according to the chronological order of each measurement under the first half period of fluctuating light on Day 3, which includes measurements at 32 time points.

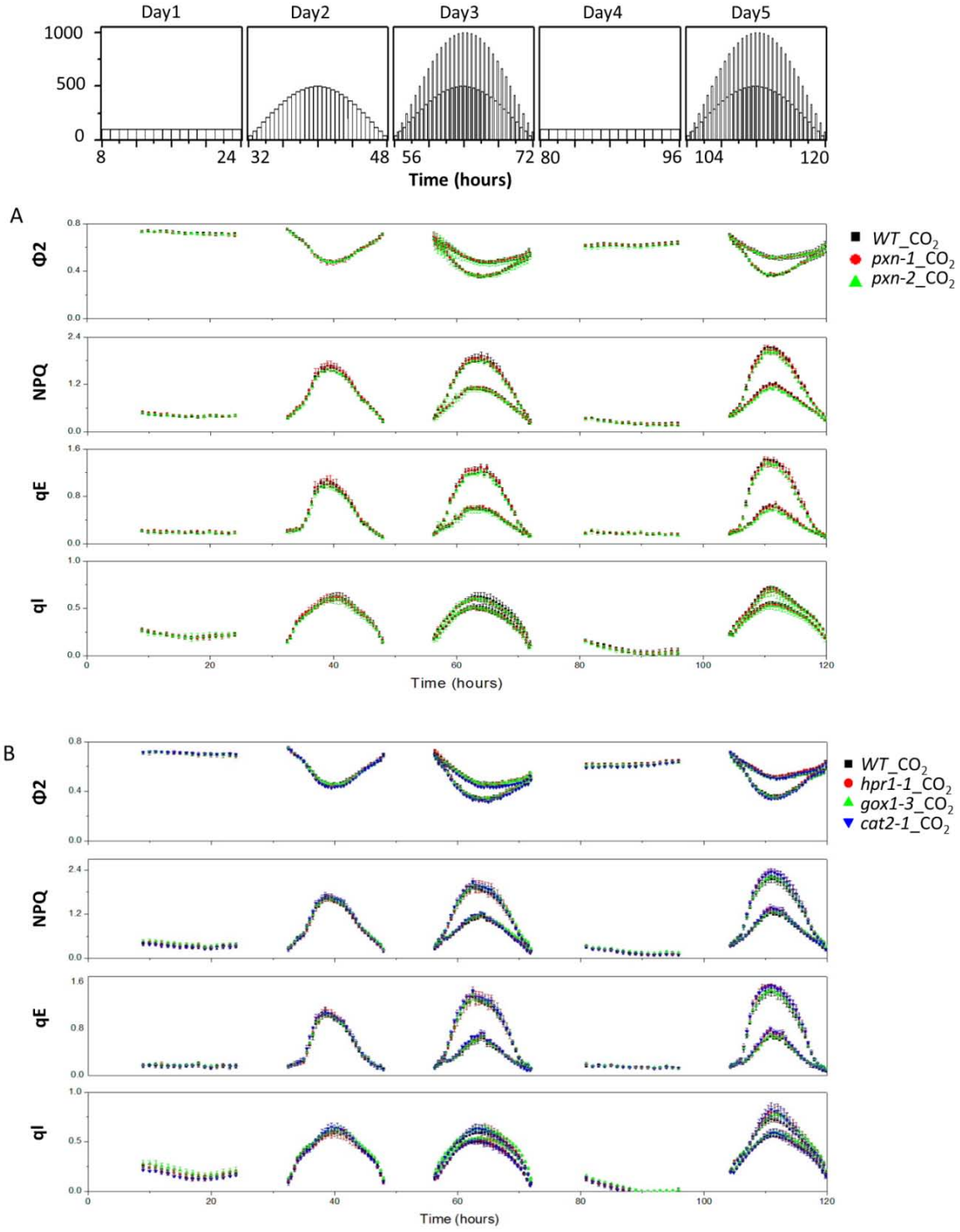

Figure 3.9. Supply of CO_2 rescued the emerging phenotype exhibited in the photorespiratory mutants and *pxn* mutants.

Figure 3.9. (cont'd)

Photorespiratory mutants and *pxn* mutants were tested under dynamically changing lights in the 5-day experiment setting in DEPI with elevated CO_2 (3000ppm). Three biological replicates were used for each genotype.

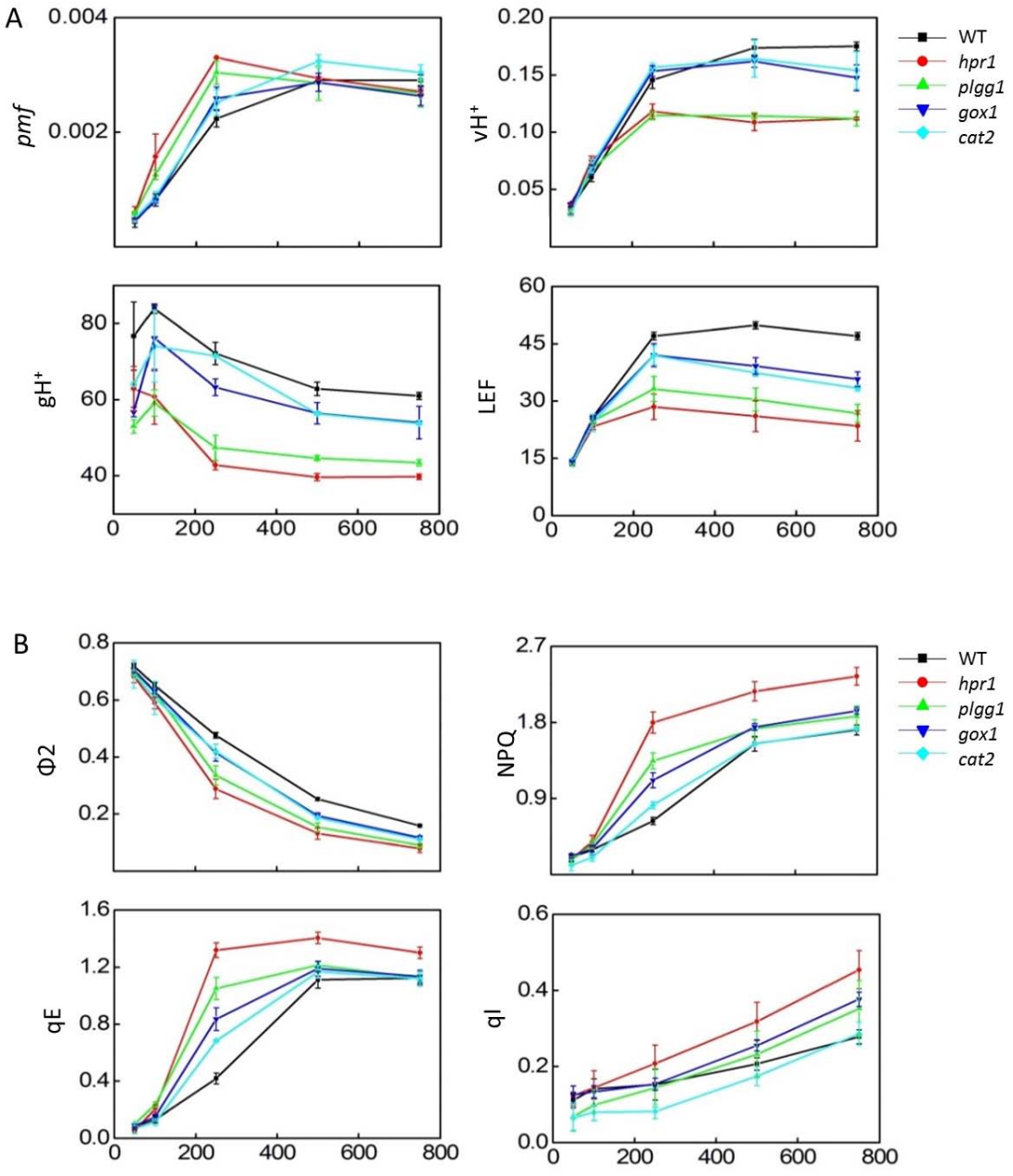

Figure 3.10. Quantitative spectroscopic analysis of photorespiratory mutants.

(A). In vivo spectroscopic assays of mutants under 50, 100, 250, 500 and 750 µmol m^{-2} s^{-1} of light. Three biological replicates were used for each genotype. (B). In vivo spectroscopic measurements of Φ2, NPQ, qE and qI in the mutants.

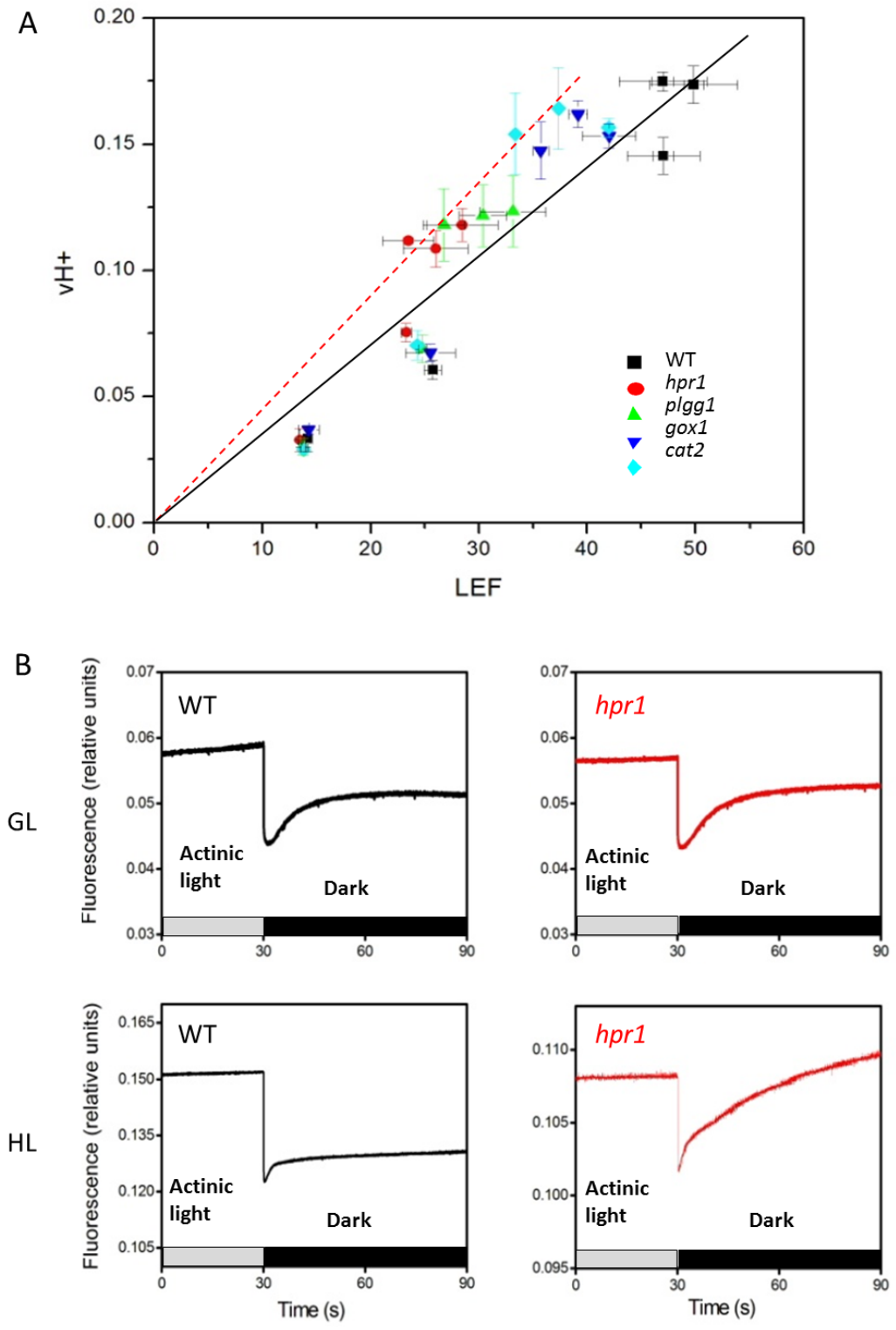

Figure 3.11. Activation of CEF in *hpr1* under high light conditions.

Figure 3.11. (cont'd)

(A). Light driven proton efflux vH^+ as a function against LEF in the mutants and WT under 50, 100, 250, 500 and 750 μmol m^{-2} s^{-1} of light. Three biological replicates were used for each genotype. B. Chlorophyll fluorescence rise post illumination in *hpr1* and WT under growth light (GL) (100 μmol m^{-2} s^{-1}) and 6 hours of HL (1000 μmol photons m^{-2} s^{-1}).

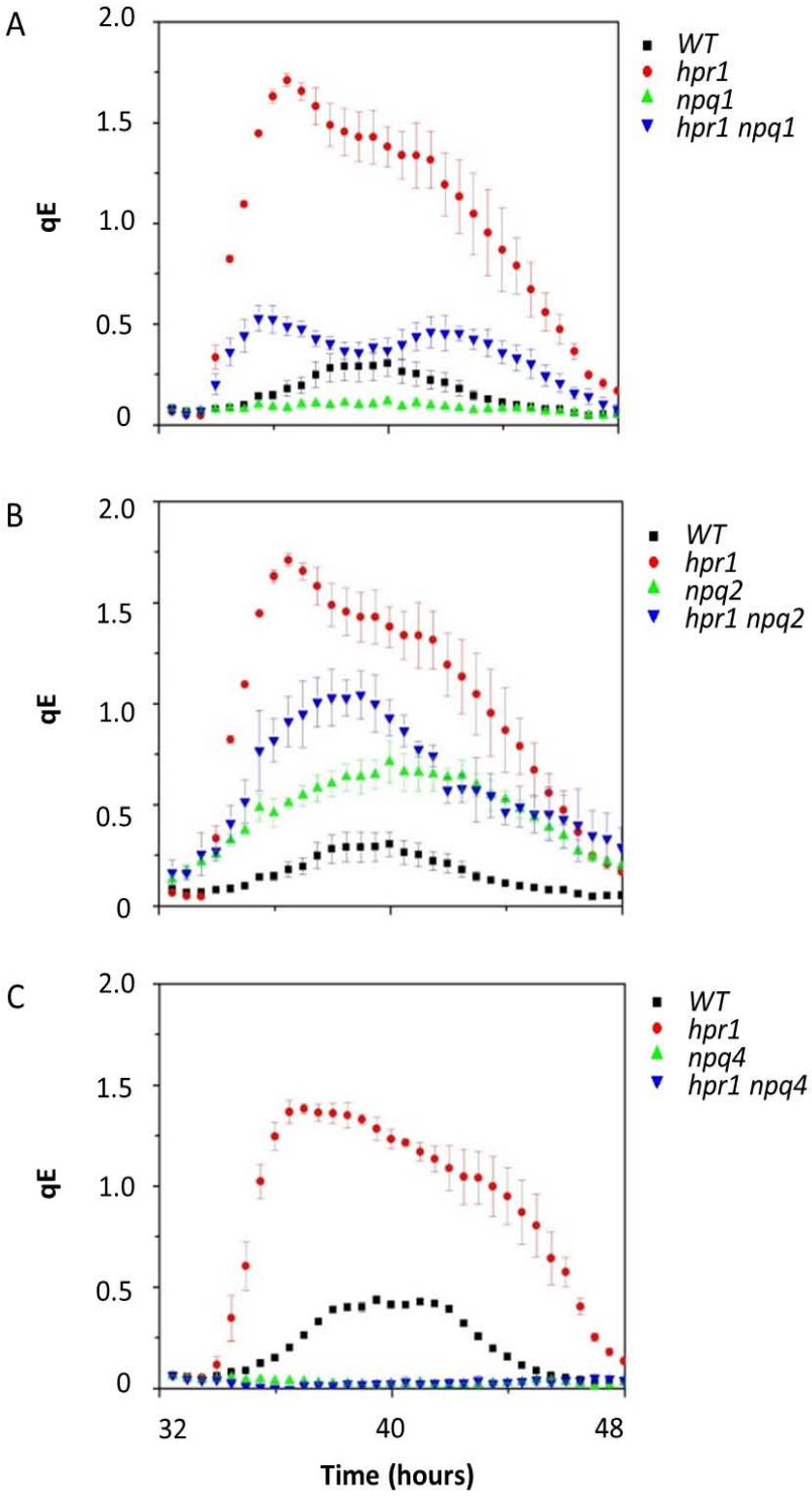

Figure 3.12. qE measurement in *hpr1 npq* double mutants.

Figure 3.12. (cont'd)

(A) qE kinetics under sinusoidal light on Day 2. (B) qE kinetics under sinusoidal light on Day 2. (C) qE kinetics under sinusoidal light on Day 2. Three biological replicates were used for each genotype.

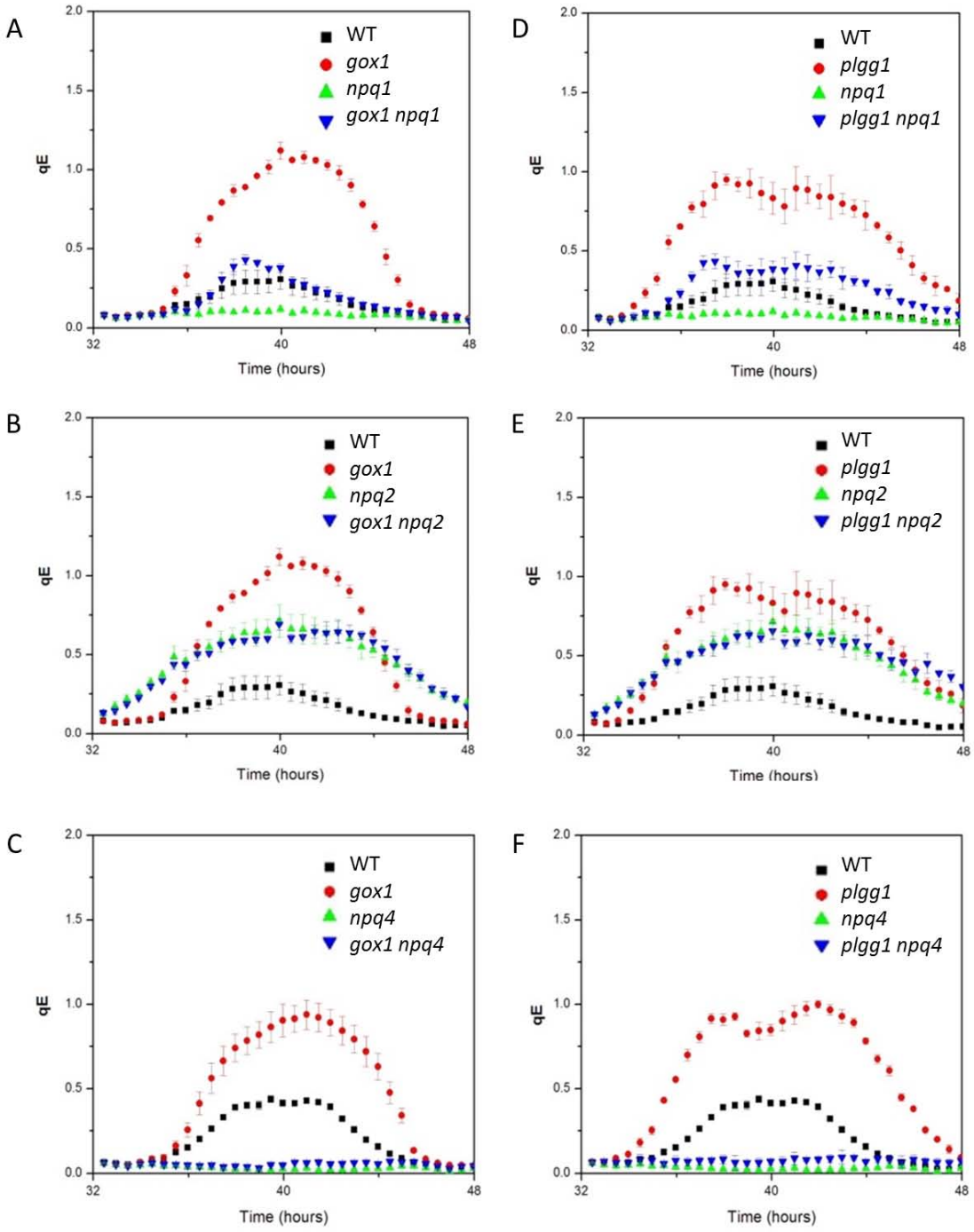

Figure 3.13. qE measurement of the *gox1 npq* and *plgg1 npq* double mutants

Figure 3.13. (cont'd)

(A-C) qE kinetics of the *gox1 npq* double mutants under sinusoidal light on Day 2. (D-F) qE kinetics of the *plgg1 npq* mutants under sinusoidal light on Day 2. Three biological replicates were used for each genotype.

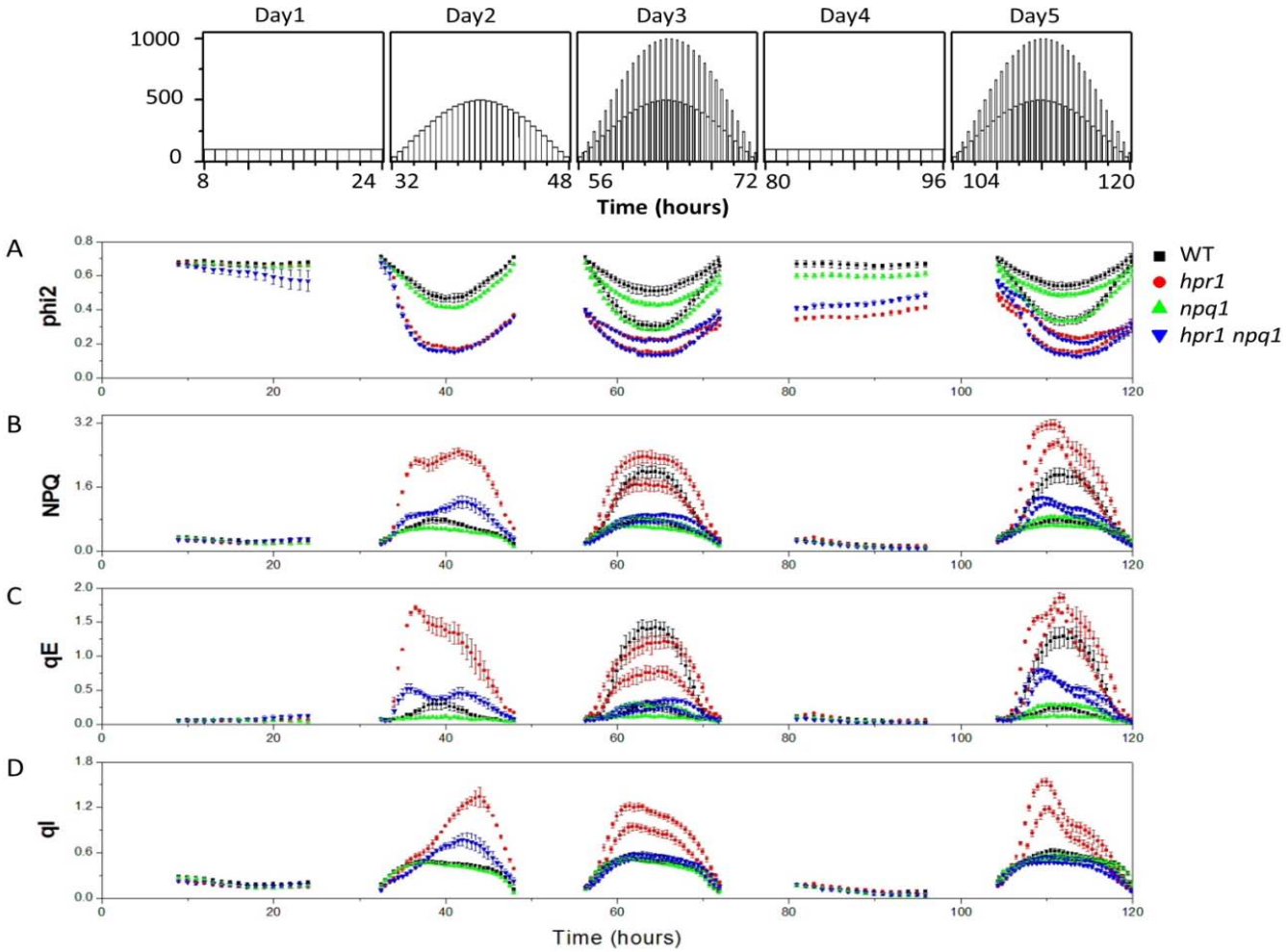

Figure 3.14. Photosynthetic measurements of *hpr1*, *npq1* and *hpr1 npq1* under dynamically changing light conditions.

Three biological replicates were used for each genotype.

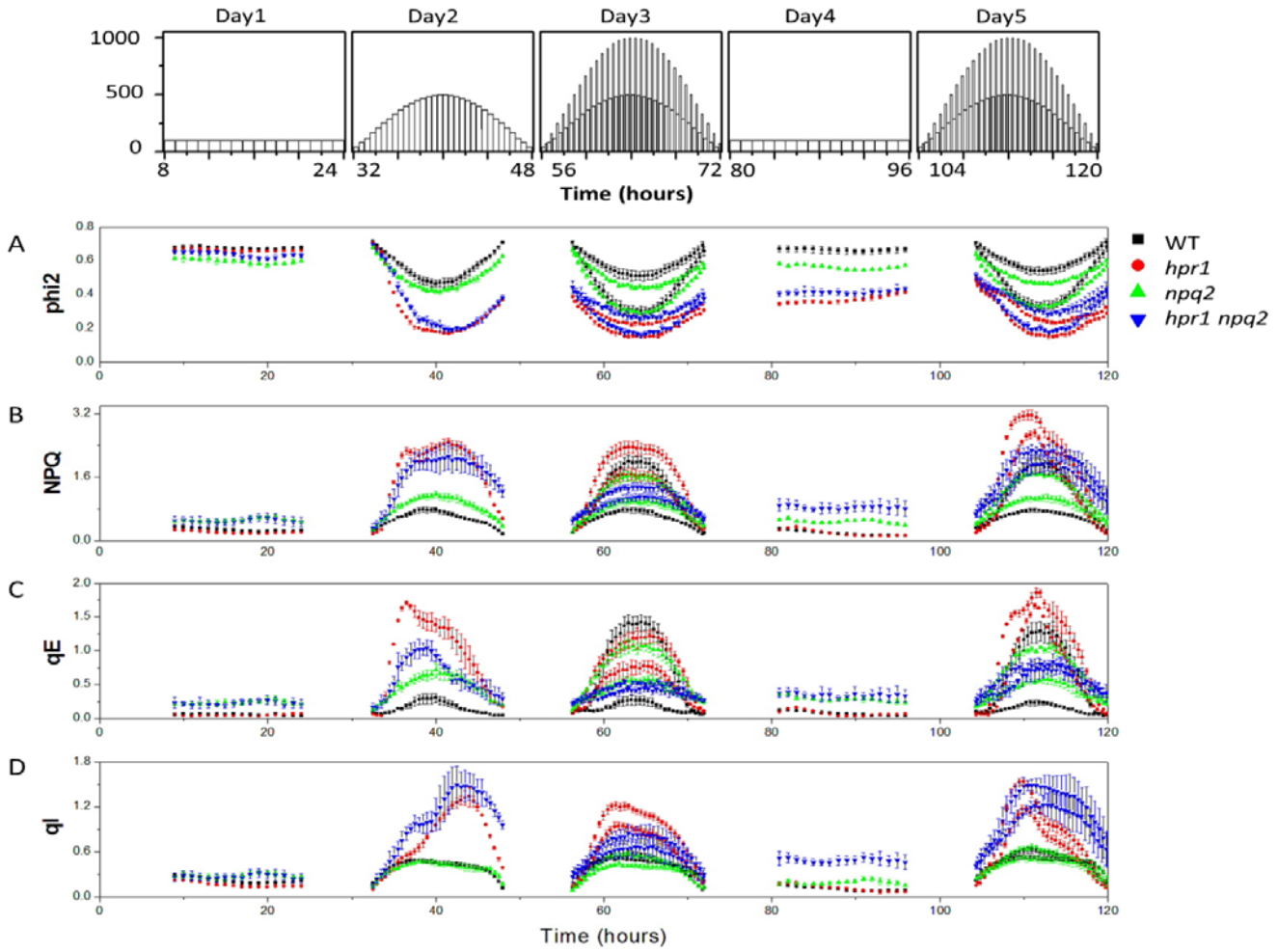

Figure 3.15. Photosynthetic measurements of *hpr1*, *npq2* and *hpr1 npq2* mutants under dynamically changing light conditions.

Three biological replicates were used for each genotype.

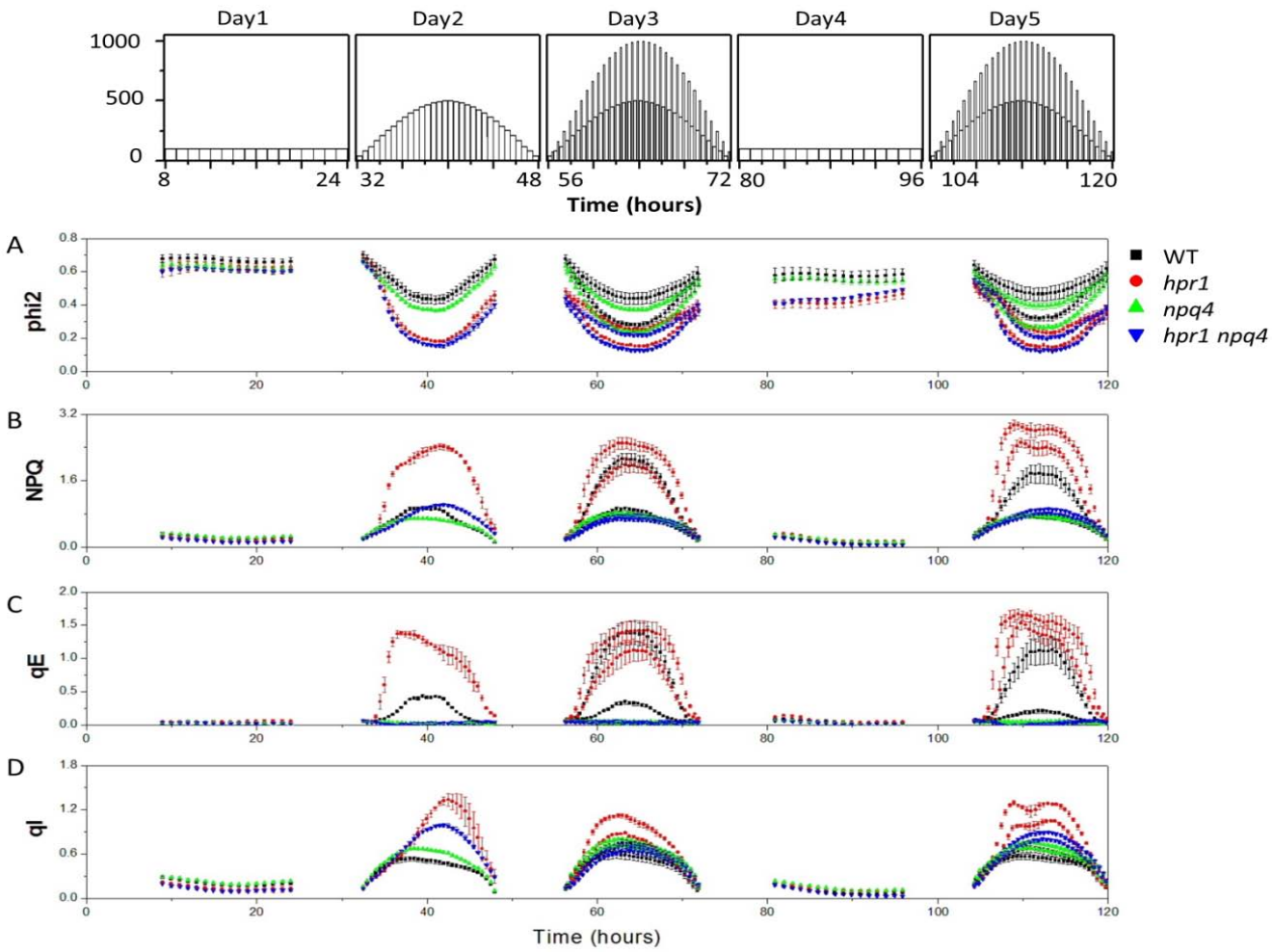

Figure 3.16. Photosynthetic measurements of *hpr1*, *npq4* and *hpr1 npq4* under dynamically changing light conditions.

Three biological replicates were used for each genotype.

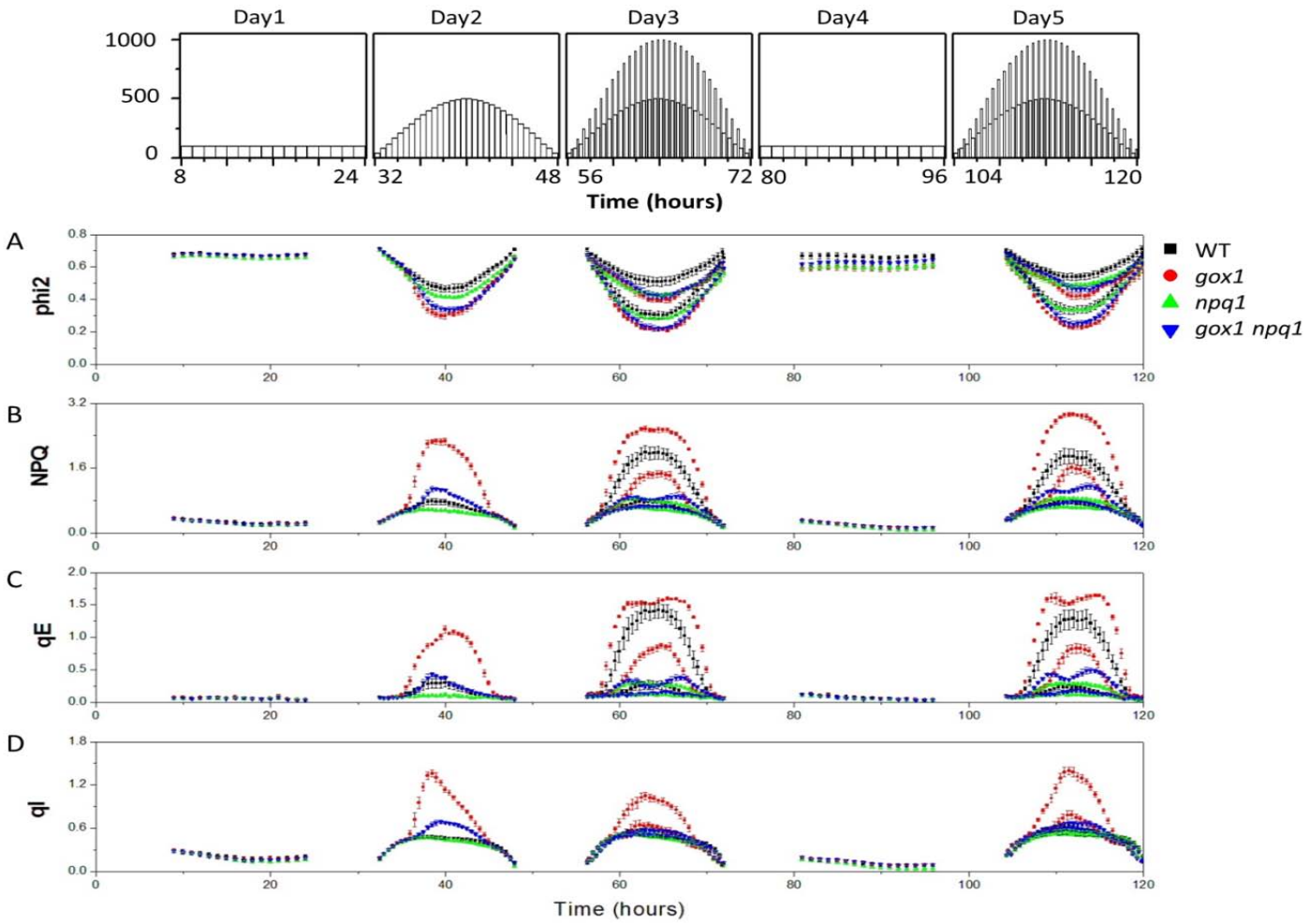

Figure 3.17. Photosynthetic measurements of *gox1*, *npq1* and *gox1 npq1* under dynamically changing light conditions.

Three biological replicates were used for each genotype.

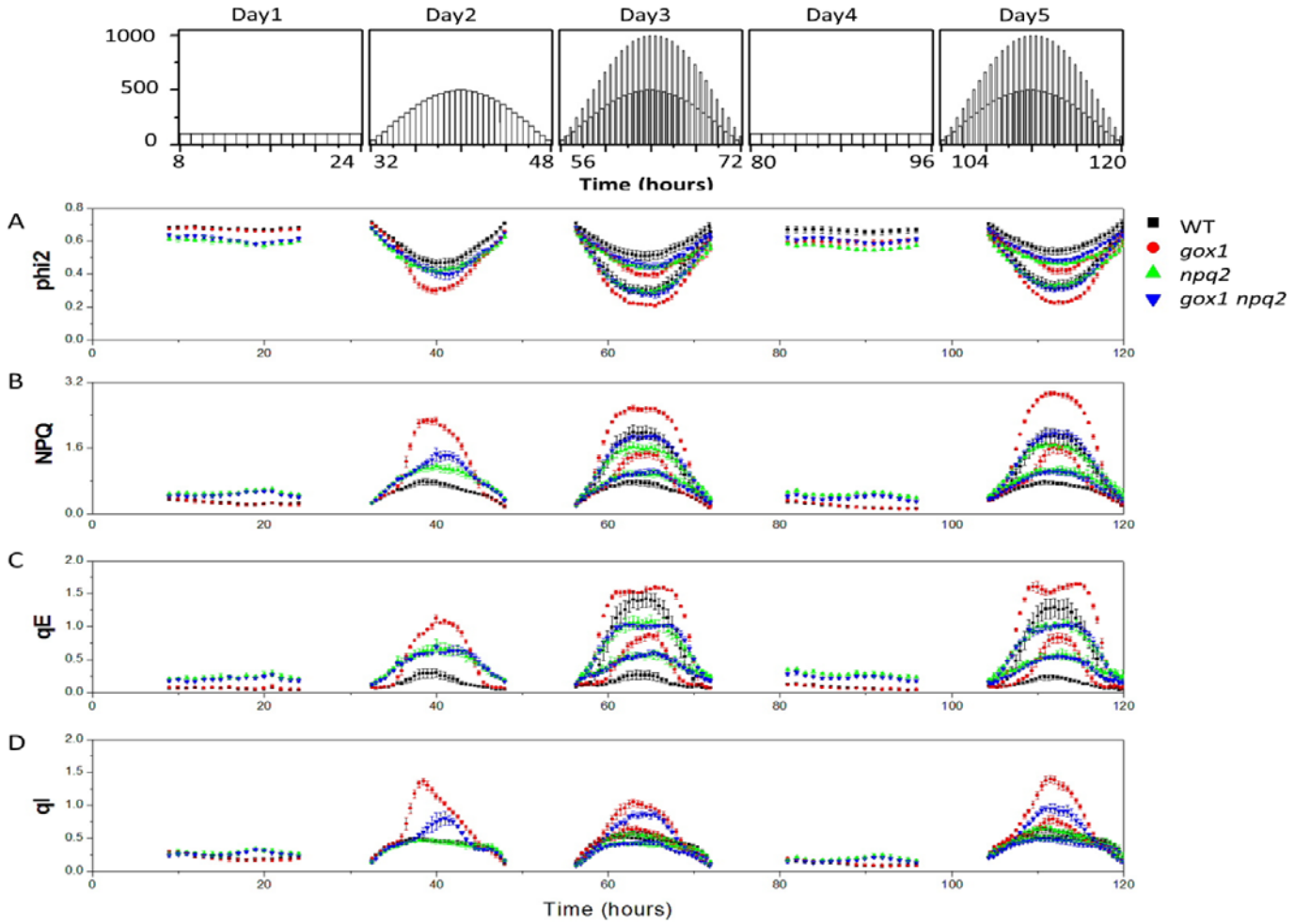

Figure 3.18. Photosynthetic measurements of *gox1*, *npq2* and *gox1 npq2* under dynamically changing light conditions.

Three biological replicates were used for each genotype.

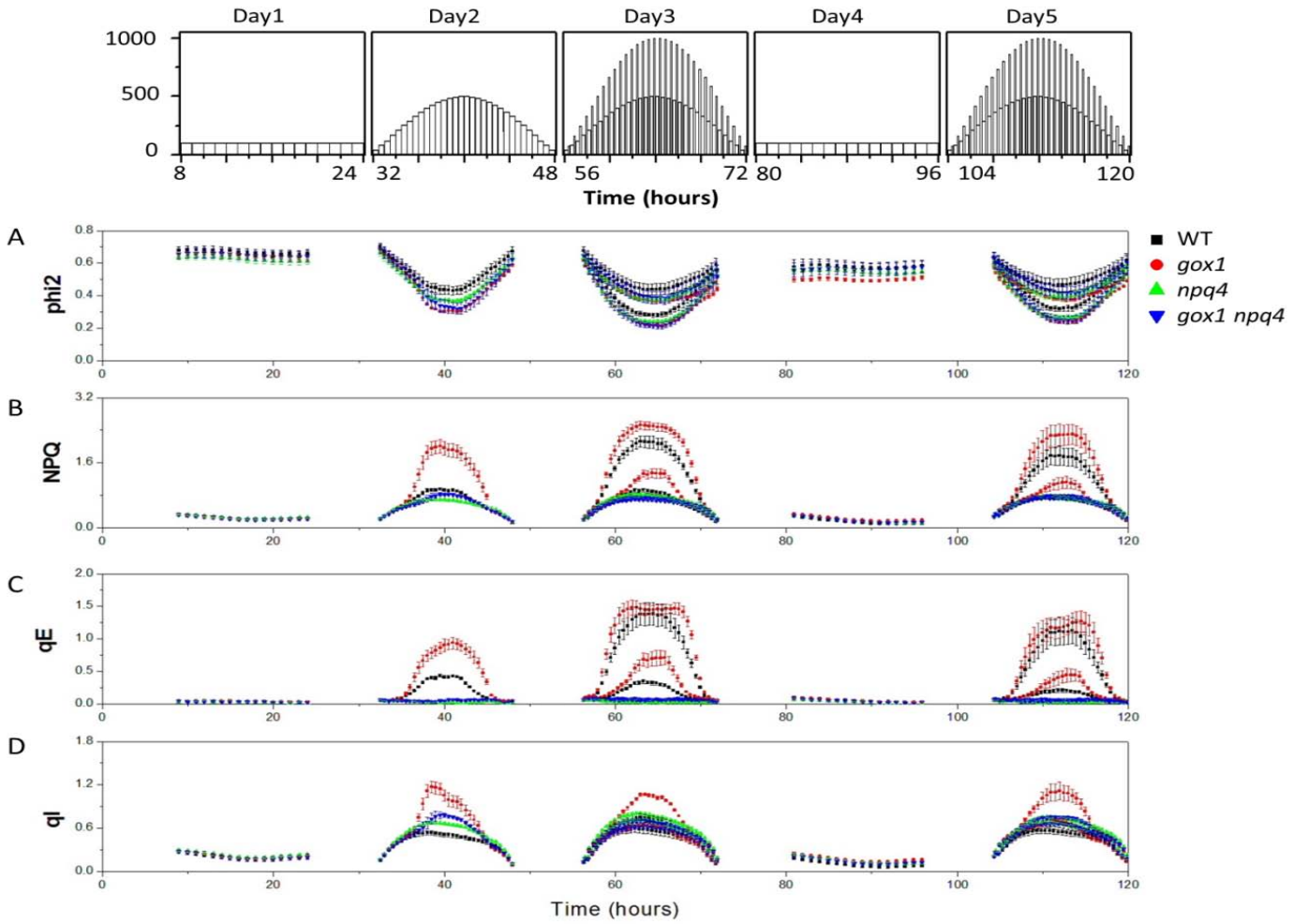

Figure 3.19. Photosynthetic measurements of *gox1*, *npq4* and *gox1 npq4* under dynamically changing light conditions.

Three biological replicates were used for each genotype.

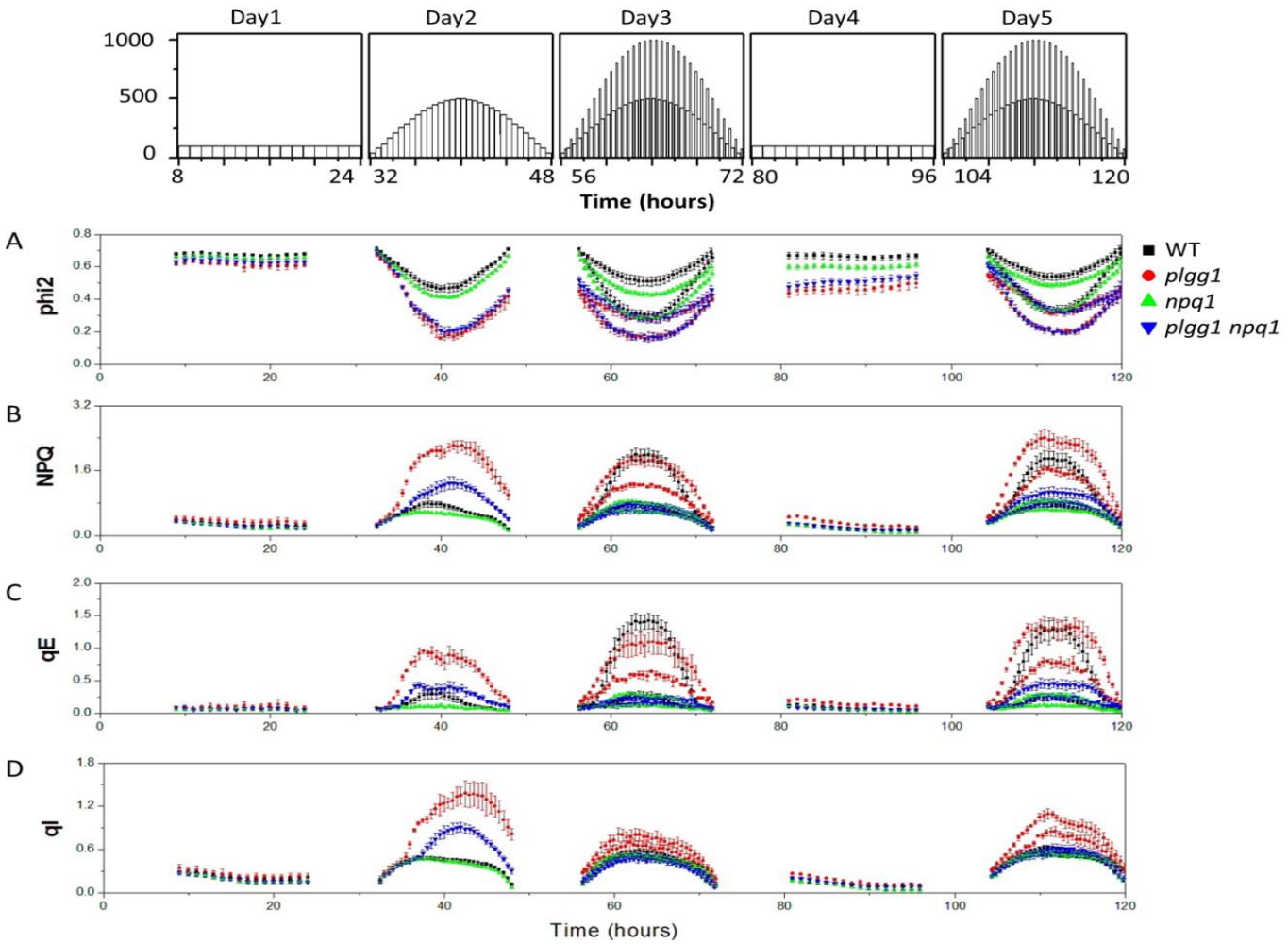

Figure 3.20. Photosynthetic measurements of *plgg1*, *npq1* and *plgg1 npq1* under dynamically changing light conditions.

Three biological replicates were used for each genotype.

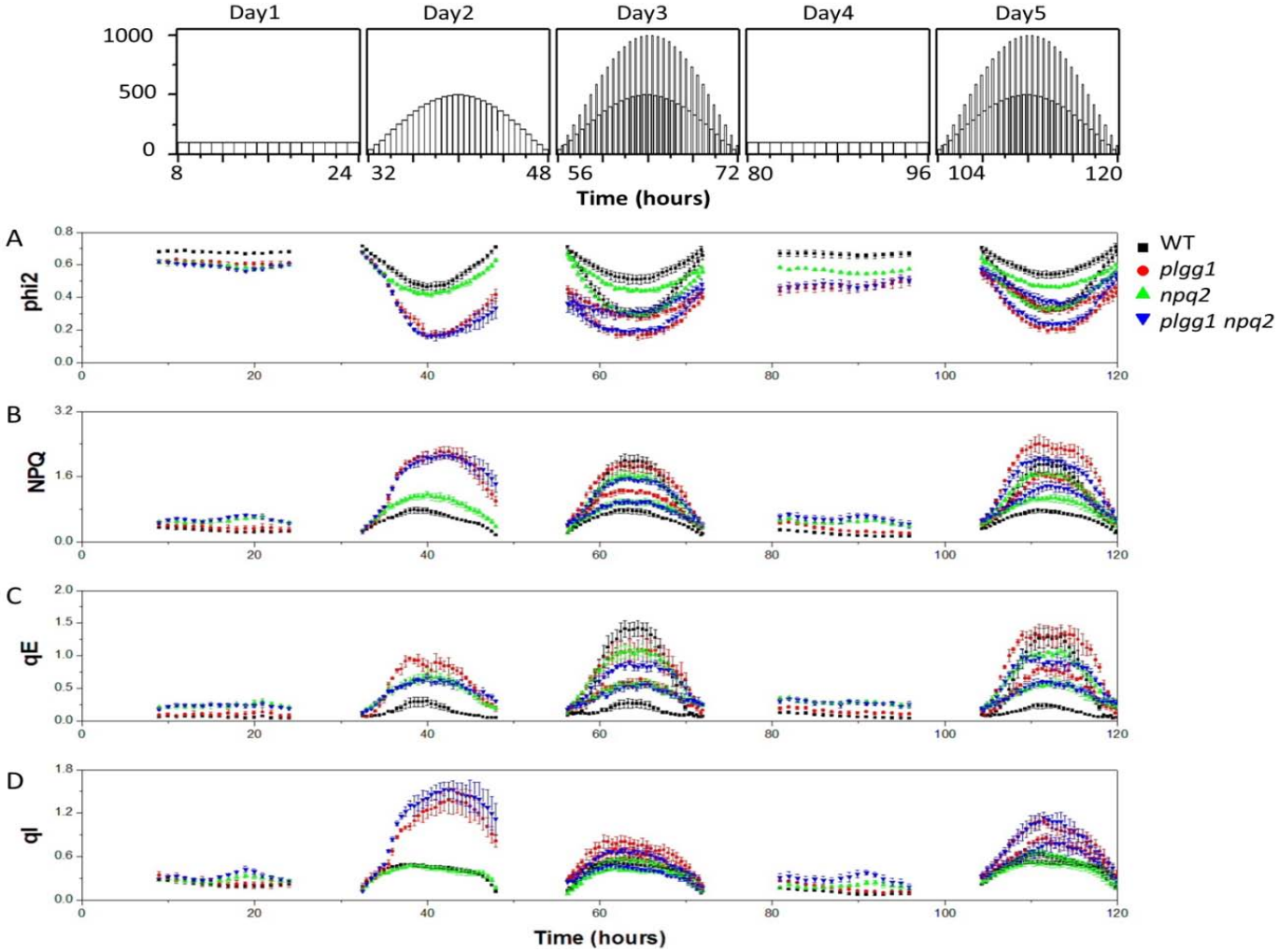

Figure 3.21. Photosynthetic measurements of *plgg1*, *npq2* and *plgg1 npq2* under dynamically changing light conditions.

Three biological replicates were used for each genotype.

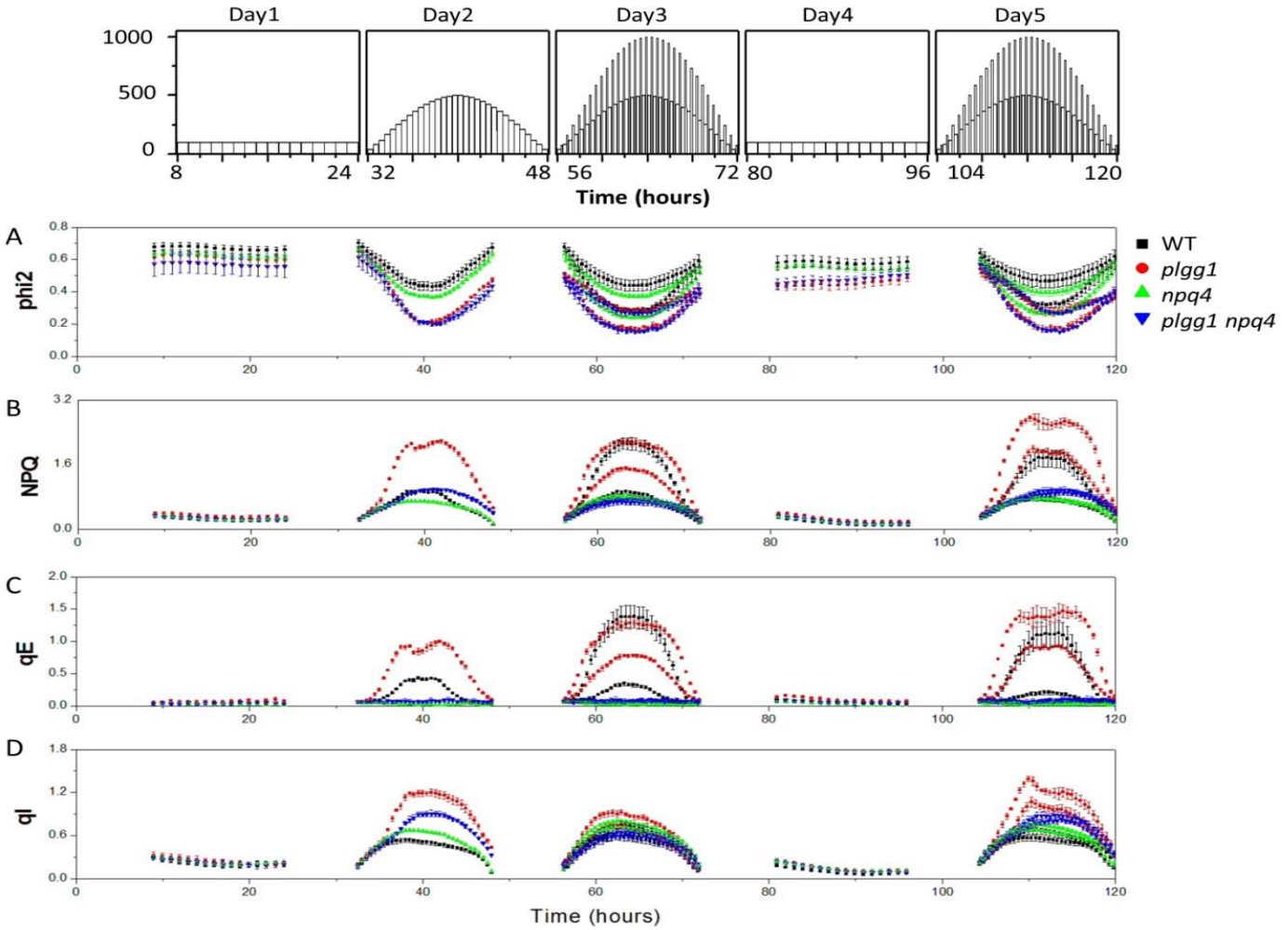

Figure 3.22. Photosynthetic measurements of *plgg1*, *npq4* and *plgg1 npq4* under dynamically changing light conditions.

Three biological replicates were used for each genotype.

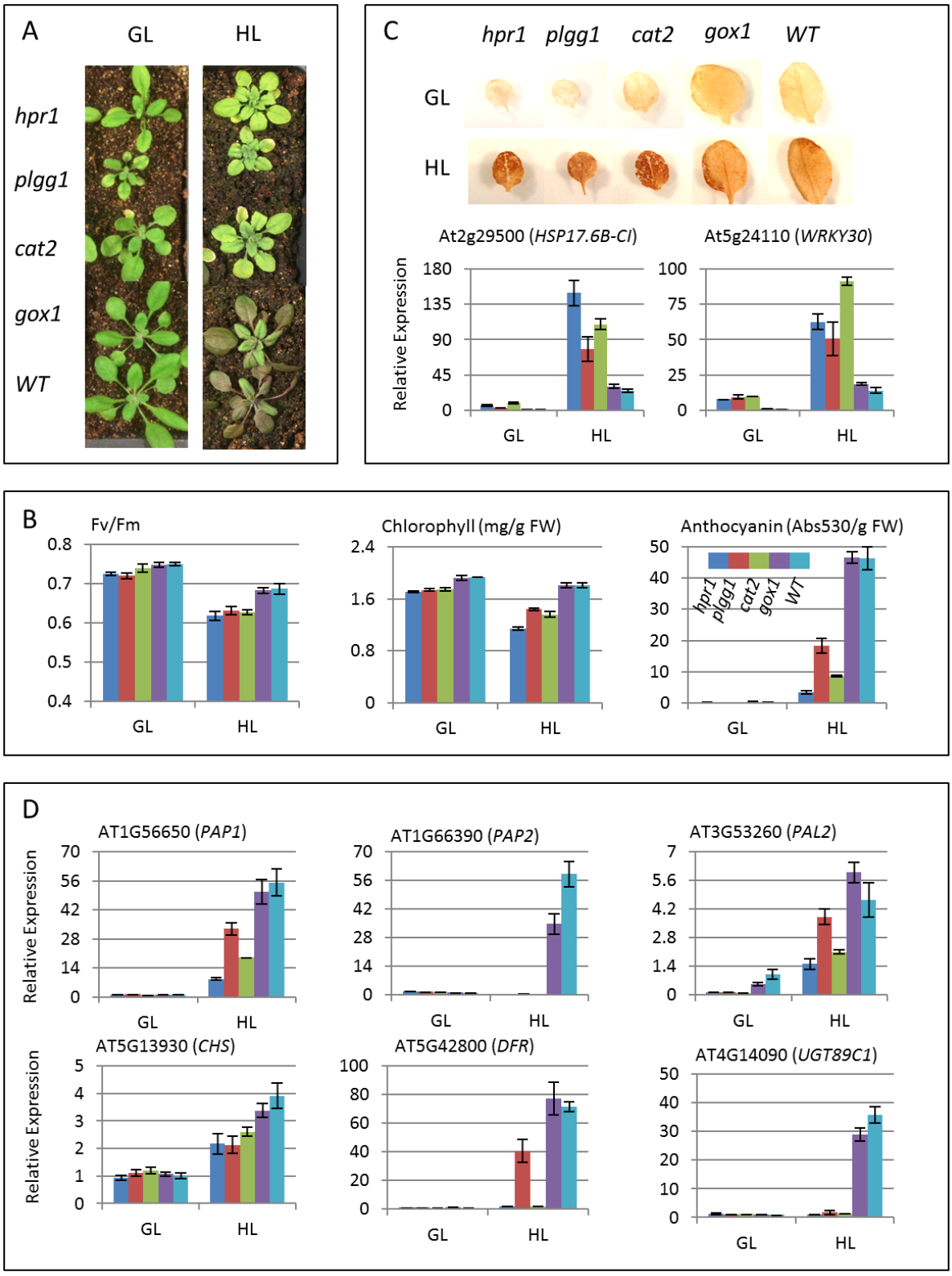

Figure 3.23. Adaptation of the photorespiratory mutants to long term HL stress.

Figure 3.23. (cont'd)

(A). 3-week-old plants grown under GL and treated with 3 days of HL. (B). Quantification of F_v/F_m, chlorophyll content and anthocyanin content. Three biological replicates were used for each genotype. (C). DAB staining of H_2O_2 in leaves of plants under GL and after 6 hours of HL treatment (top), and quantitative RT-PCR analysis of two oxidative stress-responsive genes (bottom). Three biological replicates were used for each genotype. (D). Quantitative RT-PCR analysis of six anthocyanin biosynthetic or regulatory genes. Three biological replicates were used for each genotype.

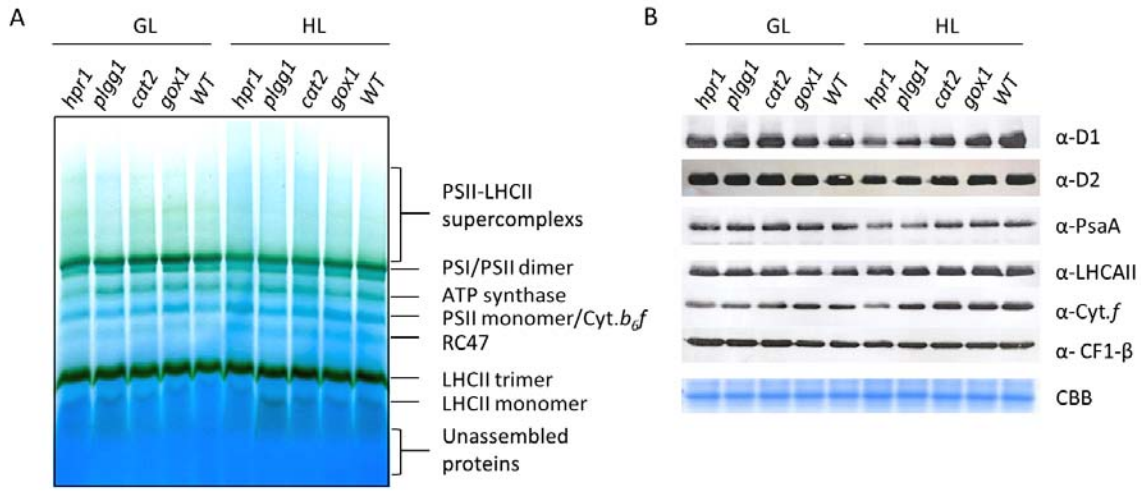

Figure 3.24. Analysis of the integrity of photosynthetic complexes and levels of photosynthetic subunits in photorespiratory mutants under high light.

(A). BN-PAGE analysis of thylakoid membrane protein complexes. Thylakoid samples were loaded on the basis of equivalent chlorophyll content (5μg) in each lane. (B). Immunoblot analysis of photosynthetic proteins. CBB, coomassie brilliant blue staining. Thylakoid samples were loaded on the basis of equal chlorophyll content (1.5μg) in each lane.

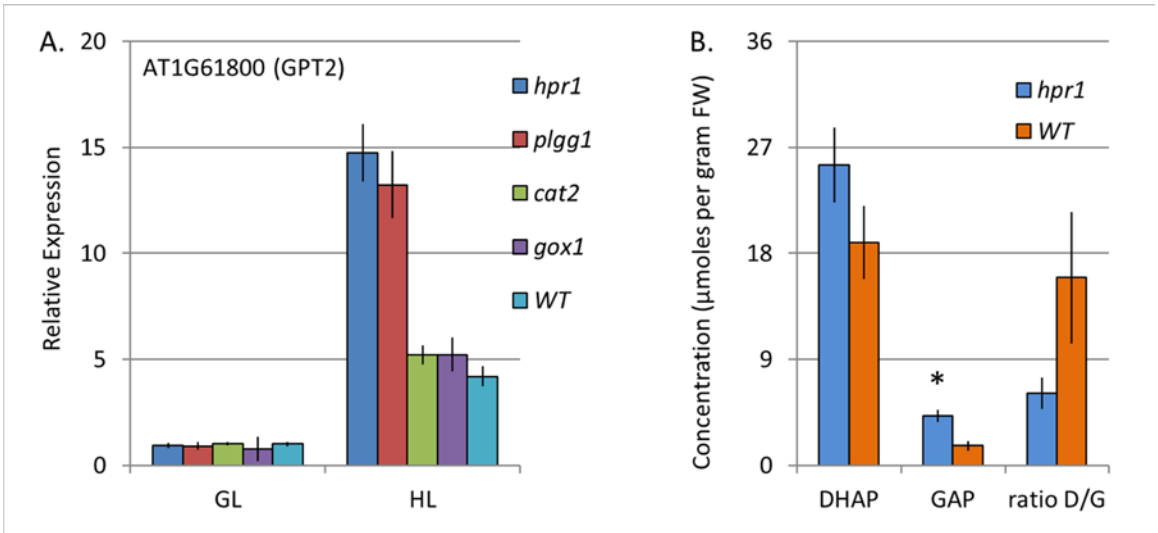

Figure 3.25. High light induction of *GPT2* expression in photorespiratory mutants and change of the amount of GAP and DHAP in *hpr1*.

(A). Quantitative RT-PCR analysis of *GPT2* transcripts in photorespiratory mutants under GL and after 6 hours of HL. Three biological replicates were used for each genotype. (B). Measurement of glyceraldehyde 3-phosphate (GAP) and dihydroxyacetone phosphate (DHAP) in *hpr1* and WT treated with 6 hours of HL. D/G, DHAP/GAP. Five biological replicates were used for each genotype. Asterisk indicates p-value < 0.01 in Student's *t* test.

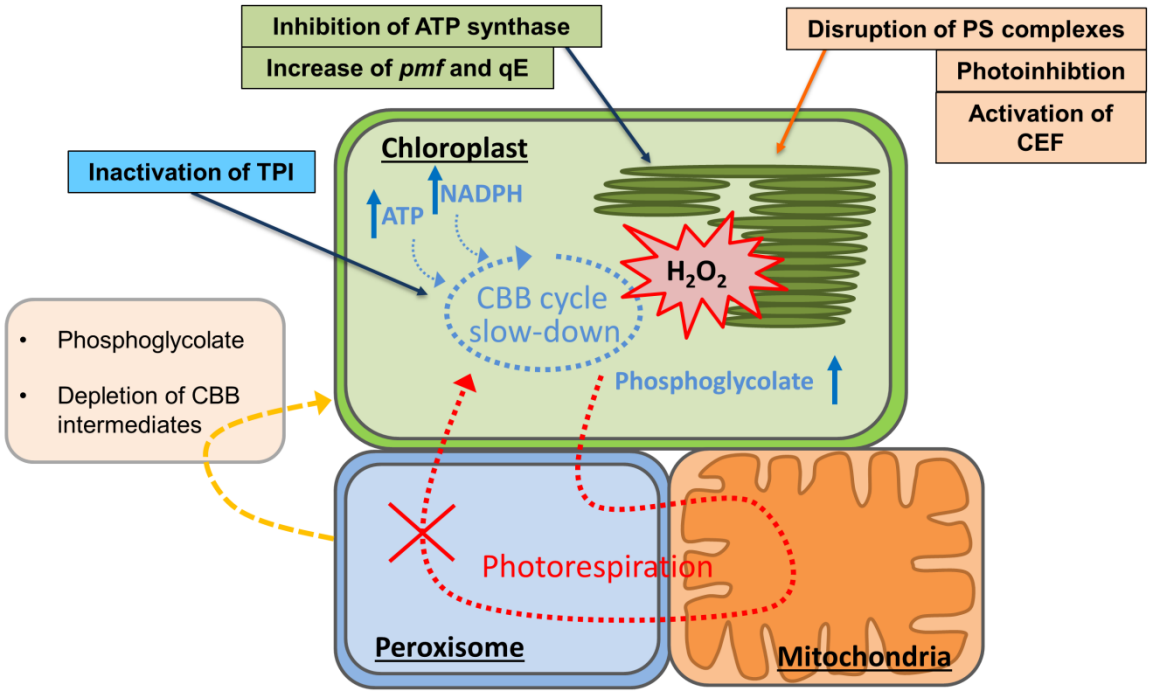

Figure 3.26. An integrated model for the role of photorespiration in modulating photosynthesis.

The photorespiration pathway initiates with the production of phosphoglycolate by Rubisco in the chloroplast, and ends with the re-feeding of glycerate to the CBB cycle, with the cooperation of chloroplasts, peroxisomes and mitochondria. The photorespiratory metabolic flow is indicated by the red dotted line. As a consequence of blocking of the photorespiration pathway, the level of phosphoglycolate is increased, which inhibits TPI activity. Meanwhile, depletion of the CBB cycle intermediates, such as glycerate, slows down the CBB cycle and causes accumulation of stromal ATP and NADPH. The accumulated ATP in stroma inhibits ATP synthase conductivity, which leads to increased *pmf* and subsequently stimulates an increase of NPQ to dissipate excessive energy. Accumulated stromal ATP and NADPH are also subsequently used to generate

Figure 3.26. (cont'd)

ROS and creates enhanced oxidative stress as well. The increased oxidative stress impacts on various photosynthetic processes, such as photoinhibition, compromised photosystem integrity, damaged photosystem subunit and activation of CEF. This integrated model provides novel mechanistic insights into the connection between photorespiration and photosynthesis.

Table 3.1. List of screened peroxisomal mutants

ATG ID	gene name	Annotation	mutant name	mutant ID	background
AT4G35090	CAT2	catalase 2	*cat2-1*	SALK_076998	Col-0
AT1G68010	HPR1	hydroxypyruvate reductase 1	*hpr1-1*	SALK_067724	Col-0
			hpr1-2	SALK_143584	Col-0
AT5G62810	PEX14	peroxin 14	*pex14*	SALK_007441	Col-0
AT4G33650 AT2G14120 AT3G19720	DRP3A DRP3B DRP5B	dynamin-related protein	*drp3A-2 drp3B-2 drp5B-2*	SALK_147485 SALK_112233 SAIL 71D_11	Col-0
AT4G33650 AT2G14120	DRP3A DRP3B	dynamin-related protein	*drp3A-2 drp3B-2*	SALK_147485 SALK_112233	Col-0
AT3G19720	DRP5B	dynamin-related protein	*drp5B-2*	SAIL 71D_11	Col-0
AT1G78590	NADK3	arabidopsis Thaliana NADH Kinase 3	*nadk3-1*	SALK_079342	Col-0
AT2G39970	PXN	peroxisomal membrane protein of 36kDa	*pxn-1*	GK_046D01	Col-0
			pxn-2	GK_830A06	Col-0
AT3G14415	GOX2	glycolate oxidase 2	*gox2-1*	SALK_082542	Col-0
			gox2-2	SALK_025574	Col-0
AT5G56290	PEX5	PTS1 peroxisomal protein receptor	*pex5*	CS3949	Col-0
AT5G43280	DCI1	delta(3,5),Delta(2,4)-dienoyl-CoA isomerase 1	*dci1-1*	SALK_002674	Col-0
AT3G58840	PMD1	peroxisome mito division factor	*pmd1-1*	CS854214	Col-0
AT4G35000	APX3	ascorbate Peroxidase 3	*apx3-1*	SALK_059352	Col-0
AT2G24580	SOX	sarcosine oxidase	*sox-1*	SALK_017108	Col-0
AT3G06810	IBR3	IBA-response 3/ acyl-CoA dehydrogenase	*ibr3-1*	SALK_033467	Col-0
AT1G11840	GLX1	glyoxylase I homolog	*glx1-1*	SALK_110070	Col-0

Table 3.1. (cont'd)

AT2G42490	CuAO	copper amine oxidase	*cuao-1*	SALK_095214	Col-0
			cuao-2	SALK_096065	Col-0
AT1G06460	Acd31.2	small heat shock protein	*acd31.2-1*	SALK_114949	Col-0
AT3G58740	CSY1	citrate synthase 1	*csy1*	SALK_007026	Col-0
AT1G55320	AAE18	similarity to acyl activating enzymes	*aae18-1*	SALK_071698	Col-0
			aae18-2	SALK_075217	Col-0
AT2G38180	GLH	hydrolase-type esterase	*glh1*	SALK_052637	Col-0
AT3G16910	AAE 7	acyl CoA activating enzyme	*aae7-1*	SALK_009373	Col-0
			aae7-2	SALK_055243	Col-0
AT5G04870	CPK1	calcium dependent protein kinase 1	*cpk1-1*	SALK_007698	Col-0
			cpk1-2	SALK_080155	Col-0
AT5G41210	GSTT1	glutathione transferase	*gstt1*	SALK_075383	Col-0
AT1G48320	sT1	small thioesterase 1	*dhnat1-1*	SAIL_1253_B02	Col-0
AT5G16370	AAE5	acyl-activating enzyme 5	*aae5-1*	SALK_009731	Col-0
AT5G48880	KAt5	3 keto-acyl-CoA thiolase 5	*kat5-1*	SALK_132871	Col-0
			kat5-2	SALK_144464	Col-0
AT2G35690	ACX5	acyl CoA oxidase in JA biosynthesis	*acx5*	SALK_009998	Col-0
AT1G77540	ATF2	Acetyltransferase	*atf2-1*	FLAG_206E09	Ws-4
AT4G12910	SCPL20	serine Carboxypeptidase-like 20	*scpl20-1*	CS818066	Col-3
			scpl20-2	SALK_147839	Col-0
AT3G17420	GPK1	glyoxysomal protein kinase 1	*gpk1-1*	SALK_047519	Col-0
			gpk1-2	SALK_047485	Col-0
AT1G11840	GLX	glyoxylase I homolog	*glx1*	SALK_059170	Col-0
AT4G39850	PXA1	ATP binding cassette transporter	*pxa1*	SALK_002100	Col-0

Table 3.1. (cont'd)

AT3G15950	UP2	unknown protein 2	*up2-1*	GK_381F11	Col-0
AT3G14420	GOX1	glycolate oxidase 1	*gox1-1*	SALK_051930	Col-0
			gox1-2	SALK_133946	Col-0
			gox1-3	SAIL_177_G11	Col-0
AT5G11910	ELT1	esterase/ lipase/ thioesterase family isoform 1	*elt1-1*	FLAG_632F03	Ws-4
AT5G44250	UP5	unknown protein	*up5-1*	SALK_107281	Col-0
AT2G42790	CSY3	citrate synthase 3	*csy3-1*	SALK_076319	Col-0
AT1G07180	NDA1	NAD(P)H dehydrogenase	*nda1*	SALK_054530	Col-0
AT1G49670	NQR	undefined, involved in oxidative stress tolerance	*nqr-1*	SALK_014601	Col-0
			nqr-2	SALK_123841	Col-0
AT3G05970	LACS6	long-chain acyl-CoA synthetase 6	*lacs6-1*	SALK_069510	Col-0
AT1G28320	DEG15	degredation of periplasmic proteins 15	*deg15-1*	SALK_022777	Col-0
AT1G49350	PLCK	pfkB-like carbohydrate kinase	*plck*	SALK_006361	Col-0
AT1G16730	UP6	unknown protein 6	*up6-1*	SALK_122395	Col-0
AT4G16760 AT2G35690	ACX1/ACX5	acyl CoA oxidase in JA biosynthesis	*acx1 acx5*	SALK_041464 SALK_009998	Col-0
AT5G12390	FIS1B	peroxisome fission	*fis1b-RNAi*	RNAi line	Col-0
AT2G38400	AGT3	glyoxylate aminotransferase 3	*agt3-1*	SALK_100364	Col-0
AT1G01710	ACH2	acyl-CoA thioesterase	*ach2-1*	SALK_134567	Col-0
			ach2-2	GK_705E01	Col-0
			ach2-3	SALK_126817	Col-0
AT1G20510	OPCL1	4-coumarate-CoA ligase	*opcl1-1*	SALK_140659	Col-0
AT3G08860	PYD4	pyriminine 4	*pyd4*	SALK_141570	Col-0
AT2G29590	sT5	small thioesterase 5	*st5-1*	SALK_089257	Col-0
			st5-2	SALK_092512	Col-0

Table 3.1. (cont'd)

AT4G28220	NDB1	NAD(P)H dehydrogenase B1	*ndb1*	SALK_087720	Col-0
AT3G48140	B12D1	senescence-associated protein/ B12D-related protein	*b12d1-1*	FLAG_548C12	Ws-4
AT1G70580	GGT2	glutamate:glyoxylate aminotransferase2	*ggt2-1*	SALK_011617	Col-0
			ggt2-2	SALK_042954	Col-0
AT4G00520	ACH	acyl-CoA thioesterase	*ach-1*	SALK_045174	Col-0
			ach-2	SALK_150023	Col-0
AT5G20070	NUDX19	nudix hydrolase homolog 19	*nudx19-1*	SALK_114456	Col-0
			nudx19-2	SALK_115339	Col-0
AT5G27600	LACS7	long-chain Acyl-CoA synthetase 7	*lacs7-1*	SALK_146444	Col-0
AT3G51840	ACX4	acyl-CoA oxidase4	*acx4-1*	SALK_000879	Col-0
			acx4-2	SALK_065013	Col-0
AT1G06290	ACX3	acyl-CoA oxidase3	*acx3-1*	SALK_128947	Col-0
			acx3-2	SALK_044956	Col-0
AT1G54340	ICDH/ IDHP1	NADP-dependent isocitrate deshydrogenase	*icdh-1*	SALK_034151	Col-0
AT1G20480	4CL3	4-coumarate-CoA ligase	*4cl3-1*	SALK_027694	Col-0
			4cl3-2	SALK_010491	Col-0
AT4G09320	NDPK1	nucleoside diphosphate kinase type 1	*ndpk1-1*	SALK_089749	Col-0
AT2G41790	PM16	peptidase family M16	*pm16-1*	SALK_056340	Col-0
			pm16-2	SALK_019128	Col-0
AT3G14150	HAOX2	hydroxy-acid oxidase isoform 2	*haox2-1*	SALK_102409	Col-0
AT2G42450	Lcp3	lipase class 3 family protein	*lcp3-1*	SALK_035053	Col-0
AT2G30660	CHYH2	ATP- dependent caseinolytic protease	*chyh2-1*	SALK_082635	Col-0
			chyh2-2	SALK_143061	Col-0
AT1G50510	IndA	indigoidine synthase A	*inda-1*	GK_681B01	Col-0

Table 3.1. (cont'd)

AT3G56460	ZnDH	zinc-binding dehydrogenase	*zndh-1*	SALK_056640	Col-0
			zndh-2	SALK_082243	Col-0
AT1G04290	sT4	acyl-CoA thioesterase	*st4-1*	SALK_087372	Col-0
			st4-2	SALK_061841	Col-0
AT5G42890	SCP2	sterol carrier protein 2	*scp2*	CS829325	Col-0
AT5G58220	TLP	transthyretin-like protein	*tlp-1*	SALK_137289	Col-0
AT5G18100	CSD3	copper/zinc superoxide dismutase 3	*csd3*	SALK_126981	Col-0
AT5G11520	ASP3	aspartate aminotransferase3	*asp3-1*	SALK_008526	Col-0
			asp3-2	SALK_063210	Col-0
			asp3-3	SALK_083372	Col-0
AT4G16760	ACX1	acyl CoA oxidase in JA biosynthesis	*acx1*	SALK_041464	Col-0
AT4G29010	AIM1	abnormal inflorescence meristem 1	*aim1*	SALK_038805	Col-0
AT1G06310	ACX6	acyl-CoA oxidase6	*acx6*	SALK_023093	Col-0
AT3G24170	GR1	glutathione reductase 1	*gr1-1*	SALK_060425	Col-0
			gr1-2	SALK_105794	Col-0
AT3G57090	FIS1A	peroxisome fission	*fis1a*	SALK_086794	Col-0
AT5G47040	Lon2	long Protease 2	*lon2-2*	SALK_043857	Col-0
AT4G05160	4CLP1	4-coumarate:CoA ligase 1	*4clp1-1*	SALK_050214	Col-0
AT3G55640	CDC	Ca2+-dependent carrier	*cadc-1*	CS832927	Col-0
			cadc-2	GK_237H07	Col-0
AT3G51660	MIF	MIF superfamily protein	*mif*	SALK_037373	Col-0
AT2G22780	PMDH1	peroxisomal NAD-malate dehydrogenase 1	*pmdh1*	SALK_047994	Col-0

Table 3.1. (cont'd)

AT5G65400	UP7	Unknown protein 7	*up7-1*	SALK_062218	Col-0
			up7-2	SALK_067081	Col-0
AT1G04710	KAT1	3 keto-acyl-CoA thiolase 1	*kat1-1*	SALK_013834	Col-0
AT5G37670	Hsp15.7	heat shock protein similar to 17.7KDa class I	*hsp15.7-1*	SALK_038951	Col-0
			hsp15.7-2	SALK_107711	Col-0
AT3G27820	MDAR4	peroxisomal monodehydroascorbate reductase 4	*mdar4*	SALK_015596	Col-0
AT5G65940	CHY1	beta-hydroxyisobutyryl-CoA hydrolase 1	*chy1-1*	SALK_025417	Col-0
			chy1-2	SALK_102725	Col-0
AT1G23310	GGT1	glutamate:glyoxylate aminotransferase1	*ggt1*	SALK_064982	Col-0
AT3G19570	SCO3	snowy cotyledon	*sco3*	SALK_021491	Col-0
AT3G06860	MFP2	multifunction protein 2	*mfp2*	SALK_098016	Col-0
AT2G43020	PAO2	polyamine oxidase 2	*pao2-1*	SALK_046281	Col-0
			pao2-2	SALK_062035	Col-0
AT1G65840	PAO4	Polyamine oxidase 4	*pao4-1*	SALK_062544	Col-0
			pao4-2	SALK_118752	Col-0
AT5G47720	ACAT1.3	acetoacetyl-CoA thiolase 1.3	*acat1.3-1*	SALK_008505	Col-0
AT3G48170	BADH	aldehyde deshydrogenase	*badh-1*	CS822971	Col-0
AT1G30520	AAE14	acyl-activating enzyme 14	*aae14*	SALK_038308	Col-0
AT4G04320	MCD	malonyl-CoA decarboxylase	*mcd-1*	SALK_069574	Col-0
			mcd-2	GK_859E12	Col-0
AT4G16210	ECHIa	enoyl-CoA hydratase/isomerase A	*echia-1*	SALK_004620	Col-0
			echia-2	SALK_024138	Col-0
AT1G20560	AAE1	acyl-activating enzyme isoform 1	*aae1-1*	SALK_041152	Col-0

Table 3.1. (cont'd)

AT2G14120	DRP3B	dynamin-related protein	*drp3b-1*	SALK_045316	Col-0
			drp3b-2	SALK_112233	Col-0
AT4G02340	EH3	epoxide hydrolase isoform 3	*eh3-1*	SALK_106529	Col-0
			eh3-2	SALK_149885	Col-0
AT3G05290	PNC1	peroxisomal adenine nucleotide carrier 1	*pnc1-1*	SALK_152091	Col-0
			pnc1-2	SALK_044502	Col-0
AT4G33650	DRP3A	dynamin-related protein	*drp3a-2*	SALK_147485	Col-0
AT1G19570	DHAR1	dehydroascorbate reductase	*dhar-1*	SALK_005382	Col-0
			dhar-2	SALK_029966	Col-0
AT5G03860	MLS	malate synthase	*mls-1*	SALK_060987	Col-0
			mls-2	SALK_109976	Col-0

Table 3.2. Primers used in this study

Hu Lab ID	Primer name	Sequence	Direction	Usage	Gene name	Gene ID
HU6151	Anth15-RTF	ATACCTTTTACAATTTGTTTAT	fw	qPCR	PAP1	AT1G56650
HU6152	Anth15-RTR	CTAATCAAATTTCACAGTC	rv	qPCR	PAP1	AT1G56650
HU6153	Anth16-RTF	TGGGAAGCCACAATAACCCC	fw	qPCR	PAP2	AT1G66390
HU6154	Anth16-RTR	CTAATCAAGTTCAACAGTCTC	rv	qPCR	PAP2	AT1G66390
HU6125	Anth2-RTF	ATGGATCAAATCGAAGCAATGTTG	fw	qPCR	PAL2	AT3G53260
HU6126	Anth2-RTR	TCGTGAACCTTTTGAGCTAATT	rv	qPCR	PAL2	AT3G53260
HU6129	Anth4-RTF	ATGGTGATGGCTGGTGCTTC	fw	qPCR	CHS	AT5G13930
HU6130	Anth4-RTR	TTAGAGAGGAACGCTGTGCA	rv	qPCR	CHS	AT5G13930
HU6141	Anth10-RTF	ATGGTTAGTCAGAAAGAGACCG	fw	qPCR	DFR	AT5G42800
HU6142	Anth10-RTR	CTAGGCACACATCTGTTGTGC	rv	qPCR	DFR	AT5G42800
HU6149	Anth14-RTF	AACTCCGTTGAGGAAGATGTGAT	fw	qPCR	UGT89C1	AT1G06000
HU6150	Anth14-RTR	TTACAAACACATCTCTGCAACG	rv	qPCR	UGT89C1	AT1G06000
HU6166	SHSP-RTF	GCGATCGTGAACGCACGTGTGGA	fw	qPCR	SHSP	AT2G29500
HU6167	SHSP-RTR	TCCATCTTCACATTCTCCGGCAACC	rv	qPCR	SHSP	AT2G29500
HU6168	WRKY30-RTF	CGCTGGACGATGGATTCAGTTGGAGA	fw	qPCR	WRKY30	AT5G24110
HU6169	WRKY30-RTR	TCGGTTCGAGGTTTTGTATCGGCATTG	rv	qPCR	WRKY30	AT5G24110

REFERENCES

REFERENCES

Albrecht, V., Simkova, K., Carrie, C., Delannoy, E., Giraud, E., Whelan, J., Small, I.D., Apel, K., Badger, M.R., and Pogson, B.J. (2010). The cytoskeleton and the peroxisomal-targeted snowy cotyledon3 protein are required for chloroplast development in Arabidopsis. The Plant cell 22, 3423-3438.

Anderson, L.E. (1971). Chloroplast and cytoplasmic enzymes. II. Pea leaf triose phosphate isomerases. Biochimica et biophysica acta 235, 237-244.

Athanasiou, K., Dyson, B.C., Webster, R.E., and Johnson, G.N. (2010). Dynamic acclimation of photosynthesis increases plant fitness in changing environments. Plant physiology 152, 366-373.

Attaran, E., Major, I.T., Cruz, J.A., Rosa, B.A., Koo, A.J., Chen, J., Kramer, D.M., He, S.Y., and Howe, G.A. (2014). Temporal Dynamics of Growth and Photosynthesis Suppression in Response to Jasmonate Signaling. Plant Physiol 165, 1302-1314.

Aung, K., and Hu, J. (2012). Differential roles of Arabidopsis dynamin-related proteins DRP3A, DRP3B, and DRP5B in organelle division. Journal of integrative plant biology 54, 921-931.

Avenson, T.J., Cruz, J.A., and Kramer, D.M. (2004). Modulation of energy-dependent quenching of excitons in antennae of higher plants. Proceedings of the National Academy of Sciences of the United States of America 101, 5530-5535.

Baker, N.R. (2008). Chlorophyll fluorescence: a probe of photosynthesis in vivo. Annual review of plant biology 59, 89-113.

Baker, N.R., Harbinson, J., and Kramer, D.M. (2007). Determining the limitations and regulation of photosynthetic energy transduction in leaves. Plant, cell & environment 30, 1107-1125.

Bauwe, H., Hagemann, M., and Fernie, A.R. (2010). Photorespiration: players, partners and origin. Trends Plant Sci 15, 330-336.

Bellafiore, S., Barneche, F., Peltier, G., and Rochaix, J.D. (2005). State transitions and light adaptation require chloroplast thylakoid protein kinase STN7. Nature 433, 892-895.

Bernhardt, K., Wilkinson, S., Weber, A.P., and Linka, N. (2012). A peroxisomal carrier delivers NAD(+) and contributes to optimal fatty acid degradation during storage oil mobilization. The Plant journal : for cell and molecular biology 69, 1-13.

Boldt, R., Edner, C., Kolukisaoglu, U., Hagemann, M., Weckwerth, W., Wienkoop, S., Morgenthal, K., and Bauwe, H. (2005). D-GLYCERATE 3-KINASE, the last unknown enzyme in the photorespiratory cycle in Arabidopsis, belongs to a novel kinase family. The Plant cell 17, 2413-2420.

Borevitz, J.O., Xia, Y., Blount, J., Dixon, R.A., and Lamb, C. (2000). Activation tagging identifies a conserved MYB regulator of phenylpropanoid biosynthesis. The Plant cell 12, 2383-2394.

Casano, L.M., Martin, M., and Sabater, B. (2001). Hydrogen peroxide mediates the induction of chloroplastic Ndh complex under photooxidative stress in barley. Plant physiology 125, 1450-1458.

Cassin-Ross, G., and Hu, J. (2014). Systematic phenotypic screen of Arabidopsis peroxisomal mutants identifies proteins involved in beta-oxidation. Plant Physiol 166, 1546-1559.

Chi, W., Sun, X., and Zhang, L. (2013). Intracellular signaling from plastid to nucleus. Annual review of plant biology 64, 559-582.

Cousins, A.B., Pracharoenwattana, I., Zhou, W., Smith, S.M., and Badger, M.R. (2008a). Peroxisomal Malate Dehydrogenase Is Not Essential for Photorespiration in Arabidopsis But Its Absence Causes an Increase in the Stoichiometry of Photorespiratory CO2 Release. Plant Physiology Vol. 148, 786-795.

Cousins, A.B., Pracharoenwattana, I., Zhou, W., Smith, S.M., and Badger, M.R. (2008b). Peroxisomal Malate Dehydrogenase Is Not Essential for Photorespiration in Arabidopsis But Its Absence Causes an Increase in the Stoichiometry of Photorespiratory CO2 Release. Plant Physiology.

Cousins, A.B., Walker, B.J., Pracharoenwattana, I., Smith, S.M., and Badger, M.R. (2011). Peroxisomal hydroxypyruvate reductase is not essential for photorespiration in Arabidopsis but its absence causes an increase in the stoichiometry of photorespiratory CO2 release. Photosynthesis research 108, 91-100.

Dutta, S., Cruz, J., Jian, Y., Chen, J., Kramer, D.M., and Osteryoung, K. (2015). Non-invasive, whole-plant imaging of chloroplast movements and chlorophyll fluorescence reveals photosynthetic phenotypes independent of chloroplast photorelocation defects in chloroplast division mutants. Plant Journal.

Dyson, B.C., Allwood, J.W., Feil, R., Xu, Y., Miller, M., Bowsher, C.G., Goodacre, R., Lunn, J.E., and Johnson, G.N. (2015). Acclimation of metabolism to light in Arabidopsis thaliana: the glucose 6-phosphate/phosphate translocator GPT2 directs metabolic acclimation. Plant, cell & environment 38, 1404-1417.

Eberhard, S., Finazzi, G., and Wollman, F.A. (2008). The dynamics of photosynthesis. Annu Rev Genet 42, 463-515.

Edwards, G.E., and Baker, N.R. (1993). Can CO2 assimilation in maize leaves be predicted accurately from chlorophyll fluorescence analysis? Photosynthesis research 37, 89-102.

Eisenhut, M., Ruth, W., Haimovich, M., Bauwe, H., Kaplan, A., and Hagemann, M. (2008). The photorespiratory glycolate metabolism is essential for cyanobacteria and might have been conveyed endosymbiontically to plants. Proceedings of the National Academy of Sciences of the United States of America 105, 17199-17204.

Engel, N., van den Daele, K., Kolukisaoglu, U., Morgenthal, K., Weckwerth, W., Parnik, T., Keerberg, O., and Bauwe, H. (2007). Deletion of glycine decarboxylase in Arabidopsis is lethal under nonphotorespiratory conditions. Plant physiology 144, 1328-1335.

Fagarasanu, A., Mast, F.D., Knoblach, B., and Rachubinski, R.A. (2010). Molecular mechanisms of organelle inheritance: lessons from peroxisomes in yeast. Nat Rev Mol Cell Biol 11, 644-654.

Fahnenstich, H., Scarpeci, T.E., Valle, E.M., Flugge, U.I., and Maurino, V.G. (2008). Generation of hydrogen peroxide in chloroplasts of Arabidopsis overexpressing glycolate oxidase as an inducible system to study oxidative stress. Plant Physiol 148, 719-729.

Fernandez, A.P., and Strand, A. (2008). Retrograde signaling and plant stress: plastid signals initiate cellular stress responses. Current opinion in plant biology 11, 509-513.

Foyer, C.H., Bloom, A.J., Queval, G., and Noctor, G. (2009). Photorespiratory metabolism: genes, mutants, energetics, and redox signaling. Annual review of plant biology 60, 455-484.

Fristedt, R., Willig, A., Granath, P., Crevecoeur, M., Rochaix, J.D., and Vener, A.V. (2009). Phosphorylation of photosystem II controls functional macroscopic folding of photosynthetic membranes in Arabidopsis. The Plant cell 21, 3950-3964.

Fu, Z.Q., and Dong, X. (2013). Systemic acquired resistance: turning local infection into global defense. Annual review of plant biology 64, 839-863.

Genty, B., Briantais, J.-M., and Baker, N.R. (1989). The relationship between the quantum yield of photosynthetic electron transport and quenching of chlorophyll fluorescence. Biochimica et Biophysica Acta 990, 87-92.

Gotoh, E., Matsumoto, M., Ogawa, K., Kobayashi, Y., and Tsuyama, M. (2010). A qualitative analysis of the regulation of cyclic electron flow around photosystem I from

the post-illumination chlorophyll fluorescence transient in Arabidopsis: a new platform for the in vivo investigation of the chloroplast redox state. Photosynthesis research 103, 111-123.

Gou, J.Y., Felippes, F.F., Liu, C.J., Weigel, D., and Wang, J.W. (2011). Negative regulation of anthocyanin biosynthesis in Arabidopsis by a miR156-targeted SPL transcription factor. The Plant cell 23, 1512-1522.

Hall, C.C., Cruz, J., Wood, M., Zegarac, R., DeMars, D., Carpenter, J., Kanazawa, A., and Kramer, D. (2013). Photosynthetic Measurements with the Idea Spec: an Integrated Diode Emitter Array Spectrophotometer/Fluorometer. Photosynthesis Research for Food, Fuel and the Future, 184-188.

Hartl, M., and Finkemeier, I. (2012). Plant mitochondrial retrograde signaling: post-translational modifications enter the stage. Front Plant Sci 3, 253.

Havaux, M., Bonfils, J.P., Lutz, C., and Niyogi, K.K. (2000). Photodamage of the photosynthetic apparatus and its dependence on the leaf developmental stage in the npq1 Arabidopsis mutant deficient in the xanthophyll cycle enzyme violaxanthin de-epoxidase. Plant Physiol 124, 273-284.

Hayashi, M., Nito, K., Toriyama-Kato, K., Kondo, M., Yamaya, T., and Nishimura, M. (2000). AtPex14p maintains peroxisomal functions by determining protein targeting to three kinds of plant peroxisomes. The EMBO journal 19, 5701-5710.

Heinzmann, U., and Seitz, U. (1977). Synthesis of phenylalanine ammonia-lyase in anthocyanin-containing and anthocyanin-free callus cells of Daucus carota L. Planta 135, 63-67.

Hofmann, N.R. (2011). The evolution of photorespiratory glycolate oxidase activity. The Plant cell 23, 2805.

Hou, X., Fu, A., Garcia, V.J., Buchanan, B.B., and Luan, S. (2015). PSB27: A thylakoid protein enabling Arabidopsis to adapt to changing light intensity. Proceedings of the National Academy of Sciences of the United States of America 112, 1613-1618.

Hu, J., Baker, A., Bartel, B., Linka, N., Mullen, R.T., Reumann, S., and Zolman, B.K. (2012). Plant peroxisomes: biogenesis and function. The Plant cell 24, 2279-2303.

Hunt, S. (2003). Measurements of photosynthesis and respiration in plants. Physiologia plantarum 117, 314-325.

Igarashi, D., Miwa, T., Seki, M., Kobayashi, M., Kato, T., Tabata, S., Shinozaki, K., and Ohsumi, C. (2003). Identification of photorespiratory glutamate:glyoxylate

aminotransferase (GGAT) gene in Arabidopsis. The Plant journal : for cell and molecular biology 33, 975-987.

Islinger, M., Grille, S., Fahimi, H.D., and Schrader, M. (2012). The peroxisome: an update on mysteries. Histochem Cell Biol 137, 547-574.

Joliot, P., and Johnson, G.N. (2011). Regulation of cyclic and linear electron flow in higher plants. Proceedings of the National Academy of Sciences of the United States of America 108, 13317-13322.

Kanazawa, A., and Kramer, D.M. (2002). In vivo modulation of nonphotochemical exciton quenching (NPQ) by regulation of the chloroplast ATP synthase. Proceedings of the National Academy of Sciences of the United States of America 99, 12789-12794.

Kasahara, M., Kagawa, T., Oikawa, K., Suetsugu, N., Miyao, M., and Wada, M. (2002). Chloroplast avoidance movement reduces photodamage in plants. Nature 420, 829-832.

Kaur, N., and Hu, J. (2011). Defining the plant peroxisomal proteome: from Arabidopsis to rice. Front Plant Sci 2, 103.

Kramer, D., Cruz, J., Hall, C., KOVAC, W.K., and Zegarac, R. (2013). Plant phenometrics systems and methods and devices related thereto. United States Patent WO 2013181433 A2.

Krause, G.H., and Jahns, P. (2003). Pulse Amplitude Modulated Chlorophyll Fluorometry and its Application in Plant Science. Light-Harvesting Antennas in Photosynthesis 13.

Krause, G.H., and Weis, E. (1991). Chlorophyll fluorescence and photosynthesis: the basics. Annual Review of Plant Physiology 42, 313-349.

Kügler, M., Jänsch, L., Kruft, V., Schmitz, U.K., and Braun, H.-P. (1997). Analysis of the chloroplast protein complexes by blue-native polyacrylamide gel electrophoresis (BN-PAGE). Photosynthesis research Volume 53, pp 35-44.

Kulheim, C., Agren, J., and Jansson, S. (2002). Rapid regulation of light harvesting and plant fitness in the field. Science 297, 91-93.

Li, J., and Hu, J. (2015). Using Co-Expression Analysis and Stress- Based Screens to Uncover Arabidopsis Peroxisomal Proteins Involved in Drought Response. PLoS ONE.

Li, X.P., Bjorkman, O., Shih, C., Grossman, A.R., Rosenquist, M., Jansson, S., and Niyogi, K.K. (2000). A pigment-binding protein essential for regulation of photosynthetic light harvesting. Nature 403, 391-395.

Liepman, A.H., and Olsen, L.J. (2003). Alanine aminotransferase homologs catalyze the glutamate:glyoxylate aminotransferase reaction in peroxisomes of Arabidopsis. Plant physiology 131, 215-227.

Liu, J., and Last, R.L. (2015). A land plant-specific thylakoid membrane protein contributes to photosystem II maintenance in Arabidopsis thaliana. The Plant journal : for cell and molecular biology 82, 731-743.

Liu, J., Yang, H., Lu, Q., Wen, X., Chen, F., Peng, L., Zhang, L., and Lu, C. (2012). PSBP-DOMAIN PROTEIN1, a Nuclear-Encoded Thylakoid Lumenal Protein, Is Essential for Photosystem I Assembly in Arabidopsis. The Plant cell.

Livingston, A.K., Cruz, J.A., Kohzuma, K., Dhingra, A., and Kramer, D.M. (2010). An Arabidopsis mutant with high cyclic electron flow around photosystem I (hcef) involving the NADPH dehydrogenase complex. The Plant cell 22, 221-233.

Long, S.P., and Bernacchi, C.J. (2003). Gas exchange measurements, what can they tell us about the underlying limitations to photosynthesis? Procedures and sources of error. J Exp Bot 54, 2393-2401.

McBride, H., and Sedwick, C. (2014). Heidi McBride: mitochondria are well connected. The Journal of cell biology 206, 454-455.

Mhamdi, A., Noctor, G., and Baker, A. (2012). Plant catalases: peroxisomal redox guardians. Archives of biochemistry and biophysics 525, 181-194.

Mullen, R.T., and Trelease, R.N. (2006). The ER-peroxisome connection in plants: development of the "ER semi-autonomous peroxisome maturation and replication" model for plant peroxisome biogenesis. Biochimica et biophysica acta 1763, 1655-1668.

Neuspiel, M., Schauss, A.C., Braschi, E., Zunino, R., Rippstein, P., Rachubinski, R.A., Andrade-Navarro, M.A., and McBride, H.M. (2008). Cargo-selected transport from the mitochondria to peroxisomes is mediated by vesicular carriers. Current biology : CB 18, 102-108.

Ng, S., Giraud, E., Duncan, O., Law, S.R., Wang, Y., Xu, L., Narsai, R., Carrie, C., Walker, H., Day, D.A., et al. (2013a). Cyclin-dependent kinase E1 (CDKE1) provides a cellular switch in plants between growth and stress responses. J Biol Chem 288, 3449-3459.

Ng, S., Ivanova, A., Duncan, O., Law, S.R., Van Aken, O., De Clercq, I., Wang, Y., Carrie, C., Xu, L., Kmiec, B., et al. (2013b). A membrane-bound NAC transcription factor, ANAC017, mediates mitochondrial retrograde signaling in Arabidopsis. The Plant cell 25, 3450-3471.

Nishiyama, Y., Allakhverdiev, S.I., and Murata, N. (2006). A new paradigm for the action of reactive oxygen species in the photoinhibition of photosystem II. Biochimica et biophysica acta 1757, 742-749.

Niyogi, K.K., Grossman, A.R., and Bjorkman, O. (1998). Arabidopsis mutants define a central role for the xanthophyll cycle in the regulation of photosynthetic energy conversion. The Plant cell 10, 1121-1134.

Niyogi, K.K., and Truong, T.B. (2013). Evolution of flexible non-photochemical quenching mechanisms that regulate light harvesting in oxygenic photosynthesis. Current opinion in plant biology 16, 307-314.

OH, L., and JV, P. (1972). A flexible system of enzymatic analysis. Academic Press, Orlando.

Oikawa, K., Matsunaga, S., Mano, S., Kondo, M., Yamada, K., Hayashi, M., Kagawa, T., Kadota, A., Sakamoto, W., Higashi, S., et al. (2015). Physical interaction between peroxisomes and chloroplasts elucidated by in situ laser analysis. Nature plants 1.

Page, M., Sultana, N., Paszkiewicz, K., Florance, H., and Smirnoff, N. (2012). The influence of ascorbate on anthocyanin accumulation during high light acclimation in Arabidopsis thaliana: further evidence for redox control of anthocyanin synthesis. Plant, cell & environment 35, 388-404.

Pick, T.R., Brautigam, A., Schulz, M.A., Obata, T., Fernie, A.R., and Weber, A.P. (2013). PLGG1, a plastidic glycolate glycerate transporter, is required for photorespiration and defines a unique class of metabolite transporters. Proceedings of the National Academy of Sciences of the United States of America 110, 3185-3190.

Pieuchot, L., and Jedd, G. (2012). Peroxisome assembly and functional diversity in eukaryotic microorganisms. Annu Rev Microbiol 66, 237-263.

Pracharoenwattana, I., Cornah, J.E., and Smith, S.M. (2007). Arabidopsis peroxisomal malate dehydrogenase functions in beta-oxidation but not in the glyoxylate cycle. The Plant journal : for cell and molecular biology 50, 381-390.

Quan, S., Switzenberg, R., Reumann, S., and Hu, J. (2010). In vivo subcellular targeting analysis validates a novel peroxisome targeting signal type 2 and the peroxisomal localization of two proteins with putative functions in defense in Arabidopsis. Plant Signal Behav 5, 151-153.

Quan, S., Yang, P., Cassin-Ross, G., Kaur, N., Switzenberg, R., Aung, K., Li, J., and Hu, J. (2013). Proteome analysis of peroxisomes from etiolated Arabidopsis seedlings

identifies a peroxisomal protease involved in beta-oxidation and development. Plant Physiol 163, 1518-1538.

Reumann, S., Quan, S., Aung, K., Yang, P., Manandhar-Shrestha, K., Holbrook, D., Linka, N., Switzenberg, R., Wilkerson, C.G., Weber, A.P., et al. (2009). In-depth proteome analysis of Arabidopsis leaf peroxisomes combined with in vivo subcellular targeting verification indicates novel metabolic and regulatory functions of peroxisomes. Plant Physiol 150, 125-143.

Rochaix, J.D. (2011). Regulation of photosynthetic electron transport. Biochimica et biophysica acta 1807, 375-383.

Rochaix, J.D. (2014). Regulation and dynamics of the light-harvesting system. Annual review of plant biology 65, 287-309.

Rojas, C.M., Senthil-Kumar, M., Wang, K., Ryu, C.M., Kaundal, A., and Mysore, K.S. (2012). Glycolate oxidase modulates reactive oxygen species-mediated signal transduction during nonhost resistance in Nicotiana benthamiana and Arabidopsis. The Plant cell 24, 336-352.

Sacksteder, C.A., Kanazawa, A., Jacoby, M.E., and Kramer, D.M. (2000). The proton to electron stoichiometry of steady-state photosynthesis in living plants: A proton-pumping Q cycle is continuously engaged. Proceedings of the National Academy of Sciences of the United States of America 97, 14283-14288.

Schnarrenberger, C., Flechner, A., and Martin, W. (1995). Enzymatic Evidence for a Complete Oxidative Pentose Phosphate Pathway in Chloroplasts and an Incomplete Pathway in the Cytosol of Spinach Leaves. Plant Physiol 108, 609-614.

Schrader, M., and Fahimi, H.D. (2008). The peroxisome: still a mysterious organelle. Histochem Cell Biol 129, 421-440.

Schumann, U., and Subramani, S. (2008). Special delivery from mitochondria to peroxisomes. Trends in cell biology 18, 253-256.

Schwarte, S., and Bauwe, H. (2007). Identification of the photorespiratory 2-phosphoglycolate phosphatase, PGLP1, in Arabidopsis. Plant Physiol 144, 1580-1586.

Sharkey, T.D., and Weise, S.E. (2012). Autotrophic Carbon Dioxide Fixation. Advances in Photosynthesis and Respiration Volume 34.

Shikanai, T. (2007). Cyclic electron transport around photosystem I: genetic approaches. Annual review of plant biology 58, 199-217.

Shikanai, T., Endo, T., Hashimoto, T., Yamada, Y., Asada, K., and Yokota, A. (1998). Directed disruption of the tobacco ndhB gene impairs cyclic electron flow around photosystem I. Proceedings of the National Academy of Sciences of the United States of America 95, 9705-9709.

Shirokane, Y., Ichikawa, K., and Suzuki, M. (2000). A novel enzymic determination of maltose. Carbohydrate research 329, 699-702.

Smith, J.J., and Aitchison, J.D. (2013). Peroxisomes take shape. Nat Rev Mol Cell Biol 14, 803-817.

Somerville, C.R., and Ogren, W.L. (1980). Photorespiration mutants of Arabidopsis thaliana deficient in serine-glyoxylate aminotransferase activity. Proceedings of the National Academy of Sciences of the United States of America 77, 2684-2687.

Strand, D.D., Livingston, A.K., Satoh-Cruz, M., Froehlich, J.E., Maurino, V.G., and Kramer, D.M. (2015). Activation of cyclic electron flow by hydrogen peroxide in vivo. Proceedings of the National Academy of Sciences of the United States of America 112, 5539-5544.

Sulpice, R., and McKeown, P.C. (2015). Moving toward a comprehensive map of central plant metabolism. Annual review of plant biology 66, 187-210.

Sylak-Glassman, E.J., Malnoe, A., De Re, E., Brooks, M.D., Fischer, A.L., Niyogi, K.K., and Fleming, G.R. (2014). Distinct roles of the photosystem II protein PsbS and zeaxanthin in the regulation of light harvesting in plants revealed by fluorescence lifetime snapshots. Proceedings of the National Academy of Sciences of the United States of America 111, 17498-17503.

Takahashi, S., Bauwe, H., and Badger, M. (2007). Impairment of the photorespiratory pathway accelerates photoinhibition of photosystem II by suppression of repair but not acceleration of damage processes in Arabidopsis. Plant physiology 144, 487-494.

Takizawa, K., Cruz, J.A., Kanazawa, A., and Kramer, D.M. (2007). The thylakoid proton motive force in vivo. Quantitative, non-invasive probes, energetics, and regulatory consequences of light-induced pmf. Biochimica et biophysica acta 1767, 1233-1244.

Tanaka, A., and Makino, A. (2009). Photosynthetic research in plant science. Plant & cell physiology 50, 681-683.

Tessmer, O.L., Jiao, Y., Cruz, J.A., Kramer, D.M., and Chen, J. (2013). Functional approach to high-throughput plant growth analysis. BMC systems biology 7 Suppl 6, S17.

Thazar-Poulot, N., Miquel, M., Fobis-Loisy, I., and Gaude, T. (2015). Peroxisome extensions deliver the Arabidopsis SDP1 lipase to oil bodies. Proceedings of the National Academy of Sciences of the United States of America 112, 4158-4163.

Thordal-Christensen, H., Zhang, Z., Wei, Y., and Collinge, D.B. (2002). Subcellular localization of H2O2 in plants. H2O2 accumulation in papillae and hypersensitive response during the barley-powdery mildew interaction. Plant Journal.

Tikkanen, M., Grieco, M., Nurmi, M., Rantala, M., Suorsa, M., and Aro, E.M. (2012). Regulation of the photosynthetic apparatus under fluctuating growth light. Philosophical transactions of the Royal Society of London Series B, Biological sciences 367, 3486-3493.

Timm, S., Florian, A., Arrivault, S., Stitt, M., Fernie, A.R., and Bauwe, H. (2012a). Glycine decarboxylase controls photosynthesis and plant growth. FEBS Lett 586, 3692-3697.

Timm, S., Florian, A., Wittmiss, M., Jahnke, K., Hagemann, M., Fernie, A.R., and Bauwe, H. (2013). Serine acts as a metabolic signal for the transcriptional control of photorespiration-related genes in Arabidopsis. Plant physiology 162, 379-389.

Timm, S., Mielewczik, M., Florian, A., Frankenbach, S., Dreissen, A., Hocken, N., Fernie, A.R., Walter, A., and Bauwe, H. (2012b). High-to-low CO2 acclimation reveals plasticity of the photorespiratory pathway and indicates regulatory links to cellular metabolism of Arabidopsis. PLoS One 7, e42809.

Timm, S., Nunes-Nesi, A., Parnik, T., Morgenthal, K., Wienkoop, S., Keerberg, O., Weckwerth, W., Kleczkowski, L.A., Fernie, A.R., and Bauwe, H. (2008). A cytosolic pathway for the conversion of hydroxypyruvate to glycerate during photorespiration in Arabidopsis. The Plant cell 20, 2848-2859.

Vanderauwera, S., Zimmermann, P., Rombauts, S., Vandenabeele, S., Langebartels, C., Gruissem, W., Inze, D., and Van Breusegem, F. (2005). Genome-wide analysis of hydrogen peroxide-regulated gene expression in Arabidopsis reveals a high light-induced transcriptional cluster involved in anthocyanin biosynthesis. Plant Physiol 139, 806-821.

Vivancos, P.D., Driscoll, S.P., Bulman, C.A., Ying, L., Emami, K., Treumann, A., Mauve, C., Noctor, G., and Foyer, C.H. (2011). Perturbations of amino acid metabolism associated with glyphosate-dependent inhibition of shikimic acid metabolism affect cellular redox homeostasis and alter the abundance of proteins involved in photosynthesis and photorespiration. Plant Physiol 157, 256-268.

Voll, L.M., Allaire, E.E., Fiene, G., and Weber, A.P. (2004). The Arabidopsis phenylalanine insensitive growth mutant exhibits a deregulated amino acid metabolism. Plant Physiol 136, 3058-3069.

Voll, L.M., Jamai, A., Renne, P., Voll, H., McClung, C.R., and Weber, A.P. (2006). The photorespiratory Arabidopsis shm1 mutant is deficient in SHM1. Plant physiology 140, 59-66.

Wang, Y., and Wu, W.H. (2013). Potassium transport and signaling in higher plants. Annual review of plant biology 64, 451-476.

Waterham, H.R., and Wanders, R.J. (2012). Metabolic functions and biogenesis of peroxisomes in health and disease. Biochimica et biophysica acta 1822, 1325.

Wellburn, A.R. (1994). The spectral determination of chlorophylls a and b, as well as total carotenoids, using various solvents with spectrophotometers of different resolution. Journal of Plant Physiology 144, 307-313.

Winkel-Shirley, B. (2002). Biosynthesis of flavonoids and effects of stress. Current opinion in plant biology 5, 218-223.

Xu, H., Zhang, J., Zeng, J., Jiang, L., Liu, E., Peng, C., He, Z., and Peng, X. (2009). Inducible antisense suppression of glycolate oxidase reveals its strong regulation over photosynthesis in rice. Journal of experimental botany 60, 1799-1809.

Yamori, W., Takahashi, S., Makino, A., Price, G.D., Badger, M.R., and von Caemmerer, S. (2011). The roles of ATP synthase and the cytochrome b6/f complexes in limiting chloroplast electron transport and determining photosynthetic capacity. Plant physiology 155, 956-962.

Zelitch, I., Schultes, N.P., Peterson, R.B., Brown, P., and Brutnell, T.P. (2009). High glycolate oxidase activity is required for survival of maize in normal air. Plant Physiol 149, 195-204.

Zeng, X.Q., Chow, W.S., Su, L.J., Peng, X.X., and Peng, C.L. (2010). Protective effect of supplemental anthocyanins on Arabidopsis leaves under high light. Physiologia plantarum 138, 215-225.

Zhang, L., Paakkarinen, V., Wijk, K.J.v., and Aro, E.-M. (1999). Co-translational assembly of the D1 protein into photosystem II. J Biol Chem.

Zhang, X., and Hu, J. (2009). Two small protein families, DYNAMIN-RELATED PROTEIN3 and FISSION1, are required for peroxisome fission in Arabidopsis. The Plant journal : for cell and molecular biology 57, 146-159.

Zhang, X., and Hu, J. (2010). The Arabidopsis chloroplast division protein DYNAMIN-RELATED PROTEIN5B also mediates peroxisome division. The Plant cell 22, 431-442.

CHAPTER 4

CONCLUSIONS AND FUTURE PERSPECTIVES

Peroxisomes house a wide array of metabolic reactions essential for plant growth and development. These organelles also dynamically interact with other organelles to support cellular functions. However, our knowledge regarding the role of peroxisomal proteins in various biological processes, including plant stress response and photosynthesis, is still incomplete. The objectives of my dissertation studies were to determine the role of peroxisomes in modulating environmental stress response and photosynthesis at a systems level, using *in silico* analysis, mutant screens followed by in-depth physiological and biochemical characterizations. Knowledge gained from my dissertation studies provides new insights into the connection between peroxisomal function and drought stress response and between photorespiration and photosynthesis, and opens new potential directions for future research on environmental stress response, photosynthesis, photorespiration and interorganellar communication.

4.1. Comprehensive analysis of transcriptional regulation on genes encoding peroxisomal proteins across developmental stages and under various environmental stresses

In Chapter 2, I presented the studies on transcriptional regulation of genes encoding peroxisomal proteins across developmental stages and under various environmental stresses. We found that many genes that function in the same pathway, such as glyoxylate cycle and photorespiration, tend to be co-expressed. For example, genes that encode glyoxylate cycle enzymes isocitrate lyase (ICL), malate synthase (MLS), and citrate synthase 1 (CSY1) were co-up-regulated during seed maturation,

presumably in preparation of their role in seed germination. Genes encoding the peroxisomal proliferation factors PEX11b, PEX11c and PEX11d were co-up-regulated under hypoxia conditions, consistent with a previous finding that hypoxia stress stimulates peroxisomal extension over the endoplasmic reticulum (Sinclair et al., 2009). Individual genes that showed dramatic up-regulations under certain conditions, such as >150-fold transcript increase of a heat shock protein gene *AtHsp15.7* under high light (HL), may shed light on the possible roles of these proteins in pertinent stress responses. Besides drought stress, other environmental stresses, such as high light, bacterial pathogen *Pseudomonas syringae* pv. *Tomato* DC3000 and bacterial elongation factor elf18, also significantly regulated the transcript levels of a large number of genes encoding peroxisomal proteins. This peroxisome-centered gene expression analysis provides a comprehensive view of transcript level changes of Arabidopsis peroxisomal genes, and is a starting point for selecting potential key players in stress response for further investigations.

Future directions: Based on our peroxisome-centered gene expression analysis, we can narrow down our focus to promising candidate genes. Uncharacterized genes that cluster with genes functioning in well known pathways are likely to play a role in that pathway. Mutant analysis of the heat shock protein gene *AtHsp15.7* under HL treatment is a worthy experiment to pursue, as this gene is dramatically up-regulated by HL. In addition to drought response screens, mutant screens can also be performed using other stress assays, such as pathogen infections and cold treatment, under which a significant number of genes show altered transcript levels. We also need to keep in mind that many

genes play a significant role in stress response but are not transcriptionally regulated under stress conditions.

4.2. LON2 protease and the photorespiratory enzyme hydroxypyruvate reductase 1 (HPR1) play important roles in drought response

In Chapter 2, I discovered that mutants of LON2 protease and hydroxypyruvate dehydrogenase HPR1 exhibited enhanced drought susceptibility, with faster chlorophyll degradation and water loss, and inhibited photosynthetic efficiency and anthocyanin induction under drought conditions. Unlike *LON2*, gene expression of *HPR1* was not highly induced by drought or the drought-related phytohormone abscisic acid. It is known that photorespiration is activated by environmental stresses, such as drought and high light (Foyer et al., 2009). The drought susceptibility exhibited by the two null mutants of *HPR1* may be mainly attributed to the block of photorespiration, which generates toxic levels of phosphoglycolate and strong accumulation of H_2O_2 that impair the photosynthetic apparatus, membrane integrity, and other cellular components. Since *LON2* was up-regulated by ABA, this protease may play a role in drought response through ABA signaling. It is also possible that the insufficient number of peroxisomes in *lon2* cannot carry out robust photorespiration, which is critical for plant survival under drought conditions.

Future directions: Whether LON2 affects drought response via photorespiration needs further investigation. Since high CO_2 can suppress photorespiration, carrying out drought tolerance experiments under high CO_2 condition may help to answer this

question. If the drought phenotype of *lon2* is rescued, we may conclude that the role of LON2 in drought is dependent on photorespiration. If not, it is more likely that LON2 itself has a direct role in drought tolerance. We may measure the abundance and morphology of peroxisomes during drought in both WT and *lon2*, which could possibly reveal the dynamics of peroxisome abundance during drought stress, and identify connections between organelle behavior and stress response. Another possibility is that the substrates for LON2 protease have a role in conferring drought tolerance, thus the identification of LON2 substrate through genetic, biochemical and/or cell biological approaches may shed light on the mechanism underlying the drought stress phenotype of *lon2*.

4.3. PXN is an additional factor in photorespiration

In Chapter 3, I presented that both *pxn* mutant alleles showed photosynthetic phenotypes under fluctuating light conditions, which can be rescued by providing high CO_2. One explanation for PXN's role is that NAD^+ delivered into peroxisome by PXN can be used as a substrate for peroxisomal malate dehydrogenases (PMDHs) to generate NADH that is needed for the reduction reaction catalyzed by the photorespiratory protein HPR1.

Future directions: The photosynthetic phenotype exhibited by the *pxn* mutants, and previously shown by the *pmdh1 pmdh2* double mutants (Cousins et al., 2008), was significant but relatively subtle, indicating that there are additional sources of NAD^+ and NADH in peroxisomes. The role of PXN in photorespiration could be further studied by

analyzing higher order mutants. Since PXN and PMDH function in NADH generation in subsequent orders, creating triple mutant *pxn pmdh1 pmdh2*, followed by photorespiratory and photosynthetic characterization could facilitate our understanding of the additive effect by PXN and PMDH.

4.4. *gox1* exhibited drastic photosynthetic phenotype under dynamic light conditions despite its normal growth in ambient air

In Chapter 3, I showed that *gox1* displayed significant photosynthetic phenotypes, including lower Φ2 and higher NPQ under high light and fluctuating light conditions. The fact that GOX1 and GOX2 are highly similar proteins and *gox1* null mutant does grow as well as WT led to an assumption that GOX1 and GOX2 are completely functionally redundant. However, we were able to reveal the phenotype of *gox1* by DEPI. This result testifies the high sensitivity and robustness of DEPI and indicates that GOX2 cannot fully substitute GOX1 under conditions in which photorespiration is strongly induced.

Future directions: *GOX1* and *GOX2* are closely linked to each other on Chromosome 3 in Arabidopsis, thus it is difficult to generate double mutants via crosses between the single mutants. To study the role of GOX in photorespiration through genetic approaches, we may generate CRISPR-CAS mediated (Feng et al., 2014; Hsu et al., 2013; Li et al., 2013) knockout lines for both GOX1 and GOX2, which will be an important genetic material for characterizing GOX functions.

4.5. Metabolites and molecules resulting from blocking photorespiration have a large impact on photosynthetic complexes and processes

In Chapter 3, I demonstrated that several photorespiratory mutants exhibited strong defects in various aspects of photosynthesis. I showed that the increased NPQs occurred in the photorespiratory mutants were attributed to elevated proton motive force (*pmf*) resulted from inhibited proton efflux across the thylakoid membrane. Meanwhile, I showed that the increased NPQs in photorespiratory mutants were completely dependent on the lumenal pH sensor protein PsbS and partially dependent on zeaxanthin. In addition, I found that cyclic electron flow (CEF) was activated in photorespiratory mutants to compensate for the ATP-to-NADPH ratio deficiency resulted from the decreased ATP synthase conductivity in photorespiratory mutants under high light (HL). Furthermore, subjecting the photorespiratory mutants to long term HL stresses led to strong photoinhibtion, enhanced reactive oxygen species (ROS), deficiency in anthocyanin accumulation, compromised photosynthetic complex integrity and reduced abundance of key photosystem subunits. Last but not least, we provided biochemical evidence that the activity of the CBB cycle enzyme triose phosphate isomerase (TPI) was inhibited in the photorespiratory mutants *in vivo* under HL. Expression of the G6P transporter gene *GPT2* was concomitantly increased, suggesting enhanced re-import of glucose 6-phosphate (G6P), which would activate the oxidative branch of the pentose phosphate pathway that subsequently creates a higher demand of ATP and enhanced oxidative stress in photorespiratory mutants.

Future directions: The diverse photosynthetic phenotypes exhibited on photorespiratory mutants may lead us to a few future directions to pursue. First, the

quantitatively and kinetically different phenotypes exhibited on mutants of genes in photorespiration, such as *hpr1, plgg1* and *cat2*, prompted us to speculate the relative importance and rate-limiting effect of each step in photorespiration. Photorespiratory metabolite flow data might be integrated with our genetics data to generate a quantitative model of photorespiration.

Decreased ATP synthase conductivity in *hpr1* and *plgg1* is the cause for higher *pmf* and NPQ, but the molecular mechanisms underlying the inhibitory effect on ATP synthase are still elusive. I speculate that the depletion of glycerate in *hpr1* and *plgg1* results in a slow-down of the CBB cycle, which increases the amount of ATP in stroma. Elevated levels of stromal ATP can possibly have a negative feedback effect on ATP conductivity. *hpr1* and *plgg1* provide suitable systems to study the regulation of ATP conductivity *in vivo*.

Additional enzymes and regulators involved in photorespiration need to be further discovered. Conducting a suppressor screen on *hpr1* could facilitate the discovery of these proteins. The obvious HL phenotype in *hpr1*, including small and pale green rosette compared to larger and purple rosette in WT, can help us to design an easy assay to look for *hpr1* suppressors under HL. Possible suppressors may include mutants of genes that negatively regulate photorespiration, positively regulate light absorption in photosystems, or positively regulate the production of H_2O_2.

In summary, results from my thesis work make a significant step towards deepening our understanding of the role of peroxisomes in modulating environmental

stress response and photosynthesis at the molecular level. These findings will not only contribute to the knowledge of organelle biology and plant biology, but also provide valuable information to biotechnological endeavors to improve crop plants for higher yields and better quality.

REFERENCES

REFERENCES

Cousins, A.B., Pracharoenwattana, I., Zhou, W., Smith, S.M., and Badger, M.R. (2008). Peroxisomal Malate Dehydrogenase Is Not Essential for Photorespiration in Arabidopsis But Its Absence Causes an Increase in the Stoichiometry of Photorespiratory CO2 Release. Plant Physiology *Vol. 148*, 786-795.

Feng, Z., Mao, Y., Xu, N., Zhang, B., Wei, P., Yang, D.L., Wang, Z., Zhang, Z., Zheng, R., Yang, L., *et al.* (2014). Multigeneration analysis reveals the inheritance, specificity, and patterns of CRISPR/Cas-induced gene modifications in Arabidopsis. Proceedings of the National Academy of Sciences of the United States of America *111*, 4632-4637.

Foyer, C.H., Bloom, A.J., Queval, G., and Noctor, G. (2009). Photorespiratory metabolism: genes, mutants, energetics, and redox signaling. Annual review of plant biology *60*, 455-484.

Hsu, P.D., Scott, D.A., Weinstein, J.A., Ran, F.A., Konermann, S., Agarwala, V., Li, Y., Fine, E.J., Wu, X., Shalem, O., *et al.* (2013). DNA targeting specificity of RNA-guided Cas9 nucleases. Nature biotechnology *31*, 827-832.

Li, J.F., Norville, J.E., Aach, J., McCormack, M., Zhang, D., Bush, J., Church, G.M., and Sheen, J. (2013). Multiplex and homologous recombination-mediated genome editing in Arabidopsis and Nicotiana benthamiana using guide RNA and Cas9. Nature biotechnology *31*, 688-691.

Sinclair, A.M., Trobacher, C.P., Mathur, N., Greenwood, J.S., and Mathur, J. (2009). Peroxule extension over ER-defined paths constitutes a rapid subcellular response to hydroxyl stress. The Plant journal : for cell and molecular biology *59*, 231-242.